

Ruthenium(II) *cis*-
triaminocyclohexane complexes as
anti-cancer compounds

Aimee Joanna Gamble

A thesis submitted for the degree of
Doctor of Philosophy

University of York
Department of Chemistry

August 2012

Abstract

Ruthenium complexes are promising candidates for the treatment of cancers. Two ruthenium(III) complexes have previously completed phase I clinical trials and half-sandwich ruthenium(II) η^6 -arene complexes are receiving much interest as anti-cancer agents. A range of new ruthenium(II) complexes have been prepared with a κ^3 -*N fac*-coordinating six electron donor, *cis*-1,3,5-triaminocyclohexane (*cis*-tach), replacing the η^6 -arene ligand. It is hypothesised that the *cis*-tach ligand will allow highly active complexes with good water solubility.

Initial access to ruthenium(II) *cis*-tach complexes was established with triphenylphosphane ligands, yielding the complexes [RuCl(*cis*-tach)(PPh₃)₂]Cl [**1**]Cl and [RuCl₂(*cis*-tach)(PPh₃)] [**2**]. The complexes adopt a piano-stool type structure, similar to η^6 -arene complexes. Use of labile dmsoligands in [RuCl(dmsol)₂(*cis*-tach)]Cl [**8**]Cl permitted the preparation of a range of complexes. Those with N–N and P–P bidentate chelating ligands, following the formula [Ru(dmsol)(N–N)(*cis*-tach)]²⁺ and [RuCl(P–P)(*cis*-tach)]⁺ were studied. Complexes with N–N chelating ligands were found to be inert to substitution in aqueous solution compared to the *bis*-dmsol complex [**8**]Cl, and were inactive in tumour growth inhibition.

Complexes with chelating diphosphane ligands are highly water-soluble, with excellent *in vitro* activity in the inhibition of tumor cell growth. The activity of two complexes (P–P = dppp, dppb) was found to exceed that of cisplatin. A structure-activity relationship is discussed. Two compounds were selected for further study (P–P = dppe [**16**]Cl, dppp [**17**]Cl) for good water solubility and high activity respectively. These complexes undergo rapid hydrolysis of the ruthenium-chlorido bond to give the corresponding aqua complexes. The interaction of these complexes with small models of biomolecules and DNA was also investigated.

Contents

Abstract	i
Contents.....	ii
Figures, Tables and Schemes	viii
Accompanying Material.....	xiii
Acknowledgements	xiv
Declaration	xvi
Chapter 1. Introduction.....	1
1.1 Preamble.....	1
1.2 Platinum-Based Cancer Therapy.....	3
1.2.1 Cisplatin	3
1.2.2 Cisplatin: Mechanism of Action	3
1.2.3 Second-Generation Platinum Drugs.....	8
1.2.4 The Ongoing Development of Metallodrugs	8
1.3 Ruthenium Complexes as Anti-cancer Agents.....	9
1.3.1 Ruthenium Ammine Complexes	9
1.3.2 NAMI-A and KP1019: Ruthenium Complexes in Clinical Trials.....	10
1.3.3 The “Activation by Reduction” Theory: Ruthenium(II).....	12
1.4 Classical Ruthenium(II) η^6 -Arene Complexes	14
1.4.1 1,2-Ethylenediamine Complexes	14
1.4.2 Structure-Activity Relationships.....	15
1.4.3 Mechanism of Action.....	18
1.4.4 Osmium Analogues	21
1.4.5 Conclusions.....	22
1.5 Non-Classical RAPTA Complexes	23
1.5.1 Initial Discovery.....	23
1.5.2 Mechanism of Action.....	25
1.5.3 Structural Modifications.....	28
1.5.3.1 Phosphane and Arene Modification.....	28
1.5.3.2 Aquation-Resistant Complexes.....	30
1.5.3.3 Targeted Therapy.....	31
1.5.4 Conclusions	32

1.6	Other Non-Classical Ruthenium(II) η^6 -Arene Compounds	33
1.6.1	Catalytic Anti-cancer agents	33
1.6.2	Complexes Designed to Inhibit Enzymes	34
1.7	Ruthenium η^6 -Arene Complexes: Conclusions	36
1.8	Is the η^6 -Arene Ligand Vital for Anti-cancer Activity?	38
1.9	The <i>cis</i> -1,3,5-Triaminocyclohexane Ligand.....	41
1.9.1	Synthesis of <i>cis</i> -tach Complexes.....	42
1.9.2	<i>cis</i> -Tach Compounds as Anti-cancer Agents	45
1.10	Aim of this Project.....	47
Chapter 2.	Ruthenium(II) <i>cis</i> -tach Triphenylphosphane Complexes	48
2.1	Introduction	48
2.2	Reaction of <i>cis</i> -tach with $[\text{RuCl}_2(\text{PPh}_3)_3]$	50
2.2.1	Formation of [1] Cl	50
2.2.2	Conversion of [1] Cl to [2]	56
2.2.3	Conclusions	61
2.3	Solid-State Structural Comparisons	62
2.4	Preparation of $[\{\text{RuCl}(\text{PPh}_3)(\textit{cis}\text{-tach})\}_2(\mu\text{-Cl})]^+$	64
2.5	Synthesis and Reactivity of Solvent Complexes	68
2.5.1	Dimethylsulfoxide Complexes.....	68
2.5.2	Acetonitrile Complexes.....	69
2.5.3	Reactivity of the Acetonitrile Complexes	73
2.5.4	Conclusions	74
2.6	<i>In Vitro</i> Biological Evaluation.....	75
2.7	Chapter Conclusions.....	76
Chapter 3.	Ruthenium(II) <i>cis</i> -tach Dimethylsulfoxide Precursor Complexes.....	78
3.1	Introduction	78
3.2	Preparation of $[\text{RuCl}(\text{DMSO-}S)_2(\textit{cis}\text{-tach})]\text{Cl}$	80
3.2.1	Synthesis and Characterisation	80
3.2.2	X-Ray Crystallography	83
3.2.3	Conclusions	84
3.3	Solid-State Structure of $[\text{RuCl}_2(\text{DMSO-}S)(\textit{cis}\text{-tach})]$	86
3.4	Comparison of X-Ray Structures	88
3.5	<i>In Vitro</i> Biological Evaluation.....	90
3.6	Aquation Studies	91

3.7	Reactions with Nucleosides.....	99
3.8	Chapter Conclusions.....	101
Chapter 4.	Ruthenium(II) <i>cis</i> -tach Complexes with <i>N-N</i> Chelates.....	103
4.1	Introduction	103
4.2	Synthesis and Characterisation.....	106
4.2.1	Polypyridyl Complexes.....	106
4.2.2	1,2-Ethylenediamine Complex.....	112
4.2.3	Analysis of the DMSO Ligand.....	116
4.2.4	Conclusions	122
4.3	<i>In Vitro</i> Biological Evaluation.....	122
4.4	Attempted Preparation of Chlorido Analogues	123
4.4.1	Use of η^4 -1,5-Cyclooctadiene Precursor Compounds.....	124
4.4.2	Use of Acetonitrile Precursor Compounds	126
4.4.3	Conclusions	127
4.5	Chapter Conclusions.....	127
Chapter 5.	Ruthenium (II) <i>cis</i> -tach Complexes with P–P Chelating Ligands	129
5.1	Introduction	129
5.2	Preparation of Complexes with P–P Chelating Ligands	131
5.2.1	Synthesis and Characterisation	131
5.2.2	X-Ray Crystallography	133
5.2.3	Discussion	140
5.2.3.2	$^{31}\text{P}\{^1\text{H}\}$ NMR Chemical Shifts.....	140
5.2.3.3	^1H NMR Chemical Shift of Amine Groups	142
5.2.3.4	Ruthenium–Chlorido Bond Lengths.....	143
5.2.4	Conclusions	145
5.3	<i>In Vitro</i> Biological Evaluation.....	145
5.3.1	Antiproliferative Activity.....	145
5.3.2	Structure-Activity Relationship	149
5.3.3	Conclusions	152
5.4	Chapter Conclusions.....	152
Chapter 6.	Aquation and Biomolecule Interactions of Ruthenium(II) <i>cis</i> -tach Diphosphane Complexes.....	154
6.1	Introduction	154
6.2	Identity of Aquation Products	155

6.2.1	Aquation of [16]Cl and [17]Cl	155
6.2.2	Coordination of Buffer	158
6.2.3	Aquation at Physiologically-Relevant Concentrations	159
6.2.4	Stability of Aquation Products with Time	161
6.2.5	Influence of Salts to Moderate Ionic Strength	162
6.2.6	Conclusions	162
6.3	Determination of the pK_a of the Aqua Ligand in [16a]^{x+} and [17a]^{x+}	163
6.3.1	UV/Vis pH Titrations	163
6.3.2	¹ H NMR pH Titrations	164
6.3.3	Conclusions	166
6.4	Kinetics of Aquation.....	167
6.4.1	Kinetics of Aquation and Anation of [16]Cl	167
6.4.2	Kinetics of Aquation and Anation of [17]Cl	172
6.4.3	Discussion and Conclusions.....	173
6.5	Equilibrium of Aquation/Anation.....	174
6.5.1	Results	175
6.5.2	Calculated Distribution of Species in Biological Environments.....	176
6.5.3	Conclusions	178
6.6	Interactions of [16]Cl and [17]Cl with Nucleosides.....	179
6.6.1	Interaction of [16]Cl with DNA Model Complexes	180
6.6.2	Interaction of [17]Cl with DNA Model Complexes	184
6.6.3	Interaction of [16]Cl and [17]Cl with Plasmid DNA.....	187
6.6.4	Conclusions	188
6.7	Interaction of [16]Cl and [17]Cl with a Model Protein: Glutathione.....	189
6.8	Chapter Conclusions.....	191
Chapter 7.	Conclusions and Future Work.....	193
7.1	Thesis Conclusions.....	193
7.2	Future Work.....	195
Chapter 8.	Experimental	197
8.1	General	197
8.1.1	X-Ray Crystallography	198
8.1.1.1	Bruker Smart Apex	198
8.1.1.2	Oxford Diffraction SuperNova	198
8.1.2	<i>In Vitro</i> Biological Evaluation	199

8.1.3	^1H and $^{13}\text{C}\{^1\text{H}\}$ NMR Assignments.....	200
8.1.4	Synthesis of <i>cis</i> -tach.....	202
8.1.4.1	<i>cis,cis</i> -1,3,5-Cyclohexanetris(benzyl carbamate).....	202
8.1.4.2	<i>Cis,cis</i> -1,3,5-triaminocyclohexane trihydrobromide	202
8.1.4.3	<i>Cis,cis</i> -1,3,5-triaminocyclohexane (<i>cis</i> -tach)	202
8.2	Chapter 2 Experimental.....	203
8.2.1	Reaction of $[\text{RuCl}_2(\text{PPh}_3)]$ with <i>cis</i> -tach.....	203
8.2.2	$[\text{RuCl}(\text{PPh}_3)_2(\textit{cis}\text{-tach})]\text{PF}_6$, [1] PF_6	203
8.2.3	$[\text{RuCl}_2(\text{PPh}_3)(\textit{cis}\text{-tach})]$, [2]	204
8.2.4	$[\{\text{RuCl}(\text{PPh}_3)(\textit{cis}\text{-tach})\}_2(\mu\text{-Cl})]\text{BPh}_4$, [3] BPh_4	205
8.2.5	$[\{\text{RuCl}(\text{PPh}_3)(\textit{cis}\text{-tach})\}_2(\mu\text{-Cl})]\text{PF}_6$, [3] PF_6	206
8.2.6	Dissolution of [2] in d_6 -DMSO	206
8.2.7	$[\text{RuCl}(\text{DMSO-}S)(\text{PPh}_3)(\textit{cis}\text{-tach})]\text{Cl}$, [4] Cl	206
8.2.8	$[\text{RuCl}(\text{NCMe})(\text{PPh}_3)(\textit{cis}\text{-tach})]\text{PF}_6$, [5] PF_6	207
8.2.9	$[\text{Ru}(\text{NCMe})_2(\text{PPh}_3)(\textit{cis}\text{-tach})](\text{PF}_6)_2$, [6] $(\text{PF}_6)_2$	208
8.2.10	Reaction of [5] PF_6 with dppm.....	209
8.3	Chapter 3 Experimental.....	209
8.3.1	$[\text{RuCl}(\text{DMSO-}S)_2(\textit{cis}\text{-tach})]\text{Cl}$, [8] Cl	209
8.3.2	$[\text{RuCl}_2(\text{DMSO-}S)(\textit{cis}\text{-tach})]$, [9]	210
8.3.3	Aquation of [8] Cl : Mass Spectrometry	210
8.3.4	Aquation of [8] Cl : NMR Kinetics.....	210
8.3.5	Aquation of [8] Cl : pH Study.....	211
8.3.6	Reaction of [8] Cl with Nucleosides	211
8.4	Chapter 4 Experimental.....	212
8.4.1	$[\text{Ru}(\text{bipy})(\text{DMSO-}S)(\textit{cis}\text{-tach})](\text{Cl})_2$, [10] $(\text{Cl})_2$	212
8.4.2	$[\text{Ru}(\text{DMSO-}S)(\text{phen})(\textit{cis}\text{-tach})](\text{Cl})_2$, [11] $(\text{Cl})_2$	212
8.4.3	$[\text{Ru}(\text{DMSO-}S)(\text{en})(\textit{cis}\text{-tach})](\text{Cl})_2$, [12] $(\text{Cl})_2$	213
8.4.4	Reaction of [11] $(\text{Cl})_2$ with Guanosine.....	214
8.4.5	$[\text{RuCl}(\eta^4\text{-COD})(\textit{cis}\text{-tach})]\text{PF}_6$, [13] PF_6	214
8.4.6	Reaction of [13] PF_6 with 2,2'-bipyridine.....	215
8.4.7	$\text{Ru}(\text{NCMe})_3(\textit{cis}\text{-tach})](\text{Cl})_2$, [14] $(\text{Cl})_2$	215
8.4.8	Reaction of [14] $(\text{Cl})_2$ with 2,2'-bipyridine.....	215
8.5	Chapter 5 Experimental.....	216
8.5.1	$[\text{RuCl}(\text{dppm})(\textit{cis}\text{-tach})]\text{Cl}$, [15] Cl	216

8.5.2	[RuCl(dppe)(<i>cis</i> -tach)]Cl, [16] Cl.....	217
8.5.3	[RuCl(dppp)(<i>cis</i> -tach)]Cl, [17] Cl.....	218
8.5.4	[RuCl(dppb)(<i>cis</i> -tach)]Cl, [18] Cl.....	219
8.5.5	[RuCl(dppv)(<i>cis</i> -tach)]Cl, [19] Cl.....	219
8.5.6	[RuCl(dppben)(<i>cis</i> -tach)]Cl, [20] Cl.....	220
8.6	Chapter 6 Experimental.....	221
8.6.1	NMR Spectroscopy.....	221
8.6.2	Mass Spectrometry of Aquation Products.....	222
8.6.3	[Ru(OH ₂)(dppe)(<i>cis</i> -tach)](OTf) ₂ , [16a] (OTf) ₂	222
8.6.4	[Ru(OH ₂)(dppp)(<i>cis</i> -tach)](OTf) ₂ , [17a] (OTf) ₂	223
8.6.5	NMR Sample Preparation – Aquation Experiments.....	223
8.6.6	pH Titrations.....	224
8.6.7	Kinetics of Aquation.....	225
8.6.8	Equilibrium Constants.....	226
8.6.9	NMR Sample Preparation – Guanine and GSH Experiments.....	226
8.6.10	Mass Spectroscopy of [16] Cl with Guo.....	227
8.6.11	Interaction of Ruthenium Complexes with pUC18 Plasmid DNA.....	227
8.6.12	DFT Calculations.....	227
Appendix I.	ORTEP Diagrams of [17–20] Cl.....	229
Appendix II.	Preparation of a Metallocene Analogue.....	234
Appendix III.	X-Ray Crystallography Data.....	235
Compound Codes.....		245
Abbreviations.....		246
References.....		250

Figures, Tables and Schemes

Figure 1.1: Structure of cisplatin.....	3
Figure 1.2: DNA structural distortions from platination.....	5
Figure 1.3: Platinum(II) complexes approved or currently in clinical trials.....	7
Figure 1.4: NAMI-A and KP1019.	10
Figure 1.5: Piano-stool structure of ruthenium(II) η^6 -arene complexes.	12
Figure 1.6: Structures of RM175 and HC11.	14
Figure 1.7: Cytotoxic Ru(II) η^6 -arene complexes with <i>O,O</i> - and <i>N,O</i> - ligands.	17
Figure 1.8: X-ray crystal structure of $[\text{Ru}(\text{en})(\text{EtG})(\eta^6\text{-tha})]^{2+}$	20
Figure 1.9: Structures of cytotoxic osmium(II) η^6 -arene complexes.	22
Figure 1.10: Structures of RAPTA-C and the <i>N</i> -Me modified complex.	23
Figure 1.11: Docking geometry of a RAPTA complex with the active site of cathepsin B and structure of a fluorescent tagged RAPTA complex.....	26
Figure 1.12: Modifications of the arene and PTA ligand inRAPTA complexes.	29
Figure 1.13: A phosphite-carbohydrate ligand as a PTA replacement	30
Figure 1.14: Aquation resistant RAPTA-C analogues.....	31
Figure 1.15: ethaRAPTA.	32
Figure 1.16: Ruthenium(II) kinase inhibitors	35
Figure 1.17: Ttcn analogues of ruthenium η^6 -arene complexes.	38
Figure 1.18: Ruthenium(II) tacn complexes assessed for anti-tumour activity..	40
Figure 1.19: Hypothesised structure of Ru(II) κ^3 <i>cis</i> -tach complexes.	41
Figure 1.20: Examples of <i>cis</i> -tach metal complexes.....	44
Figure 1.21: Structure of a platinum <i>cis</i> -tach complex.....	46
Figure 1.22: Hypothesised structure of Ru(II) κ^3 <i>cis</i> -tach complexes.	47
Figure 2.1: Structure of Dichlorido-tris(triphenylphosphane) ruthenium(II).....	48
Figure 2.2: ^1H NMR spectra of <i>cis</i> -tach and [1]Cl.....	51
Figure 2.3: Possible ^1H NMR symmetry environments for the <i>cis</i> -tach ligand.....	52
Figure 2.4: ORTEP diagram of [1]PF ₆	54
Figure 2.5: Type II and V X–H... π hydrogen-bonds defined by Malone.....	56
Figure 2.6: ORTEP diagram of [2].	58
Figure 2.7: ORTEP diagram of the hydrogen-bonded dimer of [2].....	60
Figure 2.8: ORTEP diagram of [3]BPh ₄	65

Figure 2.9:	$^{31}\text{P}\{^1\text{H}\}$ NMR spectrum of the reaction between [5] PF ₆ and dppm.....	73
Figure 2.10:	Proposed structure of the pendant-phosphane complex [8] PF ₆	74
Figure 3.1:	Anti-tumor ruthenium (II) DMSO complexes.....	79
Figure 3.2:	ORTEP diagram of [8] PF ₆	82
Figure 3.3:	Intermolecular hydrogen-bonds in the crystal packing of [8] PF ₆	84
Figure 3.4:	ORTEP diagram of [9]	85
Figure 3.5:	Intermolecular hydrogen-bonds in the crystal packing of [9]	87
Figure 3.6:	^1H NMR spectrum resulting from the aquation of [8] Cl.....	92
Figure 3.7:	Proposed structures of the aquation products of [8] Cl	93
Figure 3.8:	DynaFit plot of the aquation of [8] Cl.	95
Figure 3.9:	^1H NMR spectrum of the NH ₂ protons in [8b] ⁿ⁺	96
Figure 3.10:	Possible structures of guanosine adduct of [8] ⁺	100
Figure 4.1:	Polypyridyl Ru(II) complexes evaluated for antitumor activity.....	103
Figure 4.2:	Ru(II) η^6 -arene polypyridyl-based complexes	104
Figure 4.3:	ORTEP diagram of [10] (PF ₆) ₂	107
Figure 4.4:	ORTEP diagram of [11] (PF ₆) ₂ (MeOH).....	109
Figure 4.5:	Intermolecular hydrogen-bonds in [10] (PF ₆) ₂	110
Figure 4.6:	Intermolecular hydrogen-bonds in [11] (PF ₆) ₂ (MeOH).	111
Figure 4.7:	ORTEP diagram of [12] (Cl)(PF ₆).	113
Figure 4.8:	Some Intermolecular hydrogen-bonds in [12] (Cl)(PF ₆).....	114
Figure 4.9:	Hydrogen-bonds between the chains of cations in [12] (Cl)(PF ₆).	115
Figure 4.10:	Schematic diagram of the solid state structure of [12] (Cl)(PF ₆).	116
Figure 4.11:	Proximity of the DMSO to bipy in [10] (PF ₆) ₂	121
Figure 5.1:	Anti-tumor Ru(II) complexes with P–P ligands.....	130
Figure 5.2:	ORTEP diagram of [15] PF ₆	134
Figure 5.3:	Intermolecular hydrogen-bonds in [15] PF ₆	135
Figure 5.4:	ORTEP diagram of [16] PF ₆	136
Figure 5.5:	Diagram of the trigonal structures in [16] PF ₆	138
Figure 5.6:	ORTEP diagrams of [17–20] Cl.....	139
Figure 5.7:	^1H - ^1H NOESY NMR spectrum of [16] Cl.	142
Figure 5.8:	Dose-response curves in A549 and A2780	146
Figure 5.9:	Schematic representation of the diphosphane complexes	150
Figure 7.1:	$^{31}\text{P}\{^1\text{H}\}$ NMR spectra of [17] Cl with various Cl ⁻ concentrations.....	156
Figure 7.2:	^1H NMR spectra of [17] Cl with 0, 10 or 20 mM sodium phosphate...	158

Figure 6.3: Low concentration ^1H NMR spectra of [16]Cl in H_2O	160
Figure 6.4: Low concentration ^1H NMR spectra of [17]Cl in H_2O	160
Figure 6.5: ^1H NMR of [17]Cl in H_2O after 1 and 48 h at 37°C	161
Figure 6.6: Initial UV/Vis pH titration for [16a]^{x+} and [17a]^{x+}	164
Figure 6.7: ^1H NMR pH titration of [16a]^{x+} and [17a]^{x+}	166
Figure 6.8: Time-evolution UV/Vis difference spectra for the aquation [16]Cl . ..	168
Figure 6.9: Time-dependence of absorbance for the aquation of [16]Cl	168
Figure 6.10: Arrhenius and Eyring plots for the aquation and anation of [16]Cl ..	171
Figure 6.11: Time-dependence of absorbance for the aquation of [17]Cl	172
Figure 6.12: Plots of chlorido/aquated species vs. $[\text{Cl}^-]$ for [16]⁺ and [17]⁺	176
Figure 6.13: Structure of EtG and GMP	180
Figure 6.14: ^1H NMR spectra of [16]Cl and the reaction with EtG.....	181
Figure 6.15: ^1H NMR spectra of [16]Cl and the reactions with EtG and GMP.....	182
Figure 6.16: Possible structures of [16c]²⁺ , geometry optimised by DFT.	183
Figure 6.17: ^1H NMR spectra of [17]Cl and the reaction with EtG and GMP	185
Figure 6.18: GEMSA of [16]Cl and [17]Cl with pUC18 plasmid DNA.....	186
Figure 6.19: Structure of GSH.	189
Figure 6.20: $^{31}\text{P}\{^1\text{H}\}$ NMR spectra of reactions with GSH.....	190
Figure 7.1: <i>R,R</i> - and <i>S,S</i> -chiraphos.	195
Figure 9.1: <i>cis</i> -tach ^1H and $^{13}\text{C}\{^1\text{H}\}$ NMR assignments.....	200
Figure 9.2: PPh_3 and $\text{DMSO-}S$ ^1H and $^{13}\text{C}\{^1\text{H}\}$ NMR assignments.....	201
Figure 9.3: bipy and phen ^1H and $^{13}\text{C}\{^1\text{H}\}$ NMR assignments.....	201
Figure 9.4: Diphosphane ^1H and $^{13}\text{C}\{^1\text{H}\}$ NMR assignments.	201
Figure I.1: ORTEP diagram of [17]Cl(H₂O)_{2.15}.MeOH	229
Figure I.2: ORTEP diagram of [18]Cl(H₂O)₄	230
Figure I.3: ORTEP diagram of [19]Cl(H₂O)_{1.5}	231
Figure I.4: ORTEP diagram of [20]Cl(CH₃OH)₃	232
Figure II.1: ORTEP diagram of [18]PF₆	233

Table A: CIF files provided on CD with this thesis.	xiii
Table 1.1: <i>In vitro</i> activity of Ru and Os <i>N,N</i> -, <i>N,O</i> - and <i>O,O</i> - complexes.....	13
Table 1.2: Initial <i>in vitro</i> biological evaluation of RAPTA complexes.....	24
Table 1.3: <i>In vitro</i> evaluation of catalytic ruthenium and osmium complexes.....	33
Table 1.4: <i>In vitro</i> biological evaluation of ttcn complexes.....	39
Table 2.1: Comparison of bond lengths in [1] ⁺ and [2] with analogous complexes.	63
Table 2.2: Biological evaluation of [4]Cl in A549 and A2780.....	75
Table 3.1: Comparison of bond lengths in [8] ⁺ and analogous complexes.....	88
Table 3.2: Comparison of bond lengths in [9] and analogous complexes.	89
Table 3.3: Rate and equilibrium constants for the aquation of [8]Cl.....	95
Table 3.4: Ratios of species in the aquation of [8]Cl at various pH.....	98
Table 4.1: IR, ¹ H NMR and bond lengths of the DMSO ligand in [10–12] ²⁺	118
Table 4.2: Comparison of data for DMSO in <i>cis</i> -tach and other <i>fac</i> -complexes....	120
Table 5.1: Selected data for the complexes [15–20]Cl.....	132
Table 5.2: Selected bond angles and ³¹ P{ ¹ H} NMR chemical shifts for [15–20] ⁺	141
Table 5.3: Comparison of the Ru–Cl bond length in [Ru ^{II} Cl(L)(<i>fac</i> -ligand)] ⁿ⁺	144
Table 5.4: IC ₅₀ and slope values for [15–20]Cl in A549 and A2780.....	147
Table 6.1: NMR and MS data for [Ru(L)(P–P)(<i>cis</i> -tach)] ^{x+} , L = Cl or OH _x	157
Table 6.2: Rate and equilibrium constants for the aquation of [16]Cl.....	169
Table 6.3: <i>E</i> _a , Δ <i>H</i> [‡] and Δ <i>S</i> [‡] for the aquation and anation of [16] ⁺ and [16a] ²⁺	171
Table 6.4: Aquation data for various ruthenium anti-tumour complexes.....	177
Table 9.1: ESI-MS data for the aquation of [8]Cl.....	210
Table 9.2: ESI-MS data for the reaction of [8] ⁺ and Guo and Ado.....	211
Table 9.3: ESI-MS data for reaction of [11] ²⁺ with Guo.	214
Table 9.4: ESI-MS data for aquation of [16]Cl and [17]Cl in H ₂ O and D ₂ O.	222
Table 9.5: ESI-MS data for the reaction of [16]Cl with Guo.	227
Table II.1: Comparison of Ru–C bond lengths of RuCp in various complexes.	233

Scheme 1.1: The mechanism of action of cisplatin.....	4
Scheme 1.2: Redox switch of a cytotoxic ruthenium(II) complex.....	16
Scheme 1.3: Aquation and DNA binding of the RAen complexes.....	18
Scheme 1.4: Aquation and hydrolysis of RAPTA-C.....	25
Scheme 1.5: Synthesis of <i>cis</i> -tach.....	42
Scheme 1.6: Coordination of <i>cis</i> -tach based ligands to a metal.....	43
Scheme 1.7: Chelation of iron(II) by tachpyr.....	45
Scheme 2.1: Conformational change of <i>cis</i> -tach on coordination to ruthenium(II)..	52
Scheme 2.2: Reaction between <i>cis</i> -tach and [RuCl ₂ (PPh ₃) ₃].....	53
Scheme 2.3: Charge-neutralisation reaction of [1]Cl.....	57
Scheme 2.4: Convenient preparation of [2].....	61
Scheme 2.5: Synthesis of [4]Cl.....	69
Scheme 2.6: Preparation of ruthenium(II) complexes with chelating ligands from a triphenylphosphane/acetonitrile precursor.....	70
Scheme 2.7: Synthesis of [5]PF ₆	71
Scheme 2.8: Synthesis of [6](PF ₆) ₂	72
Scheme 3.1: Preparation of [RuCl(en)(ttn)]OTf.....	78
Scheme 3.2: Synthesis of [RuCl(DMSO-S) ₂ (<i>cis</i> -tach)]Cl, [8]Cl.....	81
Scheme 3.3: Scheme employed for kinetics analysis of aquation of [8]Cl.....	94
Scheme 3.4: Proposed mechanism for formation of [8b] ⁿ⁺ from [8]Cl.....	97
Scheme 4.1: Synthesis of [10](Cl) ₂ and [11](Cl) ₂	106
Scheme 4.2: Synthesis of [12](Cl) ₂	112
Scheme 4.3: Canonical forms of M-S(O)(CH ₃) ₂	117
Scheme 4.4: Preparation of [13]PF ₆	125
Scheme 4.5: Preparation of [14](Cl) ₂	126
Scheme 5.1: Reaction of [8]Cl with dppm to yield [15]Cl. * Isolated yield.....	131
Scheme 5.2: Synthesis and proposed structures of [15–20]Cl.....	132
Scheme 7.1: Aquation of [16]Cl and [17]Cl.....	155
Scheme II.1: Preparation of the ruthenocene analogue [18]PF ₆	234

Accompanying Material

Compact Disc with CIF files (Table A) from single-crystal X-ray diffraction experiments (with checkCIF) is attached at the back of this thesis.

Structure*	Code	File name
[RuCl(tach)(PPh ₃) ₂]PF ₆	[1]Cl	jml0928a.cif
[RuCl ₂ (tach)(PPh ₃)]PF ₆	[2]	jml0927m.cif
[{RuCl(PPh ₃)(<i>cis</i> -tach)} ₂ (μ-Cl)]BPh ₄	[3]BPh ₄	jml0930a.cif
[RuCl(DMSO- <i>S</i>) ₂ (<i>cis</i> -tach)]Cl	[8]PF ₆	jml1003a.cif
[RuCl ₂ (DMSO- <i>S</i>)(<i>cis</i> -tach)]	[9]	jml1004m.cif
[Ru(bipy)(DMSO- <i>S</i>)(<i>cis</i> -tach)](PF ₆) ₂	[10](PF ₆) ₂	phw1001a.cif
[Ru(DMSO- <i>S</i>)(phen)(<i>cis</i> -tach)](PF ₆) ₂	[11](PF ₆) ₂	jml1001m.cif
[Ru(DMSO- <i>S</i>)(en)(<i>cis</i> -tach)]Cl(PF ₆)	[12]Cl(PF ₆)	jml1006m.cif
[RuCl(dppm)(<i>cis</i> -tach)]PF ₆	[15]PF ₆	jml1007m.cif
[RuCl(dppe)(<i>cis</i> -tach)]PF ₆	[16]PF ₆	phw1012.cif
[RuCl(dppp)(<i>cis</i> -tach)]Cl	[17]Cl	jml1134.cif
[RuCl(dppb)(<i>cis</i> -tach)]Cl	[18]Cl	jml1147_twin1_hklf4.cif
[RuCl(dppv)(<i>cis</i> -tach)]Cl	[19]Cl	jml1149.cif
[RuCl(dppben)(<i>cis</i> -tach)]Cl	[20]Cl	jml1137.cif
[RuCp(<i>cis</i> -tach)]PF ₆	[21]PF ₆	jml0929a.cif

Table A: CIF files provided on CD with this thesis. *Solvent molecules omitted from structural formula.

Acknowledgements

This thesis would not have been possible for if it were not for so many people. First of all, I would like to thank my supervisors Paul Walton and Jason Lynam for providing me with the opportunity to undertake a PhD as well as all their support, encouragement, wisdom and guidance.

The members of the Walton and Lynam group have been invaluable to helping me through this, especially Christine, Emma and Luisa as well as Áine, David, Lee, Tony, Dave, Neets and Lizzie; also a thank you to those from other groups, especially Abeda, Maria, Sharifa, Richard, and Charlie. I've had some great memories from the past 4 years, usually involving the Derry and I'll never forget the night when I fell down the stairs at the willow...

A big thank you goes to Naser, for assisting with NMR experiments and his willingness to always help, and Adrian and Rob (as well as Jason) for their hours spent solving my X-ray crystal structures. My thanks also go to Heather, David, Mathias (NMR) and Derrick (the NMR guard-dog), Trevor and Karl (MS) and Phil and Graeme (CHN). A massive thank you goes to Helen Burrell, who taught us cell culture technique and was always happy to help when there were any problems, as well as Jared Cartwright for allowing us to use his cell culture facilities. Also, Sally, Karen, Karen and Maria provided much help over in YSBL. I wish to also thank Anna Peacock and Louise Male, for their helpful discussions and the EPSRC and the University of York for funding my studies.

I also want to thank my family; my Mom, and my sister, Katherine, for always being there for me, encouraging and supporting me no matter what and keeping me afloat when times got tough. Finally, Becca deserves a massive thank you; she has supported me through everything for the past three years, put up with me while I have been writing this thesis and for just making me happy always.

To Dad.

Declaration

The research presented in this thesis was carried out at the University of York between October 2008 and January 2012. This work is, to the best of my knowledge, original and my own, except where specifically stated otherwise.

Aimee J. Gamble

Chapter 1. Introduction

1.1 Preamble

Within the UK, over 320,000 new cases of cancer were diagnosed in 2009.¹ The previous year saw an estimated 12.7 million diagnoses worldwide and 7.6 million deaths attributed to this disease.¹ On average, one in three people within the UK will develop a form of cancer at some point in their life and it is the cause of one in four deaths.¹

Cancer is a term describing over 200 diseases,¹ all of which involve unregulated cell growth.² Cancers may also invade surrounding tissues or other locations around the body *via* the lymph or blood stream (metastasis).² Generally, a single genetic mutation during cell replication is insufficient to cause cancer; a series of independent mutations must occur—all within the lineage of a single cell—and these mutations must overcome natural selection and cell control mechanisms.² The accumulation of mutations over time accounts for an increased incidence of cancer with age, owing to the greater number of times the DNA has been replicated. Cancers are rarely diagnosed within the early stages of mutations, and are only detectable when they have reached advanced stages, such as invasive carcinomas.²

There are numerous characteristics of tumour cells, which are the basis for cancerous behaviour.^{3, 4} Tumour cells are often referred to as immortal, where cells will proliferate indefinitely with no growth control. Cancer cells evolve to elude apoptotic mechanisms, allowing them to survive conditions in which normal cells are expected to die. They do not require extra-cellular growth stimulation and often produce growth factors which act on their own receptors, promoting continuous proliferation. They also exhibit increased genetic instability, which may result in changes to the chromosome or multiple replications of growth-promoting genes.

As tumours grow, the distance of oxygen diffusion to cells from blood vessels increases, resulting in low oxygen levels (hypoxia).⁵ To allow growth beyond the limits of oxygen diffusion, tumours express vascular endothelial growth factors,

promoting capillary growth from near-by blood vessels (angiogenesis).⁵ Most normal cells do not grow once detached from a tissue, however tumour cells invade other tissues resulting in secondary metastases and this is considered the point of which a tumour becomes life-threatening.^{3,4}

Tumour cells often exhibit an uncontrolled cell cycle; the over-expression of cyclins that promote the progression of the cell cycle into the synthesis (DNA replication) or mitosis phase results in unregulated cell proliferation.^{3, 4} Additionally, a cell may develop malfunctions in the control and regulation of the cell cycle, where checkpoints are not correctly completed. For example, many tumours lack a functional DNA damage-induced p53-dependant checkpoint, allowing increased likelihood of accumulating genetic mutations.^{3,4}

Classical anti-tumour drugs target the p53-dependant checkpoint of the cell cycle.³ The drugs cause modifications to DNA, typically through alkylation, which is then recognised by the cell, triggering an apoptotic pathway. However, many tumours have a defective p53 gene, thus many tumours are resistant to classical therapies.^{3,6}

It is due to the inherent and acquired drug resistance of tumours to these drugs, as well as the adverse side-effects caused by the toxicity of therapies on other tissues, that there is a need for the continual development of new anti-tumour agents. This effort is focused on both classical agents, designed to induce apoptosis by DNA damage, and non-classical drugs, designed to target other aspects of cell replication or mechanisms vital to cell maintenance.⁷

1.2 Platinum-Based Cancer Therapy

1.2.1 Cisplatin

Cis-diamminedichloridoplatinum(II) (cisplatin, Fig. 1.1) has become one of the most widely used drugs in the treatment of cancers.⁸ Its therapeutic capability was discovered by Barnett Rosenberg in 1965, over a century after its initial discovery by Michel Peyrone in 1845. Generation of cisplatin at a platinum electrode inhibited the division of *E. coli* cells, demonstrating its ability to disrupt cell growth.^{9, 10}

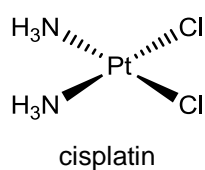


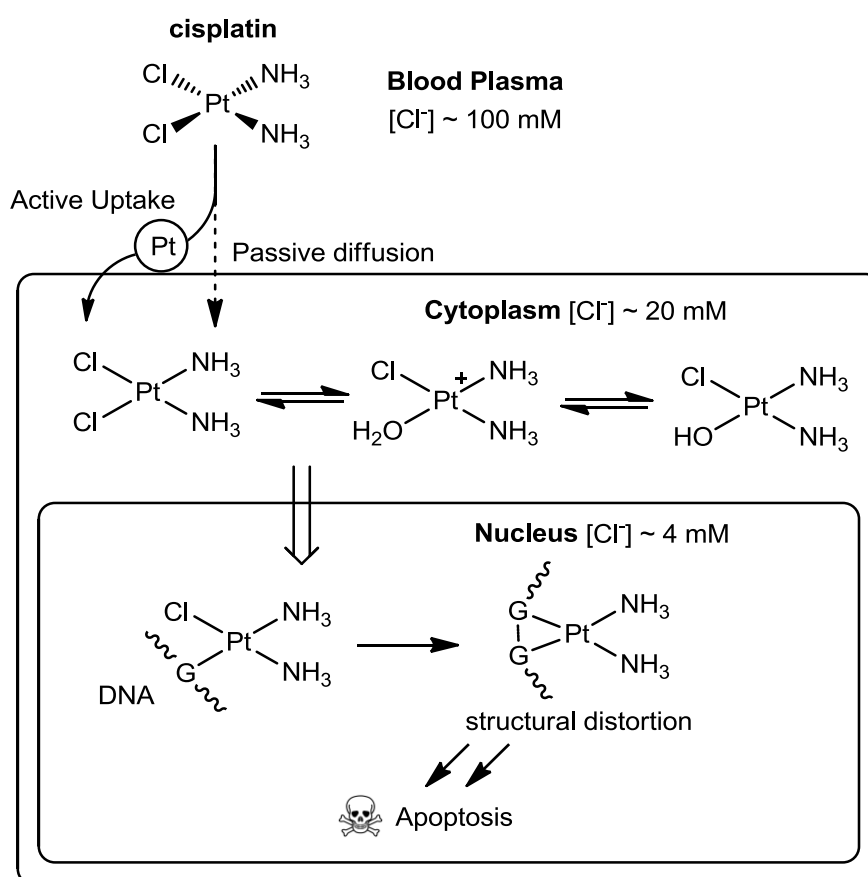
Figure 1.1: Structure of cisplatin, [*cis*-PtCl₂(NH₃)₂], the first metal complex to be approved for the treatment of cancers in the clinic.

After entering phase I trials in 1971,¹¹ cisplatin was approved for the treatment of testicular and ovarian cancers in 1978.¹² In the case of testicular cancer, the use of cisplatin resulted in the survival rate dramatically rising to *ca* 90%.¹² It is also used in the treatment of bladder, head and neck cancers, as well as the treatment of many other cancers in combination therapy with other drugs.⁸

1.2.2 Cisplatin: Mechanism of Action

After intravenous administration of cisplatin, it is transported around the body *via* the blood stream. This environment has a relatively high chloride concentration of 100 mM and substitution of the chlorido ligands with water (aquation) is largely suppressed.¹³ This reduces the likelihood of ligand-exchange reactions with biomolecules, although some do still occur, causing unwanted side-effects and drug deactivation.¹⁴

Cisplatin does bind to intercellular proteins through the sulfur donor atom of thiol groups, particularly with those containing cysteine residues such as human serum albumin.¹⁵ This does not necessarily result in deactivation and has been demonstrated to improve patient response to treatment.¹⁵ The leading hypothesis at present is that cisplatin may be transported into the cell by passive diffusion, and possibly also by organic and metal transporters such as copper transportation proteins (Scheme 1.1).¹⁶



Scheme 1.1: Chemical processes involved in the cisplatin-induced DNA damage, leading to eventual apoptosis. Resistance mechanisms may develop by the deactivation of the platinum complex *via* coordination of intracellular thiols or DNA repair.

Aquation of one or both chlorido ligands occurs under the lower intracellular chloride concentration (4–20 mM),¹³ followed by partial hydrolysis to give the unreactive hydroxy species (Scheme 1.1).¹⁷ Deactivation of cisplatin may occur

within the cell by *S*-coordination of glutathione (GSH), which is an intracellular thiol anti-oxidant; increased expression of GSH is often associated with cisplatin resistance.¹⁸ Only a small percentage of cisplatin manages to reach its target, the nucleus. An aqua ligand of the mono-aquated species $[cis\text{-PtCl}(\text{NH}_3)_2(\text{OH}_2)]^+$ is displaced by a DNA base, to give a mono-functional adduct (Scheme 1.1).¹⁹ Cisplatin preferentially binds to the N7 of guanine; formation of adducts with adenine are less favoured. This is followed by ring-closure of coordination of a second DNA base,²⁰ with intrastrand 1,2 d(GpG) cross-linking predominating (Fig. 1.2).^{21, 22}

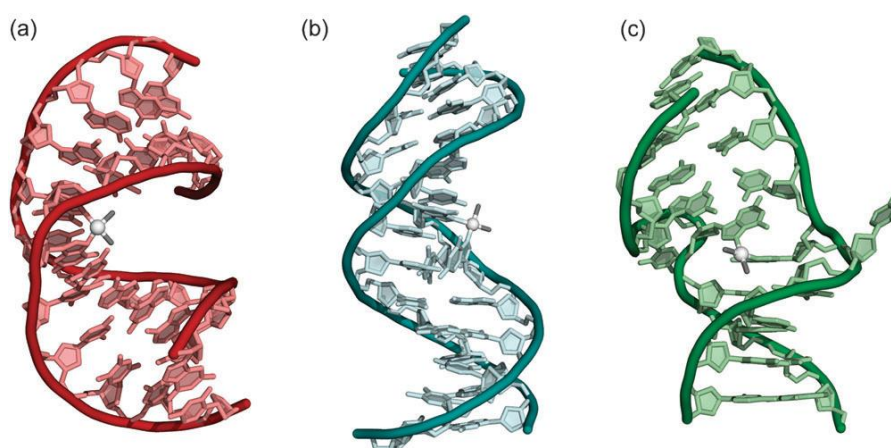


Figure 1.2: DNA structural distortions from a) intrastrand 1,2 d(GpG) (60–65 %), b) intrastrand 1,3 d(GpG) (2–3 %) and c) interstrand 1,2d(GpG) (1–5 %) platinumation. Intrastrand 1,2 d(GpA) (20–25 %) not shown. Diagram from reference 23.

The platinumation of DNA causes a bend towards the major groove of DNA (30–60°) and unwinding of the double helix (up to 23°) as shown in Fig. 1.2.²⁴ The structural distortion stalls RNA synthesis (transcription), from either the physical block of RNA polymerases, the binding of proteins, or disruption of the nucleosomal structure.²³ Following inhibition of transcription, DNA damage response is activated—which is induced by proteins such as p53 (a tumour suppressor protein)—inducing cell cycle arrest, and eventual apoptosis.²⁵

The *trans*- isomer of cisplatin, [*trans*-PtCl₂(NH₃)₂] (transplatin), is inactive in comparison to the clinical drug. This was initially rationalised due to its inability to form DNA cross-links in the same way as cisplatin.²⁶ However, platinum complexes with a *trans*-geometry, such as [*trans*-PtCl₂(pyridine)₂], have been reported with anti-cancer activity comparable to cisplatin.²⁷ These compounds are also capable causing DNA structural distortions.²⁷ It is hypothesised that the inactivity of transplatin is due to a greater kinetic instability, leading to increased deactivation of the drug.²⁶

Cisplatin has also been shown to interfere with RNA, blocking digestion and preventing reverse-transcription.²⁸ This was hypothesised to disrupt cell-wide RNA processing, accounting for cell-wide effects of cisplatin.²⁸ Furthermore, cisplatin can form DNA-protein cross-links which inhibit DNA polymerisation or DNA repair by the nucleotide excision repair system.²⁹

Despite the success of cisplatin, problems are experienced with its clinical use. Resistance may be acquired by one of several mechanisms, including reduced cellular drug uptake, DNA damage repair, detoxification by intracellular thiols or lack of response to damaged DNA.³⁰ Furthermore, treatment of cancers in the clinic with cisplatin is limited by side-effects, associated with kidney and nervous system toxicity, nausea and vomiting among others.³¹ This has prompted the development of platinum drugs displaying increased activity, reduced side effects or the ability to overcome resistance mechanisms.⁸

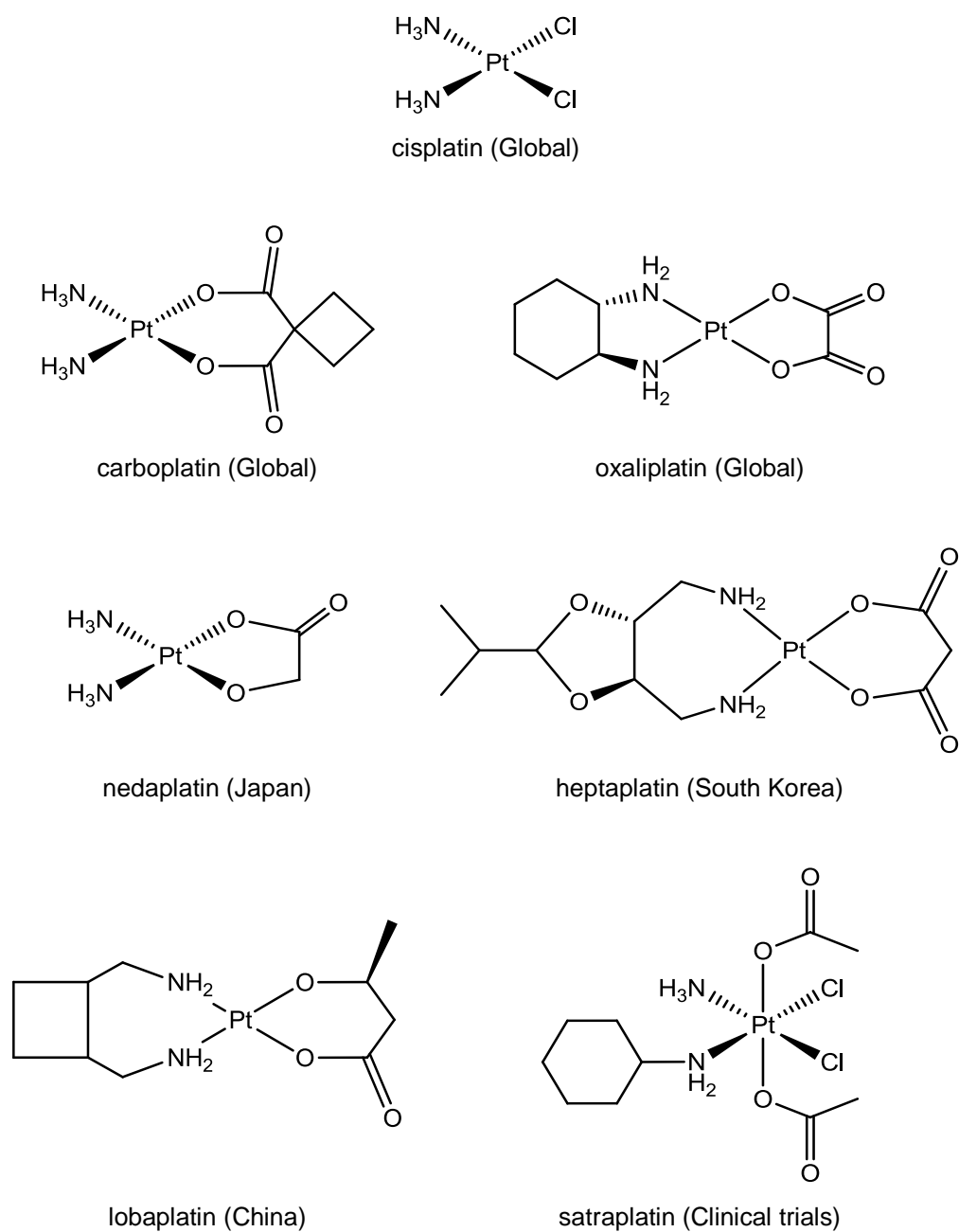


Figure 1.3: Platinum(II) complexes which have been approved for clinical use (region in parenthesis) and satraplatin, an orally-active platinum(IV) complex currently in clinical trials.

1.2.3 Second-Generation Platinum Drugs

Carboplatin, diammine(1,1-cyclobutanedicarboxylato-*O,O'*)platinum(II) (Fig. 1.3) was developed to reduce the side effects experienced with cisplatin. It is structurally similar, but a dicarboxylate replaces the *cis*-dichlorido ligands.³² The chelating leaving group provides the complex with a reduced rate of aquation, and therefore a decreased general toxicity.³³ This has allowed the administration of a higher dose in comparison to cisplatin with diminished side effects.⁸ Since global approval in 1989, the use of carboplatin in the treatment of ovarian cancer has surpassed that of cisplatin.⁸ However, as carboplatin forms identical DNA adducts to cisplatin, it is unable to overcome the majority of resistance mechanisms.³⁴

Some cisplatin cross-resistance was first overcome by (1*R*,2*R*-diaminocyclohexane)oxalatoplatinum(II) (oxaliplatin, Fig. 1.3), which was approved globally in 2005 for the treatment of colorectal cancer.^{19,35} Oxaliplatin is a member of the same family as cisplatin and carboplatin but is distinguished by its chelating diamine ligand. The bio-transformations of oxaliplatin are similar to cisplatin and carboplatin,³⁶ with a similarly high affinity for guanine.³⁵ The bulky cyclohexane ring of the chelating diamine prevents binding of DNA repair proteins, reducing (but not entirely eliminating) cross-resistance.³⁷ The importance of chirality was also assessed, with the *R,R*- more effective than the *S,S*- isomer.³⁷

1.2.4 The Ongoing Development of Metallo drugs

A further three complexes have each been approved for clinical use in the market of a single nation (Fig. 1.3).⁸ Many platinum(II) and platinum(IV) complexes have since entered clinical trials including satraplatin, an orally active Pt(IV) complex (Fig. 1.3).³⁸ Increasingly, the focus of research is directed towards the use of other transition metals for the treatment of cancers.³⁹ This is in an effort to overcome the difficulties of the platinum-based compounds such as the inherent toxicity to all tissues (including healthy cells), undesired side-effects and the development of cross-resistance.^{8, 40} Employment of different metals may also allow the development of anti-tumour agents with alternative modes of action and reactivity with biomolecules.

1.3 Ruthenium Complexes as Anti-cancer Agents

In a continuing drive to find alternatives to platinum-based anti-tumour drugs, non-platinum transition metals have since been widely studied with titanium, gallium and ruthenium compounds reaching clinical trials.^{41, 42} Ruthenium complexes have gathered much interest, as highlighted by several reviews.^{41, 43-47} The ligand exchange kinetics of ruthenium are similar to those observed with platinum in aqueous solution, with timescales comparable to cellular processes.⁴⁸ Although in many cases ruthenium complexes have a similar affinity to DNA, they do show differences to platinum compounds.⁴⁰ Much excitement surrounding ruthenium has originated from the hypothesis that ruthenium complexes could be transported into tumour cells by transferrin,⁴⁹ due the protein having a similar affinity with some ruthenium complexes as to iron,⁵⁰ but also the lower general toxicity compared to platinum. Both of these properties have been observed in specific cases, but have since been largely discounted for ruthenium compounds in general.⁵¹ Despite this, ruthenium is still regarded as the most promising alternative to platinum-based cancer therapy.

1.3.1 Ruthenium Ammine Complexes

The first ruthenium compounds to be realised for their potential as anti-cancer agents were discovered in 1976 by Durig and co-workers. They observed that the ruthenium(III) complex [*fac*-Ru(NH₃)₃Cl₃] inhibited the growth of *E. coli* cells at similar concentrations to those of cisplatin.⁵² Later, Clarke and co-workers evaluated the cytotoxic properties of a Ru(II) analogue, [*cis*-Ru(NH₃)₄Cl₂], which also exhibited anti-cancer properties.⁵³ While these complexes were active, poor water solubility prevented further investigation into their use as pharmaceuticals.⁵⁴

1.3.2 NAMI-A and KP1019: Ruthenium Complexes in Clinical Trials

At present, the only two ruthenium-based compounds to have successfully entered phase I clinical trials are the ruthenium(III) complexes NAMI-A and KP1019 (Fig. 1.4).⁵⁵ Although structurally similar, the two complexes display different behaviour *in vivo*.

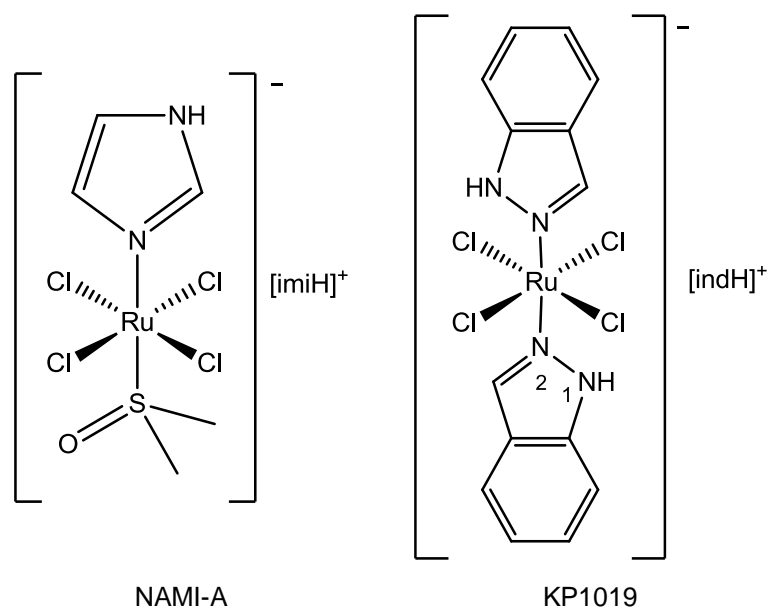


Figure 1.4: NAMI-A and KP1019, two ruthenium(III) complexes in clinical trials for use in cancer treatment. The numbering scheme used for the nitrogen atoms in indazole is given for KP1019.

$(\text{imiH})[\text{trans-RuCl}_4(\text{S-DMSO})(\text{N-im})]$ (NAMI-A, Fig. 1.4) initially failed *in vitro* screening for anti-cancer activity, but was shown to inhibit the development and growth of metastasis tumours *in vivo*, particularly in the lungs.⁵⁶ This is a useful property given the relative success of Pt(II) complexes in the treatment of primary tumours. NAMI-A has been shown to inhibit metastasis invasion by impeding the adhesion of cells to substrates,⁵⁷ as well as controlling angiogenesis (development of blood vessels) by the inhibition of endothelial cell functions.⁵⁸ The biological activity of NAMI-A first arises from a two-step aquation and a reduction process to ruthenium(II),⁵⁹ although the latter has yet to be observed *in vivo*.⁵⁹ Apoptosis is caused by the blocking of mitogen-activated protein kinase/extracellular signal-

regulated kinase signalling pathways and activation of caspase-3.^{60, 61} More recently, the Os(III) analogue of NAMI-A, (imiH)[*trans*-OsCl₄(S-DMSO)(N-imi)] was reported with reasonable antiproliferative activity *in vitro* with IC₅₀ of 103 μM (concentration of drug required to inhibit 50% of cell growth) in the HT-29 colon carcinoma cell line (NAMI-A IC₅₀ = 340 μM). The osmium complexes were also shown to be kinetically stable in aqueous solution compared to the ruthenium variant.⁶² NAMI-A has successfully completed phase I trials,⁶³ and is currently undergoing phase II studies.

(indH)[*trans*-RuCl₄(N2-ind)₂] (KP1019, Fig. 1.4) was discovered by its effect on the growth of chemically induced tumours in mice and reported in 1989 by Keppler.⁶⁴ The imidazole analogue (*c.f.* NAMI-A) (imiH)[*trans*-RuCl₄(N-imi)₂] was reported two years earlier by the same group.⁶⁵ In contrast to NAMI-A, KP1019 is cytotoxic and displays both *in vitro* and *in vivo* activity against colorectal tumours cells.^{66, 67} The *in vitro* activity of KP1019 is an order of magnitude greater than that of NAMI-A, with an IC₅₀ of 20 μM vs. 340 μM in the HT-29 colon carcinoma cell line.⁶⁶

KP1019 has been demonstrated to form Ru(III) adducts with proteins such as transferrin, assisting with the transportation of the complex into cancer cells.⁶⁸ It has been suggested that reduction of the ruthenium(III) centre to ruthenium(II) occurs *in vivo*,⁴⁹ although this is yet to be confirmed.⁵¹ The target of KP1019 is thought to be the DNA bases, forming strong mono-functional adducts with guanine and adenine,⁶⁹ at the N7 position.⁷⁰ KP1019 was shown to form bi-functional adducts with DNA, but to a lesser extent than cisplatin,⁷¹ and with a smaller degree of structural distortion.⁷¹ The DNA damage and oxidative stress caused by KP1019 is thought to result in apoptosis by the intrinsic mitochondrial pathway.⁷² Recently, KP1019 successfully completed phase I clinical trials, with a phase II study planned.⁷³ Although an osmium(III) analogue of KP1019 has not yet been reported, Os(IV) compounds following a similar structural motif, including [*trans*-OsCl₄(N1-ind)₂], have been shown to have promising cytotoxic properties.⁷⁴

1.3.3 The “Activation by Reduction” Theory: Ruthenium(II)

An important step in the activation of ruthenium(III) complexes is proposed as the *in vivo* reduction to ruthenium(II), where reduction occurs in the highly reducing and often hypoxic conditions found in tumours.^{53, 75} This was hypothesised by Clarke in the “activation by reduction” theory as Ru(II) coordinates biomolecules rapidly in comparison to Ru(III).⁵⁴ This has resulted in increased efforts in the study of ruthenium(II) complexes to aid in the design of new anti-cancer compounds.

In the past decade, a new class of ruthenium(II) compounds featuring the η^6 -arene ligand (Fig. 1.5) have proved promising for use as anti-cancer agents. It is proposed that in these complexes the desired +2 oxidation state at the metal centre is stabilised by the arene ligand, providing air and water stable compounds.^{76, 77} The ruthenium(II) η^6 -arene moiety forms a piano-stool type structure, with three *fac*-coordination sites available for fine-tuning by various ligands to obtain the desired properties.

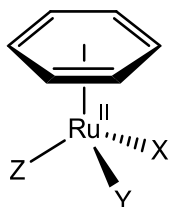


Figure 1.5: Piano-stool structure of ruthenium(II) η^6 -arene complexes.

The cytotoxic potential of ruthenium(II) η^6 -arene complexes was first realised when the anti-cancer activity of an existing agent, metronidazole, was enhanced by coordination to a $[\text{RuCl}_2(\eta^6\text{-C}_6\text{H}_6)]$ fragment.⁷⁶ Since, anti-tumour ruthenium(II) η^6 -arene compounds were simultaneously developed by Sadler and Dyson in 2001,^{78, 79} and since have been the subject of many studies.

	M	η^6 -arene	L	X	refs	IC ₅₀ (μ M)	
						A549	A2780
	Ru	benzene	en	Cl	⁷⁸		20
	Ru	<i>p</i> -cymene	en	Cl	^{78, 80}		10
RM175	Ru	biphenyl	en	Cl	^{81, 82}	3.0	5
	Ru	biphenyl	en	I	⁸³		5
	Ru	biphenyl	en	N ₃	⁸³		4
	Ru	dha	en	Cl	⁸⁰		2
HC11	Ru	tha	en	Cl	^{80, 81}	0.5	0.4
	Ru	indan	bipy	Cl	⁸²		>100
	Ru	indan	phen	Cl	⁸²		55
	Ru	<i>p</i> -cymene	tmeda	Cl	⁸²		>100
	Ru	<i>p</i> -cymene	dab	Cl	⁸²		11
	Ru	biphenyl	dab	Cl	⁸²		5
	Ru	tha	dab	Cl	⁸²		23
	Ru	<i>p</i> -cymene	gly	Cl	⁸²		>100
	Ru	<i>p</i> -cymene	pico	Cl	⁸⁴		42.5
	Ru	benzene	acac-Me ₂	Cl	⁸²		>50
	Ru	<i>p</i> -cymene	acac-Me ₂	Cl	⁸²		19
	Ru	dha	acac-Me ₂	Cl	⁸²		70
	Ru	<i>p</i> -cymene	acac- ^t Bu ₂	Cl	⁸²		14
	Ru	<i>p</i> -cymene	Acac-Ph ₂	Cl	⁸²		11
	Os	bip	en	Cl	⁸⁵	10	7.6
	Os	tha	en	Cl	⁸⁵	6.4	9.4
	Os	bip	pico	Cl	⁸⁶	8	4.2
		cisplatin			^{80, 81}	2.6	0.6
		carboplatin			⁸⁰		6

Table 1.1: *In vitro* activity of ruthenium and osmium *N,N*-, *N,O*- and *O,O*-complexes, following the general formula of $[M^{II}(X)(\eta^6\text{-arene})(L)]^{n+}$. IC₅₀ values are given for the A549 and A2780 cell lines. Lower values indicate a greater cytotoxic activity.

1.4 Classical Ruthenium(II) η^6 -Arene Complexes

1.4.1 1,2-Ethylenediamine Complexes

Since their initial discovery in 2001, Sadler and co-workers have studied complexes following the general formula $[\text{RuX}(\eta^6\text{-arene})(\text{L})]^{n+}$, where X is a leaving group and L is an *N,N*-, *N,O*- or *O,O*- chelating ligand.⁷⁸ A summary of these complexes and *in vitro* activity by growth-inhibition assays, the IC_{50} value, is given in Table 1.1. The IC_{50} is defined as the concentration required to inhibit cell growth by 50 %.

The lead complex (RM175, Fig. 1.6) from the initial report by Sadler and co-workers consists of η^6 -biphenyl as the η^6 -arene, 1,2-ethylenediamine (en) as the chelating ligand (L) and chlorido as the leaving group (X). Complexes of this type with the en ligand are abbreviated to RAen. RM175 was found to be equipotent to carboplatin in A2780 human ovarian cancer cells.⁷⁸ Reduction in the size of the arene to *para*-cymene and η^6 -benzene resulted in reduced activity. It was later reported that use of highly extended aromatics, such as 1,4,9,10-tetrahydroanthracene (tha) in the complex HC11 (Fig. 1.6) resulted in greater activities than the smaller arene ligands.⁸⁰ The lead compound, HC11 is equipotent to cisplatin in the A2780 ovarian cancer cell line.⁸⁰ These complexes are cytotoxic; they exhibit both *in vitro* and *in vivo* activity against primary tumour cells, similar to KP1019.

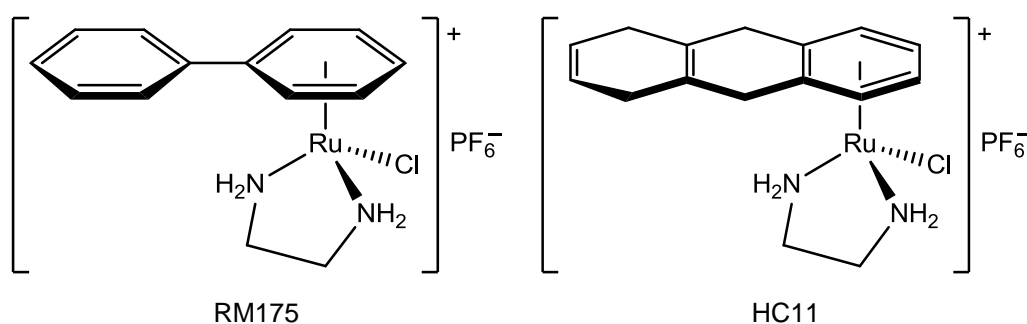


Figure 1.6: Structures of RM175 and HC11, two leading ruthenium(II) η^6 -arene anti-tumour complexes developed by Sadler.

The cross-resistance profiles of these complexes were assessed with the cisplatin-resistant cell line, A2780cis and multi-drug/adriamycin resistant cell line, A2780^{AD}. These cell lines display acquired resistance to clinical drugs. For example, A2780cis, which is obtained from the repeated exposure of the A2780 cell line to cisplatin, has increased DNA-repair and glutathione expression.^{87, 88} The resistance factor (RF) is defined as the ratio of IC₅₀ values obtained in the resistant and sensitive cell lines; a value of one denotes identical activity in both cell lines, with lower values indicating improved activity in the drug-resistant cell line. For example, the RF for cisplatin is 10 and 8 for the A2780cis and A2780^{AD} cell lines respectively. RM175 and HC11 both retained activity in A2780cis (RF 0.5–1), but activity was lost in the multi-drug resistant cell line (RF >15).⁸⁰ Therefore, it was hypothesised that the RAen complexes have a different mechanism of action compared to cisplatin.

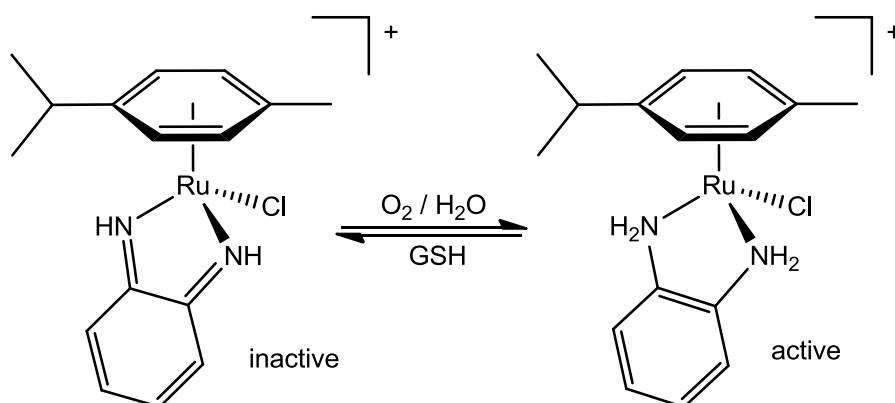
1.4.2 Structure-Activity Relationships

Structure-Activity relationships (Table 1.1) further demonstrated the importance of the identity of the arene ligand; the greatest activity is observed with extended hydrophobic systems.⁸² This increased hydrophobicity was hypothesised to provide the complex with a greater ability to passively diffuse through cell membranes, and to form stronger interactions with DNA *via* intercalation.⁸⁹ Studies of the *ortho*-, *meta*- and *para*-terphenyl ligands (terpy) in [RuCl(terpy)(en)]⁺ have also supported the hypothesis that extended hydrophobic systems enhance cytotoxicity by increased intercalation of this group with DNA. The *para*-terpy complex displayed high activity with IC₅₀ of 4 μM in A2780 (cisplatin 2.8 μM) and was an order of magnitude more potent than the *ortho*- and *meta*- isomers.⁸⁹

Modification of the leaving group to iodo and azido failed to alter the *in vitro* activity of the en complexes. This was attributed to these ligands undergoing exchange with chloride, resulting from the high intercellular chloride concentrations.⁸³

Variation of the en ligand by modification of the alkyl backbone also resulted in little effect on the *in vitro* cytotoxicity.⁸² However, removal of hydrogen-bonding donors by employment of *N,N,N',N'*-tetramethylethylene-1,2-diamine (tmeda) and 2,2'-bipyridyl (bipy) derivatives, resulted in inactive compounds.⁸² This supports the hypothesis that en assists in the stabilisation of the DNA-Ru adduct by formation of hydrogen-bonds with the DNA bases.⁹⁰ Since these studies, polypyridyl complexes have been shown to be capable of photo-activated DNA binding,⁹¹ with promising *in vitro* activity.⁹²

Introduction of 1,2-diaminobenzene (dab, Scheme 1.2) as the chelating ligand resulted in little change in activity to the parent en complexes in the A2780 cell line. However, the resistance factor (RF) for the multi-drug resistant variant A2780^{AD} was significantly improved to 0.8–2 from >45. Optimum activity was achieved when dab was accompanied by smaller extended arenes, suggesting a limit of lipophilicity for optimum cytotoxicity.⁸² The ruthenium dab complexes were shown to undergo oxidation to *ortho*-benzoquinonediimine.⁹³ The resulting imine complexes are biologically less active, allowing a potential switch mechanism, where the complex is activated by the reduction of the imine ligand to dab by the intracellular antioxidant glutathione, or from the greater reducing environment of tumour cells (Scheme 1.2).⁹³



Scheme 1.2: Reduction/Oxidation of the *ortho*-benzoquinonediimine/1,2-diaminobenzene chelating ligand (L) in the complex $[\text{RuCl}(\eta^6\text{-}p\text{-cym})(\text{L})]$, which is capable of acting as a switch mechanism.

Antiproliferative activity was retained on use of *O,O*-chelating diketones (Fig. 1.7) in comparison to *en*, with activity loosely correlating with lipophilicity of the diketone.⁸² In contrast to the *en* complexes, the activity dependence upon the size of the arene is no longer applicable; the η^6 -benzene complex, and those with an extended arene, such as 9,10-dihydroanthracene (dha), were found to be less active than the *p*-cymene and biphenyl complexes.⁸² These complexes rapidly aquate and it was hypothesised that bulkier arene ligands, such as *p*-cymene and biphenyl, protect the chelating ligand from displacement and deactivation.⁹⁴ Coordination of the β -diketone curcumin, a natural product, gave active compounds which display moderate activity *in vitro* with IC₅₀ of 23 μ M in the A2780 cell line (vs. cisplatin 1.3 μ M).⁹⁵

Use of mixed *N,O*-chelating ligands, such as natural amino acids, in Sadler's structure-activity relationship studies failed to provide active candidates.⁸² However, some moderately active compounds have since been reported, such as [RuCl(η^6 -*p*-cym)(pico)] (pico = picolinate) by McGowan and co-workers (Fig. 1.7).⁸⁴

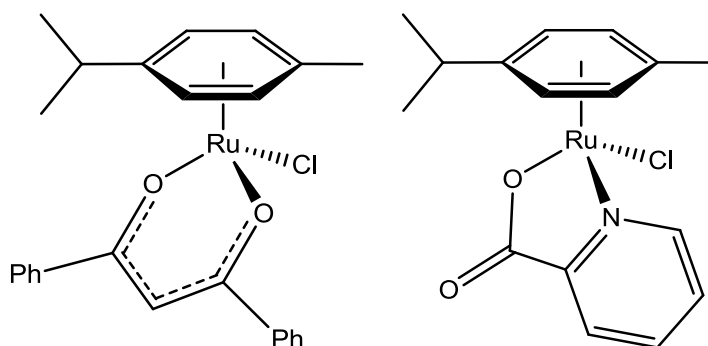
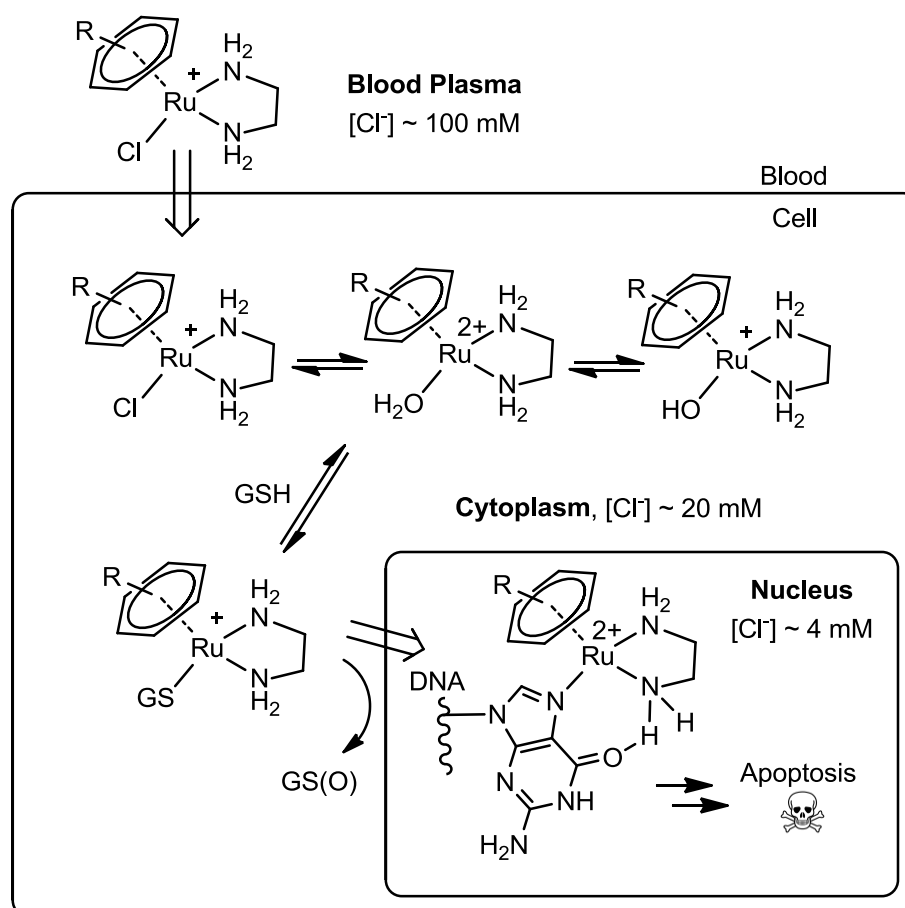


Figure 1.7: Structures of cytotoxic ruthenium(II) η^6 -arene complexes [RuCl(η^6 -*p*-cym)(acac)] (left) and [RuCl(η^6 -*p*-cym)(pico)] (right) with *O,O*- and *N,O*-chelating ligands.

1.4.3 Mechanism of Action

Studies with the ruthenium RAen complexes RM175 and HC11 revealed that the reaction of these species with nucleobases proceeds *via* the corresponding aqua-adduct $[\text{Ru}(\text{OH}_2)(\eta^6\text{-arene})(\text{en})]^{2+}$ (Scheme 1.3).⁹⁶ Further investigations demonstrated that aquation is rapid, with first-order rates which are greater than twenty times that of cisplatin.⁹⁷ The pK_{a} s of the resulting complexes were determined as 7.71 and 8.01 respectively, so therefore hydrolysis is expected to be largely suppressed at physiological pH with the more reactive aqua adduct dominating.⁹⁷



Scheme 1.3: Proposed aquation and DNA binding of the RAen complexes, causing a break of an adjacent base pairing and eventual apoptosis. Delivery of the complex to DNA is hypothesised to be *via* coordination of glutathione.

It is predicted that at therapeutic-relevant concentrations of the RAen complexes, the chlorido species dominates in the relatively high chloride concentrations of blood plasma (>89%). However, upon transportation into the cell where chloride concentrations are lower, 45–65% of the bulk will exist as the aqua adduct with 9–25% as the hydroxy complex.⁹⁷ Exposure of analogous complexes with other halides to physiological chloride concentrations results in the formation of the chlorido complex, thus rendering the alternative leaving groups redundant, and therefore producing no effect on cytotoxicity when used *in vivo*.⁸³

Similar to cisplatin, DNA is hypothesised as the eventual target for the RAen complexes, but only a single covalent bond is formed between the ruthenium centre and purine base by displacement of the aqua ligand (Scheme 1.3).^{90, 96, 98} There is strong preference for binding to the N7 of guanine, verified by interactions of RM175 with an oligonucleotide and analysis by negative ion ESI-MS.⁷⁸ DNA ruthenation is similar to the platination by cisplatin and correlates to cytotoxic potency with the RAen complexes binding DNA stronger than cisplatin.^{51, 99} The DNA base selectivity of RAen complexes is in the order of guanine(N7) > thymine(N3) > cytosine(N3) > adenine(N7) > adenine(N1) as determined by reactions with the mononucleosides.⁹⁶ The guanine adduct was the thermodynamically favoured product in competitive reactions.⁹⁶ With modification of the chelating ligand from en to the anionic acetylacetonate (acac), the rate and extent of hydrolysis are not only increased,⁸² but the affinity for adenine was found to be greater than guanine.⁹⁶ This was thought to be due to specific hydrogen-bond recognition of the complex by the bases.

The structural features which assist in the binding of RAen complexes to DNA *via* guanine were demonstrated in the crystal structures of the 9-ethyl guanine adduct of HC11 (Fig. 1.8).⁹⁰ The selectivity towards the N7 of guanine is enhanced by hydrogen-bond formation between the en NH protons and the O6 of guanine and the hydrophobic interactions of the extended arenes with the DNA core by intercalation,^{100, 101} resulting in the unwinding of DNA by at least 14°.¹⁰²

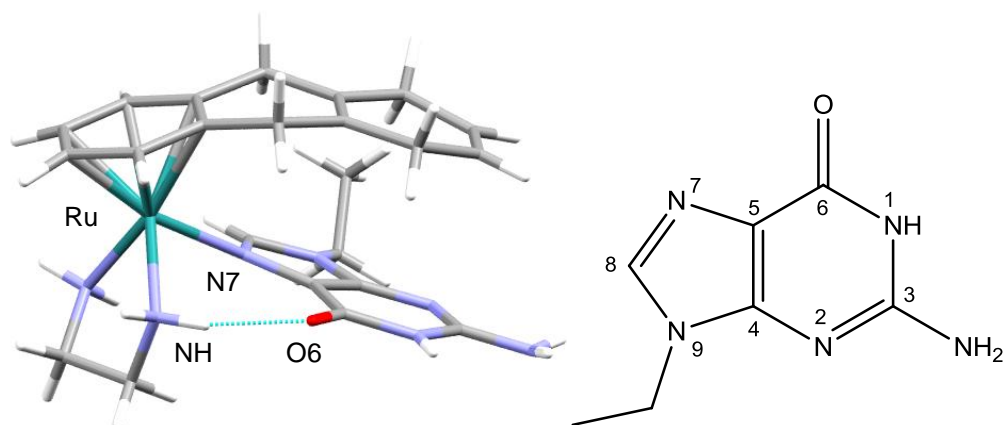


Figure 1.8: Left: X-ray crystal structure of $[\text{Ru}(\text{en})(\text{EtG})(\eta^6\text{-tha})]^{2+}$, showing the hydrogen-bond between the en NH and the O6 of guanine, and the arene-nucleobase stacking.⁹⁰ Right: Structure and numbering scheme of 9-Ethylguanine (EtG)

Ab initio studies based on $[\text{RuCl}(\eta^6\text{-}p\text{-cymene})(\text{en})]^+$ additionally suggested that binding of this complex to duplex DNA results in a break in an adjacent Watson-crick base pair.¹⁰³ The mechanisms of aquation and Ru-DNA adduct formation have also been investigated using computational methods.^{104, 105} It is hypothesised that this structural distortion is recognised by the cell and it has been shown that RM175 causes cell-cycle arrest and apoptosis by a p53 (tumour suppressor protein) and Bax (apoptosis-inducing protein) dependant mechanism.¹⁰⁶

Although the Ru-G adduct is resistant to hydrolysis, at the elevated temperatures for annealing DNA the ruthenium moiety is capable of migrating to other G residues in DNA suggesting that the complex may be easily removed from damaged DNA.⁹⁹ Therefore, DNA may not be the ultimate target of the RAen complexes. This is in contrast to cisplatin where stable, strong adducts are formed and suggests an additional contribution to the differing mechanism of these two compounds.²⁴ Ruthenium migration occurs *via* a $\text{S}_{\text{N}}1$ pathway, with complex dissociation assisted by the solvent and followed by coordination of a nearby guanine-N7.

The en complexes exhibit high selectivity for DNA bases over other biomolecules, including cytochrome c and L-histidine.¹⁰⁷ Furthermore, competitive reactions with

glutathione showed that in addition to the Ru-guanine adduct being thermodynamically favoured, the abundant intracellular reducing agent may be involved in the ruthenation of DNA by delivering the complex to the nucleus, thereby protecting it.¹⁰⁸ In contrast, glutathione is capable of the detoxification of cisplatin, and up-regulation is associated with cisplatin resistance.^{18, 109}

In addition to DNA, a potential target for the RAen complexes was identified as protein tyrosine phosphatase 1B, a key target for the treatment of breast and ovarian cancers. The *para*-cymene complex $[\text{RuCl}(\eta^6\text{-}p\text{-cym})(\text{en})]^+$ inhibits the enzyme with an IC_{50} of 19 μM .¹¹⁰ Preferential binding of the ruthenium complex was demonstrated with employment of the model compound 2-mercaptobenzanilide, even in the presence of excess glutathione.¹¹⁰ This study also demonstrated the ability for the en ligand to be labilised at low pH by thiol coordination.

1.4.4 Osmium Analogues

The importance of the metal used in these compounds was investigated by Sadler with the preparation of osmium analogues of RM175 and its related compounds. The ethylenediamine complex $[\text{OsCl}(\eta^6\text{-bip})(\text{en})]\text{PF}_6$ (Fig. 1.9) was initially found to be inactive and this was thought to be due to the slow aquation and domination of the inactive hydroxy species $[\text{Os}(\text{OH})(\eta^6\text{-bip})(\text{en})]^+$ with $\text{p}K_a$ 6.3.⁹⁴ Modification of the chelating ligand to *O,O*- donors in $[\text{OsCl}(\eta^6\text{-}p\text{-cym})(\text{L})]$ L = acac or maltolato, provided complexes which readily aquate with a biologically accessible $\text{p}K_a$ of 7.6. These complexes rapidly form adducts with guanine and adenosine bases, but in both cases formation of the dimer $[\{\text{Os}(\eta^6\text{-}p\text{-cym})\}(\text{OH})_3\{\text{Os}(\eta^6\text{-}p\text{-cym})\}]^+$ resulted in an inactive species.^{94, 111}

To overcome these difficulties, *N,O*- donor ligands were employed to combine the stability of the complexes containing en with the more ideal aquation reactivity of the acac ligand. The complex $[\text{OsCl}(\eta^6\text{-bip})(\text{pico})]$ (Fig. 1.9) readily aquates without dimer formation, giving a highly active complex *in vitro* with an IC_{50} of 4.2 μM (equipotent to carboplatin) for the A2780 cell line.⁸⁶ This line of compounds have since been optimised by variation of substituent groups on the pyridyl ring.¹¹² The

arene ligand is also thought to be important in the activity of these compounds, with a similar hydrophobicity trend as the ruthenium complexes.¹¹³

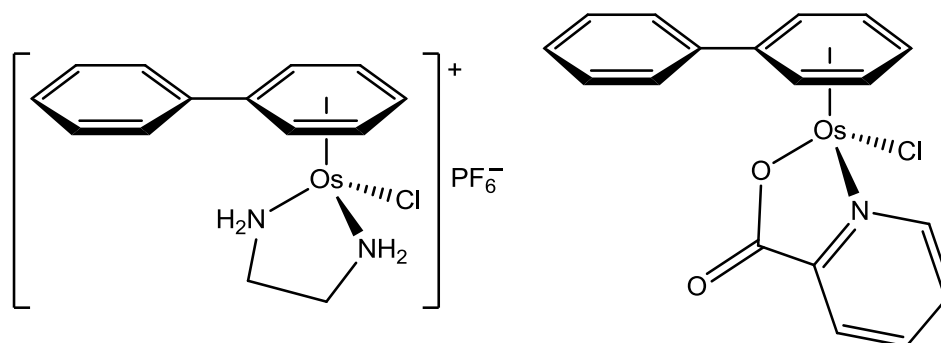


Figure 1.9: Structures of cytotoxic osmium(II) η^6 -arene complexes $[\text{OsCl}(\eta^6\text{-bip})(\text{en})]\text{PF}_6$, an analogue of RM175 (left) and $[\text{OsCl}(\eta^6\text{-bip})(\text{pico})]$, designed to balance the reactivity of *N,N*- and *O,O*-chelating ligands (right)

Re-evaluation of $[\text{OsCl}(\eta^6\text{-bip})(\text{en})]\text{PF}_6$ showed that the decomposition of the complex in DMSO prior to its use in growth inhibition assays accounted for its apparent inactivity.⁸⁵ Use of freshly prepared solutions of $[\text{OsCl}(\eta^6\text{-arene})(\text{en})]\text{BF}_4$ (arene = bip or tha) were found to be highly active *in vitro* with IC_{50} of 7.6 μM in A2780, equipotent to RM175 and carboplatin.⁸⁵ The osmium en complexes have an affinity for guanine and adenine bases, similar to their ruthenium analogues,⁸⁵ and have been demonstrated to bind to DNA as a potential biological target.¹¹⁴ Although highly active, the osmium en complexes are two orders of magnitude less reactive than the ruthenium variants.⁸⁵ This may reduce the occurrence of side effects in clinical use, in a similar manner to the reduced reactivity of carboplatin compared to cisplatin.

1.4.5 Conclusions

The RAen family of compounds are capable of high activities when a suitably hydrophobic arene ligand (e.g. tha) is employed. The *in vitro* activities of these complexes are comparable to carboplatin and cisplatin. Although they are hypothesised to inhibit tumour growth by a classical mechanism, they have been demonstrated to overcome some platinum cross-resistance. Although highly

promising, there are also efforts to develop ruthenium(II) η^6 -arene complexes which employ non-classical mechanisms.

1.5 Non-Classical RAPTA Complexes

1.5.1 Initial Discovery

Ruthenium (II) arene complexes containing *P*-1,3,5-triaza-7-phosphatricyclo-[3.3.1.1]decanephosphine (PTA), termed ‘RAPTA’, were initially reported in 2001. The *para*-cymene derivative, $\text{RuCl}_2(p\text{-cym})(\text{PTA})$ ‘RAPTA-C’ (Fig. 1.10) exhibited pH dependent DNA damage, with the greatest damage occurring at the pH proposed to occur within cancer cells ($\text{pH} < 7$).^{79, 115} Molecular dynamics simulations showed that RAPTC-C induces a localised kink in duplex DNA by forming intrastrand cross-links between guanine bases.¹⁰³

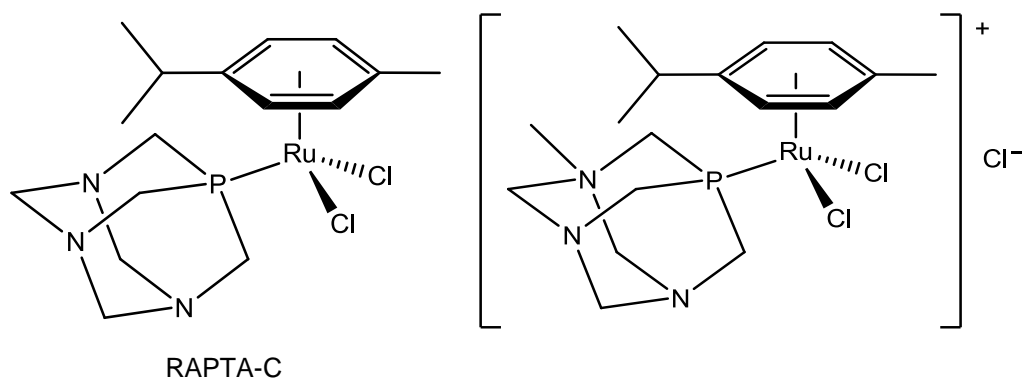


Figure 1.10: Structures of the anti-metastatic agent RAPTA-C (left) and the *N*-Me modified complex (right), in which selectivity for tumour cells is lost.

The *In vitro* biological activity of several RAPTA compounds was investigated with the TS/A mouse adenocarcinoma cancer and HBL-100 human mammary (non-tumour) cell lines (Table 1.2). These studies revealed that RAPTA complexes are moderately active against the cancer cell line, but inactive in the non-tumour cells (up to $300 \mu\text{M}$).¹¹⁶

It was proposed that potential binding of RAPTA complexes to biomolecular targets at pH values typical of hypoxic cells involved *N*-protonation of the PTA ligand,

potentially forming a secondary hydrogen-bond interaction. To explore this hypothesis, an *N*-methylated analogue of the PTA ligand was prepared. This modification resulted in the increased cytotoxicity to both tumour and healthy cell lines, but with the loss of selectivity to the cancer cells (Table 1.2).¹¹⁶

	η^6 -arene	L	IC ₅₀ / μ M	
			TS/A	HBL-100
RAPTA-B	benzene	PTA	231	> 300
RAPTA-T	toluene	PTA	74	> 300
RAPTA-C	<i>p</i> -cym	PTA	> 300	> 300
	<i>p</i> -cym	MePTA ⁺	> 300	246
RAPTA-H	C ₆ Me ₆	PTA	199	> 300

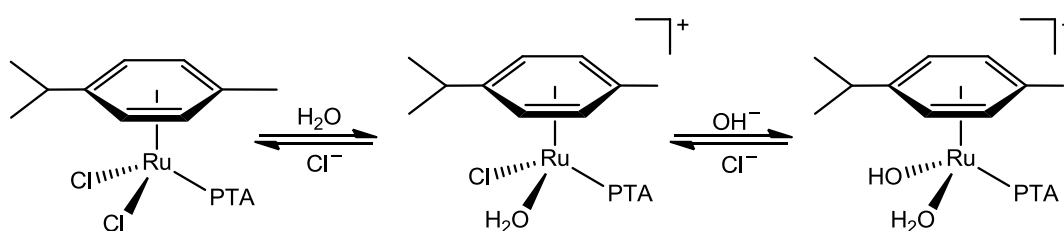
Table 1.2: Initial *in vitro* biological evaluation of RAPTA complexes with TS/A (adenocarcinoma) and healthy HBL-100 cells following the formula [Ru^{II}Cl₂(η^6 -arene)(L)]ⁿ⁺.

Due to having similar behaviour *in vitro* to NAMI-A, both RAPTA-C and RAPTA-B were selected for *in vivo* evaluation on CBA sub-strain of mice bearing the MCa mammary carcinoma.¹¹⁶ Like the *in vitro* studies, reduction of primary tumour growth was not observed, but activity was seen against secondary lung metastases, indicating that like NAMI-A, RAPTA-C acts as an anti-metastatic agent.¹¹⁶

Given the similarities with NAMI-A, the RAPTA series were considered to be a viable contender for further studies. In addition to a high selectivity against secondary metastasis tumours, RAPTA compounds were also discovered to possess anti-angiogenic (anti-blood vessel development) properties.¹¹⁷ Although the RAPTA complexes are not as cytotoxic as those with the en ligand, they exhibited a significant enough selectivity for tumours over healthy cells, providing a distinct therapeutic advantage.

1.5.2 Mechanism of Action

Studies on the aquation and hydrolysis of RAPTA-C (Scheme 1.4) highlighted the important steps needed for the activation of these complexes in biological systems. Under physiologically relevant conditions, the major product was found to be the mono-aqua adduct, $[\text{RuCl}(p\text{-cymene})(\text{OH}_2)(\text{PTA})]^+$, along with a smaller amount of $[\text{Ru}(\text{OH})(p\text{-cymene})(\text{OH}_2)(\text{PTA})]^+$.¹¹⁸ Aquation of this complex is two orders of magnitude faster than cisplatin, and approximately three times faster than the RAen complexes described earlier.



Scheme 1.4: Aquation and hydrolysis reactions of RAPTA-C which are accessible under physiologically-relevant conditions. It is proposed these reactions occur when the complex enters the cell, where the chloride concentration is lower than in the blood.

In order to optimise the pK_a of the aqua ligand to match the pH of tumour cells, Computational studies (Density Functional Theory) suggested incorporation of fluorinated analogues of the arene ligands such as $\eta^6\text{-C}_6\text{H}_5\text{CF}_3$ into the complexes.¹¹⁹ This resulted in an improvement of *in vitro* activity by ten-fold in the A2780 cell line (IC_{50} 38 μM vs. 353 μM for the *p*-cymene analogue). This is hypothesised to be the result of suppression of hydrolysis of the aqua ligand selectively in the lower pH environment of tumour cells.¹¹⁹

In contrast to cisplatin and the RAen complexes, the RAPTA family of complexes are not believed to reduce tumour growth through coordination to DNA, since no correlation between DNA interactions and activity was observed.^{116, 120} Therefore investigations were directed towards the interaction of RAPTA compounds with proteins. Recent work has found that even in the nucleosomal core, where the DNA

concentration is at its highest, RAPTA-C preferentially forms stable adducts with chromatin at specific histone protein sites in favour of ruthenium-DNA interactions.¹²¹

RAPTA-T was found to inhibit steps associated with metastasis *in vitro* such as detachment and re-adhesion of tumour cells.¹²² Therefore, RAPTA-T was evaluated for its ability to bind or inhibit potential target enzymes in these processes. RAPTA-T was found to be a potent inhibitor of cathepsin B, a protease commonly over expressed in tumours, and it also showed limited inhibition of thioredoxin reductase, an enzyme essential for cell growth.¹²³ Molecular docking studies have suggested that RAPTA complexes may bind to an important cysteine residue within the active site of cathepsin B (Fig. 1.11).¹²³

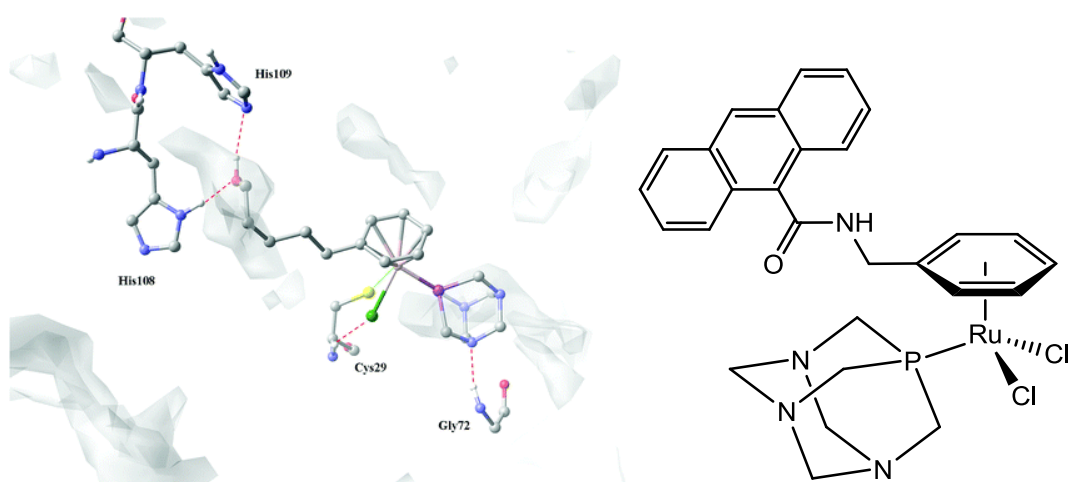


Figure 1.11: Left: Docking geometry of $[\text{RuCl}_2(\eta^6\text{-C}_6\text{H}_5(\text{CH}_2)_5\text{OH})(\text{PTA})]$ with the active site of the enzyme cathepsin B. A cysteine thiol is coordinated to the ruthenium complex and the arene participates in hydrogen bonds with histidine residues. Diagram taken from ref.¹²³ Structure of fluorescent anthracene tagged RAPTA complex used to investigate accumulation of the complex within cells by emission studies (right).

The eventual target for RAPTA-C and RAPTA-T remains unknown and efforts to identify its biological targets are ongoing. The distribution of RAPTA complexes in the cell was investigated by tethering the RAPTA moiety to anthracene to act as a fluorescent label for the complex (Fig. 1.11).¹²⁴ The fluorophore-labelled complexes showed similar cellular uptake and *in vitro* cytotoxicity to RAPTA-C and RAPTA-T. Although the cellular distribution of the anthracene-tagged complex may not reflect those of the whole RAPTA family, fluorescence emission studies revealed that the complex does not accumulate in the cell nucleus; this evidence was proposed to support the hypothesis that RAPTA complexes do not target DNA.¹²⁴ Further studies are focusing on the possible conjugation of functionalised RAPTA complexes to biomolecular targets, but at present, only results which demonstrate the proof-of-concept are so far reported.¹²⁵

Cysteine-rich intracellular compounds, such as glutathione (GSH), are known to be involved in the detoxification of cisplatin and the increased expression of GSH is often associated with cisplatin resistance.¹⁸ GSH was also demonstrated to cleave RAPTA-C from the model protein ubiquitin, resulting in detoxification of the complex.¹²⁶ Furthermore, the protein metallothionein-2, which is also responsible for resistance to metallo-drugs by the displacement of zinc, was shown to abstract RAPTA-C from ubiquitin, with a greater ability compared to cisplatin.¹²⁷

Eventual apoptosis induced by RAPTA-C, in *Ehrlich ascites* carcinoma cells was found to occur by the triggering of the mitochondrial apoptotic pathway causing increased levels of p53 (tumour suppressor protein).¹²⁸ In addition, with increased expression of p21 (regulator of cell cycle suppression) levels and reduced cyclin E levels (required for progression of cell cycle from G₁ to S) were also observed.¹²⁸

1.5.3 Structural Modifications

A series of structural modifications to the RAPTA complexes have been made not only to improve their activity, but to suggest at possible mechanisms of action. The osmium analogue of RAPTA-C, $[\text{OsCl}_2(\eta^6\text{-}p\text{-cymene})(\text{PTA})]$ has been studied but to a lesser extent. It was found to exhibit similar DNA binding and *in vitro* activity profiles to the ruthenium analogue.^{120, 129} No clear conclusions were formed on the influence of the metal on *in vivo* activity.

1.5.3.1 Phosphane and Arene Modification

The η^6 -arene ligand was modified to include hydrogen-bonding substituents in an effort to increase anti-tumour activity, by enhancing complex-DNA interactions. This either reduced or failed to affect the anti-tumour activity of the complexes.¹³⁰ However, an improvement of *in vitro* cytotoxicity against primary tumours was achieved by the inclusion of these hydrogen-bonding capable arenes and a triphenylphosphane ligand (Fig. 1.12). Although this resulted in improved cellular uptake of the complex and increased the affinity of the complex for DNA, the complex was no longer of selectivity for cancer cells over healthy cells.¹³¹ In contrast to the improved DNA binding, poorer selectivity for the proteins ubiquitin (directs protein recycling) and cytochrome c (involved in electron transport) was observed with the complexes containing the triphenylphosphane ligand.¹³¹ This supports the hypothesis that the biological effects of the RAPTA complexes are due to interactions with proteins rather than DNA. Replacement of the triphenylphosphane ligand with PPh_2R , where R incorporates an extended perfluorinated alkyl chain, results in highly cytotoxic compounds ($\text{IC}_{50} = 1\text{--}11 \mu\text{M}$ at 37°C), with thermo-responsive properties; a small activity increase ($\Delta\text{IC}_{50} = 0.3\text{--}2 \mu\text{M}$) was found at elevated temperatures (42°C).¹³²

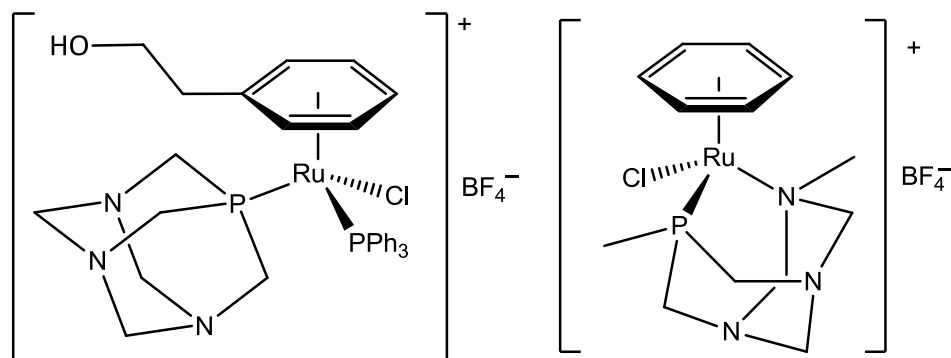


Figure 1.12: Left: Modification of the RAPTA complexes to include a hydrogen bonding substituent on the arene ligand, designed to improve uptake and DNA binding. Right: Structure of $[\text{RuCl}(\eta^6\text{-benzene})(\text{PTN})]\text{BF}_4$, where a modification of the RAPTA structure has been made to include the ruthenium centre in the adamantane structure of the PTA ligand.

A structural variation of the PTA moiety, 3,7-dimethyl-7-phospha-1,3,5-triazabicyclo[3.3.1]nonane (PTN) was introduced to evaluate the effect of a P–N chelate without altering the acid-base properties and solubility of the complexes (Fig. 1.12). Although the ability for the complex to bind DNA was reduced in comparison to the PTA analogues, the complex retained anti-tumour activity and affinity for the protein ubiquitin, therefore suggesting that the primary targets of the RAPTA compounds are likely to be proteins rather than DNA.¹³³

Further modifications of the phosphane ligand were possible by employing a phosphite-carbohydrate ligand (Fig. 1.13).¹³⁴ In aqueous solution, the initial aquation and hydrolysis of the Ru–Cl bonds occurs followed by the hydrolysis of the phosphite P–O bonds. Both of these processes were found to be suppressed with high chloride concentrations.¹³⁴ The reported complexes were selective towards a range of tumour cells in comparison to healthy cells, including the cisplatin-resistant A2780cisR cell line.¹³⁴

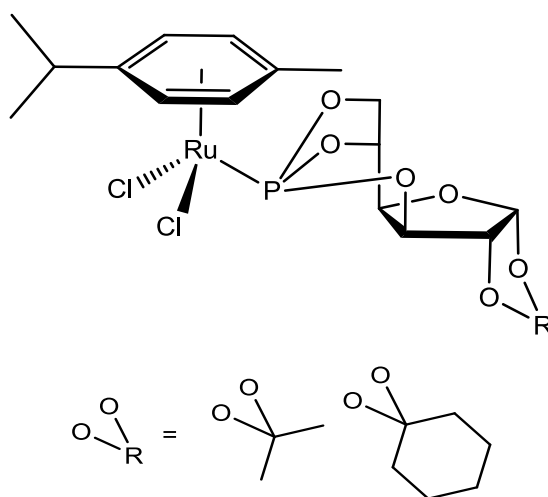


Figure 1.13: Structure of ruthenium(II) η^6 -arene complexes with a phosphite-carbohydrate ligand to provide increased structural variation over PTA *via* the R group, which were evaluated for activity against tumour cells.

1.5.3.2 Aquation-Resistant Complexes

In an effort to improve activity of the RAPTA compounds, the *cis*-chlorido ligands were replaced with chelating *O,O*-donor ligands, in a similar manner to the development of the second generation platinum drugs. These complexes were designed to suppress the aquation of the RAPTA complexes. The structural modification was achieved with both a dicarboxylate and oxalate group, giving carboplatin and oxaliplatin analogues, named carbo-RAPTA and oxali-RAPTA respectively (Fig. 1.14).¹³⁵ However, this failed to enhance the antiproliferative activity of the complexes in comparison to the *cis*-chlorido analogues. Interactions of the three RAPTA complexes were observed with the proteins cytochrome c and lysozyme, with preferential binding to surface histidines.¹³⁶

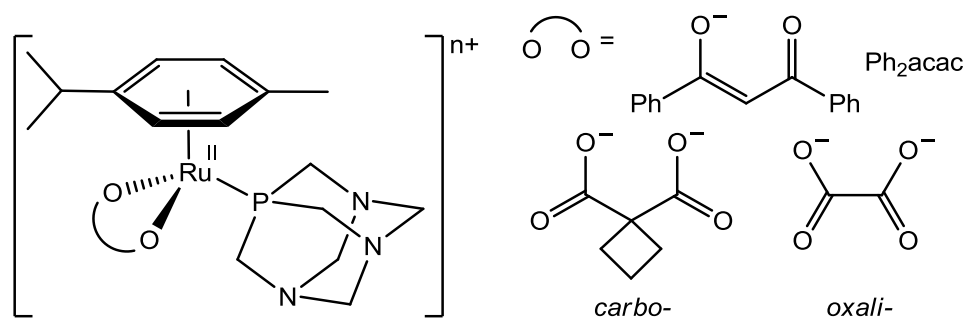


Figure 1.14: RAPTA-C analogues of the second generation platinum drugs, carboplatin and oxaliplatin, and the Ph₂acac based complex, a highly active complex designed to resist aquation.

Following the ruthenium(II) η^6 -arene 1,3-diketonato complexes developed by Sadler which are as cytotoxic as their en analogues, Dyson and co-workers prepared a series of PTA-acac complexes (Fig. 1.14), designed to resist aquation.¹³⁷ Unlike the parent RAPTA complexes, the acac derivatives were found to be cytotoxic *in vitro*. As expected, the complexes of ligands with lipophilic groups exhibited the greatest antiproliferative abilities, with IC₅₀ values of 50 and 14 μ M reported for [Ru(Ph₂acac)(*p*-cym)(PTA)]⁺ in the A549 and A2780 cell lines respectively.¹³⁷ Although initially over-looked, the successful employment of the acac ligand as a leaving group in ruthenium anti-tumour complexes lead to the development of highly cytotoxic Pt(II) acac complexes including [Pt(Ph₂acac)(NH₃)₂]⁺NO₃⁻.¹³⁸

1.5.3.3 Targeted Therapy

The GST inhibitor ethacrynic acid was incorporated into the η^6 -arene ligand in the RAPTA motif (Fig. 1.15) to direct the complex to target glutathione S-transferases (GST). These enzymes are responsible for removing xenobiotics from a cell; therefore inhibition of these enzymes results in an accumulation of potentially toxic compounds. GSTs, especially GSTP1-1, are frequently over-expressed in solid tumours.¹³⁹

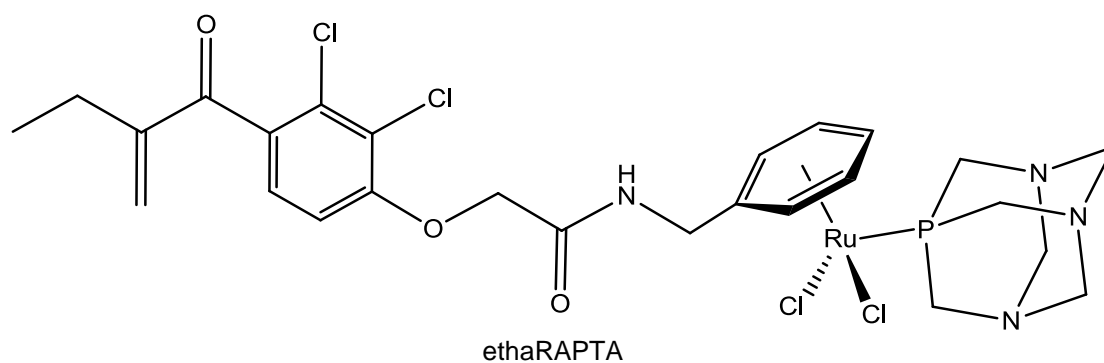


Figure 1.15: Structure of the RAPTA moiety functionalised with ethacrynic acid through an amide linker, designed to inhibit GST enzymes, which are responsible for removing xenobiotics from the cell.

Ethacrynic acid is incorporated by an amide linker in ethaRAPTA (Fig. 1.15). The ethacrynic moiety is able to bind to the active site in addition to the ruthenium centre binding to its cysteine target.¹³⁹ The affinity of this ruthenium complex for GST P1-1 was greater than ethacrynic acid alone.¹³⁹ A two-wave apoptosis is induced by ethaRAPTA, proposed to be the result of initial binding to GSTP1-1 through the ethacrynic acid group, followed by the release of the metal fragment from drug processing.¹⁴⁰ Ethacrynic acid was also employed as a ligand in the cisplatin Pt(IV) analogue [*cis,trans,cis*-PtCl₂(Ea)₂(NH₃)₂] (Ea = ethacrynic acid). It is proposed that intracellular reduction of this complex to Pt(II) results in generation of cisplatin and ethacrynic acid, targeting both the inhibition of GSTs and cisplatin-induced DNA damage.¹⁴¹

1.5.4 Conclusions

Although many details about the mechanism by which RAPTA compounds inhibit tumour growth remains unknown, they are highly promising with activity selectively against metastases. Compounds of this type are potentially powerful in the treatment of cancers, as the point at which a tumour becomes life threatening is considered to be at which the primary tumour metastasises. The cross-resistance of the RAPTA complexes with cisplatin remains largely unknown. Aside from these complexes, many other non-classical complexes have been investigated; some are discussed in the next section.

1.6 Other Non-Classical Ruthenium(II) η^6 -Arene Compounds

1.6.1 Catalytic Anti-cancer agents

The mechanism by which a metal complex inhibits cell proliferation is not limited to the coordination of biomolecules or the disruption of an existing biological pathway. A promising family of compounds are the ruthenium(II) η^6 -arene iodo-phenylazopyridine complexes, reported by Sadler and co-workers (Table 1.3).¹⁴²

				IC ₅₀ (μM)	
M	η^6 -arene	R	X	A549	A2780
Ru	<i>p</i> -cymene	NMe ₂	Cl	> 100	> 100
Ru	<i>p</i> -cymene	NMe ₂	I	3	4
Os	<i>p</i> -cymene	NMe ₂	Cl	5.23	1.8
Os	<i>p</i> -cymene	NMe ₂	I	0.38	0.14
Ru	biphenyl	NMe ₂	Cl	49	44
Ru	biphenyl	NMe ₂	I	2	3
^b		NMe ₂		14	> 100
Ru	biphenyl	H	I	> 100	> 100
^b		H		> 100	> 100
cisplatin ^a				4.10	1.8

Table 1.3: Structure and *in vitro* biological evaluation of catalytic ruthenium and osmium complexes as anti-tumour agents. The iodo complexes are inert to substitution with water and have been shown to catalyse the oxidation of glutathione. *a*) only reported with Os complexes, *b*) free ligand.

These phenylazopyridine complexes, with a hydroxy or dimethylamino substituent, were found to be highly active in the growth inhibition of both A2780 and A549 cell lines.¹⁴² The iodo complexes are inert to aquation, whereas the chlorido analogues readily aquate and are significantly less active.¹⁴³

The antiproliferative activity of these complexes is hypothesised to involve reduction of the azopyridine ligand by intracellular reducing agents, such as glutathione. Reduction of the free ligand is biologically inaccessible but its coordination to the metal allows for this process to occur. It is proposed that these complexes catalyse the oxidation of glutathione (GSH) to glutathione disulfide (GSSG), leading to an accumulation of reactive oxygen species, and eventual cell death.¹⁴²

Osmium analogues of these complexes have also been studied, with activity measured to be over an order of magnitude greater than that of the ruthenium compounds or cisplatin.¹⁴⁴ Again, the iodo complexes which were inert to aquation were found to display the greatest activity, with aquation-capable chlorido complexes significantly less active.¹⁴⁴ However, unlike the Ru(II) complexes, they have not been shown to catalyse the oxidation of GSH, but it is still hypothesised that they catalyse the generation of other reactive oxygen species within the cell.¹⁴⁵

1.6.2 Complexes Designed to Inhibit Enzymes

A series of half-sandwich η^5 -C₅H₅ ruthenium(II) carbonyl complexes, which are inert to substitution, have been developed to mimic the natural product staurosporin.¹⁴⁶ Both staurosporin and the ruthenium mimics selectively inhibit protein kinases, which are responsible for the transfer of phosphate to various substrates and is vital for many cellular functions, including signalling pathways.¹⁴⁷ Development of these ruthenium complexes allowed for a larger variety of structural modifications to be screened for inhibition activity.¹⁴⁷

The complex DW1/2, a racemic mixture of two isomers (Fig. 1.16) was found to have a high affinity for the kinase GSK3 β and Pim-1 enzymes.^{148, 149} These complexes were found to successfully inhibit the activity of GSK3 β and PI3K leading to p53 mediated apoptosis.¹⁵⁰ These complexes are highly active in inhibiting the growth of

1205 Lu melanoma cells, with IC_{50} values below $1 \mu\text{M}$.¹⁵¹ The dependence on the geometry of the complex was demonstrated by the observation of identical dose-response curves for both ruthenium and osmium analogues.¹⁵¹ These complexes do not involve reactivity of the metal centre in their mode of action.

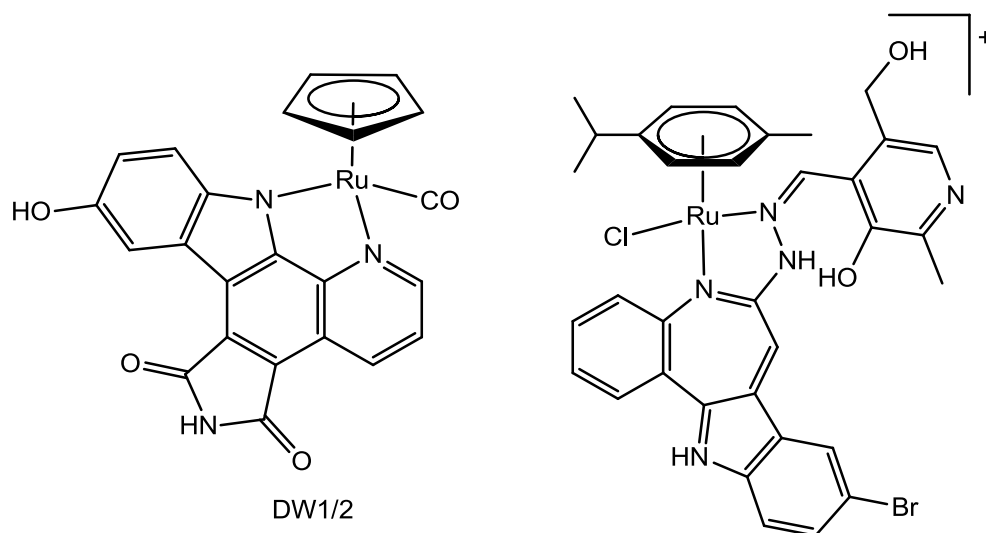


Figure 1.16: Left: DW1/2, a half-sandwich ruthenium(II) complexes that selectively inhibits protein kinases. Right: Ruthenium(II) η^6 -arene complex with a paullone derived ligand which inhibits cyclin-dependant kinases.

Highly cytotoxic ruthenium(II) η^6 -arene complexes with ligands based on the biologically active paullones (Fig. 1.16) were also demonstrated to inhibit enzymes, with IC_{50} values as low as $0.5 \mu\text{M}$.¹⁵² The paullone ligand occupies the active site of cyclin-dependant kinases, which control progression of the cell cycle.¹⁵³ However, as with DW1/2 it is hypothesised that the antiproliferative activity of the complex results from ligand-protein interactions with the metal acting as a scaffold.¹⁵²

Other kinase inhibitor ligands based on indirubin have recently been incorporated into ruthenium(II) η^6 -arene complexes with excellent *in vitro* cytotoxic activity with IC_{50} values as low as $0.3 \mu\text{M}$.¹⁵⁴ Although these complexes were demonstrated to aquate, it was hypothesised that coordination of biomolecules by the displacement of the aqua ligand did not account for activity, with the inert osmium analogues most active. Again, it was proposed that activity originates from the inhibition of kinases by the ligand, with the metal an innocent in the mechanism.

1.7 Ruthenium η^6 -Arene Complexes: Conclusions

The number of reported ruthenium(II) η^6 -arene anti-cancer compounds, although a relatively young area, is vast.^{76, 155, 156} Many more types of ruthenium(II) complexes have been studied;^{7, 42, 46, 55, 157} some of these are discussed later in this thesis. Numerous ruthenium(II) η^6 -arene complexes have been identified which are highly effective in the inhibition of tumour cell growth. However, to potentially replace platinum based chemotherapeutics in the clinic, one or more of several problems with these drugs must be overcome.

A significant problem experienced with Pt(II) compounds for the treatment of tumours is acquired resistance.^{158, 159} Therefore, new complexes which exploit other pathways of inhibiting growth are desirable, thereby avoiding these resistance mechanisms. The RAen complexes developed have been demonstrated to retain activity in cisplatin-resistant cells with some even overcoming multi-drug resistance.^{80, 82} These complexes are among the most cytotoxic of the ruthenium(II) compounds reported, but they selectively bind to the N7 of guanine in DNA like cisplatin.⁹⁶ Resistance is possibly overcome by differing reactivity with intracellular thiols (which detoxify cisplatin),¹⁰⁸ and through causing different structural distortions of DNA.^{90, 98} Although the cross-resistance of RAen complexes and cisplatin is yet to be observed, some DNA repair mechanisms developed by tumour cells may affect the activity of these ruthenium compounds.

The most promising complexes for overcoming both the inherent and acquired resistance of Pt(II) complexes are those with non-classical mechanisms.⁷ It is these types of compounds which have the greatest potential for use in the clinic. Relatively little is known about the mechanism of action for the most promising candidates, NAMI-A and RAPTA-C, compared to the classical compounds. However, these non-classical compounds are not necessarily unaffected by cross-resistance with cisplatin.¹²⁷ For example, It has been demonstrated that GSH, which detoxifies cisplatin, can displace RAPTA-C from proteins, which are hypothesised as a potential target for these complexes.¹²⁶

An unpleasant aspect of platinum based therapy are its associated side-effects, such as the renal toxicity.^{8, 160} The reduction of these side effects may be achieved by increasing the selectivity of drugs for cancer cells over healthy tissue.¹⁶⁰ Such selectivity has already been demonstrated by the RAPTA family of complexes which, *in vivo* only inhibit the growth of secondary metastases.¹¹⁶ However, their lack of activity against primary tumours is likely to allow for their use alongside other agents, such as platinum drugs.

Although biologically active ligands have been incorporated into ruthenium complexes in an attempt to direct the complex to bind proteins or to improve the potency of the ligand, their activity is dominated by the pre-existing inhibitor and often does not exploit the chemistry available at the ruthenium centre, such as the previously discussed staurosporine mimics developed by Meggers.¹⁴⁶

Several highly potent ruthenium(II) complexes have been identified with *in vitro* cytotoxicities marginally surpassing that of cisplatin.^{80, 82, 142} However, it is often common practice to incorporate hydrophobic groups into complexes to achieve higher activity, hypothesised to be a result of increased cellular uptake of the drug by passive diffusion.^{82, 131} However, this modification also reduces the complex's water solubility, hindering any potential clinical application. There is therefore a fine balance that needs to be achieved in order to maximise both the compounds activity and bio-availability.

While ruthenium(II) η^6 -arene complexes are a promising and prospective class of compounds, there remain several challenges to overcome before they—or other piano-stool type complexes—can be seriously considered for clinical application. Ideally, a compound should begin to overcome several of the issues described here by having properties such as high potency, good water solubility, an alternative mode-of-action to cisplatin (therefore overcoming resistance mechanisms) and some selectivity for cancer cells. It is hypothesised that one possible way to achieve this may be by employing of a new *facial*-coordinating ligand.

1.8 Is the η^6 -Arene Ligand Vital for Anti-cancer Activity?

This thesis is focused on the use of an alternative neutral six-electron donor *fac*-coordinating ligand for the design of highly cytotoxic metal complexes, based on the proven piano-stool structural motif of the ruthenium(II) η^6 -arene complexes.

The requirement for the η^6 -arene ligand in ruthenium(II) anti-cancer complexes was first examined by Alessio and co-workers who replaced the arene ligand with the cyclothioether, 1,4,7-trithiacyclononane (ttn).¹⁶¹ The antiproliferative activity of ttn complexes (Fig. 1.17) were found to be comparable to the respective η^6 -arene analogues (Table 1.4), with minimal loss of activity. The en complex [RuCl(en)(ttn)]OTf was found to be the most active, but lack of data using identical cell lines prevents direct comparison with the RAEn compounds. A RAPTA analogue, [RuCl(PTA)₂(ttn)]OTf, showed similar selectivity for tumour cells over healthy cells when compared to the parent RAPTA complexes.¹⁶¹

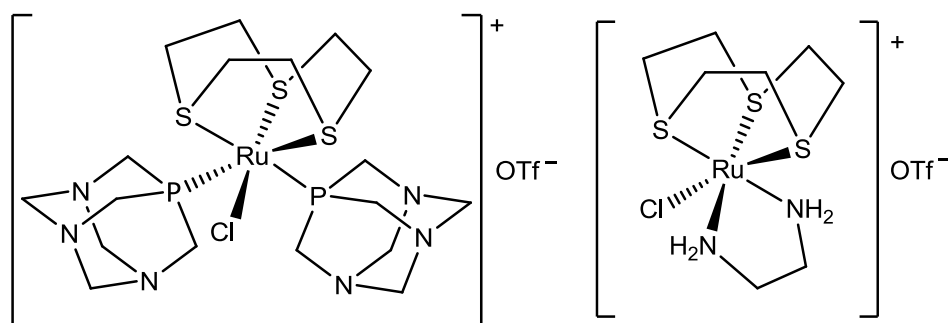


Figure 1.17: Ttn analogues of ruthenium η^6 -arene complexes. The RAPTA analogue with the PTA ligand shows similar selectivity to RAPTA-B (left) and the RM175 analogue with en is moderately active against tumour cells *in vitro* (right).

Complex	IC ₅₀ (μM)	
	TS/A	HBL-100
[RuCl ₂ (PTA)(ttcn)]	650	738
[RuCl(PTA) ₂ (ttcn)]OTf	388	>1000
[RuCl(en)(ttcn)]OTf	65	175
RAPTA-C	507	>1000
RAPTA-B	231	>1000

Table 1.4: *In vitro* biological evaluation of ttcn complexes designed to resemble the promising ruthenium η^6 -arene compounds in the TS/A carcinoma and HBL-100 healthy cell lines.¹⁶¹

Further studies on complexes of the ttcn ligand were continued with bipyridyl (bipy) ligands which had been functionalised with groups such as hydroxyl and carboxylate, capable of forming hydrogen-bonding interactions with potential target molecules. However, none of these complexes were found to be of a sufficient enough cytotoxicity *in vitro*, reflecting the findings of studies with the ruthenium(II) η^6 -arenes complexes.^{162, 163} Highly active compounds were successfully obtained by the conjugation of porphyrin rings to the bipy ligand of a ruthenium-ttcn complex, where activity was further enhanced by irradiation with visible light.¹⁶⁴ A further modification of the ruthenium ttcn compounds was explored using *N,N*-1-(2-picolyl)-4-phenyl-1*H*-1,2,3-triazole (ppt) and it was found that the cytotoxic activity of [RuCl(ttcn)(ppt)]OTf (A549, 48 h exposure) surpassed that of cisplatin and the η^6 -*p*-cymene analogue by over two-fold.¹⁶⁵

Recently, Alessio and co-workers reported an expansion of the structure-activity relationship of the ruthenium ttcn compounds with *N,N*-, *N,O*- and *O,O*- ligands; but *in vitro* activity was only reported for [RuCl(ttcn)(dach)]PF₆ (dach = *trans*-1,2-diaminocyclohexane) which failed to improve on the cytotoxicity of [RuCl(ttcn)(en)]PF₆.¹⁶⁶ This study also focussed on the use of a new *fac*-coordinating ligand, 1,4,7-triazacyclononane (tacn) for the development of ruthenium(II) anti-cancer compounds (Fig. 1.18). When accompanied with an *N,N*-

chelating ligand and DMSO as a leaving group, no detectible antiproliferative activity was observed (up to 300 μM).

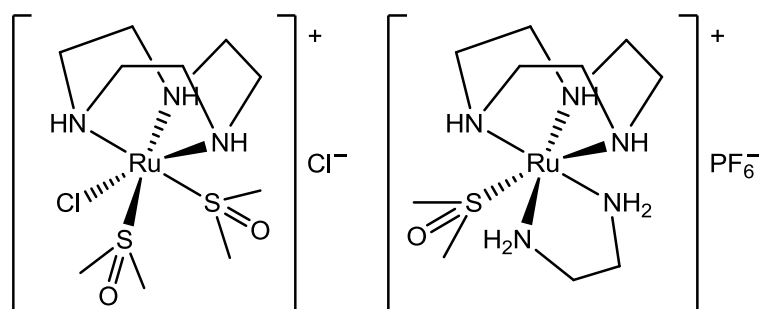


Figure 1.18: Ruthenium(II) tacn complexes $[\text{RuCl}(\text{DMSO-S})_2(\text{tacn})]\text{Cl}$ (left) and $[\text{Ru}(\text{DMSO-S})(\text{en})(\text{tacn})]\text{PF}_6$ (right) developed by Alessio and co-workers and assessed for *in vitro* anti-tumour activity. Activity was not observed for either complex up to 300 μM .

Use of the *fac*-ligand ttcn has permitted the design of novel ruthenium(II) complexes which were inspired by the promising activity of the ruthenium(II) η^6 -arene compounds. These complexes do show some activity, but complexes with the ttcn are yet to show any significant advantages over the η^6 -arenes. Therefore the replacement of the arene with another *fac*-ligand is a viable strategy for the preparation of highly active anti-cancer compounds.

1.9 The *cis*-1,3,5-Triaminocyclohexane Ligand

There is an ongoing drive to discover more potent anti-cancer compounds with less severe side effects and which overcome cross-resistance with existing chemotherapeutics. Novel use of ligands and new types of complexes are essential in this quest for more effective chemotherapeutic agents. With the promising activity of ruthenium(II) compounds, there is the opportunity to explore other *facially*-capping ligands.

Cis-1,3,5-triaminocyclohexane (*cis*-tach) is capable of acting as a neutral, *facially*-coordinating six-electron donor ligand, similar to the η^6 -arene ligands (Fig. 1.19). Incorporation of the *cis*-tach ligand in the design of ruthenium(II) complexes may introduce advantageous properties for application as anti-cancer agents. The amine groups of *cis*-tach provide three key functions (in order of priority): increased water solubility, interaction with biomolecules by hydrogen-bonding (*cf.* RM175), and *possible* increased reactivity, resulting from the strong σ -donors *trans*- to potential leaving groups. The cyclohexane ring also provides a hydrophobic face to the complex, hiding the hydrophilic metal core.

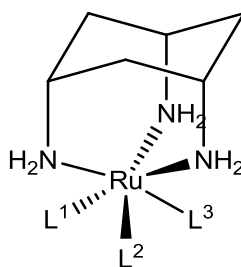
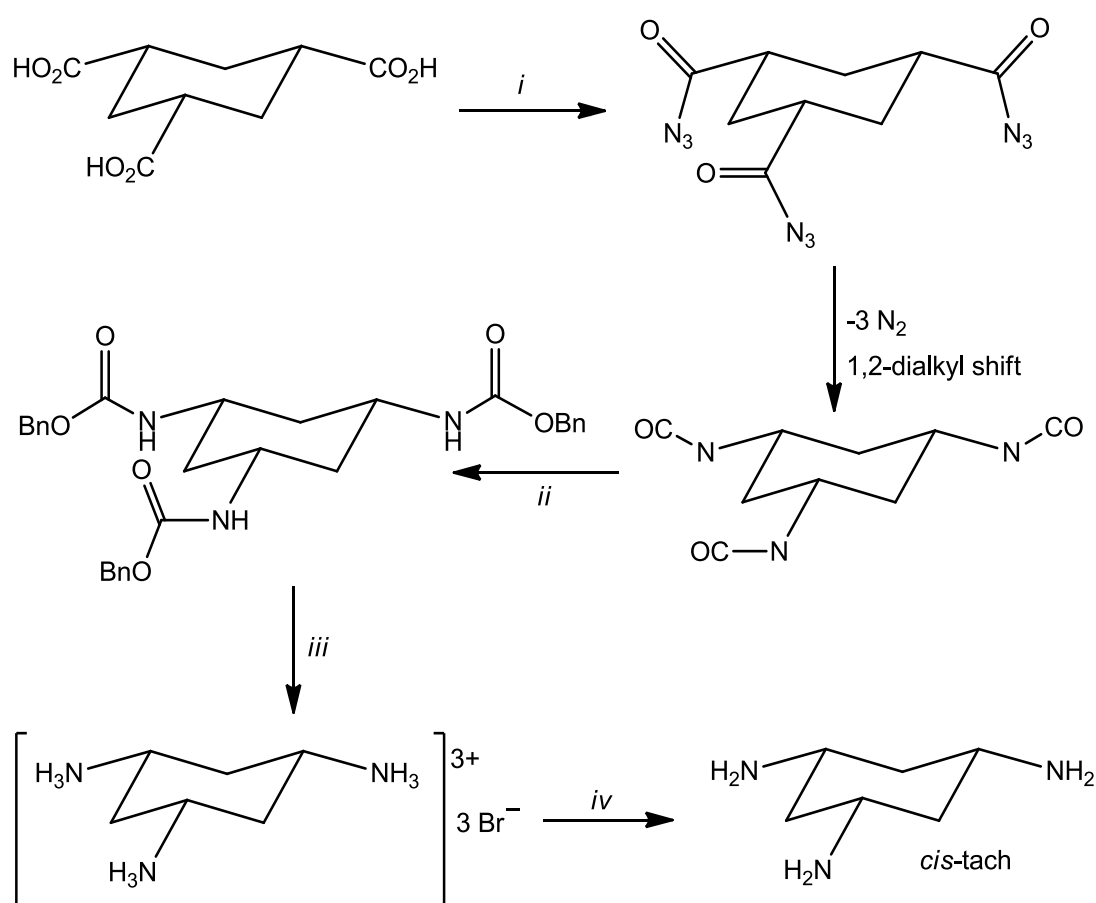


Figure 1.19: Hypothesised structure that the ruthenium(II) κ^3 *cis*-tach complexes will adopt, where *cis*-tach acts as a six-electron *fac*-coordinating ligand.

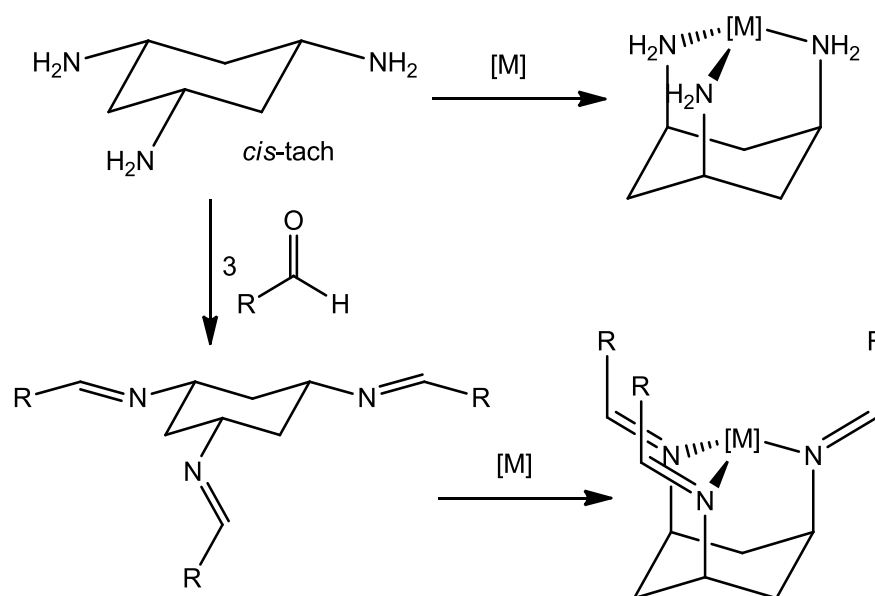
1.9.1 Synthesis of *cis*-tach Complexes

A summary of the synthesis of *cis*-tach is given in Scheme 1.5.¹⁶⁷ The *cis*- ligand is obtained from reaction of *cis*-1,3,5-cyclohexanecarboxylic acid with diphenylphosphoryl azide (DPPA) by a Curtius rearrangement, giving *cis*-1,3,5-cyclohexanetrakis(benzylcarbamate).¹⁶⁷ The carbamates is cleaved by hydrobromic acid, yielding the hydrobromide salt of *cis*-tach.¹⁶⁷ The preparation of the free ligand is finally achieved by removal of the hydrogen bromide by passing through an anion-exchange column followed by purification by sublimation.¹⁶⁸



Scheme 1.5: Synthesis of *cis*-tach. Reagents and conditions: *i*) triethylamine, DPPA, *ii*) benzyl alcohol, reflux, *iii*) HBr (33% in acetic acid by weight), *iv*) anion exchange column, sublimation.

When free in solution, the amine groups of *cis*-tach adopt an equatorial conformation. On coordination to a metal centre, a ring-flip process occurs (Scheme 1.6), enforcing an axial conformation of the amine groups with an adamantane-type structure forming. This provides a rigid and highly directional basis for metal-complex design.



Scheme 1.6: Coordination of *cis*-tach ligands to a metal, adopting an all-axial geometry of the amine ligands (top). The ligand can be functionalised with “arms” on the nitrogen group, prepared by the condensation reaction with aldehydes.

Some early coordination complexes of *cis*-tach took the form of $[M(\textit{cis}\text{-tach})_2]^{n+}$,^{169, 170} akin to the organometallic sandwich complexes (Fig. 1.20). *Cis*-tach is easily *N*-functionalised by a condensation reaction with a range of aldehydes (Scheme 1.6),¹⁷¹ and has been used as to preparing a variety of new ligands. The additional arms may also coordinate to the metal in a hexadentate fashion, such as the tris(acetic acid) modified *cis*-tach ligand (tachta, Fig. 1.20),¹⁷² or may be innocent in metal coordination.

Walton and co-workers have also demonstrated the preparation of mono-substituted *cis*-tach based complexes (Fig. 1.20) formed by the cleavage of two arms upon coordination to a metal centre but this approach is limited to arms based on benzaldehyde derivatives.^{173, 174} This was overcome by Walton and co-workers by

using cinnamaldehydes to functionalise *cis*-tach and the resulting ligands were employed in the small-molecule modelling studies on of the secondary coordination spheres of enzyme active sites (Fig. 1.20).^{174, 175}

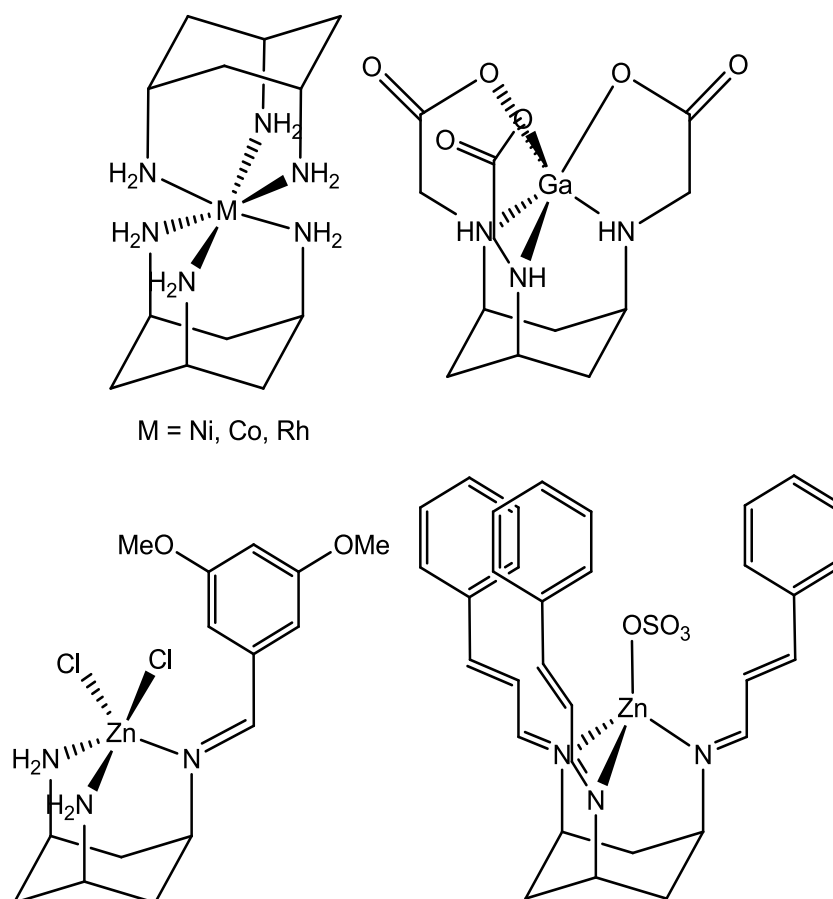
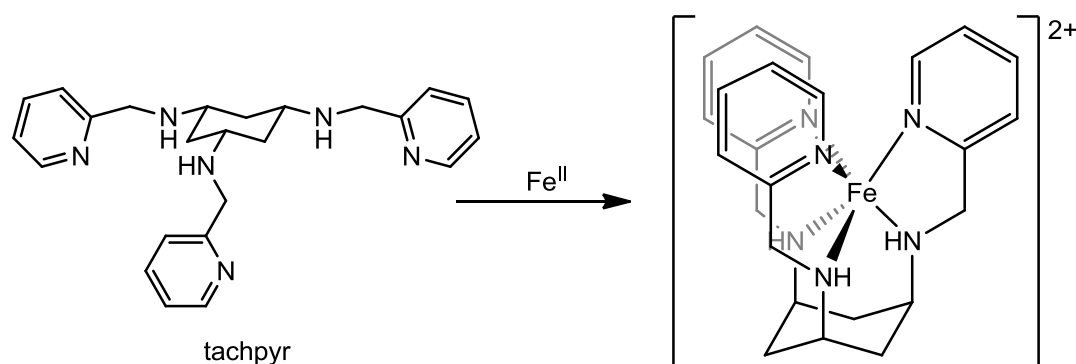


Figure 1.20: Examples of *cis*-tach metal complexes with or without modified amine groups and the possible metal-coordination motifs accessible. These include the sandwich-type complexes $[M(\textit{cis}\text{-tach})_2]^{n+}$ (top left), hexadentate coordination with $[\text{Ga}(\textit{tachta})]$ (top right), mono-arm *cis*-tach complexes obtained from the cleavage of benzaldehyde derived arms (bottom left) and cinnamaldehyde-functionalised *cis*-tach, used to obtain non-coordinating arms resistant to cleavage (bottom right)

A range of structural motifs are accessible with *cis*-tach, all offering a rigid and highly directional basis for complex design. Although its ruthenium chemistry is previously unexplored, the *cis*-tach ligand has been widely and successfully used in coordination chemistry. Therefore, it is an ideal candidate to be used for investigating the design of new complexes with anti-tumour properties.

1.9.2 *cis*-Tach Compounds as Anti-cancer Agents

Compounds derived from *cis*-tach have previously been studied for their anti-tumour activity. Modification of the amine groups of *cis*-tach with 2-pyridylmethylene groups (by reaction with 2-pyridinecarboxaldehyde and its subsequent reduction) gave tachpyr,¹⁶⁷ a highly cytotoxic compound with an IC₅₀ of 4.6 μM in the A549 lung adenocarcinoma cell line.¹⁷⁶ It was hypothesised that the activity originated from tachpyr strongly binding iron(III) as a hexadentate ligand with reduction to iron(II) (Scheme 1.7).^{177, 178} This is thought to inhibit ferritin synthesis causing iron depletion.¹⁷⁶ Eventual apoptosis is caused by a p53-independent mitochondrial caspase pathway and this is advantageous for treating tumours with defective p53 pathways with these compounds.^{179, 180}



Scheme 1.7: Chelation of iron(II) by tachpyr. It is proposed that coordination of intracellular iron results in a partially-oxidised form of tachpyr.

Zinc was also identified as a potential metal targeted by tachpyr, with the ligand chelating 13% of cellular zinc in comparison to 9% of cellular iron.¹⁸¹ The pre-treatment of the cells with zinc or iron prevented apoptosis, suggesting a link between metal depletion and cytotoxicity.¹⁸¹ *N*-methylation of the pyridine rings results in loss of activity, hypothesised to be due to the reduced strength of binding iron(II) or zinc(II).¹⁸² It has also been shown that the ring-flip process is not a significant step in the activity of the complexes.¹⁸³ Since the initial discovery of tachpyr, a number of cytotoxic and anti-angiogenic chelating complexes have been studied which are based on tachpyr.^{184, 185}

Although the anti-cancer abilities of other functionalisations of *cis*-tach have been investigated,^{186, 187} there still remains no directly cytotoxic metal complexes which incorporate the *cis*-tach ligand. It is therefore the aim of the work described in this thesis to design, prepare and evaluate such complexes for use as anti-cancer agents, with ruthenium as the chosen metal.

It is worth noting that platinum(IV) half-sandwich type complexes of κ^3 -*cis*-tach have been studied, although to a limited extent (Fig. 1.21).^{188, 189} This complex is yet to be studied for its anti-cancer properties, but such work may form the basis of an interesting future study.

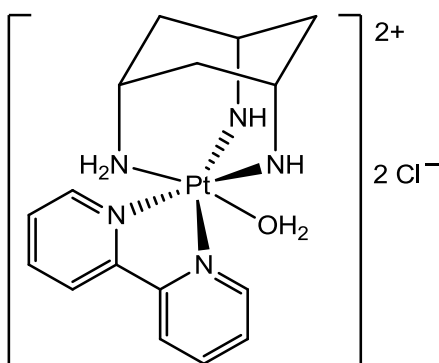


Figure 1.21: Structure of a platinum *cis*-tach complex. Two of the *cis*-tach amine groups are deprotonated, therefore acting as a dianionic ligand.

1.10 Aim of this Project

This thesis is focused on the use of novel *cis*-tach coordination complexes as metallo-anti-cancer agents. The *cis*-tach ligand is capable as acting as a neutral, six-electron, *fac*-coordinating ligand in a similar fashion to the η^6 -arene ligand in the ruthenium(II) half sandwich compounds presented earlier (Fig. 1.22).

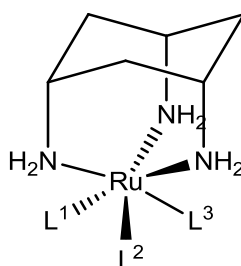


Figure 1.22: Hypothesised structure that the ruthenium(II) κ^3 *cis*-tach complexes will adopt, where *cis*-tach acts as a six-electron *fac*-coordinating ligand.

The hypothesis of this project is that by using the *cis*-tach ligand in ruthenium(II) coordination compounds, the resulting complexes will display anti-proliferative properties with good water solubility. At present, many ruthenium(II) compounds with high potency *in vitro* possess limited water solubility due to the dominance of hydrophobic groups within them.

Investigations will first concentrate on establishing the preparation of ruthenium(II) *cis*-tach complexes and the development of a general precursor compound. This will be used in the subsequent preparation of further ruthenium(II) *cis*-tach complexes, where the properties of the complex can be fine-tuned by the co-ligand. The aqueous chemistry, as well as the binding of these candidates to biomolecules is of interest to begin assessing their chemistry under physiological conditions. However, most importantly, selected compounds will be assessed for their ability to inhibit tumour cell growth by *in vitro* techniques.

Chapter 2. Ruthenium(II) *cis*-tach Triphenylphosphane Complexes

2.1 Introduction

As the preparation of ruthenium(II) *cis*-tach complexes was previously unexplored, a synthetic procedure for obtaining κ^3 -*cis*-tach complexes had to be established.

There are various challenges in the synthesis of ruthenium(II) complexes containing a *facially*-coordinating six electron donor, the first of which is the reduction of the ruthenium(III) chloride hydrate to a suitable ruthenium(II) species. This can be performed before, during or after the coordination of the *fac*-ligand. A zinc reduction method may be utilised, where a ruthenium(III) complex of the ligand is reduced to ruthenium(II) in the presence of a suitable co-ligand.¹⁹⁰ Alternatively, reaction of ruthenium(III) chloride with a partially reduced modification of the ligand can be employed in the synthesis of the η^6 -arene half-sandwich complexes.¹⁹¹ Alternatively, the ligand may be coordinated to a ruthenium(II) precursor prepared in a previous synthetic step.¹⁹² It is proposed that a successful method for the preparation of such compounds is the latter, with reaction of *cis*-tach with ruthenium(II) precursor complexes. The overall yield of target complexes with respect to *cis*-tach may be enhanced by use of this method.

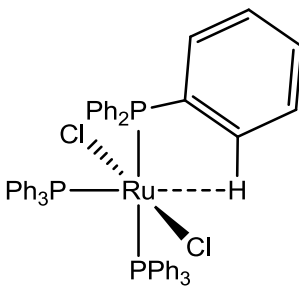


Figure 2.1: Structure of Dichlorido-tris(triphenylphosphane) ruthenium(II).^{193, 194}

Dichlorido-tris(triphenylphosphane) ruthenium(II) is formally a sixteen-electron complex capable of readily binding introduced ligands.¹⁹⁵ The compound owes its reactivity to the electron deficiency of the ruthenium centre, where the bulky

triphenylphosphane groups prevent coordination of a fourth phosphane ligand and satisfaction of the 18-electron rule. The complex is stabilised by an agostic interaction from the *ortho*-hydrogens of the phenyl rings to the metal centre (Fig 2.1).¹⁹⁶ Furthermore, the triphenylphosphane ligands are relatively labile, potentially allowing for additional electron donors to coordinate. The complex [RuCl₂(PPh₃)₃] has been demonstrated to react with a variety of *facial*-coordinating ligands including η⁵-cyclopentadienyl (Cp) and tris(pyrazolyl)borate (Tp), both resulting in the neutral species [RuCl(X)(PPh₃)₂] (X = Cp or Tp).^{197, 198} Additionally, neutral ligands have been successfully coordinated to this precursor, including ttcn, to yield the neutral species [RuCl₂(ttcn)(PPh₃)].¹⁹⁹

Ruthenium(II) phosphane complexes have been extensively studied for the catalytic transformations of organic molecules, including olefin metathesis and the *anti*-Markovnikov hydration of terminal alkynes.²⁰⁰⁻²⁰⁴ Recently, ruthenium(II) phosphane complexes capable of inhibiting tumour growth, such as RAPTA-C have been extensively studied.^{79, 116, 118, 131, 136, 137} This series of compounds have been discussed in detail in section 1.5.

The ruthenium(II) complex [RuCl₂(PPh₃)₃] is a suitable candidate to investigate the synthetic possibilities of *cis*-tach with ruthenium. It was hypothesised that ruthenium(II) κ³-*cis*-tach compounds could be accessible from this precursor. The reaction of *cis*-tach with [RuCl₂(PPh₃)₃] is explored, and the resulting products and their reactivity are discussed, as well as the assessment of selected compounds for biological activity.

2.2 Reaction of *cis*-tach with [RuCl₂(PPh₃)₃]

2.2.1 Formation of [1]Cl

In order to investigate the potential of *cis*-tach to act as a six electron *facial*-coordinating ligand with ruthenium, [RuCl₂(PPh₃)₃] was added to a suspension of one equivalent of *cis*-tach in CD₂Cl₂. Upon dissolution of the ruthenium complex a solution formed accompanied by an immediate colour change from dark brown to orange. After standing for 30 min the reaction had visually appeared to reach completion as a yellow solution was formed. The ³¹P{¹H} NMR spectrum of the solution exhibits a single sharp resonance at δ_P 47.3 ppm, assigned to [1]Cl, and is distinctly different to that of the starting material, a broad resonance at δ_P 41.0 ppm. In addition, liberated triphenylphosphane (δ_P -5.6 ppm) is observed, in a ratio of half that of the ruthenium complex, suggesting two phosphane ligands remain coordinated to the metal.

The ¹H NMR spectrum of [1]Cl, generated *in situ* from the reaction between *cis*-tach and one equivalent of [RuCl₂(PPh₃)₃] in CD₂Cl₂ allows for inspection of the *cis*-tach proton environments. Assessment of the phenyl protons cannot be performed due to the resonances for liberated triphenylphosphane coinciding with those of the complex. The *cis*-tach region (δ_H 3.8–0.7 ppm) of the ¹H NMR spectrum of [1]Cl and the uncoordinated ligand is given in Fig. 2.2.

The *CH* and *CH*₂ protons were assigned by cross-peaks in the 2D ¹H-¹³C correlation spectrum (HSQC), with the nature of the adjacent carbon determined by the ¹³C{¹H} DEPT-135 spectrum. The *NH*₂ resonances were assigned from the remaining resonances by observation of a cross-peak in the 2D ¹H-¹H COSY spectrum with the *CH* groups; a cross-peak in the 2D ¹H-¹³C correlation spectrum (HSQC) was not observed for these resonances. Relative integrations of the *cis*-tach resonances in the ¹H NMR totalled fifteen, as expected for this ligand which contains fifteen protons. Distribution of the integrations was consistent with the expected ¹H chemical environments present within the ligand.

Coordination of *cis*-tach to the metal centre is expected to result in a shift of the amine proton resonances to a higher δ_{H} . The large shift of all amine resonances from δ_{H} 1.04 to 2.15, 3.44 and 3.57 ppm suggests that the amine groups are coordinated to the metal in a κ^3 fashion.

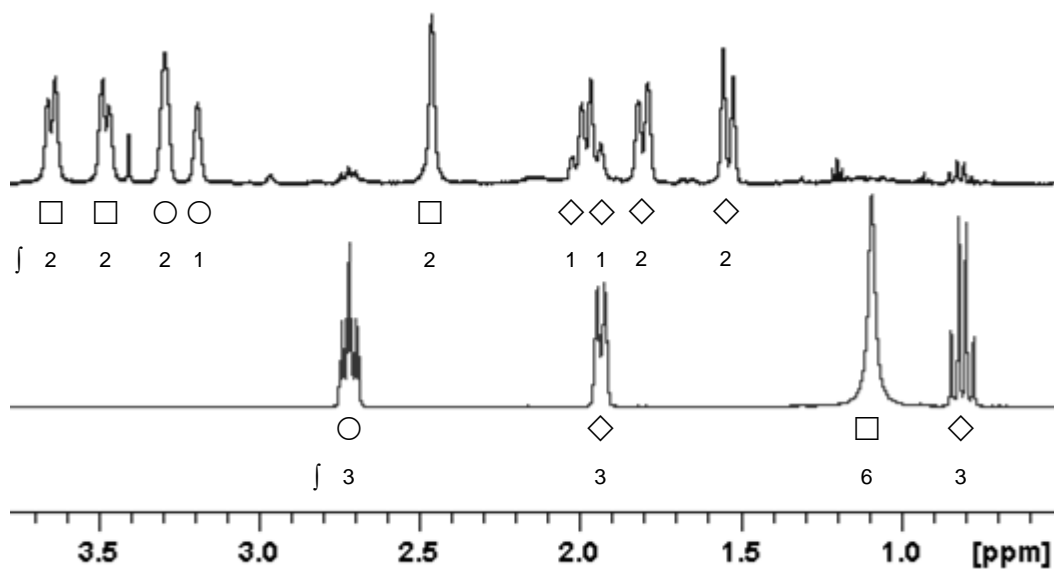
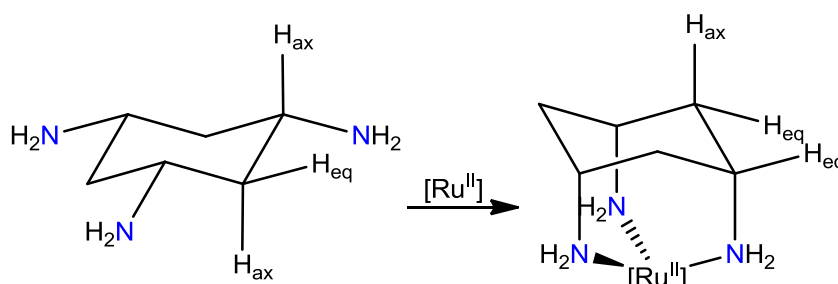


Figure 2.2: ¹H NMR spectra of *cis*-tach (bottom) and [1]Cl (top) in CD₂Cl₂. Key: □ NH₂, ○ CH, ◇ CH₂. Relative integrations are given underneath symbol.

The absence of visible axial-axial $^3J_{\text{HH}}$ coupling (~ 10 Hz) in the cyclohexane ring resonances suggests that a ring-flip process has occurred (Scheme 2.1), with the amine groups adopting an all-axial geometry in a chair conformation. This would occur if all the amine groups are coordinated to a metal centre. The expected $^3J_{\text{HH}}$ coupling for axial-equatorial (~ 4 Hz) and equatorial-equatorial (~ 4 Hz) cyclohexane protons could not be determined.



Scheme 2.1: Conformational change of *cis*-tach from equatorial amine groups to axial on coordination to a ruthenium(II) complex, resulting in a κ^3 complex.

It is possible to identify the symmetry environment of the *cis*-tach ligand and therefore the symmetry about the ruthenium from the number of ^1H NMR resonances. A summary of the three symmetry environments and number of resonances expected for *cis*-tach is shown in Fig. 2.3.

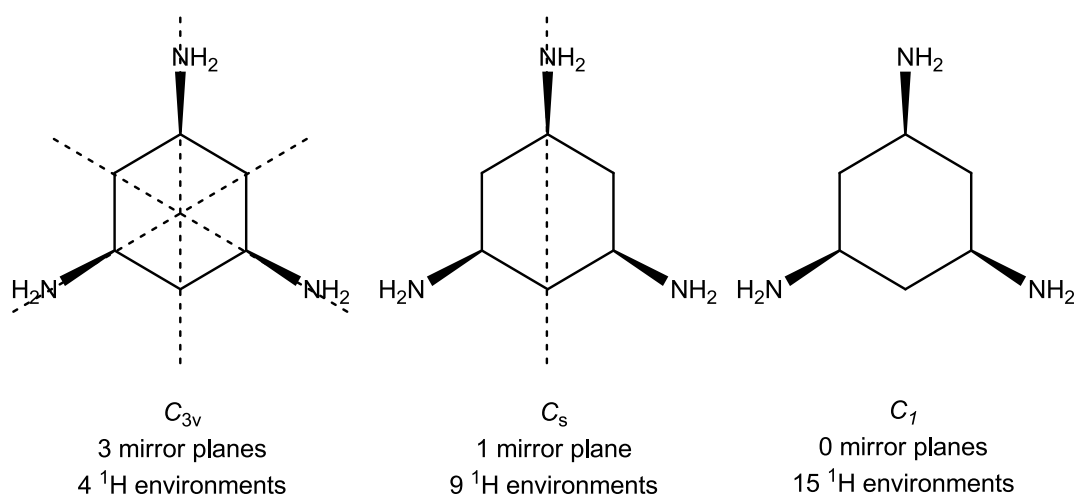
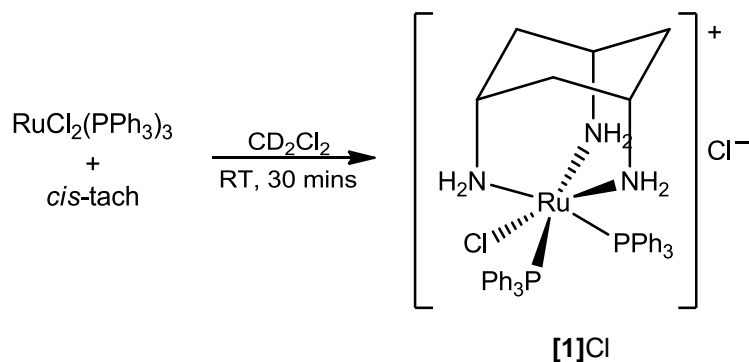


Figure 2.3: The three different possible symmetry environments for the *cis*-tach ligand when κ^3 coordinated to a metal centre and the number of resonances expected for the ligand in the ^1H NMR spectrum.

The resonances for the *cis*-tach ligand of [1]Cl in the ^1H NMR spectrum consists of nine signals, two of which are near coincidental and appear as a quartet. This suggests the symmetry about the ruthenium centre is C_s . Therefore the complex may be one of the two possibilities which would exhibit this symmetry with a κ^3 *cis*-tach

ligand, $[\text{RuCl}(\text{cis-tach})(\text{PPh}_3)_2]^+$ and $[\text{RuCl}_2(\text{cis-tach})(\text{PPh}_3)]$ —assuming a chlorido ligand completes the coordination sphere of the metal, satisfying the eighteen-electron rule. Given the $^{13}\text{P}\{^1\text{H}\}$ integrations of the complex vs. free triphenylphosphane (2:1) described earlier, it is initially proposed that the identity of **[1]Cl** is $[\text{RuCl}(\text{cis-tach})(\text{PPh}_3)_2]\text{Cl}$ (Scheme 2.2). This assignment is in accordance with that reported for a similar reaction with tacn as the *fac*-ligand,²⁰⁵



Scheme 2.2: Reaction between *cis*-tach and $[\text{RuCl}_2(\text{PPh}_3)_3]$. The product, formed after 30 mins at RT, is proposed as the κ^3 complex $[\text{RuCl}(\text{cis-tach})(\text{PPh}_3)_2]\text{Cl}$, **[1]Cl**.

Isolation of the cationic species as the hexafluorophosphate salt, **[1]PF₆**, was attempted by chloride metathesis of **[1]Cl** with NaPF_6 in CH_2Cl_2 solution. The excess triphenylphosphane and resulting insoluble NaCl were removed by filtration followed by precipitation with pentane. The resonance for the PPh_3 ligands of **[1]PF₆** in the $^{31}\text{P}\{^1\text{H}\}$ NMR spectrum is identical to that of **[1]Cl**, with δ_{P} 47.3 ppm. This allowed for spectroscopic information to be gained regarding the phenyl groups of the triphenylphosphane ligands and determination of the identity of the complex.

The resonances corresponding to the *cis*-tach ligand in the ^1H NMR spectrum obtained for **[1]PF₆** are mostly identical to that of **[1]Cl**, with small changes in chemical shift relating to the altered properties of the anion. Those relating to the aromatic protons of the phosphane ligands suggest that each phenyl ring is equivalent and that there is free rotation around the Ru-P bond. The integration of these resonances accounts for two phosphane ligands for each *cis*-tach. Furthermore, the $^{13}\text{C}\{^1\text{H}\}$ NMR spectrum provides evidence for the number of phosphane ligands.

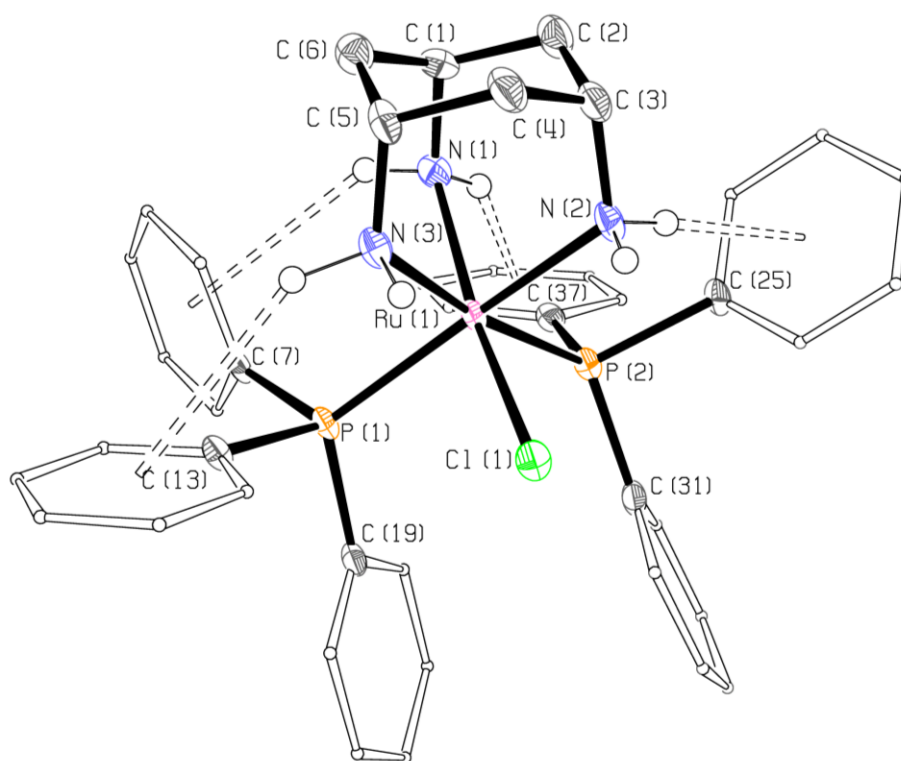


Figure 2.4: ORTEP (50% probability ellipsoids) diagram of one cation of two in the asymmetrical unit of **[1]PF₆**. Hydrogen atoms (except for amino hydrogens) and the counter ion are omitted for clarity. Selected bond lengths (\AA) and angles ($^\circ$): Ru(1)–N(1) 2.144(4), Ru(1)–N(2) 2.180(4), Ru(1)–N(3) 2.176(4), Ru(1)–Cl(1) 2.424(1), Ru(1)–P(1) 2.339(1), Ru(1)–P(2) 2.354(1), N(1)–Ru(1)–N(2) 87.87(17), N(1)–Ru(1)–N(3) 87.75(17), N(2)–Ru(1)–N(3) 82.19(17), P(1)–Ru(1)–P(2) 98.53(5), P(1)–Ru(1)–Cl(1), 89.09(4), P(2)–Ru(1)–Cl(1) 97.28(5), N(1)–Ru(1)–Cl(1) 167.56(13), N(2)–Ru(1)–Cl(1) 81.67(13), N(3)–Ru(1)–Cl(1) 84.18(12). Selected hydrogen-bond (D–H...A–X) lengths (\AA) and angles ($^\circ$) D...A, H...A, D–H...A, H...A–X, H...X (A = centroid and X = plane of respective phenyl ring of atom *): N(1)–H(1b)...C(7)* 4.09, 3.27, 145, 39.7, 2.52 (V); N(1)–N(1a)...C(37)* 4.13, 3.36, 149, 36.3, 2.71 (V); N(2)–H(2c)...C(25)* 3.33, 2.43, 176, 64.4, 1.05 (II); N(3)–H(3b)...C(13)* 3.96, 3.03, 149, 48.1, 2.03 (V). Malone hydrogen-bond type is given in parenthesis.²⁰⁶

The *ipso* carbons of the phenyl groups are observed as triplets due to virtual coupling with $|^1J_{PC} + ^3J_{PC}| = 37$ Hz. The observed virtual coupling results from a J_{CP} with a ^{31}P nuclei strongly coupled to another ^{31}P with identical chemical shift, $\Delta\nu_{\text{P-P}} = 0$. This therefore appears as though the ^{13}C nucleus is equally coupled to two ^{31}P nuclei, finally confirming the identity of $[\mathbf{1}]^+$ as $[\text{RuCl}(\text{cis-tach})(\text{PPh}_3)_2]^+$.

The assigned identity of $[\mathbf{1}]\text{PF}_6$ is further supported by the $^{31}\text{P}\{^1\text{H}\}$ NMR; integration of the PPh_3 resonance correlates with approximately double that of PF_6 , suggesting two phosphanes per cation. The ESI mass spectrum also exhibits a major signal with the expected m/z (790.2) and ruthenium/chlorine isotope pattern for $[\mathbf{1}]^+$. The species $[\text{Ru}(\text{NCMe})(\text{cis-tach})(\text{PPh}_3)_2]^+$ is also observed in the mass spectrum with m/z 941.2 (10%); this complex is presumed to be generated in the preparation of the sample in acetonitrile for mass spectrum acquisition.

Single crystals suitable for X-Ray diffraction analysis were obtained from slow diffusion of pentane into a dichloromethane solution of $[\mathbf{1}]\text{PF}_6$. An ORTEP diagram and selected bond angles and lengths are given in Fig. 2.4.

The resulting structural determination of $[\mathbf{1}]\text{PF}_6$ demonstrates that the *cis-tach* ligand adopts a κ^3 *facial*-coordination mode, forming a distorted adamantane structure with ruthenium. The entire complex resembles the piano-stool type structures of the η^6 -arene complexes. The structure of the ruthenium centre is that of a distorted octahedron, due to the geometrical constraints of the *cis-tach* and triphenylphosphane ligands. For example, the phosphane ligands have a P(1)–Ru(1)–P(2) bite-angle of $98.53(5)^\circ$ compared to ideal the octahedral angle of 90° ; this results from the steric crowding of the phenyl groups when in a *cis* configuration. There is further distortion in the adamantane structure, as the metal is not located in the exact centre between the amine groups. This is seen from the average Ru–N bond lengths, of 2.144(4) and 2.178(6) Å for those *trans*- to chlorido [N(1)] and phosphane [N(2) and N(3)] ligands respectively. The bite-angle of the *cis-tach* amines also vary due to this distortion, where the N(2)–Ru(1)–N(3) angle is $82.19(17)^\circ$, compared to the average of the remaining two angles of $87.8(2)^\circ$.

Hydrogen-bonds are present in the crystal structure, between the NH groups of *cis*-tach and the π -system of an adjacent phenyl ring of the phosphane ligand. The contact geometries of hydrogen-bonds to an aromatic π system were defined by Malone;²⁰⁶ those present in [1]PF₆ can be described as type II or V (Fig. 2.5).

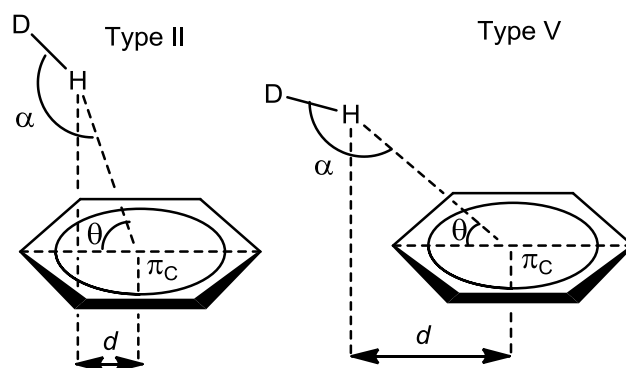


Figure 2.5: Type II (left) and V (right) D–H... π hydrogen-bonds defined by Malone. Type II: $d(\pi_C\cdots H) \leq 3.05 \text{ \AA}$, $\theta \geq 53^\circ$, $150^\circ \leq \alpha \leq 180^\circ$, $d > 0.5 \text{ \AA}$. Type V: $d(\pi_C\cdots H) \leq 4.0 \text{ \AA}$, $\theta \leq 90^\circ$, $90^\circ \leq \alpha \leq 180^\circ$, $d > 1.4 \text{ \AA}$.

In both of these geometries, the N–H group is highly directional towards the centroid of the phenyl ring. An almost perfectly perpendicular and linear hydrogen-bond would be of type I. The difference between type II and V is in the proximity of the hydrogen-bond donor to the centroid. In type II, the perpendicular of the hydrogen to the phenyl plane is within the ring system, whereas in type V it falls outside.

Isolation of [1]⁺ as the hexafluorophosphate salt was met with difficulty, due to formation of a new ruthenium species when standing in CH₂Cl₂ solution. It was not possible to isolate [1]PF₆ with analytical purity. This is discussed in more detail in the next section.

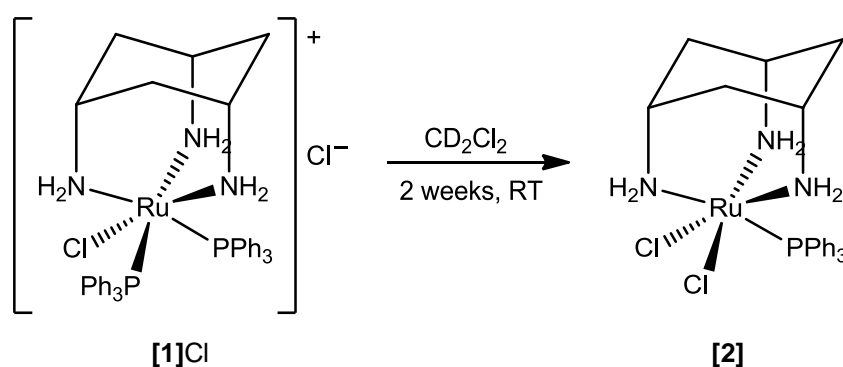
2.2.2 Conversion of [1]Cl to [2]

After two weeks, the ³¹P{¹H} NMR spectrum of [1]Cl in CD₂Cl₂—which was formed *in situ* from the reaction of [RuCl₂(PPh₃)₃] and *cis*-tach—was recorded again. The signal for [1]Cl at δ_P 47.3 ppm was no longer observed, with a new singlet

resonance at δ_{P} 66.0 ppm, of a new ruthenium *cis*-tach complex, [2]. The relative integration of triphenylphosphane to this had also increased, to double that of the metal complex.

The new complex, [2], was of C_s symmetry about *cis*-tach, evident from eight resonances for the ligand in the in the ^1H NMR spectrum. The expected nine chemical environments of *cis*-tach appear as eight signals as two geminal CH_2 resonances are coincidentally isochronous, appearing as a singlet. The κ^3 coordination of *cis*-tach is also retained from [1]Cl. This is evidenced by the absence of axial-axial cyclohexane J couplings, suggesting an all-axial conformation of the amine groups, and downfield amine resonances (δ_{H} 1.85–4.77 ppm), similar to those for [1]Cl.

Given the displacement of a triphenylphosphane group, based on $^{31}\text{P}\{^1\text{H}\}$ NMR integrations, it is proposed that [2], $[\text{RuCl}_2(\textit{cis}\text{-tach})(\text{PPh}_3)]$ is the product from the charge-neutralisation of [1]Cl (Scheme 2.3). It is hypothesised that this reaction is aided by steric repulsion of the triphenylphosphane ligands, aiding displacement. This complex, along with [1]Cl, are the only two plausible κ^3 *cis*-tach products accessible from the reactants employed.



Scheme 2.3: Charge-neutralisation reaction between the chloride anion and $[\text{RuCl}(\textit{cis}\text{-tach})(\text{PPh}_3)_2]^+$ ([1]⁺), yielding the neutral complex $[\text{RuCl}_2(\textit{cis}\text{-tach})(\text{PPh}_3)]$ ([2]) from displacement of a phosphane ligand.

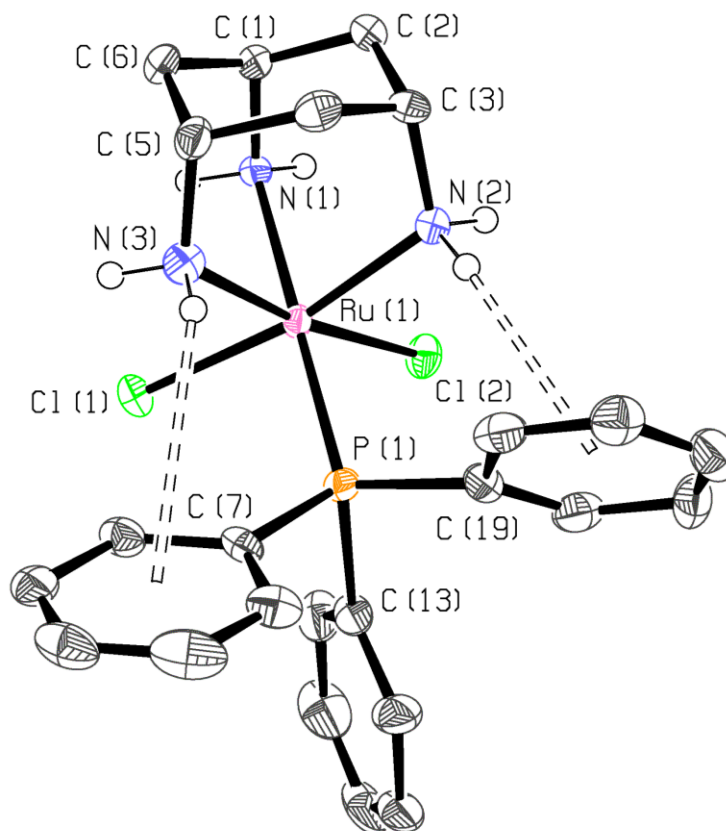


Figure 2.6: ORTEP (50% probability ellipsoids) diagram of one complex of two in the asymmetrical unit of [2]. Hydrogen atoms (except for amino hydrogens) and the solvent of crystallisation are omitted for clarity. Selected bond lengths (\AA) and angles ($^\circ$): Ru(1)–N(1) 2.172(5), Ru(1)–N(2) 2.110(5), Ru(1)–N(3) 2.115(5), Ru(1)–Cl(1) 2.446(2), Ru(1)–Cl(2) 2.447(2), Ru(1)–P(1) 2.245(2), N(1)–Ru(1)–N(2) 86.4(2), N(1)–Ru(1)–N(3) 85.22(19), N(2)–Ru(1)–N(3) 91.3(2), Cl(1)–Ru(1)–Cl(2) 97.09(6), P(1)–Ru(1)–Cl(1) 92.57(6), P(1)–Ru(1)–Cl(2) 94.67(6), N(1)–Ru(1)–P(1) 178.91(14), N(2)–Ru(1)–P(1) 94.45(15), N(3)–Ru(1)–P(1) 95.42(15). Selected hydrogen-bond (D–H...A–X) lengths (\AA) and angles ($^\circ$) D...A, H...A, D–H...A, H...A–X, H...X (A = centroid and X = plane of respective phenyl ring of atom *): N(3)–H(3b)...C(7)* 4.11, 3.36, 141, 44.9, 2.38 (V); N(2)–H(2c)...C(19) 3.72, 2.88, 152, 55.5, 1.63 (II). Malone hydrogen-bond type is given in parenthesis.²⁰⁶

The complex could be isolated with analytical purity by slow diffusion of diethyl ether into a dichloromethane solution with a single molecule of DCM as solvent of crystallisation was also present. Removal of the excess triphenylphosphane by washing of the crystals with diethyl ether allowed inspection of the phenyl resonances in the ^1H NMR spectrum. The relative integration of the phenyl protons of 1:1 PPh_3 :*cis*-tach agrees with the proposed assignment of the complex. Furthermore, the resonances for the *ipso* carbons of the phenyl rings in the $^{13}\text{C}\{^1\text{H}\}$ NMR spectrum appear as doublets with $^1J_{\text{CP}} = 36.0$ Hz. This multiplicity is due to the ^{13}C nucleus coupling to a single ^{31}P nucleus; therefore only one triphenylphosphane ligand is coordinated to the metal complex.

The ESI mass spectrum of a sample of [2] exhibits three ions with ruthenium isotope patterns, all of which may originate from the proposed structure of [2]. The most abundant signal, $[\text{RuCl}(\text{NCMe})(\textit{cis}\text{-tach})(\text{PPh}_3)]^+$ (m/z 569.1, 100%) is formed from the displacement of a chlorido ligand with acetonitrile, which is present from sample preparation for mass spectrometry. Other less intense signals are observed for the ions $[\text{RuCl}(\textit{cis}\text{-tach})(\text{PPh}_3)]^+$ (m/z 528.1, 25%) and $[\text{Ru}(\textit{cis}\text{-tach})(\text{PPh}_3)]^{2+}$ (m/z 246.6, 10%), resulting from the loss of one and two chlorido ligands respectively. The loss of a chlorido ligand in these three species allows the formation of a cationic species able to be observed by mass spectrometry. Single crystals suitable for X-Ray diffraction analysis were obtained from isolation of [2] as described above. An ORTEP diagram and selected bond angles and lengths are given in Fig. 2.6.

The asymmetric unit of the structure contains two molecules of [2] and a single disordered dichloromethane. Additional disordered solvent was found to be present, which was accounted for using the SQUEEZE algorithm.^{207, 208} The *cis*-tach ligand adopts the same κ^3 *fac*-coordination mode as in [1]PF₆ with the ruthenium centre again that of a distorted octahedron. The adamantane structure is also distorted, evident from the differing Ru–N bond lengths, caused by the *trans*-influence of the phosphane and chlorido ligands. These bond lengths follow the same trend as observed in [1]PF₆. This distortion is most apparent from the bite-angles of *cis*-tach with ruthenium. The N(2)–Ru(1)–N(3) angle is 91.3(2)° compared to the remaining two of an average 85.81(27)°. Although the steric hindrance of the ruthenium centre is reduced in complex [2] on comparison to [1]PF₆, the remaining angles are greater

than that expected for an ideal octahedron. This is due to the inherently small bite-angles of the *fac*-coordinating ligand and the chlorido and phosphane ligands compensating with larger angles. This is most notable in the largest *cis*-angle, Cl(1)–Ru(1)–Cl(2) of 97.09(6)°, which is additionally due to the electrostatic repulsion of the two ligands.

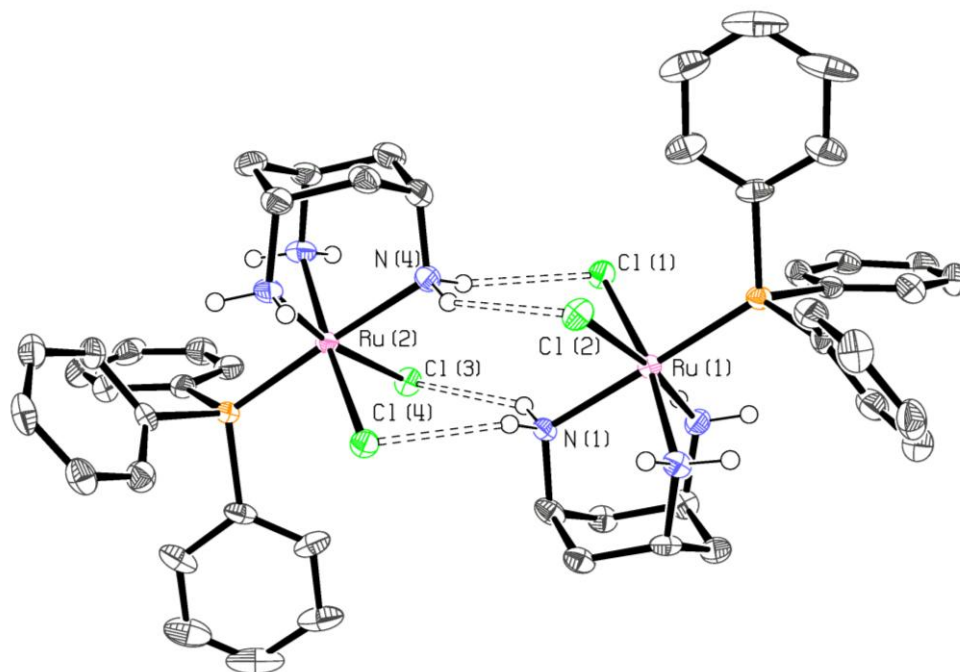
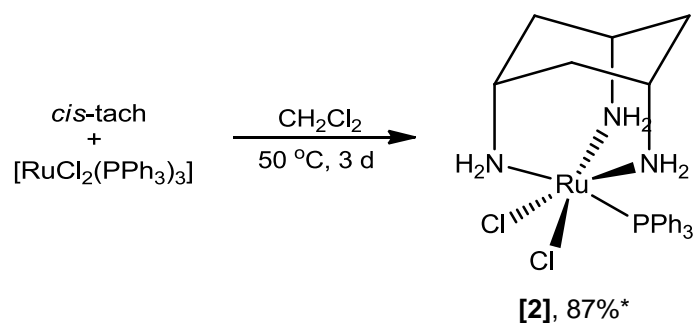


Figure 2.7: ORTEP (50% probability ellipsoids) diagram of the hydrogen-bonded dimer of [2]. Hydrogen atoms (except for amino hydrogens) and solvent of crystallisation are omitted for clarity. Selected hydrogen-bond (D–H...A–X) lengths (Å) and angles (°) D...A, H...A, D–H...A, H...A–X: N(1)–H(1a)...Cl(4)–Ru(2) 3.319(5) 2.541(1) 142.6(3) 93.16(5) (x, y–1, z); N(1)–H(1b)...Cl(3)–Ru(2) 3.436(5) 2.622(1) 147.8(3) 91.61(5) (x, y–1, z). Symmetry transformations used to generate equivalent atoms are given in parenthesis.

In the unit cell, two molecules of [2] form a hydrogen-bonded dimer, with interactions between an amine group and the two chlorido ligands of the other complex, shown in Fig. 2.7. These hydrogen-bonds have a high Ru–Cl...H angular preference of approximately 95°, resultant from the halogen *p*-type lone pair orbitals.²⁰⁹ Intra-molecular hydrogen-bonds are also present in the structure, with Malone type II and V interactions between the amine protons and the aromatic rings.

The synthetic procedure to obtain **[2]** on larger scales (~50 mg) was modified to improve reaction times. This was achieved by heating of the reaction mixture to 50 °C in a sealed vessel for three days (Scheme 2.4). The complex was isolated with analytical purity by crystallisation on addition of pentane to the reaction mixture.



Scheme 2.4: Convenient preparation of **[2]** from the reaction of $[\text{RuCl}_2(\text{PPh}_3)_3]$ and *cis*-tach. * Isolated yield.

2.2.3 Conclusions

It has been shown that *cis*-tach rapidly reacts with dichlorido-tris(triphenylphosphane) ruthenium(II) resulting in the formation of a kinetic product, **[1]**⁺. Over time, charge neutralisation occurs from the exchange of triphenylphosphane with the chloride anion, to yield **[2]** as the thermodynamically favoured product, which is isolable. An analogous tacn complex of **[1]**⁺ has been reported,²⁰⁵ but it is not evident that similar conversion to the neutral species occurs in this complex. The isolation of $[\text{RuCl}(\text{tacn})(\text{PPh}_3)_2]\text{Cl}$ is achieved by recrystallisation from the slow diffusion of diethyl ether into a dichloromethane solution, resulting in an analytically pure sample. Therefore, it is likely that such a process does not occur with the tacn analogue. This indicates that ruthenium *cis*-tach and tacn complexes may exhibit differing reactivity to each other.

2.3 Solid-State Structural Comparisons

The popularity of triphenylphosphane as a ligand in ruthenium(II) chemistry provides an abundance of structurally similar compounds with other *facial*-coordinating ligands for comparison. Analysis of the geometrical properties of [1]PF₆ and [2] with analogous compounds may provide an insight into the electronic differences of the ligands. With increased electron density located on the metal, the Ru–Cl bond is expected to elongate from a weakening of the σ -interaction. Furthermore, the triphenylphosphane ligand can provide information regarding the π -donor abilities of the metal as phosphanes act as both σ -donors and π -acceptors. There is a low lying unoccupied $\sigma^*(\text{P–C})$ orbital located on the phosphane, with correct symmetry for π -overlap with the metal *d* orbitals.²¹⁰ Therefore, a larger degree of π back-bonding from ruthenium to the phosphane ligand is expected to influence the average bond lengths, with shorter Ru–P and longer P–C bonds. The P–C bond may be considered a better indicator of the Ru–P π -bonding character, as this is not influenced by the strength of the σ -donation.

It is hypothesised that *cis*-tach is a strong σ -donor ligand and lacks π -bonding capabilities, as it has no suitable orbitals. Therefore, in comparison to *fac*-ligands capable of π -back bonding, the average P–C bond length is expected to be longer for *cis*-tach complexes. The average Ru–Cl, Ru–P and P–C bond lengths for [1]PF₆, [2] and analogous compounds are given in Table 2.1.

In comparison to other neutral *facial*-coordinating ligands, the Ru–Cl bonds in [1]⁺ and [2] are significantly longer, with the exception of [RuCl₂(PPh₃)(ttcn)] which is comparable to *cis*-tach in this instance. Unsurprisingly, the replacement of the *cis*-tach ligand in [1]⁺ with η^5 -cyclopentadienyl results in a significantly longer Ru–Cl bond, due to the anionic nature of this ligand. The observed trend agrees with the hypothesis, for the *cis*-tach ligand is a strong σ -donor, thus weakening the Ru–Cl bond through the *trans*-influence.²¹¹ The η^6 -arenes are weaker donors, and are able to accept electron density from the metal by π back-bonding.

Complex	ref	Average bond length (Å)		
		Ru–Cl	Ru–P	P–C
[RuCl(PPh ₃) ₂ (η ⁵ -C ₅ H ₅)]	²¹²	2.448(1)	2.326(1)	1.842(3)
[1]PF ₆ [RuCl(PPh ₃) ₂ (<i>cis</i> -tach)] ⁺		2.420(1)	2.343(1)	1.848(3)
[RuCl(PPh ₃) ₂ (κ ³ -Tp)]	¹⁹⁸	2.412(2)	2.340(2)	1.830(1)
[RuCl(PPh ₃) ₂ (κ ³ -Tpm)] ⁺	²¹³	2.400(2)	2.363(2)	1.844(4)
[RuCl(PPh ₃) ₂ (η ⁶ - <i>p</i> -cym)] ⁺	²¹⁴	2.391(1)	2.385(1)	1.837(2)
[RuCl(PPh ₃) ₂ (η ⁶ -C ₆ H ₅ CH ₃)] ⁺	²¹⁵	2.390(3)	2.394(3)	1.827(2)
[2] [RuCl ₂ (PPh ₃)(<i>cis</i> -tach)]		2.453(1)	2.238(1)	1.842(2)
[RuCl ₂ (PPh ₃)(ttn)]	¹⁹⁹	2.452(2)	2.345(2)	1.834(3)
[RuCl ₂ (PPh ₃)(κ ³ <i>N</i> -P(py) ₃)]	²¹⁶	2.433(1)	2.352(1)	1.850(3)
[RuCl ₂ (PPh ₃)(η ⁶ - <i>p</i> -cym)]	²¹⁷	2.415(1)	2.344(1)	1.833(2)
[RuCl ₂ (PPh ₃)(η ⁶ -C ₆ Me ₆)]	²¹⁸	2.411(1)	2.360(2)	1.836(2)
[RuCl ₂ (PPh ₃)(η ⁶ -C ₆ H ₆)]	²¹⁹	2.409(2)	2.364(1)	1.833(2)

Table 2.1: Comparison of selected bond lengths for [1]PF₆ and [2] with analogous compounds. Average bond lengths are calculated as the weighted mean.²²⁰

The Ru–P bond lengths in both *cis*-tach complexes are shorter than in the complexes with other neutral *fac*-ligands, again with the exception of ttn. The largest difference in this parameter is seen with the *bis*-phosphane complexes, where the *cis*-tach complex [1]⁺ has a significantly shorter Ru–P bond than the η⁶-arene complexes, this is expected due to a possible greater degree of back-bonding from the metal. However, the hypothesis fails when applied to the dichlorido complexes, where the Ru–P bond of the *cis*-tach complex [2] is similar to that of η⁶-*p*-cymene. Surprisingly, there is no significant difference between the P–C bond length of the *cis*-tach complexes and other *fac*-ligands; this bond length may be more influenced by steric or other factors. Alternatively, the influence of the metal may be smaller than the precision of the values obtained. Therefore, no conclusions can be extrapolated from these data.

The parameters examined here suggest that *cis*-tach complexes may in some cases resemble those of Cp to a greater extent than the η⁶-arenes. This is therefore

expected to be reflected in the chemistry of ruthenium(II) *cis*-tach complexes. For example, chlorido ligands may be more easily displaced than for the η^6 -arenes, without the requirement for weakly coordinating anions to isolate cationic complexes. This property may be advantageous for the design of anti-tumour compounds without the need for potentially toxic counter-ions. Furthermore, it may assist in substitution of chlorido leaving groups with biologically-relevant species. This will be discussed later in this thesis.

2.4 Preparation of $[\{\text{RuCl}(\text{PPh}_3)(\textit{cis}\text{-tach})\}_2(\mu\text{-Cl})]^+$

In order to investigate the stability of [2] with time, a CD_2Cl_2 solution was monitored over a period of two weeks. Over this time, the resonance for [2] in the $^{31}\text{P}\{^1\text{H}\}$ NMR spectrum was observed to broaden. This effect was attributed to rapid inter-conversion of [2] with another species on the NMR timescale. Low temperature NMR studies did improve the appearance of the resonance of [2], although it was not possible to resolve two signals.

Addition of triphenylphosphane to the solution did not alter the width of the resonance. However, a sharpening in the signal was observed in the presence of $^n\text{Bu}_4\text{NCl}$ suggesting loss of a chlorido ligand as the origin of the observation. In the absence of any potential ligands, the exchange must involve the coordination of the solvent or another molecule of [2], forming a dimer. Addition of NaPF_6 resulted in the precipitation of sodium chloride, promoting the formation of [3] PF_6 . This complex is characterised by a sharp, singlet resonance in the $^{31}\text{P}\{^1\text{H}\}$ NMR spectrum at δ_{P} 60.2 ppm. The number of *cis*-tach resonances in the ^1H NMR spectrum indicated a C_1 symmetry environment of the ligand. The ligand also remained as a *fac*- κ^3 ligand, evidenced by the expected cyclohexane *J* coupling and chemical shifts of the amine protons. Although one NH resonance is upfield compared to the free ligand at δ_{H} 0.77 ppm, there is geminal coupling of $^2J_{\text{HH}} = 15.3$ Hz to a resonance at δ_{H} 1.61 ppm; it is proposed the upfield chemical shift is due to the local environment of this proton, such as participation in a hydrogen-bond.

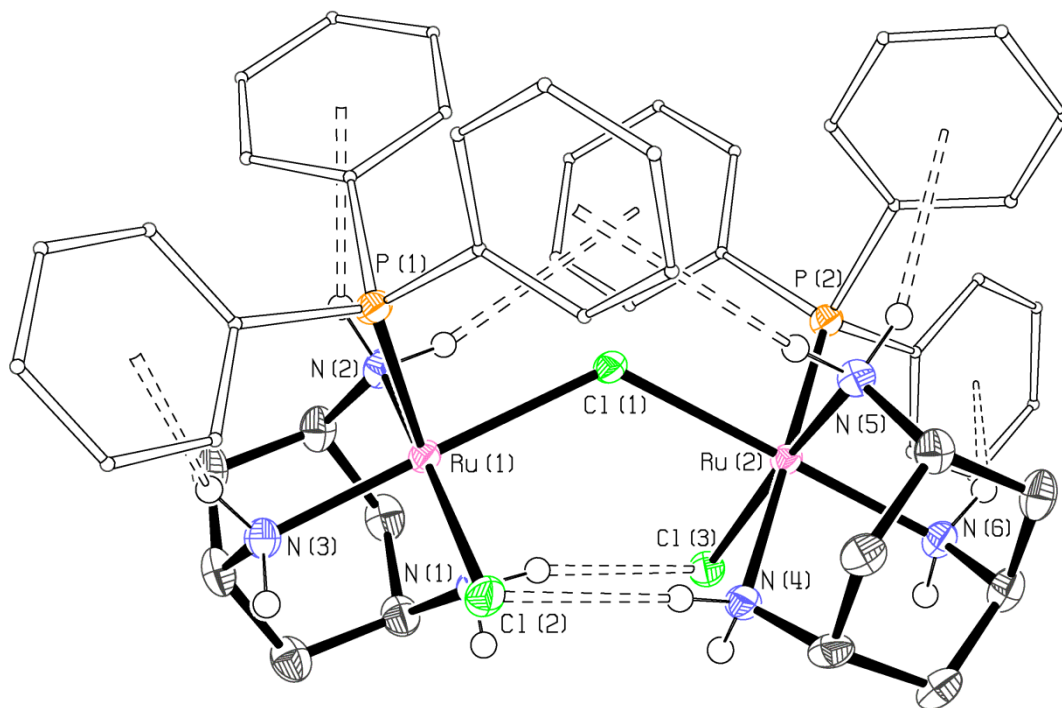


Figure 2.8: ORTEP (50% probability ellipsoids) diagram of the asymmetric unit of [3]BPh₄. Hydrogen atoms (except for amino hydrogens), solvent of crystallisation and counter ion are omitted for clarity. Selected bond lengths (Å) and angles (°): Ru(1)–N(1) 2.159(3), Ru(1)–N(2) 2.112(2), Ru(1)–N(3) 2.111(3), Ru(2)–N(4) 2.155(3), Ru(2)–N(5) 2.119(2), Ru(2)–N(6) 2.116(2), Ru(1)–P(1) 2.2664(8), Ru(2)–P(2) 2.2655(8), Ru(1)–Cl(1) 2.4606(8), Ru(2)–Cl(1) 2.4505(7), Ru(1)–Cl(2) 2.4392(8), Ru(2)–Cl(3) 2.4387(8), N(1)–Ru(1)–N(2) 86.44(10), N(1)–Ru(1)–N(3) 86.38(10), N(2)–Ru(1)–N(3) 91.72(10), N(3)–Ru(1)–Cl(1) 173.85(7), P(1)–Ru(1)–Cl(1) 89.74(3), P(1)–Ru(1)–Cl(2) 95.84(3), Cl(1)–Ru(1)–Cl(2) 97.35(3), Ru(1)–Cl(1)–Ru(2) 128.01(3). Selected hydrogen-bond (D–H...A–X) lengths (Å) and angles (°) D...A, H...A, D–H...A, H...A–X, H...X: N(1)–H(1a)...Cl(3)–Ru(2) 3.219(3), 2.39(4), 164(3), 88.0(8); N(4)–H(4c)...Cl(2)–Ru(1) 3.305(3), 2.45(4), 176(3), 89.6(8).

As ruthenium μ -dichlorido dimers are well known, this new species was considered to be a complex of that type. Although the *cis*-tach ligand is expected to exhibit C_s symmetry in the ^1H NMR spectrum, it was hypothesised that hydrogen-bonding may disrupt the symmetry. However, the $^{31}\text{P}\{^1\text{H}\}$ NMR integrations of the hexafluorophosphate anion suggest one equivalent of anion per two triphenylphosphane ligands, and does not agree with the hypothesis.

Attempts to obtain single crystals of $[\mathbf{3}]\text{PF}_6$ were unsuccessful, but employment of tetraphenylborate as the anion gave single crystals suitable for X-ray diffraction analysis. The resonance for the ruthenium complex in the $^{31}\text{P}\{^1\text{H}\}$ NMR spectrum of $[\mathbf{3}]\text{BPh}_4$ is identical to that for $[\mathbf{3}]\text{PF}_6$. Resonances in the ^1H NMR spectrum were observed to shift due to the effect of the anion. An ORTEP diagram of the structural solution and selected bond angles and lengths are given in Fig. 2.8.

The structural determination is of a mono μ -chlorido dimer and is consistent with the evidence from the ^1H and $\{^1\text{H}\}^{31}\text{P}$ NMR spectra. Prior to this, the ESI mass spectrum of this complex was unable to provide further insight into the identity of $[\mathbf{3}]^+$, due to similarity to the starting complex, $[\mathbf{2}]$. However, the molecular ion, $[\mathbf{3}]^+$ was observed in the ESI mass spectrum on further inspection with m/z 1091.1496 ($< 1\%$). The identity of the bulk material was confirmed as $[\mathbf{3}]\text{BPh}_4 \cdot 1\frac{1}{2}\text{CH}_2\text{Cl}_2$ by elemental analysis and reflects the composition of the crystal structure.

The assignment of $[\mathbf{3}]^+$ as $[\{\text{RuCl}(\text{PPh}_3)(\text{cis-tach})\}_2(\mu\text{-Cl})]^+$ is as the product of chlorido substitution by another molecule of $[\mathbf{2}]$ and the formation of a μ -chlorido bridge between the two metal centres. The mono- μ -chlorido bridging mode is uncommon for ruthenium and is only achievable in this case due to the ability of *cis*-tach to form hydrogen-bonding interactions between the two units, stabilising the structure. Few X-ray crystal structures of single-molecule diruthenium(II) complexes with a similar μ -chlorido motif have been reported.^{221, 222} Most of these feature bulky ligands around the metals rather than hydrogen bonds, although the X-ray structure of $[\{\text{Ru}(\text{NCMe})_5\}_2(\mu\text{-Cl})](\text{OTf})_3$ has been reported.²²³

The asymmetric unit in the resulting crystal structure consists of one $[\mathbf{3}]\text{BPh}_4$ with one and a half molecules of dichloromethane, disordered across two sites. There is a

significant peak of residual electron density, believed to be due to the ruthenium atoms from a minor twin. The ruthenium *cis*-tach moiety displays the same structural distortions as [1]PF₆ and [2] and the ruthenium centre is again a distorted octahedron. The hydrogen-bonding network and the resulting geometrical constraints is responsible for the unusually large Ru(1)–Cl(2)–Ru(2) angle of 128.01(3)° compared to the ideal 90°.²⁰⁹ Four hydrogen-bonds complete the bridging structure, with the two ruthenium centres rotated by 104.61° around the Ru(1)–Ru(2) axis. A minor stabilisation is provided from two mutual NH– π inter-nuclear hydrogen-bonds (type V) between the *cis*-tach and a triphenylphosphane. Furthermore stronger hydrogen-bonds are formed between the *cis*-tach and chlorido ligands, with Ru–Cl...H angles close to the ideal 90°. The structure is completed by two hydrogen-bonds between the amine and phenyl groups around each metal centre with bond lengths and angles similar to that of [2]. The resulting structure is in agreement with the recorded NMR spectra, where both *cis*-tach ligands are within a C₁ environment.

Conclusions

It has been shown that [2], over a period of weeks, forms an equilibrium with a new species, [3]⁺, formed from the loss of a chlorido ligand and coordination of a second molecule of [2]. The identity of this new complex was determined by single crystal X-ray crystallography. The two ruthenium centres are bonded by a single μ -chlorido bridging ligand, with mutual hydrogen-bonding systems between the two monomer units aiding stabilisation of the structure. The structural motif of the dimeric [3]BPh₄ is uncommon for ruthenium(II) compounds, as complexes containing a second μ -ligand are the norm. This effectively demonstrates the different coordination chemistry accessible with *cis*-tach in comparison to the η^6 -arene ligands.

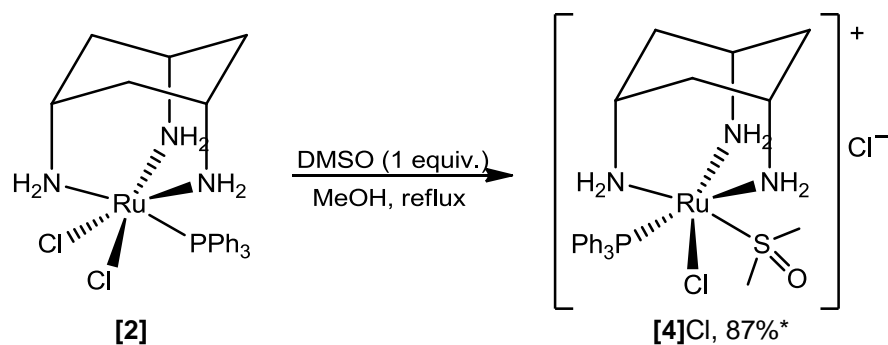
2.5 Synthesis and Reactivity of Solvent Complexes

2.5.1 Dimethylsulfoxide Complexes

Complex [2] was of great interest for biological evaluation due to the simplicity of the molecule, and presence of a stable phosphane ligand. However, poor water solubility hindered assessment of [2] by MTT assay. Dimethylsulfoxide (DMSO) is a common solvent used to aid solubility of compounds in aqueous media for biological evaluation, due to its low toxicity. Therefore, the solvation of [2] in DMSO was investigated with the view of obtaining an aqueous solution of [2].

A resonance at δ_p 49.7 in the $^{31}\text{P}\{^1\text{H}\}$ NMR spectrum of [2] recorded in d_6 -DMSO confirmed the presence of a single ruthenium phosphane complex; liberated PPh_3 was not observed. The *cis*-tach protons in the ^1H NMR spectrum exhibited resonances corresponding to a species in a C_1 symmetry environment, in contrast to the C_s symmetry of the starting complex. It was therefore hypothesised that a new species had formed, from exchange of a chlorido ligand with the solvent to give $[\text{RuCl}(\text{DMSO})(\textit{cis}\text{-tach})(\text{PPh}_3)]\text{Cl}$, [4]Cl.

The direct dissolution of [2] in DMSO followed by dilution with water was not desirable for the preparation of samples for *in vitro* biological evaluation. A molecule of dichloromethane—a highly toxic compound—in the crystallisation of [2] would adversely affect any results obtained.²²⁴ To overcome this problem, [4]Cl was prepared and isolated prior to any *in vitro* experiments. This was achieved by heating [2] under reflux in methanol with one equivalent of DMSO. This gave the cationic complex [4]Cl in good yield (87%, Scheme 2.5) with analytical purity as $[\text{4}]\text{Cl} \cdot \frac{1}{2}\text{DMSO}$.



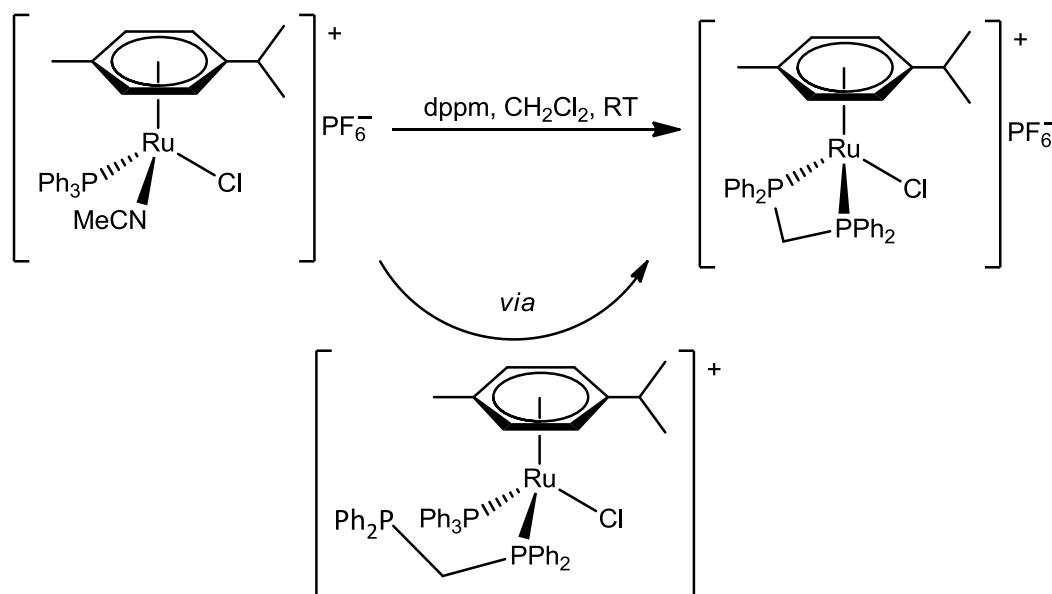
Scheme 2.5: Synthetic procedure for obtaining the DMSO complex [RuCl(DMSO-*S*)(*cis*-tach)(PPh₃)]Cl (**[4]Cl**) from the reaction between **[2]** and one equivalent of DMSO. *Isolated yield.

ESI mass spectrometry confirmed the identity of **[4]**⁺, with a molecular ion observed at *m/z* 606.1, displaying the expected isotope pattern. This signal was observed without fragmentation or other species. The coordination of DMSO was evidenced by resonances at δ_H 3.20 and 2.69 ppm for the two methyl groups of the ligand in the ¹H NMR spectrum. These chemical shifts are indicative of an *S*-bound coordination mode.²²⁵ The inequivalence of the DMSO methyl groups reflects the *C*₁ symmetry environment of *cis*-tach. Therefore, **[4]**⁺ is chiral and expected to be a racemic mixture of the *R*- and *S*-enantiomers. The water solubility of **[4]Cl** is improved compared to **[2]**; first, the complex is ionic, and therefore capable of forming electrostatic interactions with water. Secondly, both the *cis*-tach and DMSO ligands are capable of participating in hydrogen-bonds with the solvent, further stabilising the solvated state. This complex was evaluated for *in vitro* activity and is discussed later.

2.5.2 Acetonitrile Complexes

The synthetic diversity available from **[2]** was explored with the aim of preparing complexes containing common solvents as ligands. These solvent complexes may allow a convenient synthetic methodology for the preparation of complexes incorporating other ligands by displacement of acetonitrile. Not only may other κ¹ ligands be introduced, but complexes with chelating ligands may be accessible. Complexes of this type have been demonstrated in the preparation of η⁶-arene

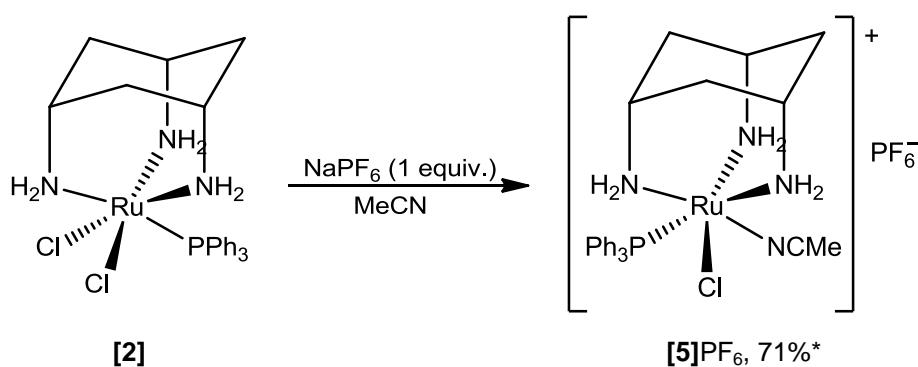
complexes with chelating diphosphanes (Scheme 2.6). The acetonitrile is substituted by the diphosphane ligand and results in the subsequent displacement of the triphenylphosphane and ring closure, yielding the chelate complex.²²⁶



Scheme 2.6: Preparation of η^6 -*p*-cymene ruthenium(II) complexes with chelating ligands such as dppm from a triphenylphosphane/acetonitrile precursor. The diphosphane coordinates by displacement of the acetonitrile ligand forming a pendant-phosphane complex. This is followed by ring-closure with substitution of triphenylphosphane, promoted by the chelate effect.

The applicability of this method in the preparation of new *cis*-tach complexes was investigated. The dissolution of **[2]** in acetonitrile was expected to readily yield $[\text{RuCl}(\text{NCMe})(\text{cis-tach})(\text{PPh}_3)]^+$, as the chloride ligand is believed to be easily displaced. The neutral complex **[2]** was found to be poorly soluble in acetonitrile, requiring treatment with an equimolar amount of sodium hexafluorophosphate to facilitate the formation of an acetonitrile complex in solution. After 30 min stirring at room temperature, the product was isolated by removal of the solvent *in vacuo*. Dissolving the residue in DCM allowed for the removal of NaCl by filtration and the product was precipitated by addition of diethyl ether to this solution.

The formation of a new species from this reaction is evidenced by a resonance at δ_P 60.61 ppm in the $^{31}\text{P}\{^1\text{H}\}$ NMR spectrum, recorded in CD_2Cl_2 . Similar to the reaction of **[2]** with DMSO, resonances suggesting a C_1 *cis*-tach symmetry environment were evident in the ^1H NMR spectrum as well as a resonance corresponding to the coordinated acetonitrile ligand at δ_H 2.29 ppm. The identity of the new complex is proposed as $[\text{RuCl}(\text{NCMe})(\text{cis-tach})(\text{PPh}_3)]\text{PF}_6$, **[5]** PF_6 (Scheme 2.7).



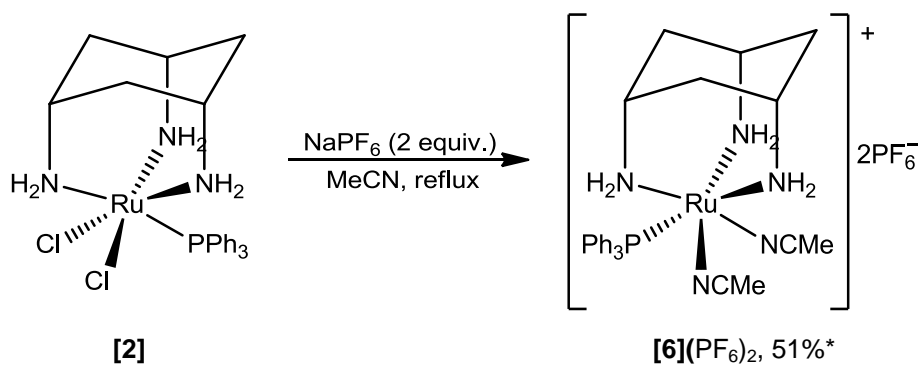
Scheme 2.7: Synthesis of the acetonitrile complex $[\text{RuCl}(\text{NCMe})(\text{cis-tach})(\text{PPh}_3)]\text{PF}_6$ (**[5]** PF_6) from chloride metathesis of **[2]** with NaPF_6 in acetonitrile. *Isolated yield.

During isolation of this complex, washing with diethyl ether resulted in minor loss of acetonitrile and small quantities of the dimeric species **[3]** PF_6 was observed in the $^{31}\text{P}\{^1\text{H}\}$ NMR spectrum. The identity of **[5]** PF_6 was supported by the observation of the expected molecular ion (m/z 569.11) and isotope pattern in the ESI mass spectrum. Elemental analysis of the isolated compound indicated the presence of residual dichloromethane and diethyl ether from the synthesis, but a sample of sufficient analytical purity could not be obtained, the largest discrepancy being in nitrogen content (found 6.61% vs. calc. 7.06%).

Milder conditions are required for the preparation of **[5]** PF_6 from **[2]** (room temperature) in comparison to the analogous reaction with $[\text{RuCl}_2(\eta^6\text{-}p\text{-cymene})(\text{PPh}_3)]$,²²⁶ where the *p*-cymene complex must be heated at reflux (80 °C+) in acetonitrile. The difference in the required conditions reflects the more labile

chlorido ligand in the *cis*-tach complexes, as hypothesised from the comparison of structural parameters in [1]PF₆ and [2] with analogous η⁶-arene complexes, owing to the stronger σ-donor properties of the *cis*-tach ligand.

Displacement of the second chlorido ligand with acetonitrile was possible by heating [2] at reflux in acetonitrile with two equivalents of NaPF₆ for 4h (Scheme 2.8). The resulting complex was isolated in the same manner as [5]PF₆. The ³¹P{¹H} NMR spectrum of the product in CD₂Cl₂ contains a single resonance from the triphenylphosphane ligand at δ_P 55.93 ppm. The coordination of a second acetonitrile is evidenced by the integration of the resonance for coordinated acetonitrile at δ_H 2.40 ppm, corresponding to two ligands per *cis*-tach. This is reflected in the restoration of *cis*-tach resonances of a C_s symmetry environment. This new species is the product of displacement of the chlorido ligands in [2] by metathesis with NaPF₆ in acetonitrile and coordination of two solvent molecules, giving [Ru(NCMe)₂(*cis*-tach)(PPh₃)](PF₆)₂ ([6](PF₆)₂, Scheme 2.8) .



Scheme 2.8: Displacement of both chlorido ligands in [RuCl₂(*cis*-tach)(PPh₃)] with acetonitrile by metathesis with NaPF₆ with heating at reflux, giving the solvent complex [Ru(NCMe)₂(*cis*-tach)(PPh₃)](PF₆)₂, [6](PF₆)₂. *Isolated yield.

The ESI mass spectrum of [6](PF₆)₂ is in agreement with the proposed identity with a single signal observed at *m/z* 720.14, corresponding to [7+PF₆]⁺ (100%). Displacement of the chlorido ligand is again achieved with relative ease compared to other *fac*-ligands. For example, the analogous reaction with [RuCl₂(ttn)(PPh₃)] requires use of light-sensitive silver salts, which are more reactive than their sodium equivalents, as well as heating the reaction at reflux.²²⁷

2.5.3 Reactivity of the Acetonitrile Complexes

The reactivity of the acetonitrile complexes was investigated with methylenebis(diphenylphosphane) (dppm), a chelating diphosphane, with the aim to prepare $[\text{RuCl}(\text{dppm})(\text{cis-tach})]\text{PF}_6$ from displacement of the acetonitrile and triphenylphosphane ligands in $[\mathbf{5}]\text{PF}_6$. A solution of $[\mathbf{5}]\text{PF}_6$ with an excess of dppm in CD_2Cl_2 was heated at 50°C in a sealed NMR tube and monitored by NMR spectroscopy. After 45 minutes, a large quantity of a new species, $[\mathbf{7}]\text{PF}_6$, was observed in the $^{31}\text{P}\{^1\text{H}\}$ NMR spectrum (Fig. 2.9), with integration corresponding to approximately 40% conversion.

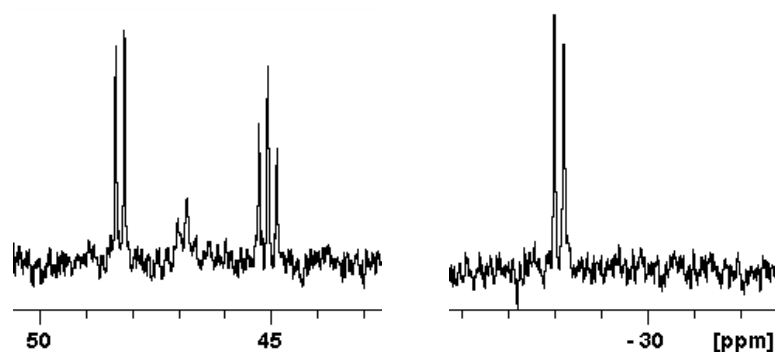


Figure 2.9: Resonances assigned to $[\mathbf{7}]\text{PF}_6$ in the resulting $^{31}\text{P}\{^1\text{H}\}$ NMR spectrum of the reaction between $[\mathbf{5}]\text{PF}_6$ and dppm in CD_2Cl_2 after 45 minutes at 50°C . The two resonances at δ_p 45–48 ppm indicate that there are two coordinated phosphane ligands in the complex, as well as a pendant phosphane, evidenced by the resonance at δ_p –28 ppm.

Two of the three phosphorus environments in $[\mathbf{7}]\text{PF}_6$ occur between δ_p 45–48 ppm; these chemical shifts are indicative of coordination to a metal centre. The two resonances are coupled to each other by a $^2J_{\text{PP}}$ of 30 Hz. The doublet of doublets is further coupled to the ^{31}P nucleus with chemical shift of –28 ppm with a $^2J_{\text{PP}}$ coupling of 33.5 Hz. This resonance appears as a triplet due to the similarity of the two coupling constants. The resonance at δ_p –28 ppm is proposed to indicate a pendant phosphane. Together with the absence of liberated triphenylphosphane, this evidence suggests the dppm ligand has coordinated in a κ^1 fashion as $[\text{RuCl}(\kappa^1\text{-dppm})(\text{cis-tach})(\text{PPh}_3)]\text{PF}_6$ (Fig. 2.10).

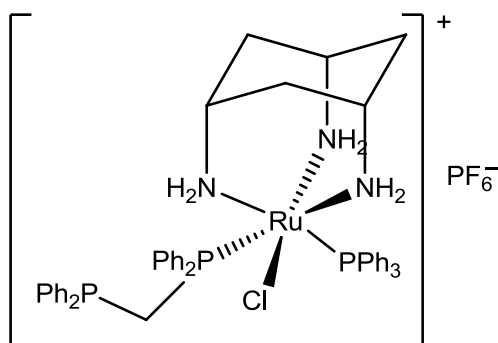


Figure 2.10: Proposed structure of the pendant-phosphane complex $[\text{RuCl}(\kappa^1\text{-dppm})(\text{cis-tach})(\text{PPh}_3)]\text{PF}_6$ (**[7]** PF_6), formed in the reaction between **[5]** PF_6 and dppm. Displacement of the triphenylphosphane ligand and ring-closure is not observed on further heating. .

The diposphane is still to undergo ring closure by displacement of the triphenylphosphane ligand to give the target complex $[\text{RuCl}(\text{dppm})(\text{cis-tach})]\text{PF}_6$. However, further heating in an attempt to obtain the target complex $[\text{RuCl}(\text{dppm})(\text{cis-tach})]\text{PF}_6$ resulted in the degradation of the sample.

2.5.4 Conclusions

The preparation of solvent complexes from **[2]** has expanded the accessible chemistry of ruthenium *cis-tach* compounds with a DMSO and two acetonitrile based complexes. However, employment of these complexes in the preparation of complexes with desirable ligands, such as chelating phosphanes, was met with difficulty. Therefore, only complexes incorporating the triphenylphosphane ligand are accessible from **[2]** due to problematic displacement of the phosphane. Therefore, alternative synthetic methods must be investigated to expand the library of ruthenium (II) *cis-tach* complexes.

2.6 *In Vitro* Biological Evaluation

As this thesis is concerned with the biological activity of ruthenium(II) *cis*-tach complexes, it was of interest to evaluate the triphenylphosphane complexes presented in this chapter. Compounds were only selected if analytically pure samples were attainable. Furthermore, complexes which displayed readily labile phosphane ligands, such as [1]Cl or insufficient water solubility were excluded from the study. Consequently, only one complex, [4]Cl, was chosen for evaluation. *In vitro* growth inhibition assays were performed using the MTT colorimetric assay with the A549 lung adenocarcinoma and A2780 ovarian carcinoma cell lines.²²⁸ The determined IC₅₀ values are given in Table 2.2.

Compound	A549		A2780	
	IC ₅₀ (μM)	slope	IC ₅₀ (μM)	slope
cisplatin	2.70(5)	0.92(5)	0.43(1)	1.36(3)
[4]Cl	194(4)	2.00(5)	67.8(10)	1.95(6)

Table 2.2: Biological evaluation of cisplatin and [RuCl(DMSO-*S*)(*cis*-tach)(PPh₃)]Cl ([4]Cl) in the A549 (lung) and A2780 (ovarian) tumour cell lines. The IC₅₀ is defined as the concentration of drug required to inhibit 50% of cell growth over a 72 h incubation.

Compound [4]Cl displayed weak anti-proliferative activity (ability to inhibit growth) in both the A549 and A2780 cell lines on comparison to the clinically used drug cisplatin. Furthermore, the dose-response profile is steeper than in cisplatin, therefore a smaller (logarithmic) concentration range spans the activity profile of the complex. Thus, the ability to control the dose in a clinical application is limited in comparison to cisplatin. Most importantly, although weakly active, [4]Cl represents the possibility for ruthenium (II) *cis*-tach complexes to be highly active anti-cancer agents with further design and development of the complexes. Therefore, structural modifications, such as [RuCl(dppm)(*cis*-tach)]⁺, the target of the reaction between [5]PF₆ and dppm, must be investigated to advance the design of ruthenium *cis*-tach complexes. In addition, the racemic mixture obtained in the preparation of the chiral

complex [4]Cl may contain only a single biologically-active enantiomer. Further development of such compounds will require investigations into the effect of the different enantiomers in a biological environment. However, complex [4]Cl has demonstrated the potential for ruthenium(II) *cis*-tach complexes to act as anti-tumour drugs, holding some promise for further developments.

2.7 Chapter Conclusions

In summary, the coordination chemistry of *cis*-tach with ruthenium has been established. *cis*-tach reacts readily with $[\text{RuCl}_2(\text{PPh}_3)_3]$ to yield the cationic species $[\text{RuCl}(\textit{cis}\text{-tach})(\text{PPh}_3)_2]\text{Cl}$ [1]Cl. The ligand was confirmed to coordinate in a κ^3 -fashion as a six electron *facial*-coordinating ligand. On standing for a period of time in dichloromethane [1]Cl undergoes a charge neutralisation reaction with chloride to $[\text{RuCl}_2(\textit{cis}\text{-tach})(\text{PPh}_3)]$, [2] with loss of PPh_3 . Furthermore, a dimerisation process is observed with complex [2], whereby abstraction of a chlorido ligand and subsequent coordination of another molecule of [2] forms $[\{\text{RuCl}(\textit{cis}\text{-tach})(\text{PPh}_3)\}_2(\mu\text{-Cl})]^+$ [3]⁺. A dimer formed by single μ -chlorido bridge is rare in ruthenium(II) chemistry.

The bond lengths in the X-ray structural solutions of the complexes [1] and [2] suggest that *cis*-tach is a strong σ -donor, resulting in increased localisation of electron density on the metal in comparison to the η^6 -arenes and is comparable to that of anionic ligands, such as Cp. Therefore, the subsequent chemistry of ruthenium *cis*-tach complexes is expected to resemble that of Cp with a greater likelihood for chlorido dissociation.

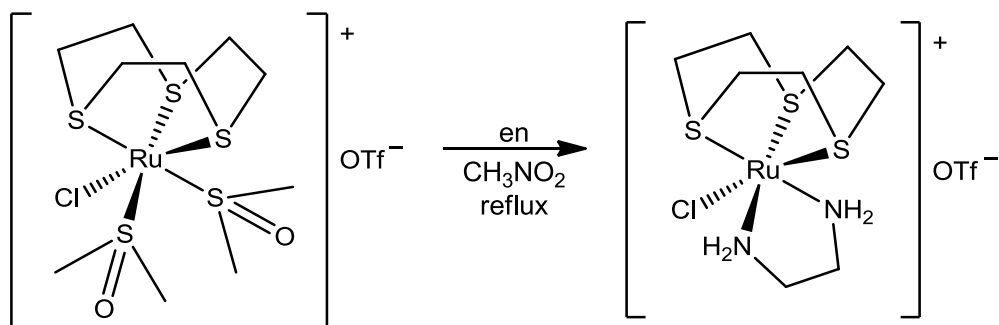
The preparation of solvent complexes based on [2] provided an increased synthetic diversity. The inclusion of the DMSO ligand in [4]Cl was observed to significantly increase water solubility in comparison to the parent compound. The anti-proliferative activity [4]Cl was shown to have poor activity against the cancer cell lines, yet demonstrated the potential for ruthenium(II) *cis*-tach complexes to act as cytotoxic agents, proving promise for the design of future compounds.

Use of acetonitrile as a synthetic precursor for further compounds was investigated, however displacement of the triphenylphosphane ligand proved difficult. Therefore, alternative synthetic methods must be investigated, whereby a common synthetic precursor to a variety of compounds is prepared. This forms the basis of the next chapter.

Chapter 3. Ruthenium(II) *cis*-tach Dimethylsulfoxide Precursor Complexes

3.1 Introduction

The preparation of ruthenium(II) *cis*-tach complexes by use of a common precursor with a desired ligand has the potential to offer a diverse library of compounds. This may be achieved by the incorporation of labile ligands providing a template for the target complex. The DMSO ligand is often employed in synthetic chemistry for this purpose.²²⁹ For example, use of 1,4,7-trithiacyclononane (ttcn) dimethylsulfoxide complexes by Alessio, Dyson and co-workers permitted the preparation of a series of moderately cytotoxic ttcn complexes (Scheme 3.1) containing PTA, en, bipy and imidazole.^{161, 162} These ligands had previously been employed in the η^6 -arene family of compounds for the development of anti-cancer compounds with varying degrees of success.^{78, 116, 163, 230} More recently, Alessio reported a series of ruthenium(II) *fac*-(DMSO-*S*)₃ complexes to replace the Ru-ttcn moiety. However, this resulted in a loss of activity, demonstrating the importance of the identity of the *fac*-ligand.²³¹



Scheme 3.1: Preparation of [RuCl(en)(ttcn)]OTf from the precursor [RuCl(DMSO-*S*)₂(ttcn)]OTf by displacement of the DMSO-*S* ligands with 1,2-ethylenediamine (en).

The use of sulfoxide ligands in ruthenium antitumor complexes was originally pioneered by Alessio, Sava and co-workers with *tetrakis*-dimethylsulfoxide halide compounds. The complex [*cis*-RuCl₂(DMSO-*S*)₃(DMSO-*O*)] exhibited antitumor activity *in vivo* against metastases, and was demonstrated to bind DNA *in vitro*, with

favourable interactions with guanine residues.^{232, 233} Although this complex displayed weak *in vivo* antitumor activity, use of [*trans*-RuCl₂(DMSO-S)₄] allowed for increased activity at doses of up to twenty times lower than the *cis*-isomer.²³⁴ The DMSO ligand was incorporated by Alessio and Sava into the imidazole ruthenium(III) complex [imiH][*trans*-RuCl₄(imi)₂], originally developed by Keppler and co-workers.⁶⁵ It was found that Na[*trans*-RuCl₄(DMSO-S)(imi)] exhibited anti-metastatic activity comparable to that of cisplatin.²³⁵ The imidazolium salt of this complex, NAMI-A entered and recently successfully completed Phase I clinical trials.⁵⁵

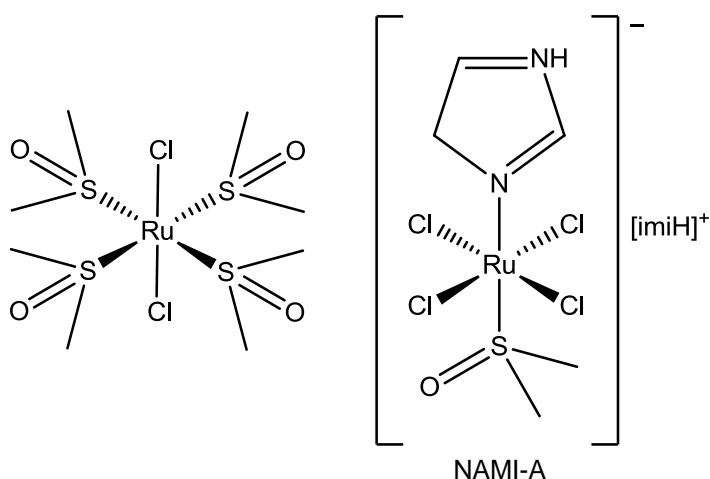


Figure 3.1: Structures of two ruthenium DMSO complexes assessed for antitumor activity, the early complex [*trans*-RuCl₂(DMSO-S)₄] (left) and the anti-metastatic agent [imiH][*trans*-RuCl₄(DMSO-S)(imi)] (NAMI-A) which has entered clinical trials (right).

To further develop ruthenium(II) *cis*-tach complexes, it was proposed to explore the coordination chemistry of *cis*-tach with dimethylsulfoxide containing precursors. The formation of an analogous complex to [RuCl(DMSO-S)₂(ttcn)]OTf may allow for the introduction of a wide variety of co-ligands into the coordination sphere of the metal. Given the precedent of ruthenium sulfoxide complexes in the literature displaying potency in the treatment of tumors, we were also interested in the *in vitro* biological activity of these novel sulfoxide complexes as well as understanding the mechanism of aquation reactions occurring in aqueous solution.

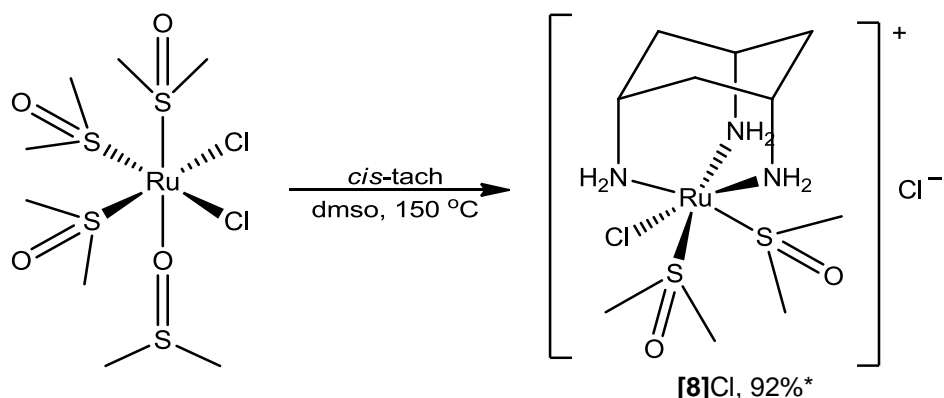
3.2 Preparation of [RuCl(DMSO-S)₂(*cis*-tach)]Cl

3.2.1 Synthesis and Characterisation

The preparation of ruthenium(II) DMSO complexes often employs [*cis*-RuCl₂(DMSO-*O*)(DMSO-*S*)₃], which is readily synthesised from the reaction of RuCl₃.xH₂O with DMSO.²³⁶ Successful treatment of this ruthenium precursor with *facially*-coordinating ligands was achieved with [9]ane-S₃ (1,4,7-trithiacyclononane), tpm (trispyrazolylmethane) and tacn (1,4,7-triazacyclononane), to generate [RuCl₂(DMSO-*S*)([9]ane-S₃)], [RuCl₂(DMSO-*S*)(tpm)] and [RuCl(DMSO-*S*)₂(tacn)]Cl respectively.^{227, 229, 237} It was hypothesised that the reaction of *cis*-tach with [*cis*-RuCl₂(DMSO-*O*)(DMSO-*S*)₃] would follow a similar route.

The conditions employed for the reaction of *cis*-tach with [*cis*-RuCl₂(DMSO-*O*)(DMSO-*S*)₃] was inspired by a similar method employed for the preparation of the analogous tacn complex.²³⁷ *cis*-tach and [*cis*-RuCl₂(DMSO-*O*)(DMSO-*S*)₃] were heated in DMSO at 130°C for 30 minutes, yielding a single product. The coordination of *cis*-tach as a κ³ *fac*-ligand to the metal is evidenced by the ¹H NMR spectrum of the material isolated by addition of ethyl acetate. Resonances accounting for all six amine protons, assigned by the absence of cross-peaks in the 2D ¹H/¹³C correlation spectrum, were detected in *d*₄-methanol, suggesting exchange between the protic solvent and the amines does not occur rapidly. Therefore the three nitrogen electron lone pairs are involved in coordination to the metal, as they are unable to participate in rapid proton exchange mechanisms with the solvent. Furthermore, all amine protons are shifted downfield (δ_H 3.75–4.5 ppm) in comparison to a non-coordinated amine (δ_H ~1 ppm). A total of nine proton environments are observed for *cis*-tach in the ¹H NMR spectrum, suggesting a C_s symmetry environment. Additionally, a single resonance for coordinated DMSO was present at δ_H 3.33 ppm with a relative integration corresponding to two ligands per complex. A single chlorido ligand is expected to complete the eighteen valence electron, six-coordinate complex [RuCl(DMSO)₂(*cis*-tach)]⁺ ([**8**]⁺, Scheme 3.2) This is evidenced by the observation of the molecular ion in the ESI mass spectrum at *m/z* 422.0271 with expected ruthenium and chlorine isotope pattern. The complex

was isolated with a chloride counter-ion by the addition of ethyl acetate to the reaction mixture in DMSO and cooling to -20°C as **[8]**Cl with analytical purity and in excellent yield (92%).



Scheme 3.2: Synthesis of $[\text{RuCl}(\text{DMSO})_2(\text{cis-tach})]\text{Cl}$ (**[8]**Cl) from $[\text{cis-RuCl}_2(\text{DMSO-O})(\text{DMSO-S})_3]$. It is proposed that two DMSO ligands coordinate to the metal centre *via* the sulfur atoms. * Isolated yield.

As DMSO is capable of coordinating to a metal through either the sulfur or oxygen atom, identification of the donor atom was of importance. ^1H NMR and IR spectroscopy techniques are both capable of providing evidence for the coordination mode of the dimethylsulfoxide ligand. The chemical shift of the DMSO ligands in the ^1H NMR spectrum at δ_{H} 3.33 ppm is indicative of an *S*-bound coordination mode.²²⁵ The IR band for the sulfur-oxygen bond stretching frequency of the bound dimethyl sulfoxide, $\nu(\text{S}=\text{O})$, appears at 1061 cm^{-1} at the lower boundary for *S*-DMSO. The difference in the stretching frequencies between *O*- (878–1035) and *S*- (1070–1233) geometries relate to the bonding character of the *S*–*O* bond.²³⁸ Oxygen coordination stabilises the resonance structure, S^+-O^- , decreasing the bond order, and thus $\nu(\text{S}=\text{O})$. Sulfur coordination stabilises the *S*=*O* electronic structure, increasing the bond order and $\nu(\text{S}=\text{O})$.²³⁹ Although the band appears outside of the literature values for *S*-DMSO complexes, complexes with other *fac*-coordinating ligands in place of *cis-tach* exhibit similar stretching frequencies. For example, the $\nu(\text{S}=\text{O})$ band in $[\text{RuCl}(\eta^5\text{-C}_5\text{Me}_5)(\text{DMSO-S})_2]$ is observed at 1060 cm^{-1} .²⁴⁰ The assignment of the DMSO ligand as a sulfur donor is consistent with many other ruthenium complexes of this type.^{166, 229}

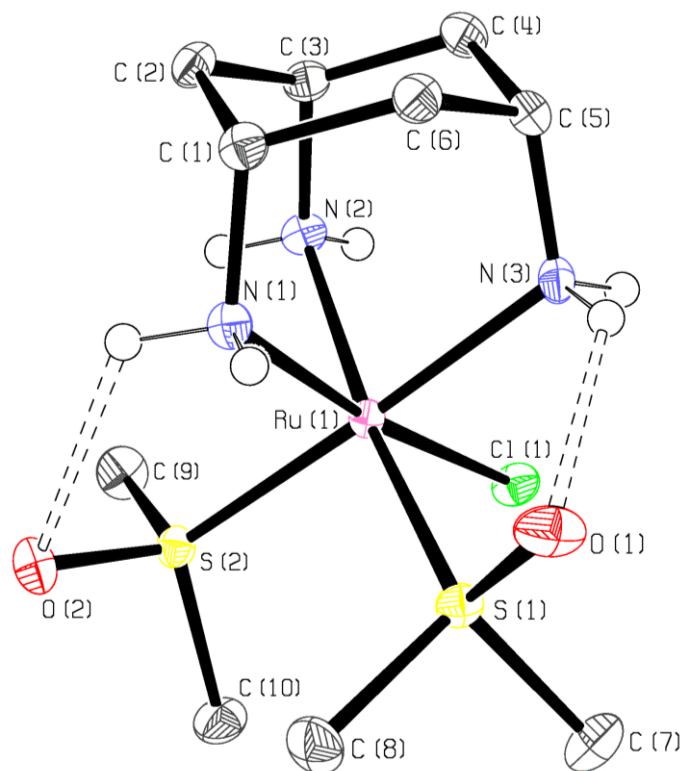


Figure 3.2: ORTEP (50% probability ellipsoids) diagram of $[8]PF_6$. Hydrogen atoms (except for amino hydrogens) and the counter ion are omitted for clarity. Selected bond lengths (\AA), angles ($^\circ$) and torsions ($^\circ$): Ru(1)–N(1) 2.1255(18), Ru(1)–N(2) 2.137(2), Ru(1)–N(3) 2.135(2), Ru(1)–Cl(1) 2.4170(6), Ru(1)–S(1) 2.2581(5), Ru(1)–S(2) 2.2524(5), S(1)–O(1) 1.5011(18), S(2)–O(2) 1.4883(17), N(1)–Ru(1)–N(2) 88.30(8), N(1)–Ru(1)–N(3) 88.49(8), N(2)–Ru(1)–N(3) 85.89(8), S(1)–Ru(1)–S(2) 97.49(2), S(1)–Ru(1)–Cl(1) 96.04(2), S(2)–Ru(1)–Cl(1) 92.37(6), N(1)–Ru(1)–Cl(1) 173.36(5), Ru(1)–S(1)–O(1) 109.62(7), Ru(1)–S(2)–O(2) 116.79(7), N(3)–Ru(1)–S(1)–O(1) 29.93(11), N(1)–Ru(1)–S(2)–O(2) $-12.40(11)$. Selected hydrogen-bond (D–H...A–X) lengths (\AA) and angles ($^\circ$) D...A, H...A, D–H...A, H...A–X: N(1)–H(1a)...O(2)–S(2) 3.143(3) 2.53(3) 124(2) 88.3 (7), N(3)–H(3b)...O(1)–S(1) 2.852(3) 2.11(3) 130(3) 95.2(9).

3.2.2 X-Ray Crystallography

Slow evaporation of a methanol solution of [8]PF₆, obtained from chloride metathesis with sodium hexafluorophosphate followed by filtration, gave crystals suitable for X-ray diffraction analysis. An ORTEP diagram and selected bond angles, lengths and torsions, as well as hydrogen-bond parameters are given in Fig. 3.2.

As for [1]PF₆ and [2], the obtained crystal structure of [8]PF₆ is that of a distorted octahedron. The ruthenium *cis*-tach moiety is again a distorted adamantane structure due to the geometrical constraints of the *cis*-tach ligand, resulting in the three N–Ru–N angles of less than the idealised 90°. The three angles of the L₃ ligand-set of DMSO and chlorido are greater than 90°, most prominent in the S(1)–Ru(1)–S(2) bite angle of 97.49(2)°. This is due to the Ru–N bond constraints of *cis*-tach, where the three “L₃” ligands are able to occupy a larger spatial region around the metal. The hexafluorophosphate anion, omitted from the ORTEP plot for clarity, is disordered between two sites in the asymmetric unit at equal occupancy.

The two DMSO ligands are rotated towards the *cis*-tach amine groups to participate in intramolecular hydrogen-bonds. The DMSO ligand containing O(1) is rotated to occupy the location between N(3) and N(1). However, the sulfoxide group is directed more towards N(3). This is evidenced by a shorter torsion angle and H...O distance of 29.93(11)° and 2.53(3) Å for O(1)/N(3) compared to –58.72(10)° and 2.77(3) Å for O(1)/N(1). When taking into account the directionality of DMSO ligand towards the hydrogen atom, the torsion angle is –3(2)° between H(3b) and O(1), suggesting an exclusive intramolecular hydrogen-bond of O(1) with N(3). The second DMSO ligand [containing O(2)] participates in intramolecular hydrogen-bonding with N(2) with a torsion angle of –12.40(11)°. Both of these intramolecular interactions have an S–O...H angle of 95.2(9) and 88.3(7)° respectively. The absence of a hydrogen-bond between N(1) and O(1) is further evident by the comparatively small S–O...H angle of 75.3(6)°.

In addition to these intramolecular interactions, two different intermolecular hydrogen-bonds between the cationic units are present in the crystal structure. These interactions form a two dimensional sheet structure, as shown in Fig. 3.3. The larger structure is comprised of a repeating set of four cations in a rhombical geometry with an angle of $67.5(1)^\circ$. Each of the cation layers is separated by hexafluorophosphate anions, which also participate in hydrogen-bonding interactions with *cis*-tach. Finally, the layers are off-set from those adjacent by a translation corresponding to one cation, or half of the rhomboidal unit.

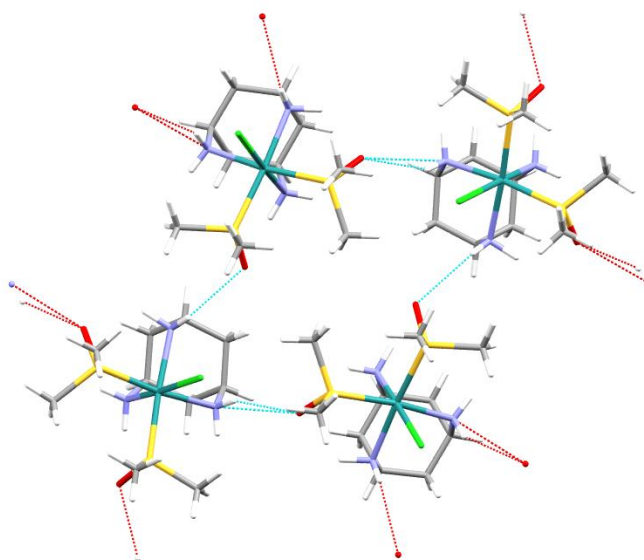


Figure 3.3: Sheet-like structure formed from intermolecular hydrogen-bonds between the *cis*-tach amine protons and DMSO oxygen of an adjacent complex in the crystal packing of **[8]**PF₆. Hydrogen bonds are drawn as D...A.

3.2.3 Conclusions

[8]Cl was prepared by reaction of $[cis\text{-RuCl}_2(\text{DMSO-}S)_3(\text{DMSO-}O)]$ with *cis*-tach and characterised by NMR and IR spectroscopy, mass spectrometry and single crystal X-ray diffraction, with the hexafluorophosphate derivative used in the latter. Two DMSO-*S* ligands were retained in the complex along with a single chlorido, giving a cationic species without the use of weakly coordinating anions. The biological activity of this complex and its aqueous chemistry forms the basis for the second half of this chapter.

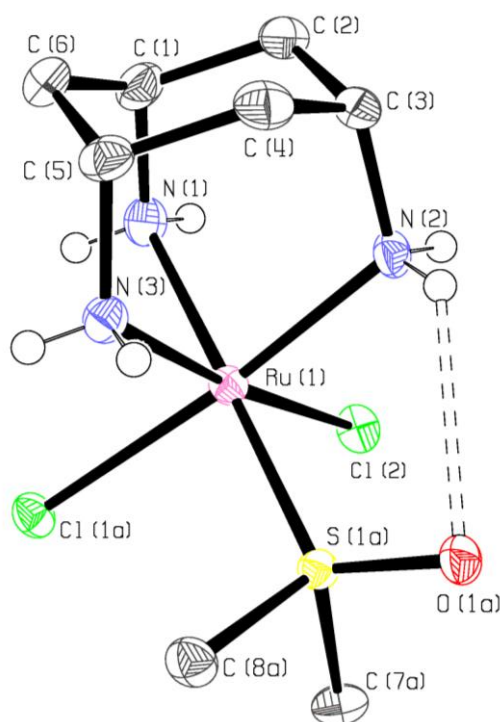


Figure 3.4: ORTEP (50% probability ellipsoids) diagram of [9]. Hydrogen atoms (except for amino hydrogens) are omitted for clarity. Cl(1a) and the DMSO ligands are disordered across the two coordination sites, where the major form is given. Selected bond lengths (\AA), angles ($^\circ$) and torsions ($^\circ$): Ru(1)–N(1) 2.154(3), Ru(1)–N(2) 2.091(3), Ru(1)–N(3) 2.131(3), Ru(1)–Cl(1a) 2.4650(12), Ru(1)–Cl(2) 2.4385(9), Ru(1)–S(1a) 2.1775(10), S(1a)–O(1a) 1.496(3), N(1)–Ru(1)–N(2) 88.08(13), N(1)–Ru(1)–N(3) 88.31(13), N(2)–Ru(1)–N(3) 90.28(13), Cl(1a)–Ru(1)–Cl(2) 95.53(3), Cl(2)–Ru(1)–S(1a) 90.69(3), Cl(1a)–Ru(1)–S(1a) 91.33(4), N(1)–Ru(1)–S(1a) 177.56(9), Ru(1)–S(1a)–O(1a) 119.54(13), N(3)–Ru(1)–S(1a)–O(1a) 1.29(18). Selected hydrogen-bond (D–H...A–X) lengths (\AA) and angles ($^\circ$) D...A, H...A, D–H...A, H...A–X: N(2)–H(2d)...O(1a)–S(1a) 3.146(4), 2.61(5), 127(5), 86(1).

3.3 Solid-State Structure of [RuCl₂(DMSO-*S*)(*cis*-tach)]

An attempt was made to synthesise [RuCl(dppm)(*cis*-tach)]PF₆ by the reaction of dppm with [8]Cl by heating at reflux in methanol. Single crystals were obtained from slow evaporation of a methanolic solution of the product of this reaction. However, the crystal was found to have the formula RuCl₂(DMSO-*S*)(*cis*-tach) [9] by X-ray diffraction analysis. This compound is the respective neutral variant of [8]Cl, formed from charge neutralisation. An ORTEP diagram and selected bond angles, lengths and torsions, as well as hydrogen-bond parameters are given in Fig. 3.4.

Once again, the complex is of a distorted octahedron and adamantane structure. The DMSO and one chlorido ligand, Cl(1a), were found to be disordered across two sites in a ratio of 93:7. An intramolecular hydrogen-bond is present between N(2) and O(1a) with a torsion angle of 1.29(18)°. This interaction has resulted in a distortion of the adamantane structure. The Ru(1)–N(2) bond length is shorter than Ru(1)–N(3), the amine generated by the C_s reflection plane of *cis*-tach (in solution), at 2.091(3) compared to 2.131(3) Å. As in the case of [8]PF₆, [9] forms an extended hydrogen-bond network in two-dimensional layers, with a total of twelve hydrogen-bonds formed between one complex and those surrounding it (Fig. 3.5).

Unfortunately, this species has only been observed by single crystal X-ray diffraction and not by any spectroscopic technique, to any extent. Therefore, further investigations of this complex were not possible.

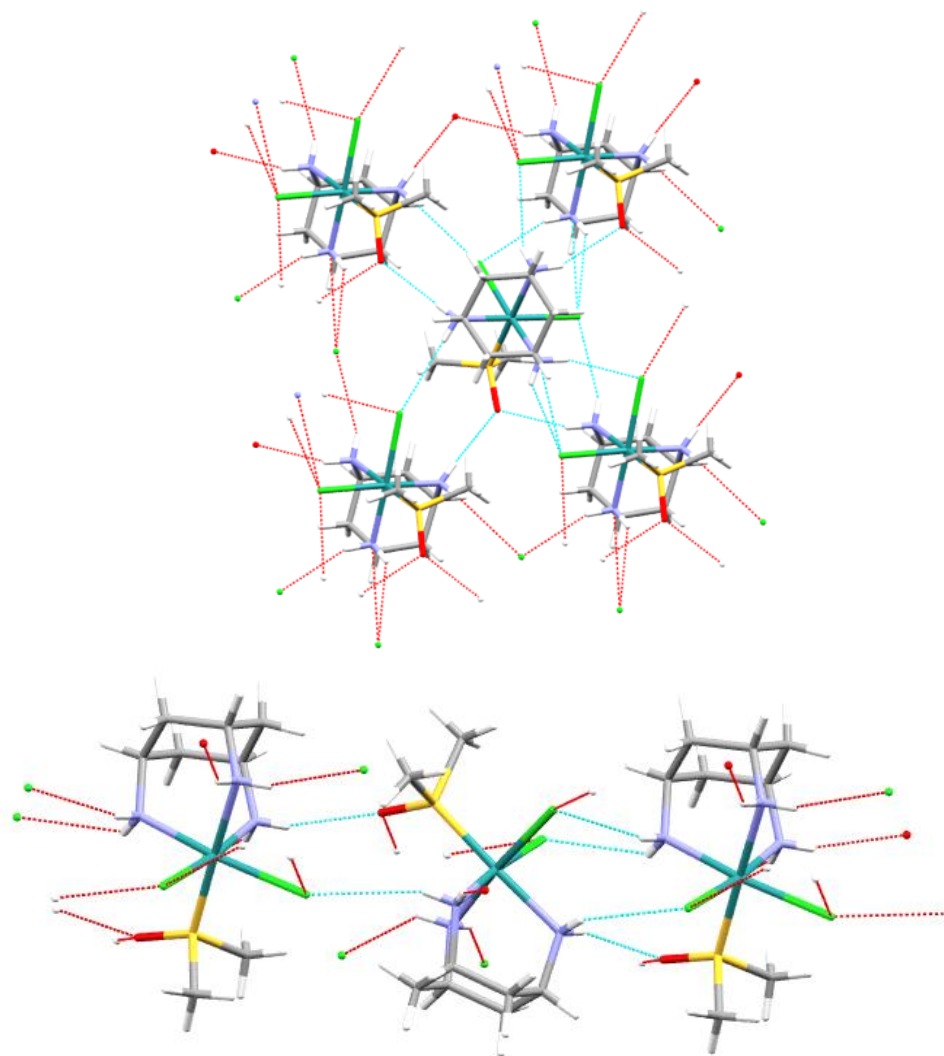


Figure 3.5: Top: Two-dimensional hydrogen-bonding motif between *cis*-tach amine protons and the chlorido and DMSO ligands of adjacent complexes in the structure of [9]. Hydrogen bonds are drawn as D...A. Bottom: Detailed view of hydrogen-bonding which is present along both axes (as seen in top diagram). Each complex donates and accepts hydrogen-bonds with an adjacent complex. The hydrogen-bonding structure alternates between two motifs. The first (left) is of NH...O and NH...Cl interactions, whereas the other (right) consists of one NH...O and three NH...Cl hydrogen-bonds. Hydrogen bonds are drawn as D...A.

3.4 Comparison of X-Ray Structures

The nature of the bonding between ruthenium and DMSO may be determined from crystallographic evidence.^{239, 241} Although the Ru–S bond is dependent upon both σ -donation and π -interactions, information regarding the π -bonding between the metal and ligand can be obtained from the S–O bond length. DFT calculations have shown that DMSO has three almost degenerate low-lying unoccupied orbitals. Two of these have strong $\sigma^*(\text{S–C})$ character and the other is predominantly $\pi^*(\text{S=O})$; with $\pi^*(\text{S=O})$ being the lowest in energy. These orbitals are involved in the back-donation of electron density from the metal, with most significant contribution to the $\pi^*(\text{S=O})$ orbital.²⁴²

In order to gain insight to the electronic influence of the *cis*-tach ligand on the Ru–DMSO moiety, selected and mean bond lengths for **[8]**PF₆ and **[9]** were compared to those of analogous complexes with other six electron *facial*-coordinating ligands in Tables 3.1 and 3.2 respectively.

<i>fac</i> -ligand	Average Bond Length (Å)		
	Ru–Cl	Ru–S	S–O
Tp ²⁴³	2.414(1)	2.27(3)	1.481(3)
[8] PF ₆ <i>cis</i> -tach	2.417(1)	2.255(5)	1.495(10)
ttn ²²⁹	2.420(1)	2.332(10)	1.483(5)
tacn ¹⁶⁶	2.426(1)	2.257(10)	1.485(4)
$\eta^5\text{-C}_5\text{Me}_5$ ²⁴⁰	2.447(3)	2.301(5)	1.476(9)

Table 3.1: Selected bond lengths from **[8]**⁺ and ruthenium(II) *fac*-ligand analogue complexes following the formula [RuCl(DMSO-*S*)₂(*fac*-ligand)]ⁿ⁺. The Ru–S and S–O bond lengths are given as the weighted mean for clarity.²²⁰

Due to the large variation of the Ru–S and S–O bond lengths in **[8]**PF₆, there is no significant difference between these parameters and those of similar complexes, with the exception of the Ru–S bond length of the $\eta^5\text{-C}_5\text{Me}_3$ and ttn complexes. Both of these bond lengths are longer than that of the *cis*-tach complex **[8]**PF₆, suggesting a

stronger Ru-DMSO bonding interaction in [8]PF₆. This is proposed to be due to increased π -back bonding from the metal centre of the *cis*-tach complex to the $\pi^*(\text{S}=\text{O})$ orbital of DMSO. There is little variation in Ru–Cl bond length between the neutral *fac*-ligands available for analysis; a significant difference is only seen on comparison with the anionic Cp* ligand.

<i>fac</i> -ligand	Bond Length (Å)			
	Ru(1)–Cl(1)	Ru(1)–Cl(2)	Ru(1)–S(1)	S(1)–O(1)
[9] <i>cis</i> -tach	2.465(1)	2.438(2)	2.178(1)	1.495(3)
η^6 - <i>p</i> -cymene ²⁴⁴	2.411(1)	2.405(1)	2.340(1)	1.477(3)
η^6 -tha ²⁴⁵	2.391(5)	2.400(6)	2.333(6)	1.48(2)

Table 3.2: Selected bond lengths from [9] and other ruthenium(II) *fac*-ligand complexes with the formula [RuCl₂(DMSO-*S*)(*fac*-ligand)].

A greater difference in bond lengths is seen when comparing [9] to η^6 -arene analogues (Table 3.2). First, both Ru–Cl bond lengths in [9] are significantly longer than those in the η^6 -*p*-cymene or η^6 -tha. This is as expected from the analysis of the triphenylphosphane crystal structures in chapter 2, where it is proposed that *cis*-tach is a stronger σ -donor and poor π -acceptor. A similar difference is seen for the Ru–S and S–O bond lengths, where the parameters for [9] suggest a greater bond-order of the metal-ligand interaction, proposed to be due to increased π character of the bond from an electron rich metal. This is also reflected in the S–O bond length (when compared to *p*-cymene only), where the longer bond length suggests a weaker bonding character, from back-donation into the $\pi^*(\text{S}=\text{O})$ orbital of DMSO. However, the involvement of the DMSO ligand in hydrogen-bonds to the *cis*-tach in the crystal structure influences the S–O bond length and therefore this parameter cannot be interpreted significantly.

3.5 *In Vitro* Biological Evaluation

The MTT assay is a rapid colorimetric assay for the quantitative determination of cell viability.²⁴⁶ A modified procedure of that reported by Carmichael and co-workers was used, and [8]Cl was assessed for antiproliferative activity with two cell lines, A549 and A2780.²²⁸ [8]Cl does not inhibit the growth of either cell line by 50% up to a concentration of 300 μ M, and is therefore considered inactive.

These results are not unexpected given the conclusions of Sadler and co-workers, where it is hypothesised that the activity can be related to the lipophilicity of the complex, which can influence the ability of the compound to enter the cell by passive diffusion through the cell membrane.^{80, 89} The low lipophilicity of [8]Cl is reflected by the insolubility of the compound in apolar solvents. [8]Cl is only readily soluble in water, methanol and DMSO, and sparsely in ethanol. This theory is further supported on comparison of the *bis*-dimethylsulfoxide complex to [4]Cl, whereby replacement of a DMSO ligand with triphenylphosphane results in moderate activity in both cell lines employed. It is evident that inclusion of a hydrophobic group is favourable for obtaining antiproliferative activity. Therefore further development of the structure of ruthenium (II) *cis*-tach complexes will focus on the incorporation of such ligands into the coordination sphere of the metal.

Although it has been shown that [8]Cl does not inhibit tumour cell growth, investigations into the aqueous chemistry of this complex were undertaken to provide a rationale for the absence of antitumor activity. The next section investigates the ligand exchange processes which occur when [8]Cl is in aqueous solution, to further aid in the understanding of the chemical identity of the species present when applied to physiological conditions.

3.6 Aquation Studies

The aquation and hydrolysis of metal complexes is an important activation step in the mechanism of the activation of several transition metal drugs, including cisplatin and the RAen and RAPTA complexes.^{97, 118, 247} Therefore, the exchange reactions which occur between **[8]**Cl and the solvent in aqueous solution was investigated. It was expected that **[8]**Cl would exchange the chlorido ligand with a single water molecule to give $[\text{Ru}(\text{OH}_2)(\text{DMSO-}S)_2(\text{cis-tach})]\text{Cl}_2$. However investigations into the identity of the aquation products revealed that additional processes are involved in the reaction between **[8]**Cl and water.

The aquation reaction of **[8]**Cl was initially investigated by ESI mass spectrometry. The mass spectrum of the complex in 50% H₂O/50% MeOH immediately after preparation consists of the single molecular ion of the chlorido complex **[8]**⁺ (*m/z* 422.0). However, pre-treatment of the sample in aqueous solution at 40°C for 18 h resulted in a change to the spectrum. Only a small quantity of the parent ion was observed, whereas the mass spectrum of the starting material under the same conditions exhibited only a signal for **[8]**⁺, with no fragmentation ions. The majority of ions observed in the mass spectrum were most likely the result of fragmentation of the aqua-adducts of **[8]**Cl. Ion fragments originating from both chlorido and DMSO dissociation were observed, at *m/z* 193.6 and 163.6 corresponding to $[\text{Ru}(\text{DMSO-}S)_2(\text{cis-tach})]^{2+}$ and $[\text{Ru}(\text{OH}_2)(\text{DMSO-}S)(\text{cis-tach})]^{2+}$ respectively. In order to gain further insight into the species formed, further reactions were monitored by ¹H NMR spectroscopy. A D₂O solution of **[8]**Cl was heated at 40°C for 24 h, after which the ¹H NMR spectrum was recorded. Selected resonances are given in Fig. 3.6.

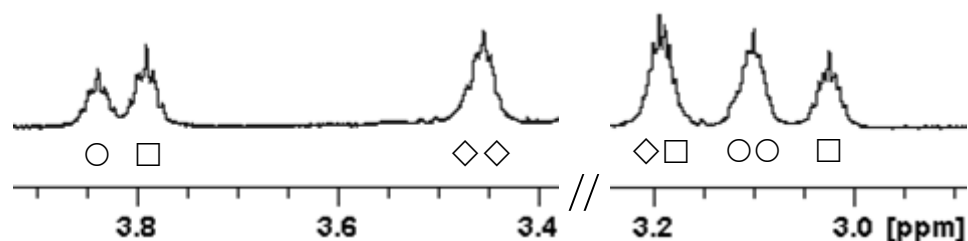


Figure 3.6: *Cis-tach* CH resonances in the ^1H NMR spectrum resulting from the aqutation of $[\mathbf{8}]\text{Cl}$. Each symbol represents a single CH proton. The DMSO-*S* resonances have been omitted for clarity with chemical shifts δ_{H} ○ 3.34, □ 3.33, ◇ 3.30 ppm. Key: ◇ $[\mathbf{8}]^+$, ○ $[\mathbf{8a}]^{n+}$, □ $[\mathbf{8b}]^{n+}$.

Aside from the starting material, resonances accounting for the formation of two new species were observed, $[\mathbf{8a}]^{n+}$ and $[\mathbf{8b}]^{n+}$ with C_s and C_1 *cis-tach* symmetry respectively. Two resonances corresponding to DMSO-*S* ligands of $[\mathbf{8a}]^{n+}$ and $[\mathbf{8b}]^{n+}$ were present both with integration proportional to one sulfoxide ligand per set of *cis-tach* resonances. Therefore both new complexes formed from the reaction of $[\mathbf{8}]\text{Cl}$ with water contained a single coordinated DMSO-*S* ligand. Over the course of the reaction the resonances for the NH_2 protons are lost through from proton-deuteron exchange with D_2O , and therefore not observed in the resulting ^1H NMR spectrum.

The product with C_1 symmetry was assigned as $[\text{RuCl}(\text{OH}_x)(\text{DMSO-}S)(\textit{cis-tach})]^{(x-1)+}$, $[\mathbf{8a}]^{n+}$. The degree of protonation of the aqua ligand cannot be assumed with the limited evidence available. The configuration of ligands in $[\mathbf{8a}]^{n+}$ represents the only plausible combination which would exhibit C_1 symmetry. A product containing an aqua and hydroxy ligand, while apparent to be C_1 symmetry, would exhibit C_s symmetry on the ^1H NMR timescale, as the proton exchange between the two ligands is relatively fast.²⁴⁸ The facile liberation of DMSO resembles the complexes $[\textit{trans-RuCl}_2(\text{DMSO-}S)_4]$ and $[\textit{cis-RuCl}_2(\text{DMSO-}S)_3(\text{DMSO-}O)]$, where the ruthenium DMSO bond is readily cleaved in water.²³⁴

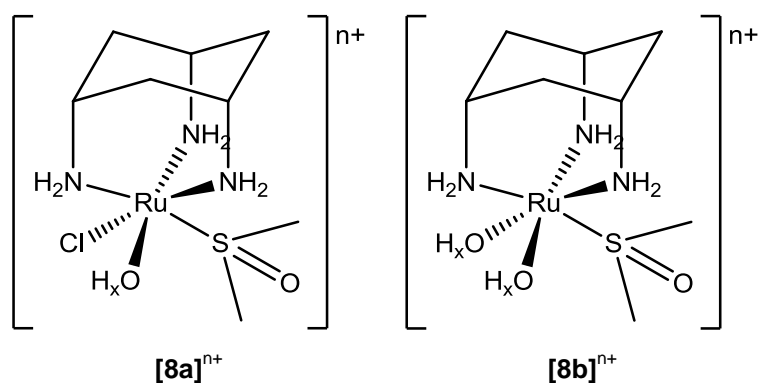
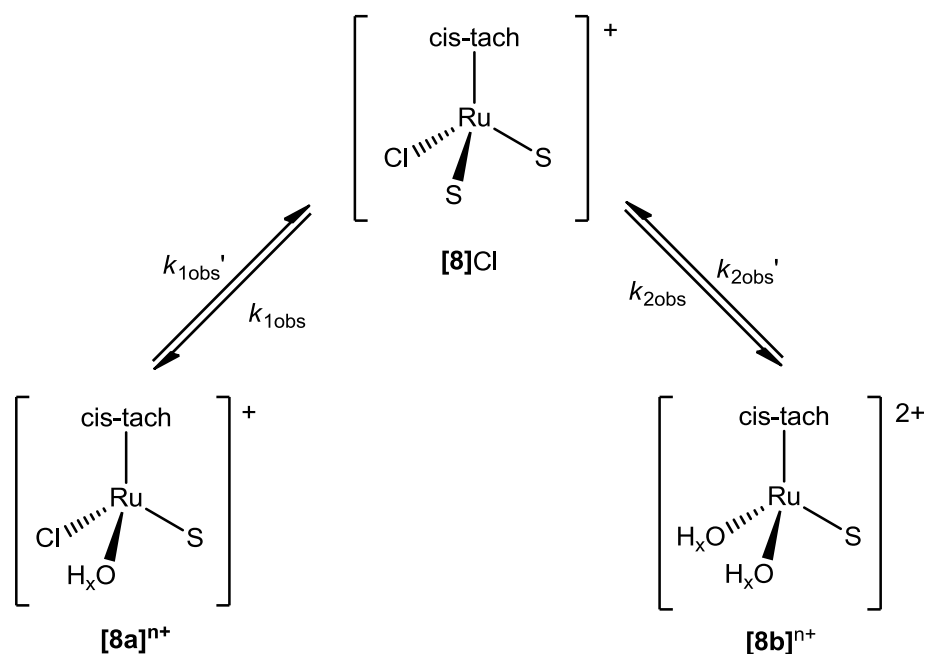


Figure 3.7: Proposed structures of the two aquation products from solvation of **[8]Cl** in aqueous solution. Exchange occurs between only DMSO-*S* and the solvent (**[8a]**ⁿ⁺) or both a chlorido ligand and DMSO-*S* with water (**[8b]**ⁿ⁺).

The C_s product **[8b]**ⁿ⁺ must contain two identical ligands to satisfy the *cis*-tach symmetry observed in the ¹H NMR spectrum. The only plausible configurations containing a single DMSO-*S* ligand are $[\text{RuCl}_2(\text{DMSO-}S)(\textit{cis}\text{-tach})]$ and $[\text{Ru}(\text{OH}_x)_2(\text{DMSO-}S)(\textit{cis}\text{-tach})]^{(2-2x)+}$, both of which agree with the ¹H NMR spectrum. Aquation of **[8]Cl** with elevated chloride concentrations (100 mM NaCl in D₂O) suppressed the formation of the species with C_s symmetry to a limited extent. This evidence suggests the identity of **[8b]**ⁿ⁺ as $[\text{Ru}(\text{OH}_x)_2(\text{DMSO-}S)(\textit{cis}\text{-tach})]^{(2-2x)+}$. Complete inhibition of the formation of both species was only achieved in D₂O solution with 100 mM of DMSO and NaCl.

It was proposed that kinetic analysis of the aquation of **[8]**⁺ would confirm the active mechanism in the formation of the two aqua complexes. This was achieved by the monitoring of a 10.8 mM solution of **[8]Cl** in D₂O by ¹H NMR spectroscopy. Spectra were recorded at 20 minute intervals and the reaction maintained at 40°C under an argon atmosphere. One equivalent of ethyl acetate was added to act a reference in data analysis. Integrals of CH protons of each ruthenium complex and the CH₃ groups of the free DMSO ligand were calculated relative to the CH₃ of the ethyl group in ethyl acetate. The resulting data were analysed using DynaFit and modelled to the following reaction Scheme given in Scheme 3.3.



Scheme 3.3: Reaction scheme employed for ^1H NMR kinetics data analysis of the aquation of $[\text{RuCl}(\text{DMSO-S})_2(\text{cis-tach})]\text{Cl}$, $[\mathbf{8}]\text{Cl}$. $\text{cis-tach} = \kappa^3\text{-}N,N',N''\text{-cis-tach}$, $S = \text{DMSO-S}$. Modification to incorporate inter-conversion between the two aqua species did not give a suitable fit for the data.

Modifying the reaction mechanism to incorporate formation of $[\mathbf{8b}]^{n+}$ via $[\mathbf{8a}]^{n+}$ did not give a suitable fit for the data (or *vice versa*, see Fig. 3.8). It is proposed that $[\mathbf{8b}]^{n+}$ is formed from chlorido dissociation from $[\mathbf{8}]\text{Cl}$, rapidly followed by DMSO loss; as opposed to the loss of the chlorido ligand in $[\mathbf{8a}]^{n+}$. Clearly there are two distinctive processes occurring in the reaction between $[\mathbf{8}]\text{Cl}$ and the solvent in aqueous solution. In addition, both products were formed with pseudo-first order kinetics, supporting the structural assignment of $[\mathbf{8b}]^{n+}$. The data were analysed using DynaFit, where the plot and reaction parameters are provided in Fig. 3.8 and Table 3.2 respectively.²⁴⁹

It is apparent from the kinetic parameters that the aquation reactions of $[\mathbf{8}]\text{Cl}$ are significantly slower than those of $[\text{RuCl}(\text{en})(\eta^6\text{-biphenyl})]\text{PF}_6$ and $[\text{RuCl}_2(\eta^6\text{-}p\text{-cymene})(\text{PTA})]$ by two orders of magnitude.^{97, 118} Furthermore, the equilibrium constants for both these processes in $[\mathbf{8}]\text{Cl}$ are lower than those for the ruthenium(II)

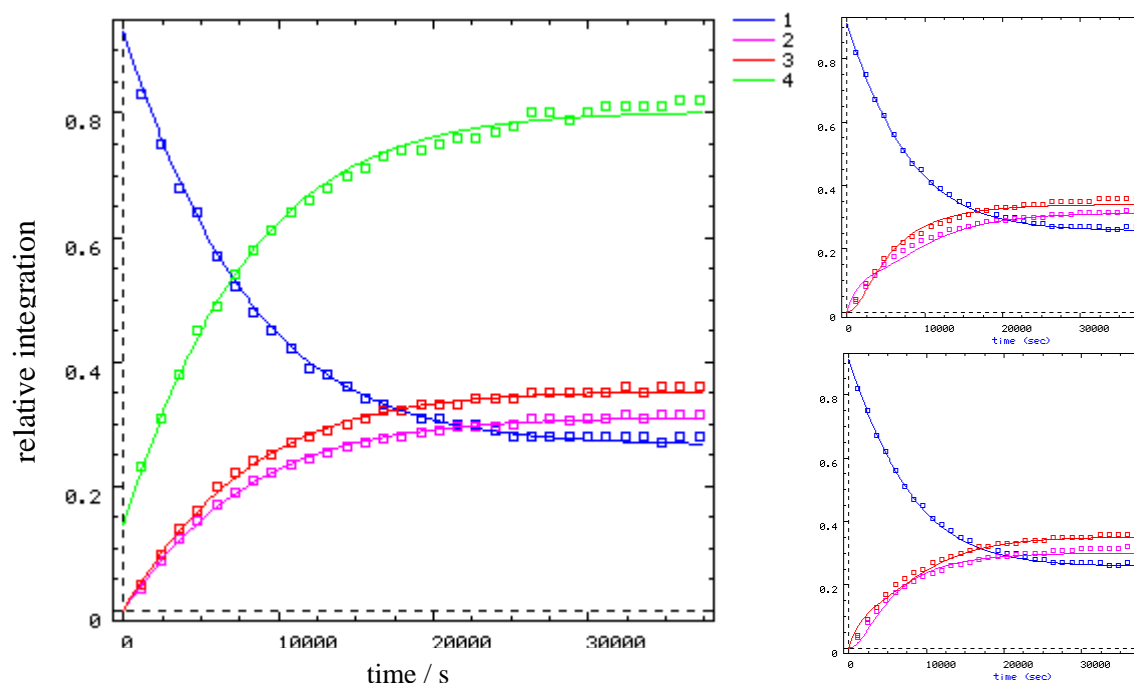


Figure 3.8: DynaFit plot of the ^1H NMR integrations and kinetic fit for the aquation reaction of $[\mathbf{8}]\text{Cl}$ (1, blue) with the mechanism in Scheme 3.3 (left), to give $[\mathbf{8a}]^{\text{n}+}$ (2, pink), $[\mathbf{8b}]^{\text{n}+}$ (3, red) and DMSO (4, green). Plots for alternative mechanisms are also given (right; DMSO trace is excluded for clarity) of $[\mathbf{8}]\text{Cl} \rightleftharpoons [\mathbf{8a}]^{\text{n}+} \rightleftharpoons [\mathbf{8b}]^{\text{n}+}$ (top) and $[\mathbf{8}]\text{Cl} \rightleftharpoons [\mathbf{8b}]^{\text{n}+} \rightleftharpoons [\mathbf{8a}]^{\text{n}+}$ (bottom).

	k (s^{-1})	K (M)
$[\mathbf{8}]\text{Cl}$		
k_1/k_1'	$(3.96 \pm 0.05) \times 10^{-5}$	$(1.11 \pm 0.31) \times 10^{-3}$
k_2/k_2'	$(4.47 \pm 0.05) \times 10^{-5}$	$(1.87 \pm 0.05) \times 10^{-4} \text{ M}^c$
$[\text{RuCl}(\eta^6\text{-bip})(\text{en})]\text{PF}_6^{97}$		
a	$(3.95 \pm 0.09) \times 10^{-3}$	$(9.1 \pm 0.9) \times 10^{-3}$
$[\text{RuCl}_2(\eta^6\text{-}p\text{-cymene})(\text{PTA})]^{118}$		
b	$(3.33 \pm 0.02) \times 10^{-3}$	$(3.8 \pm 0.2) \times 10^{-3}$

Table 3.3: Calculated rate and equilibrium constants for the first-order aquation of $[\mathbf{8}]\text{Cl}$ in D_2O at 313 K. *a*) Aquation of $[\text{RuCl}(\eta^6\text{-bip})(\text{en})]\text{PF}_6$, 310 K with 100 mM NaClO_4 in H_2O at pH 6.29; *b*) First aquation of $[\text{RuCl}_2(\eta^6\text{-}p\text{-cymene})(\text{PTA})]$ ($\text{Ru}-\text{Cl}_2 \rightarrow \text{Ru}-\text{Cl}\{\text{OH}_x\}$), 298K with 150 mM NaClO_4 in H_2O . *c*) Equilibrium constant unit of M^2 due to second-order nature of the reverse reaction.

η^6 -arene complexes by at least a factor of three. Therefore, a smaller fraction of the aquated—and potentially more reactive—species may be present compared to the RAen and RAPTA complexes at the same chloride concentrations. This slow and limited aquation may provide additional rationale for the poor antitumor activity of **[8]Cl**. It is proposed that insufficient quantities of the aqua species would be slowly generated ($t_{1/2} > 4$ h) within a physiological environment such as the cytoplasm of nucleus of a cell.

The ^1H NMR spectrum at the end of the reaction is able to provide an insight into the possibility of inter-conversion between **[8a]ⁿ⁺** and **[8b]ⁿ⁺**. Observation of the NH_2 protons of **[8b]ⁿ⁺** (only approximately 40% deuteration), but not those of **[8a]ⁿ⁺** (100% deuteration) provides evidence for the absence of exchange between the two species. It is most probable that inter-conversion can only slowly occur *via* the starting material **[8]Cl**. Further inspection of the NH_2 ^1H NMR resonances of **[8b]ⁿ⁺** reveals an unequal distribution of deuteration in the amine proton environments, as shown in Fig. 3.9.

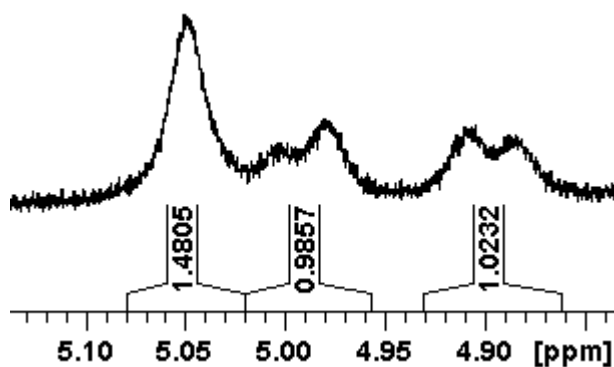
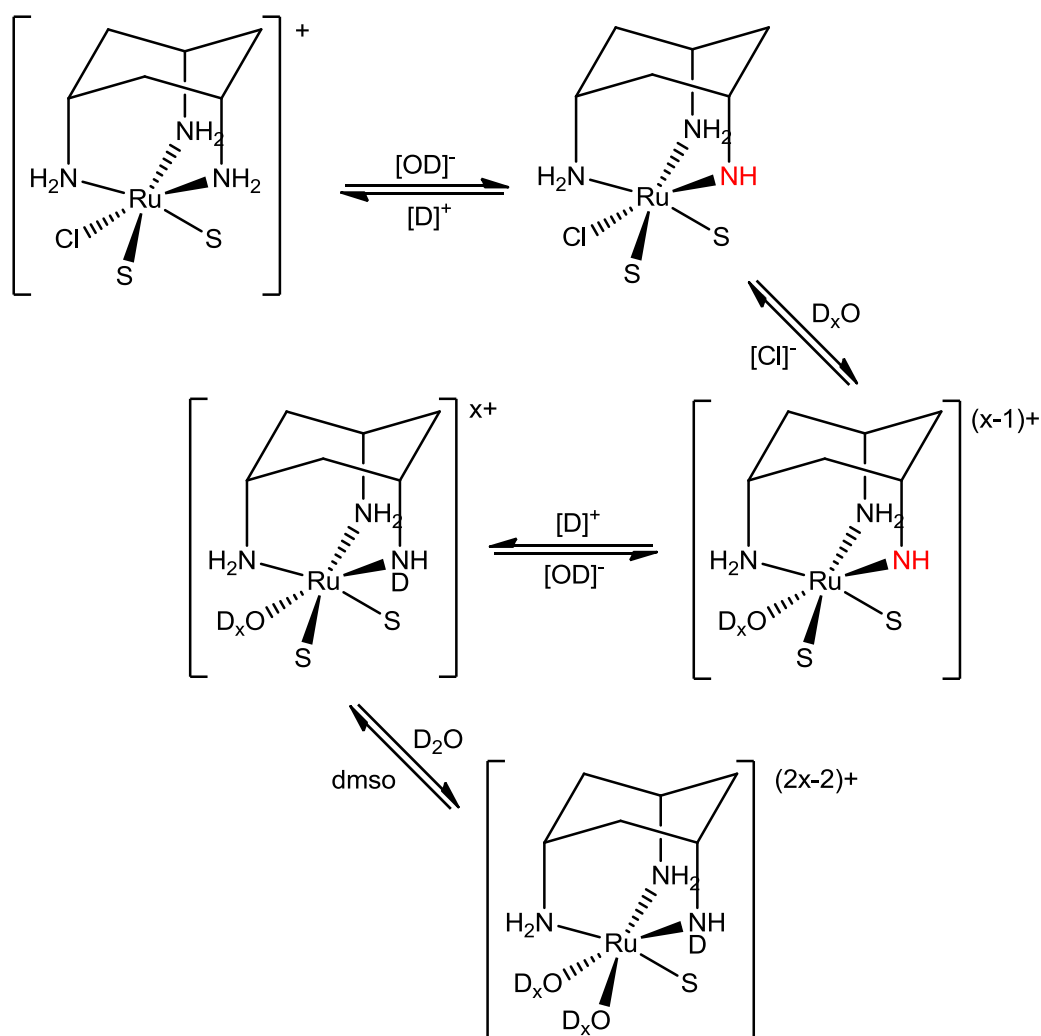


Figure 3.9: ^1H NMR spectrum of the NH_2 protons in **[8b]ⁿ⁺**, from the aquation of **[8]Cl** in D_2O . Integrations are relative to the CH signal used for kinetic analysis with integration of 2.0.

The relative integrations of the two doublet resonances of δ_{H} 4.90 and 4.99 ppm reveals a deuterium incorporation of approximately 30% more than the singlet at δ_{H} 5.05 ppm. This difference in intensity is observed in all the ^1H NMR spectra throughout the reaction and therefore not the result of increased proton – deuterium

exchange kinetics. This disparity suggests that a single deuteron has been incorporated equally into the geminal amine resonances.

The conjugate base mechanism S_N1CB , is a pathway for metal amine and ammine complexes to undergo ligand exchange. The amine group is deprotonated by a base such as the hydroxide in water, where the ligand *trans*- to the amine dissociates and is subsequently replaced by an aqua ligand. This may be applied to the proposed mechanism of formation of $[\mathbf{8b}]^{n+}$ (Scheme 3.4) and may account for the observed deuteration pattern in the ^1H NMR spectrum of $[\mathbf{8b}]^{n+}$.



Scheme 3.4: Proposed conjugate base mechanism for formation of $[\mathbf{8b}]^{n+}$ from $[\text{RuCl}(\text{DMSO-S})_2(\text{cis-tach})]\text{Cl}$, $[\mathbf{8}]\text{Cl}$, with deuteration of the *cis*-tach ligand indicated. The deprotonated NH group is highlighted in red. S = DMSO-S.

Although a second order reaction, the rate equation for the SN_1CB mechanism remains a pseudo-first order reaction with respect to ruthenium, assuming no overall change in hydroxide concentration. However, the observed rate constant would be a function of the hydroxide concentration due to its involvement in the rate determining step. Therefore, the distribution of species after 18 h at 40°C at varying pH was determined to evaluate the reaction dependence on pH. Sodium phosphate buffer was employed at pH 6.4, 7.4 and 8.2 in 10% $\text{D}_2\text{O}/90\%$ H_2O solution. The relative amounts of each complex are given in Table 3.4.

pH	$[\mathbf{8}]^+$ (%)	$[\mathbf{8a}]^{n+}$ (%)	$[\mathbf{8b}]^{n+}$ (%)
6.4	46.4	30.7	22.8
7.4	21.2	19.9	58.9
8.2	24.1	20.9	55.0

Table 3.4: Ratios of starting material and products in the aquation of $[\mathbf{8}]\text{Cl}$ at pH 6.4, 7.4 and 8.2 in 10% D_2O solution with 10 mM sodium phosphate buffer.

It is evident that a dramatically increased proportion of $[\mathbf{8b}]^{n+}$ is formed at pH 7.4 compared to at pH 6.4, providing a degree of support for the conjugate base mechanism. However, it was expected for change to be observed in the relative proportions of the species between pH 7.4 and 8.4. These ^1H NMR experiments suggest that the physiological pH of a cell, 7.4 is near the optimal pH for the aquation of $[\mathbf{8}]\text{Cl}$.

These studies on the aqueous chemistry of $[\mathbf{8}]\text{Cl}$ reveal that solvation of the complex in water results in two exchange mechanisms occurring; that of exchange between DMSO and an aqua ligand and also a classical aquation reaction which is followed by a rapid exchange of DMSO for a second aqua ligand. Both processes involve dissociation of DMSO, therefore formation of an equilibrium requires dmsO to be present, not just chloride. It is proposed that aquation is not suppressed in any biological environment, including the conditions found within the blood stream.

Therefore this complex may be deactivated before it has been able to enter the cell. The rate of aquation has been correlated to cytotoxicity in several structure-activity relationships, with complexes exhibiting faster aquation generally being more active.⁸⁶ Both aquation reactions occur at rates two orders of magnitude slower than the that of leading ruthenium(II) η^6 -arene complexes, providing a rationale for the poor *in vitro* activity of [8]Cl.

3.7 Reactions with Nucleosides

Metal-DNA interactions are thought to be involved in the mechanism of action of many anti-cancer compounds; thus, DNA is often the first target screened against potential anti-tumour compounds.^{84, 96, 233, 250} In order to investigate the potential for [8]Cl with to react with DNA, the small-molecule model guanosine (Guo) was chosen for the selectivity cisplatin and RAen complexes exhibit for this base.^{20, 96}

A 5 mM solution of [8]Cl was treated with two equivalents of Guo at 40°C for 18 hours resulting in the formation of a blue solution. The ESI mass spectrum of the solution, supplemented with 50% methanol exhibited a single major species, corresponding to loss of both a DMSO and chlorido ligand from the coordination of guanosine to the metal centre. The starting material was observed (m/z 422.1, 5%), with three signals assigned as $[\text{Ru}(\text{DMSO-}S)(\text{Guo})(\text{cis-tach})-\text{H}]^+$ (m/z 591.1, 100%) $[\text{Ru}(\text{DMSO-}S)(\text{Guo})(\text{cis-tach})]^{2+}$ (m/z 296.1, 10%) and $[\text{Ru}(\text{DMSO-}S)(\text{guanine})(\text{cis-tach})]^{2+}$ (m/z 230.1 25%). These are proposed to be fragments of a single complex with a minimum formula of $[\text{Ru}(\text{DMSO-}S)(\text{Guo})(\text{cis-tach})]^{2+}$. The structural configuration of the guanosine ligands is unable to be determined, but examples of plausible structures which may account for the fragments observed are given in Fig. 3.10.

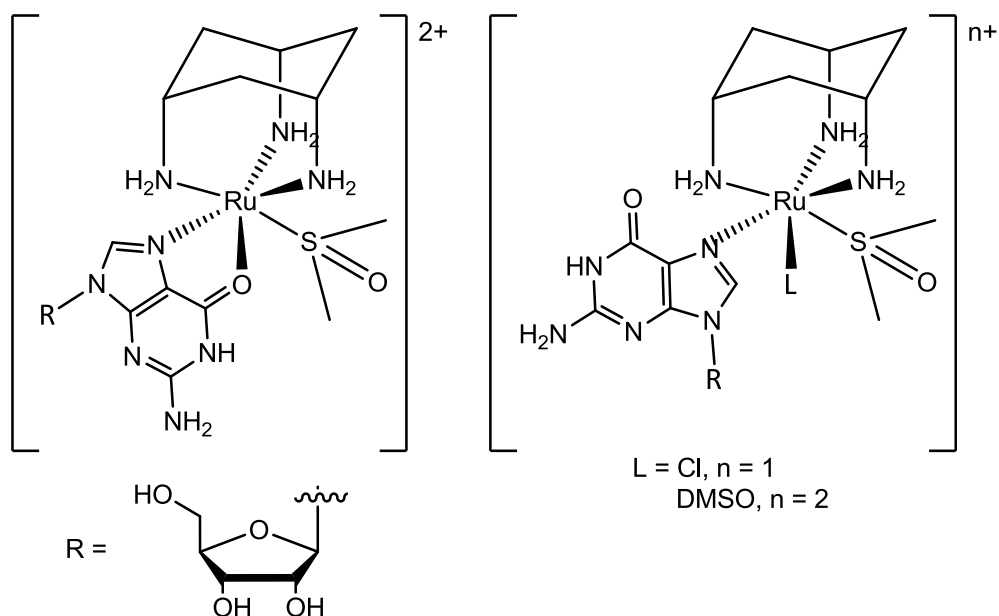


Figure 3.10: Possible structures of guanosine adducts of $[\mathbf{8}]^+$, which may produce the fragmentation observed in the ESI mass spectrum.

In addition, a minor species, $[\text{Ru}(\text{DMSO-S})(\text{Guo})_2(\text{cis-tach})]^{2+}$ (m/z 398.6, 25%) was observed in the mass spectrum. Although the structural configuration of the Guo molecules cannot be determined, the complex may contain two coordinated Guo ligands, akin to the G,G-cross-linking of cisplatin.²² However, guanosine was often observed in the ESI mass spectrum as a dimer, presumably due to hydrogen-bonding interactions; this interaction may account for a *bis*-guanosine ruthenium ion.

The cisplatin and RAen complexes have been demonstrated to form adducts not only with guanine, but also adenine.²² Therefore, the reactivity of $[\mathbf{8}]\text{Cl}$ to adenosine was investigated. Reaction of a 5mM solution of $[\mathbf{8}]\text{Cl}$ with two equivalents of adenosine at 40°C over 18 h resulted in the formation of an orange solution, suggesting a reaction had occurred. A single peak was observed in the ESI mass spectrum assigned as $[\text{Ru}(\text{DMSO-S})(\text{Ado})(\text{cis-tach})]^{2+}$ (m/z 575.1, 100%). This complex is expected to follow a similar structure to the Guo adduct.

The ability for $[\mathbf{8}]\text{Cl}$ to bind both adenosine and guanosine to an extent is unsurprising given the structural similarity of the two bases. Both contain two suitable donor atoms (Guo: N7/O6, Ado: N7/N6) which can participate in donation

to the metal centre of [8]Cl and may also result in chelation. It should be noted that adenine is unlikely to chelate in this way when part of DNA as the amine is a base-pair hydrogen-bond acceptor with thymine, thus preventing N6 coordination.

These initial reactions of [8]Cl with the nucleosides guanosine and adenosine have demonstrated that the ruthenium(II) *cis*-tach complex may interact with DNA via covalent interactions. However, the reactions described here were performed at concentrations of 5 mM of [8]Cl and when applied to physiologically-relevant concentrations, this affinity may not be significant. Further experiments including ¹H NMR spectroscopy were not performed due to the poor anti-tumour activity of [8]Cl.

3.8 Chapter Conclusions

Preparation of a cationic dimethylsulfoxide ruthenium *cis*-tach complex [8]Cl was achieved by the reaction of *cis*-tach with [*cis*-RuCl₂(DMSO-*O*)(DMSO-*S*)₃]. This complex was isolated and fully characterised by a range of spectroscopic techniques. The DMSO ligand was identified as coordinating to the metal through the sulfur atom by NMR and infra-red spectroscopy. The structural assignment was supported by the single crystal X-ray diffraction of [8]PF₆ obtained by the metathesis of [8]Cl with sodium hexafluorophosphate. In addition to the cationic complex, a single crystal of the neutral complex [9] was obtained.

[8]Cl was found to be inactive (IC₅₀ > 600 μM) in the inhibition of cancer cell growth in both the A549 and A2780 cell lines by the MTT assay. The complex does participate in ligand exchange with the solvent in aqueous solution, but the reactivity is dominated by the dissociation of one DMSO ligand. Interactions of this complex with nucleosides were observed with guanosine and adenosine. It is postulated that the poor *in vitro* activity of [8]Cl is due to the hydrophilic nature of the complex resulting in reduced cell uptake, combined with poor reactivity of the complex in aqueous solution. For example, aquation is slow and both exchange processes involve the loss of DMSO, therefore the “chloride concentration switch” does not

apply and the complex may be activated by aquation and subsequently deactivated before it can reach a suitable biological target.

However, more significantly, the advent of the precursor compound **[8]Cl** permits the design and development of new ruthenium (II) *cis*-tach compounds for application in cancer therapy. The labile DMSO ligands permit the preparation of complexes with a diverse range of ligands. Those of particular interest are chelating ligands, which have often been employed in the design of cytotoxic molecules, which are more strongly bound to the metal due to the chelate effect. The design, preparation and evaluation of ruthenium (II) *cis*-tach complexes with chelating ligands derived from **[8]Cl** form the basis of the remaining chapters in this thesis.

Chapter 4. Ruthenium(II) *cis*-tach Complexes with *N-N* Chelates

4.1 Introduction

The synthetic development of ruthenium(II) *cis*-tach complexes from the precursor $[\text{RuCl}(\text{DMSO-}S)_2(\textit{cis}\text{-tach})]\text{Cl}$ [**8**] Cl was concentrated on the incorporation of a chelating ligand to give $[\text{RuCl}(\text{L})(\textit{cis}\text{-tach})]\text{Cl}$. These ligands provide more predictable ligand exchange due to increased stabilisation from the chelate effect and reduction in the number of potential vacant coordination sites. Suitable candidates are the *N,N*-donor 2,2'-bipyridyl (bipy) and its derivatives. Ruthenium complexes containing these ligands are already well known to be highly promising anti-cancer agents.²⁵¹ Amongst the earliest examples was $[\textit{mer}\text{-RuCl}_3(\text{terpy})]$ (terpy = 2,2':2'',2'''-terpyridine) (Fig. 4.1), which is capable of forming DNA intrastrand cross links.²⁵²

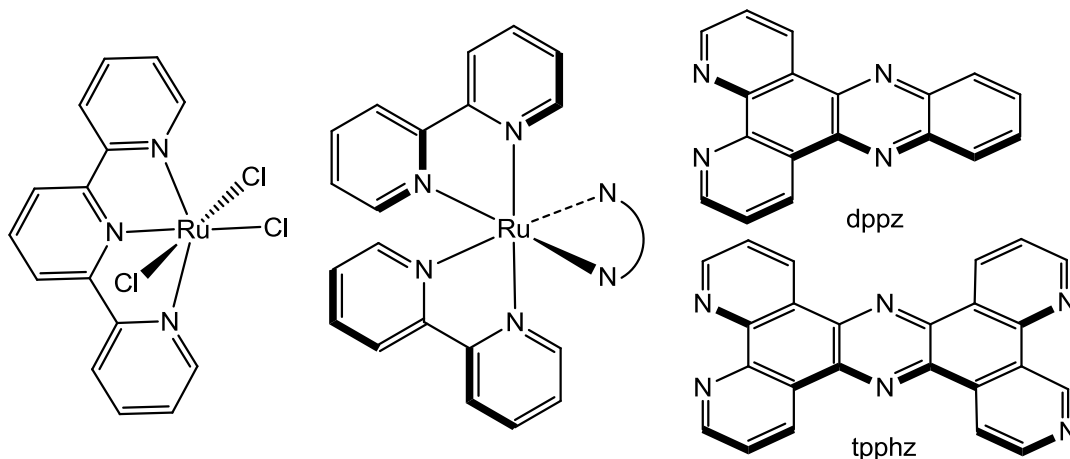


Figure 4.1: Structure of the polypyridyl ruthenium(II) complexes $[\textit{mer}\text{-RuCl}_3(\text{terpy})]$ (left) $[\text{Ru}(\text{bipy})_2(\text{N-N})]^{2+}$ (middle) where $\text{N-N} = \text{dppz}$ (top right) or tpphz (bottom right) evaluated for antitumor activity.

Since the observation that $[\text{Ru}(\text{N-N})_2(\text{dppz})]^{2+}$ (Fig. 4.1, $\text{N-N} = 2,2'$ -bipyridyl or 1,10-phenanthroline; $\text{dppz} = \text{dipyrido}[3,2\text{-}a':2',3'\text{-}c]\text{phenazine}$) reversibly binds to DNA, ruthenium(II) complexes of the general type $[\text{RuL}_3]^{2+}$ ($\text{L} = 2,2'$ -bipyridyl or derivative) have been studied more recently.²⁵³ Although in aqueous solution the luminescence of these complexes is quenched, intercalation with DNA results in an

emission from a $^3\text{MLCT}$ excited state, permitting the application of these complexes as imaging agents.²⁵⁴ Battaglia, Thomas and co-workers recently developed the two related complexes $[\text{Ru}(\text{N-N})_2(\text{tpphz})]^{2+}$ (Fig. 4.1 B, tpphz = tetrapyrido[3,2-a:2',3'-c:3'',2''-h:2''',3'''-j]phenazine) which not only act as “light-switch” complexes capable of use in imaging techniques, but are also highly cytotoxic.²⁵⁵

The immediate success of ruthenium(II) polypyridyl complexes did not extend to complexes containing η^6 -arenes as the species $[\text{RuCl}(\eta^6\text{-bip})(\text{N-N})]\text{PF}_6$ ($\text{N-N} = 2,2'$ -bipyridine and 1,10-phenanthroline)⁸² were found to be poorly cytotoxic in comparison to $[\text{RuCl}(\eta^6\text{-bip})(\text{en})]\text{PF}_6$ (RM175). The cause for the loss in activity was proposed to be the absence of hydrogen-bond donors in the complex, preventing hydrogen-bond formation with the DNA target. The effect of subtle differences on the biological activity of a complex was demonstrated by modification of the 2,2'-bipyridyl ligand with hydroxyl groups at the 3,3' positions (Fig. 4.2). Deprotonation of one hydroxyl group results in a bridging $\text{O-H}\cdots\text{O}$ which is stabilised from the resulting planarity. These compounds were found to be moderately active in the ovarian A2780 cell line.¹⁶³ Further studies with η^6 -arene complexes and extended 1,10-phenanthroline ligands have shown that these type of complexes are highly cytotoxic *in vitro* and bind to duplex DNA.²⁵⁶

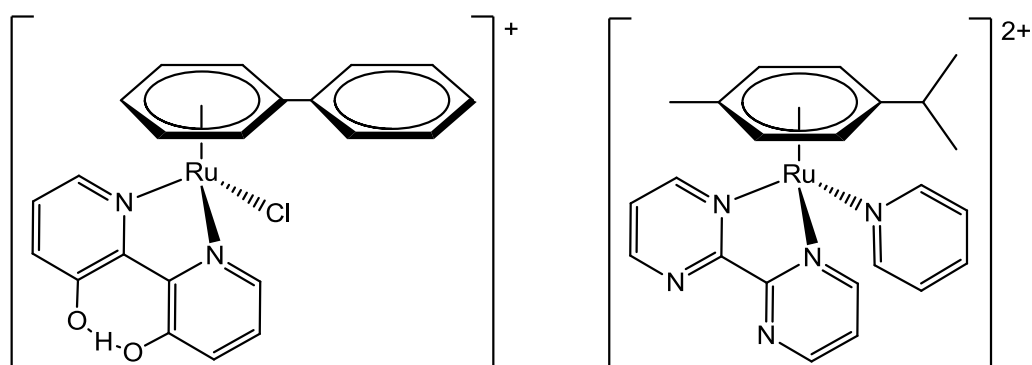


Figure 4.2: Structure of two ruthenium(II) η^6 -arene polypyridyl-based complexes studied for anti-tumour activity: $[\text{RuCl}(\text{bipy}^{175}\text{O})(\eta^6\text{-biphenyl})]\text{PF}_6$ (left) and the light-activated $[\text{Ru}(\text{py})(\text{bipyrimidine})(p\text{-cymene})](\text{PF}_6)_2$ ($\text{py} = \text{pyridine}$) (right)

The first light activated aquation of a ruthenium η^6 -arene complex was achieved by the employment of bipyrimidine (Fig. 4.2). In aqueous solution, dissociation of the

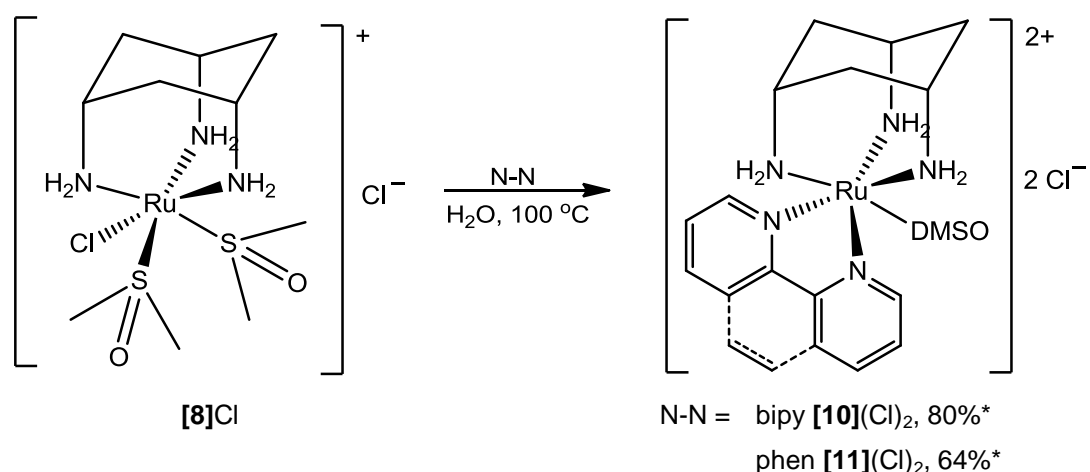
pyridine ligand is promoted by light,⁹¹ to afford the solvent complex which was demonstrated to further react with ethyl-guanine and DNA, with promising *in vitro* activity under ambient lighting conditions.⁹²

Given that polypyridyl ligands have promising application in the development of ruthenium(II) anti-cancer compounds, these complexes were of interest to investigate. Also, *cis*-tach can participate in hydrogen-bonding to target compounds, a key feature missing in the η^6 -arene bipyridyl complexes. Additionally, modification of the ligands is possible by substitution on the pyridyl rings. Investigations into the synthetic possibilities were at first focused on the ligands 2,2'-bipyridyl (bipy) and 1,10-phenanthroline (phen), and later expanded to include ethylenediamine (en). The synthesis, characterisation and X-ray structures are discussed. Initial investigations into the synthesis of these complexes were undertaken with Mr Thomas Hunter (see BSc report 2009–2010, University of York). The aqueous chemistry and *in vitro* biological evaluation of one of these complexes is also discussed.

4.2 Synthesis and Characterisation

4.2.1 Polypyridyl Complexes

The reaction of **[8]**Cl with one equivalent of the *N,N*-ligands 2,2'-bipyridine (bipy) and 1,10-phenanthroline (phen) was achieved by heating under reflux in water, resulting in a colour change of the solution from yellow to a deep red (Scheme 4.1). Isolation of the product by washing with DCM to remove the excess ligand and evaporation to dryness gave a deep orange powder. The ^1H NMR spectra of these compounds in D_2O exhibited the expected *cis*-tach resonances for a complex with C_s symmetry, alongside those for the coordinated *N,N*-chelating ligand. However, a resonance arising from coordinated DMSO was additionally observed in the ^1H NMR spectrum at δ_{H} 2.63 and 2.52 ppm for the 2,2'-bipyridyl and 1,10-phenanthroline complexes respectively. It was therefore evident that the identity of the two complexes were $[\text{Ru}(\text{bipy})(\text{DMSO})(\text{cis-tach})](\text{Cl})_2$, **[10]**(Cl) $_2$, and $[\text{Ru}(\text{DMSO})(\text{phen})(\text{cis-tach})](\text{Cl})_2$, **[11]**(Cl) $_2$. ESI mass spectrometry confirmed the identity of the two complexes; peaks were observed at m/z of 232.5573 ($[\text{M}]^{2+}$, 100%) and 244.5570 ($[\text{M}]^{2+}$, 100%) for **[10]** $^{2+}$ and **[11]** $^{2+}$ respectively. The observed isotope pattern corresponds to a dicationic ruthenium species in both cases.



Scheme 4.1: Reaction of **[8]**Cl with 2,2'-bipyridyl and 1,10-phenanthroline to give the complexes **[10]**(Cl) $_2$ and **[11]**(Cl) $_2$ respectively. Both complexes were dicationic with a DMSO ligand. * Isolated yield.

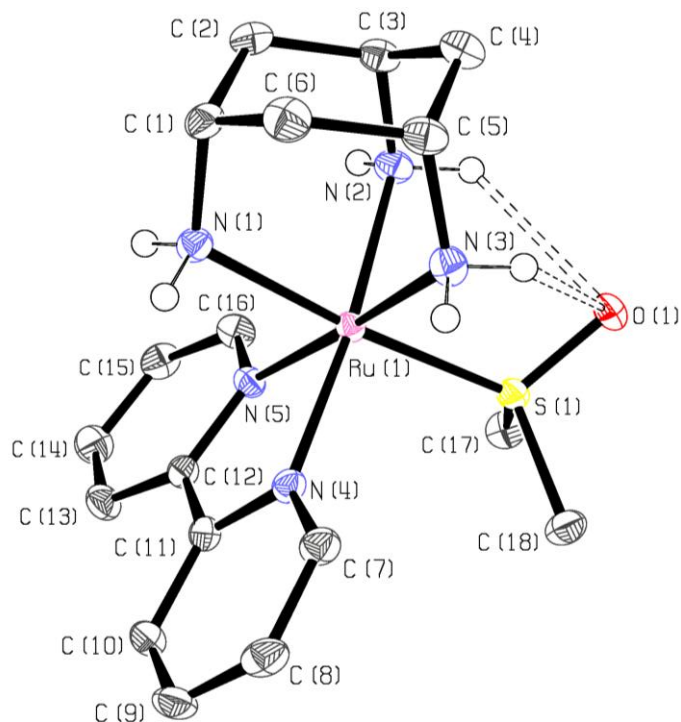


Figure 4.3: ORTEP diagram (50% probability ellipsoids) of **[10](PF₆)₂**. Hydrogen atoms (except for amino hydrogens) and counter ions are omitted for clarity. Selected bond lengths (Å), angles (°) and torsions (°): Ru(1)–N(1) 2.136(3), Ru(1)–N(2) 2.141(3), Ru(1)–N(3) 2.148(3), Ru(1)–N(4) 2.077(3), Ru(1)–N(5) 2.076(2), Ru(1)–S(1) 2.2223(8), S(1)–O(1) 1.500(2), N(1)–Ru(1)–N(2) 87.60(11), N(1)–Ru(1)–N(3) 88.71(11), N(2)–Ru(1)–N(3) 85.96(11), N(4)–Ru(1)–N(5) 78.79(10), N(4)–Ru(1)–S(1) 96.58(7), N(5)–Ru(1)–S(1) 97.37(7), N(1)–Ru(1)–S(1) 175.10(8), Ru(1)–S(1)–O(1) 112.23(9), N(2)–Ru(1)–S(1)–O(1) 40.95(13), N(3)–Ru(1)–S(1)–O(1) –45.05(13). Selected hydrogen-bond (D–H...A–X) lengths (Å) and angles (°) D...A, H...A, D–H...A, H...A–X: N(2)–H(2d)...O(1)–S(1): 3.074(4), 2.40(4), 127(3), 86.0(9); N(3)–H(3a)...O(1)–S(1): 3.126(4), 2.51(3), 130(3), 82.8(8).

Single crystals suitable for X-ray diffraction were obtained by chloride metathesis with potassium hexafluorophosphate and slow evaporation of the resulting methanol solution of the complexes. The crystals of **[10]**(PF₆)₂ were obtained by, and **[11]**(PF₆)₂(MeOH) with, Mr Thomas Hunter (see BSc report 2009–2010, University of York). ORTEP diagrams and selected bond angles, lengths, torsions and hydrogen-bond parameters are given for **[10]**(PF₆)₂ and **[11]**(PF₆)₂(MeOH) in Figs. 4.3 and 4.4 respectively.

The resulting crystal structures of **[10]**(PF₆)₂ and **[11]**(PF₆)₂(MeOH) contain similar distorted octahedron and adamantane geometries to the previously described structures in this thesis. The DMSO ligand was identified as being coordinated *via* the sulfur atom in the same fashion as the precursor complex **[8]**⁺. Spectroscopic analysis of the DMSO ligand coordination mode is discussed later in section 4.2.3. The structure of the cations **[10]**²⁺ and **[11]**²⁺ are very similar, as expected; both with hydrogen-bonds present between the DMSO oxygen and the adjacent amine groups. In both structures the DMSO ligand is orientated to reside approximately equidistant to the two adjacent amine groups, evident from bond torsions between 40 and 45°.

While the 1,10-phenanthroline ligand of **[11]**(PF₆)₂(MeOH) is geometrically constrained to a planar nature, the pyridine rings of the 2,2'-bipyridyl ligand in **[10]**(PF₆)₂ are twisted by approximately 5.5°. Additionally, the 2,2'-bipyridyl deviates from planarity with the N-Ru-N plane by an average of 10°, towards *cis*-tach. This is in contrast to 1,10-phenanthroline in **[11]**²⁺, where only a bend of 1.2° of the aromatic plane compared to the octahedron centre is observed.

In both structures, the cations are assembled into linear chains, separated by the hexafluorophosphate anions. The cations within **[10]**(PF₆)₂ are linked by two hydrogen-bonds shown in Fig. 4.5. One bond is present between an amine and DMSO oxygen and the other is between a second amine and the π -system of a pyridyl ring. From one cation to the next, there is a rotation about the ruthenium centre of 70.87(5)° - the direction of rotation alternates along the chain, with a repeating unit of two cations.

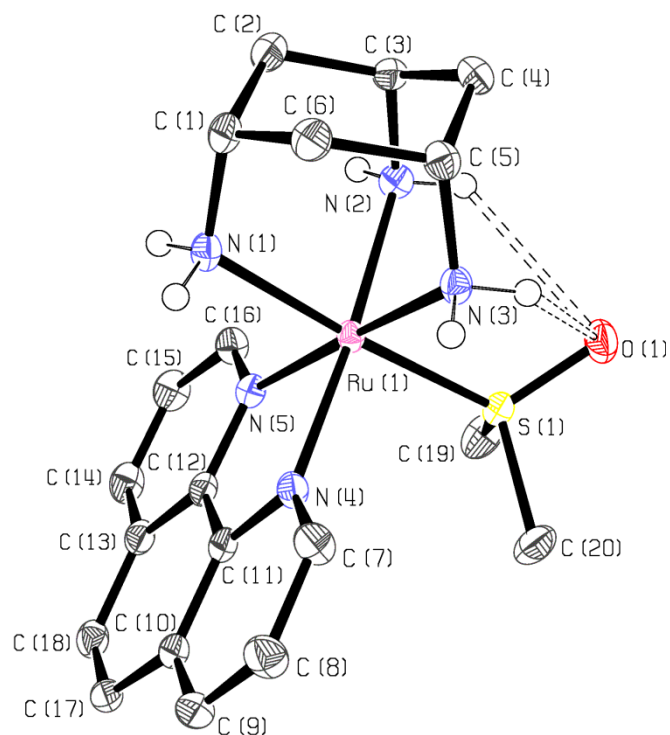


Figure 4.4: ORTEP diagram (50% probability ellipsoids) of **[11]**(PF₆)₂(MeOH). Hydrogen atoms (except for amino hydrogens), solvent and counter ions are omitted for clarity. Selected bond lengths (Å), angles (°) and torsions (°): Ru(1)–N(1) 2.1470(17), Ru(1)–N(2) 2.1470(17), Ru(1)–N(3) 2.1333(16), Ru(1)–N(4) 2.0881(17), Ru(1)–N(5) 2.1008(16), Ru(1)–S(1) 2.2145(8), S(1)–O(1) 1.5016(15), N(1)–Ru(1)–N(2) 87.79(7), N(1)–Ru(1)–N(3) 89.26(7), N(2)–Ru(1)–N(3) 85.79(7), N(4)–Ru(1)–N(5) 79.23(7), N(4)–Ru(1)–S(1) 94.64(5), N(5)–Ru(1)–S(1) 94.64(5), N(1)–Ru(1)–S(1) 176.39(5), Ru(1)–S(1)–O(1) 114.08(7), N(2)–Ru(1)–S(1)–O(1) 44.09(8), N(3)–Ru(1)–S(1)–O(1) –41.71(8). Selected hydrogen-bond (D–H...A–X) lengths (Å) and angles (°) D...A, H...A, D–H...A, H...A–X): N(2)–H(2d)...O(1)–S(1): 3.173(2), 2.57(2), 124.0(17), 82.3(6); N(3)–H(3b)...O(1)–S(1): 3.126(2), 2.48(2), 132(2), 82.6(6).

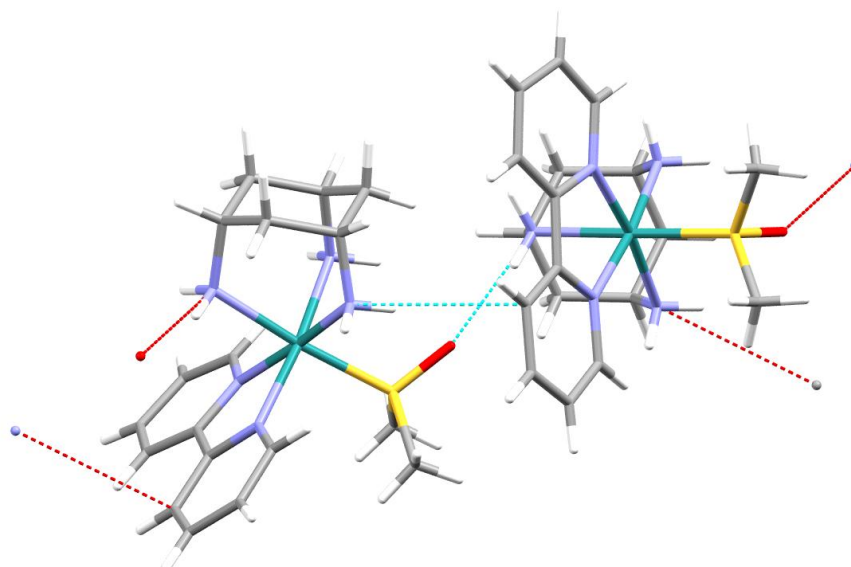


Figure 4.5: Capped stick diagram of the intermolecular hydrogen-bonds within the linear chains of cations in $[\mathbf{10}](\text{PF}_6)_2$, separated by the PF_6 anions. Hydrogen-bonds are drawn as $\text{D}\dots\text{A}$. Selected hydrogen-bond ($\text{D}-\text{H}\dots\text{A}-\text{X}$) lengths (\AA) and angles ($^\circ$) $\text{D}\dots\text{A}$, $\text{H}\dots\text{A}$, $\text{D}-\text{H}\dots\text{A}$, $\text{H}\dots\text{A}-\text{X}$: $\text{N}(1)-\text{H}(1a)\dots\text{O}(1)-\text{S}(1)$ ($x, -y+1/2, z-1/2$) 2.996(4), 2.17(3), 165(3), 157.6(8); $\text{N}(2)-\text{H}(2d)\dots\text{N}(4)^{\text{C}}-\text{N}(4)^{\text{P}}$ ($-x, y-1/2, -z+1/2$) 4.44, 3.52, 164, 57.7 (Malone type V).²⁰⁶ C and P denote the centroid and plane of the respective six-membered ring.

The cationic chain of $[\mathbf{11}](\text{PF}_6)_2(\text{MeOH})$ is different to that of $[\mathbf{10}](\text{PF}_6)_2$, with two distinctly different regions of intermolecular interactions as shown in Fig. 4.6. First, between two ruthenium complexes, which relate to each other by an inversion along the chain axis, several hydrogen-bonds are present. Two triangular hydrogen-bonding motifs are formed between an amine, DMSO oxygen and the methanol solvent. Secondly, $\pi-\pi$ interactions are present between the 1,10-phenanthroline rings of adjacent complexes.

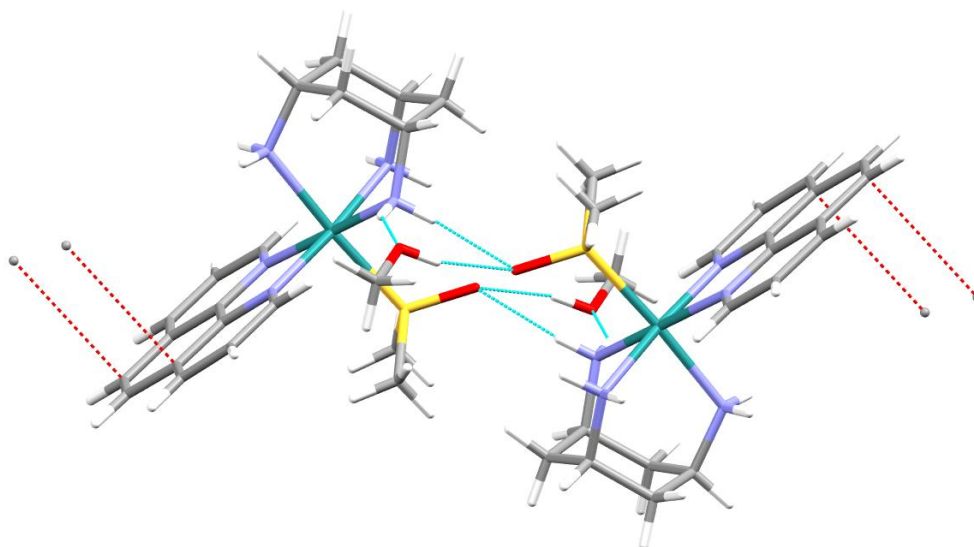


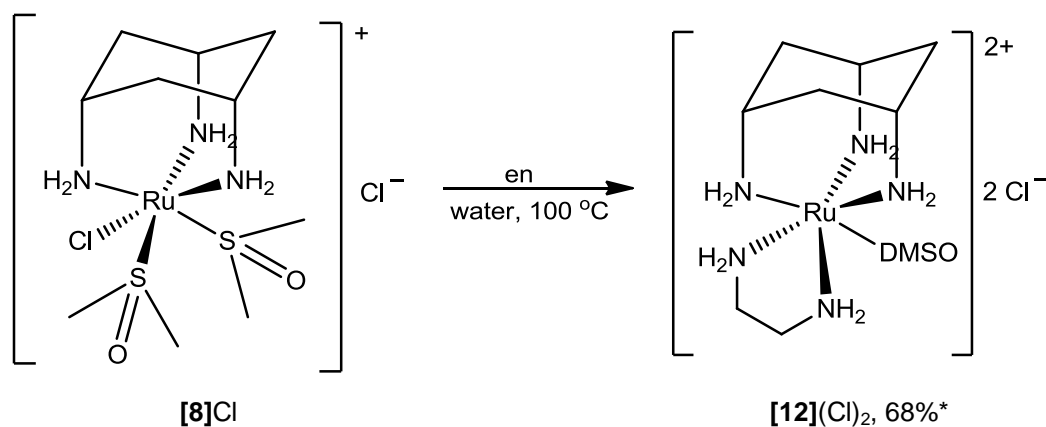
Figure 4.6: Diagram of the intermolecular hydrogen-bonds within the linear chains of cations in $[11](PF_6)_2(MeOH)$. The chains are separated by the PF_6^- anions. Selected π - π length (\AA): C(10)-C(18) ($2-x, 2-y, 1-z$) 3.334(3). Selected hydrogen-bond (D-H...A-X) lengths (\AA) and angles ($^\circ$) D...A, H...A, D-H...A, H...A-X: N(3)-H(3b)...O(1)-S(1) ($-x, -y, -z$) 3.127(2), 2.45(2), 136(2), 140.4(6); N(3)-H(3a)...O(3)-C(21) ($-x, -y, -z$) 2.951(2), 2.15(3), 152(2), 149.2(8); O(2)-H(2)...O(1)-S(1) ($x, y, z+1$) 2.839(2), 2.06(3), 155(3), 134(1).

Conclusions

Successful coordination of a chelating ligand to $[8]Cl$ was achieved with 2,2'-bipyridyl and 1,10-phenanthroline to give the complexes $[10](Cl)_2$ and $[11](Cl)_2$. These complexes were characterised by NMR spectroscopy, mass spectrometry and single crystal X-ray diffraction. In place of the expected chlorido based complex, a DMSO complex was obtained, in which the coordination mode was revealed by the resulting structural determination to be through sulfur donation. Further aspects of the nature of the metal-DMSO bonding are discussed later (section 4.2.3).

4.2.2 1,2-Ethylenediamine Complex

In addition to the two pyridyl based ligands employed in $[10]^{2+}$ and $[11]^{2+}$, the preparation of a Ru(II) *cis*-tach 1,2-ethylenediamine (en) complex was investigated to expand the family of *N,N*-chelate complexes and to attempt to prepare an RM175 analogue. Reaction of en with $[8]Cl$ followed a similar route to the previous *N,N*-chelate complexes under the same conditions, giving a yellow product (Scheme 4.2). The 1H NMR spectrum of the product in D_2O replicated that of $[10]^{2+}$ and $[11]^{2+}$, with resonances assignable to coordinated *N,N*-chelate ligand, *cis*-tach in a C_s symmetry environment and a DMSO ligand at δ_H 3.34 ppm. The proposed structure of the complex, $[Ru(en)(DMSO)(cis-tach)]^{2+}$, ($[12]^{2+}$) was confirmed by ESI mass spectrometry by the observation of a peak assigned to the molecular ion, with m/z 184.5553 (100%, $[M]^{2+}$) and an isotope pattern corresponding to a dicationic ruthenium species.



Scheme 4.2: Reaction of $[8]Cl$ with 1,2-ethylenediamine (en) to give $[Ru(en)(DMSO)(cis-tach)](Cl)_2$, $[12](Cl)_2$. A DMSO and the chlorido ligand are displaced by coordination of en, giving a DMSO-S complex. *Isolated yield.

Single crystals suitable for X-ray diffraction were obtained by chloride metathesis of $[12](Cl)_2$ with potassium hexafluorophosphate and slow evaporation of a methanol solution. ORTEP diagram and selected bond angles, lengths, torsions and hydrogen-bond parameters are given for $[12](Cl)(PF_6)$ in Fig. 4.7.

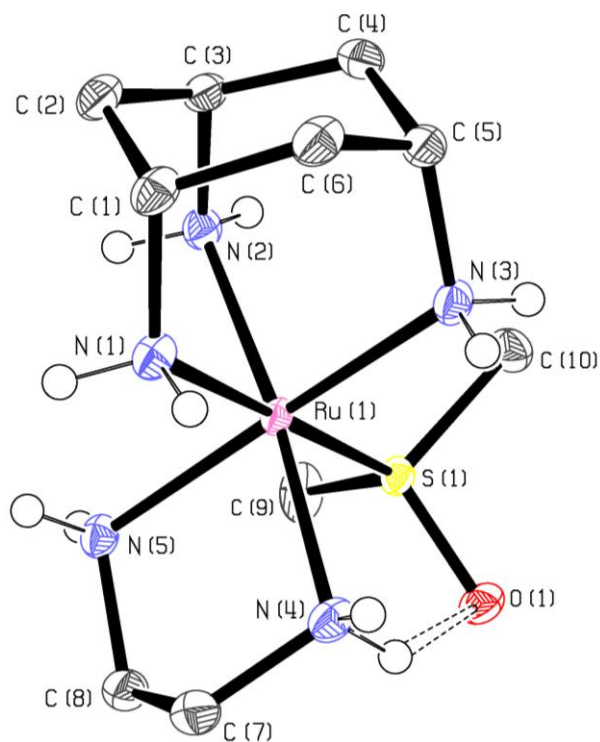


Figure 4.7: ORTEP diagram (50% probability ellipsoids) of **[12](Cl)(PF₆)**. Hydrogen atoms (except for amino hydrogens) and counter ions are omitted for clarity. Selected bond lengths (\AA), angles ($^\circ$) and torsions ($^\circ$): Ru(1)–N(1) 2.1665(13), Ru(1)–N(2) 2.1396(14), Ru(1)–N(3) 2.1316(14), Ru(1)–N(4) 2.1262(14), Ru(1)–N(5) 2.1373(14), Ru(1)–S(1) 2.1885(4), S(1)–O(1) 1.5008(12), N(1)–Ru(1)–N(2) 88.67(5), N(1)–Ru(1)–N(3) 83.26(6), N(2)–Ru(1)–N(3) 92.00(5), N(4)–Ru(1)–N(5) 81.59(5), N(4)–Ru(1)–S(1) 89.83(4), N(5)–Ru(1)–S(1) 92.68(4), N(1)–Ru(1)–S(1) 176.71(4), Ru(1)–S(1)–O(1) 117.15(5), N(4)–Ru(1)–S(1)–O(1) - 7.99(7). Selected hydrogen-bond (D–H...A–X) lengths (\AA) and angles ($^\circ$) D...A, H...A, D–H...A, H...A–X): N(4)–H(4d)...O(1)–S(1): 2.9833(19), 2.27(2), 137.9(17), 89.3(5).

The solid state structure of $[\mathbf{12}](\text{Cl})(\text{PF}_6)$ does not follow the model of $[\mathbf{10}](\text{PF}_6)_2$ and $[\mathbf{11}](\text{PF}_6)_2(\text{MeOH})$. The DMSO ligand does not participate in intramolecular hydrogen-bonding with *cis*-tach, but to the ethylenediamine ligand. This most likely results from the increased flexibility of the en ligand, whereby stronger hydrogen-bonds can be formed. The most prominent difference in the crystal structure of $[\mathbf{12}]^{2+}$ when compared to $[\mathbf{10}]^{2+}$ and $[\mathbf{11}]^{2+}$ is the partial metathesis of chloride with hexafluorophosphate, whereby a single chloride anion has been retained. The chloride resides in a hydrogen-bonding pocket, created by two cationic units as shown in Fig. 4.8. The greater capability for $[\mathbf{12}]^{2+}$ to hydrogen-bond to a chloride anion, due to the increased number of hydrogen-bond donors in comparison to $[\mathbf{10}]^{2+}$ and $[\mathbf{11}]^{2+}$ provides a rationale for the chemical composition observed.

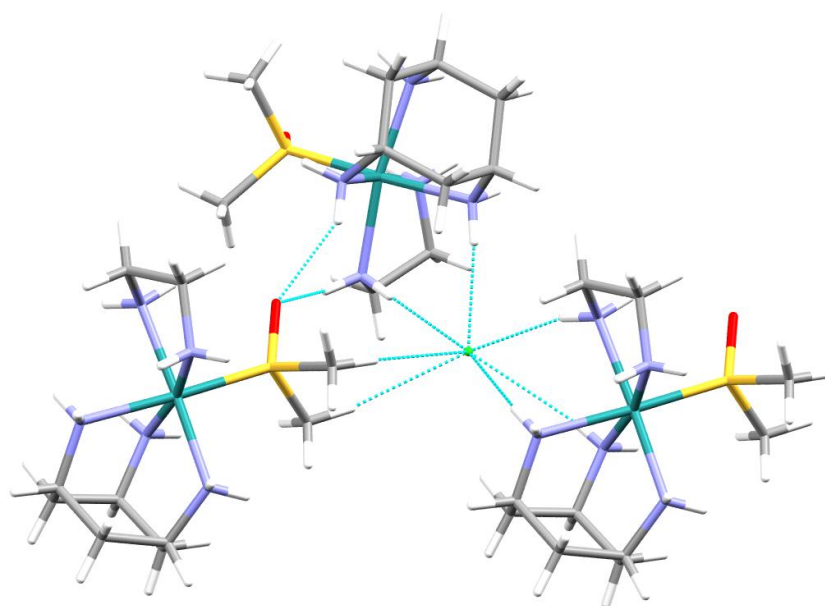


Figure 4.8: Diagram of the intermolecular hydrogen-bonds between the ruthenium complexes and chloride anions in $[\mathbf{12}](\text{Cl})(\text{PF}_6)$. Selected hydrogen-bond (D–H...A–X) lengths (Å) and angles (°) D...A, H...A, D–H...A: C(9)–H(9a)...Cl(1): 3.811(2) 2.8788(4), 159.3(1); C(10)–H(10c)...Cl(1): 3.680(2), 2.7249(4), 164.8(1).

On further inspection of the groups surrounding the chloride anion, there are two highly directional near-space interactions of 2.8788(4) and 2.7249(4) Å between two methyl protons of DMSO and the chloride anion, also shown in Fig. 4.8. As the methyl protons in DMSO carry a partial positive charge, δ^+ , they are therefore able

to participate in hydrogen-bonding to the chloride anion.²⁵⁷ This interaction completes the hydrogen-bonding cavity in which the chloride anion resides.

The cations are assembled in a hydrogen-bonded “zigzag” structure as opposed to the linear chains present in the structures [10]²⁺ and [11]²⁺. The hydrogen-bonding structure of these chains is shown in Fig. 4.9. The bonding between two of the cations consists of two intermolecular hydrogen-bonds, with *cis*-tach and 1,2-ethylenediamine of one cation acting as donor groups and the DMSO ligand of an adjacent complex an acceptor of both interactions.

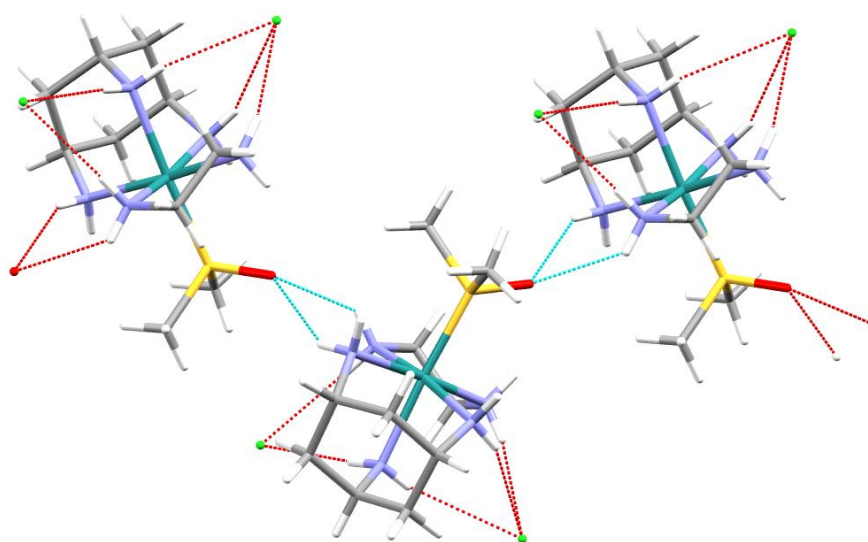


Figure 4.9: Diagram of the intermolecular interactions within the “zigzag” chains of cations in [12](Cl)(PF₆). The chains are separated by Cl and PF₆ anions. Selected hydrogen-bond (D–H...A–X) lengths (Å) and angles (°) D...A, H...A, D–H...A, H...A–X: N(2)–H(2c)...O(1)–S(1) (–x+1, y+1/2, –z+1/2) 2.9376(18), 2.17(2), 147.0(19), 138.6(6); N(5)–H(5a)...O(1)–S(1) (–x+1, y+1/2, –z+1/2) 3.1352(18), 2.54(2), 129.1(17), 122.4(5).

The chloride anions act as a template around which the chains are arranged; a schematic diagram is given in Fig. 4.10. The hexafluorophosphate anions reside between sheets of these chains to complete the structure.

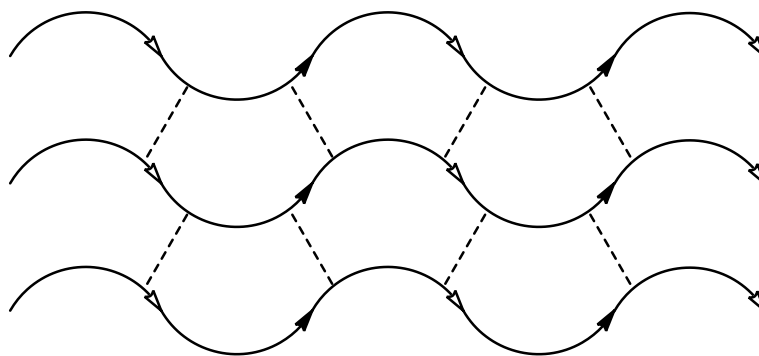


Figure 4.10: Schematic diagram of the solid state structure of $[\mathbf{12}](\text{Cl})(\text{PF}_6)$. The arrows and dotted lines represent the cation “zigzag” chain shown in Fig. 4.9 and the cation-chloride hydrogen-bonds in Fig. 4.8 respectively. The arrow tail represents the NH donor and the head the oxygen acceptor in the intra-chain hydrogen-bonds.

Conclusions

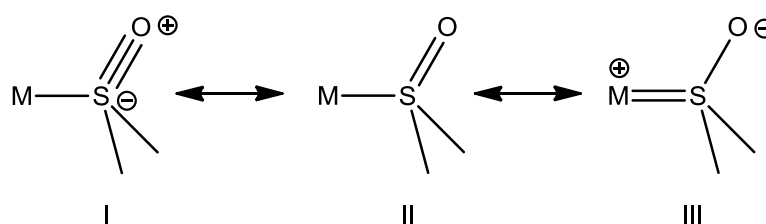
The reaction of $[\mathbf{8}]\text{Cl}$ and 1,2-ethylenediamine follows a similar route to the reaction with the polypyridyl ligands, as described previously. Again, a DMSO-*S* ligand is incorporated in the complex $[\text{Ru}(\text{DMSO-}S)(\text{en})(\text{cis-tach})](\text{Cl})_2$, $[\mathbf{12}](\text{Cl})_2$, and the spectroscopic and crystallographic properties of the DMSO in the complexes with a *N,N*-chelating ligand will be discussed in detail in the following section.

4.2.3 Analysis of the DMSO Ligand Coordination Mode

The coordination mode of the DMSO ligand in the *N,N*-chelate complexes $[\mathbf{10-12}]^{2+}$ was initially assigned by the geometry observed in the single crystal X-ray diffraction solution. A single crystal is not representative of the overall composition of the compound and bulk spectroscopic techniques are required to fully characterise the complexes. Often, IR spectroscopy is employed to determine the donor atom of DMSO in a coordination complex. Although this was straight-forward in the assignment of $[\mathbf{8}]\text{Cl}$, the $\nu(\text{S-O})$ band for the complexes $[\mathbf{10-12}](\text{Cl})_2$ range between 1015 and 1035 cm^{-1} . These are just within the expected DMSO-*O* region of 878–1035 cm^{-1} .²³⁸ In comparison, the $\nu(\text{S-O})$ bands of the recently reported analogous DMSO-*S* tacn complexes with en and bipy range between 1110 and 1077 cm^{-1} .¹⁶⁶

Therefore, further analysis of the data from all techniques is required to confidently determine the coordination geometry.

The valence bond model for describing the nature of the bonding character of the DMSO-*S* ligand is considered to be of three resonance forms, shown in Scheme 4.3.²²⁵ The resonance form experimentally proven to dominate in DMSO-*S* metal complexes is that of form II. Coordination of DMSO by the oxygen donor is considered to be dominated by the $\text{Me}_2\text{S}^+-\text{O}^-$ form. This is similar to the resonance form of free DMSO, which has been proven to be predominantly $\text{Me}_2\text{S}^+-\text{O}^-$ from crystallographic evidence.²²⁵



Scheme 4.3: Canonical forms of $\text{M-S(O)(CH}_3)_2$ contributing to the resonance hybrid.

The coordination of a sulfoxide to a metal complex *via* the sulfur atom typically results in an increase in the $\nu(\text{S-O})$ frequency from the increased bond order in comparison to the free ligand.²⁴¹ This is reflected in a decreased S-O bond length observed in the X-ray crystal structures relative to the free ligand. On the other hand, oxygen coordination results in the opposite occurring, as the $\text{Me}_2\text{S}^+-\text{O}^-$ resonance form is stabilised.²⁴¹ For both coordination modes, the shift in $\nu(\text{S-O})$ parallels the change in S-O bond length in the X-ray crystal structure. Therefore, despite the correlation, the $\nu(\text{S-O})$ frequency reflects the S-O bond order and length – not the identity of the donor atom, a common misinterpretation of infrared spectra. Crystallographic and spectroscopic parameters for the complexes **[10–12]**²⁺ are presented in Table 4.1.

	$\nu(\text{S-O})$ (cm^{-1})	$\delta_{\text{H}} \text{CH}_3$ (ppm)	Mean $r(\text{A-B})$ (\AA)	
			M-S	S-O
[10] ²⁺	1015	2.63	2.222(1)	1.500(2)
[11] ²⁺	1016	2.52	2.215(1)	1.502(2)
[12] ²⁺	1035	3.34	2.189(1)	1.501(2)
DMSO- <i>S</i>	1070–1233 ²³⁸	≥ 3.2 ²²⁵	2.260(2) ²⁴¹	1.480(1) ²⁴¹
DMSO	1055 ²⁵⁸	2.71 ²⁵⁹		1.492(1) ²⁴¹
DMSO- <i>O</i>	878–1035 ²³⁸	≤ 3.2 ²²⁵		1.545(3) ²⁴¹

Table 4.1: Infra-red, ¹H NMR and selected bond lengths of the DMSO ligand in **[10–12]**²⁺ and averages for ruthenium(II) DMSO-*S* and DMSO-*O* complexes, as well the free ligand.

The frequency of the $\nu(\text{S-O})$ band in the infrared spectra for complexes **[10–12]**²⁺ is decreased in comparison to DMSO at 1055 cm^{-1} in the solid state.²⁵⁸ This suggests that the resonance form of the DMSO ligand in these complexes is dominated by the $\text{Me}_2\text{S}^+-\text{O}^-$ form, therefore the S–O bond length for all three complexes is expected to be longer than in the free ligand. Although the S–O bond length of the free ligand has been determined by crystallography to be $1.522(2) \text{ \AA}$, poor diffraction quality has lead to the suggested value of $1.492(1) \text{ \AA}$ for a ‘true’ S–O bond length based on several DMSO-solvate and sulfoxide structures.^{239, 241, 260, 261} The X-ray diffraction data for all three complexes is in agreement with the observed $\nu(\text{S-O})$ bands in the infrared spectra, where the S–O bond lengths of approximately $1.501(2) \text{ \AA}$ are longer than the accepted value for the free ligand. Therefore, the complexes are proposed to adopt resonance form III from Scheme 4.3. The average S–O bond lengths for single-DMSO-*S* and DMSO-*O* ruthenium(II) complexes are $1.480(1) \text{ \AA}$ and $1.545(3) \text{ \AA}$ respectively.²⁴¹ Although both the S–O bond lengths and stretching frequency are within the range expected for DMSO-*O* complexes, the bulk composition of the three *cis*-tach complexes in the solid form is that of *S*-coordination.

The nature of the metal-sulfur bond can also be determined from the X-ray crystal data. All three complexes have shorter Ru–S bonds than the average for single-DMSO-*S* ruthenium(II) complexes of 2.260(2) Å.²⁴¹ This is reflected by the resonance form of **[10–12]**²⁺ as form III in Scheme 4.3 opposed to form II for the majority of DMSO-*S* complexes. This is expected based on the observations made in previous chapters of the strong ability for *cis*-tach to act as a good σ -donor ligand. This results in increased π - back donation from the electron-rich metal centre to the DMSO $\pi^*(\text{S–O})$ orbital (Section 3.3). The observed trend in Ru–S bond distances correlate to the ability for the *N,N*-chelate to act as a π -acceptor and therefore reduce the electron density of the metal, thereby decreasing the Ru–S bond order. In the case of **[12]**²⁺, the en ligand is a poor π -acceptor so is unable to remove electron density from the metal, resulting in a shorter Ru–S bond.

The difference in metal-sulfur bond order for the three complexes would be expected to be reflected in the sulfur-oxygen bond length. However, the crystal data for the complexes show this not to be the case, with S–O bond lengths approximately equal at 1.501(2) Å. It has been demonstrated that hydrogen-bonding to a sulfoxide has a profound effect on the S–O bond length.^{241, 260} It is evident from the crystal structures of **[10–12]**²⁺ that each DMSO ligand is in a distinctly different hydrogen-bonding environment. This may also account for the variation in the $\nu(\text{S–O})$ band in the infrared spectra.

The conclusions made for the bonding nature of the ruthenium(II) *cis*-tach DMSO complexes are in agreement with those for the complex $[\text{Ru}(\text{NH}_3)_5(\text{DMSO-}i>S)]^{2+}$, especially in the case of **[12]**²⁺ owing to its structural similarity. The ammine complex is reported to have a $\nu(\text{S–O})$ of 1045 cm^{-1} and Ru–S and S–O bond lengths of 2.188(3) and 1.512(7) Å respectively.^{262, 263} These bond lengths are (within error) similar to those of **[12]**²⁺.

	<i>fac</i> -ligand	L	ref.	$\nu(\text{S-O})$ (cm^{-1})	$\delta_{\text{H}} \text{CH}_3$ (ppm)	Mean $r(\text{A-B})$ (\AA) M-S	S-O
[10] ²⁺	tach	bipy		1015	2.63	2.222(1)	1.500(2)
	tacn	bipy	¹⁶⁶	1077	2.67	2.224(2)	1.498(5)
	tten	bipy	¹⁶¹	<i>a</i>	2.83	2.285(3)	1.487(8)
[11] ²⁺	tach	phen		1016	2.52	2.215(1)	1.502(2)
[12] ²⁺	tach	en		1035	3.34	2.189(1)	1.501(2)
	tacn	en	¹⁶⁶	1110	3.33	2.211(2)	1.492(3)
	(NH ₃) ₃	(NH ₃) ₂	^{262, 263}	1045	3.28	2.188(3)	1.512(7)

Table 4.2: IR, ¹H NMR and selected bond lengths of the DMSO ligand in complexes of the formula $[\text{Ru}(\text{dmsO})(\text{fac-ligand})(\kappa^2\text{-L})]^{2+}$. *a*) not assigned in literature.

The other commonly employed spectroscopic technique for the determination of the DMSO donor atom is ¹H NMR spectroscopy. Coordination to the metal results in the deshielding of the methyl protons resulting in a down-field shift.²²⁵ The proximity of the protons to the donor atom is reflected by the degree of deshielding. *O*- coordination of DMSO results in small downfield shifts of less than 0.5 ppm, whereas a large shift of ~1 ppm is observed for *S*- coordination. This conveniently applies to **[12]**²⁺ with a DMSO-*S* resonance at δ_{H} 3.34 ppm in D₂O, a shift of 0.63 ppm downfield from the free ligand at δ_{H} 2.71 ppm. Again, the observation corresponds to $[\text{Ru}(\text{NH}_3)_5(\text{DMSO-}i>S)]^{2+}$ with a DMSO-*S* resonance at δ_{H} 3.28 ppm in D₂O.²⁶² However, **[10]**²⁺ and **[11]**²⁺ do not follow the trend with resonances slightly upfield of the free ligand by 0.1 to 0.2 ppm. This observation was confirmed by the addition of trace amounts of free DMSO. An upfield shift is not accounted for by *O*-coordination, therefore it is proposed that the near-by polypyridyl ligand aromatic system is causing a shielding effect of the methyl protons. This is apparent from the X-ray crystal structure of **[10]**²⁺ in Fig. 4.11.

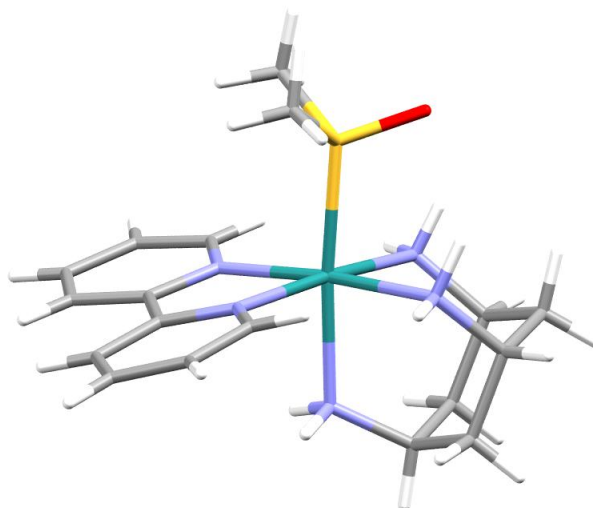


Figure 4.11: Diagram of $[10](PF_6)_2$ showing the proximity of the DMSO methyl protons to the aromatic system of the 2,2'-bipyridine ligand. The average H...bipy-plane distance is 2.98(6) Å.

A similar phenomenon was observed with DMSO-*S* and bipy for the complexes $[Ru(DMSO-S)(bipy)(ttcn)]^{2+}$ and $[Ru(DMSO-S)(bipy)(tacn)]^{2+}$ with DMSO-*S* resonances at δ_H 2.83 and 2.67 ppm respectively in D_2O , also attributed to the shielding cone of the aromatic system.^{161, 166} A rationale for the greater shielding of the methyl protons in the *cis*-tach and tacn complexes may be due to the geometrical constraints from hydrogen-bonding to the *fac*-ligand. This hinders the rotation of the Ru–S bond and the positioning of the methyl groups away from the π system.

The apparently strong ruthenium–sulfur bond, evident from the crystal structures of $[10-12]^{2+}$, is consistent with the inability for the remaining DMSO ligand to undergo a substitution reaction with the solvent during synthesis. Preparation of these complexes in water, heated at reflux provides further evidence that the DMSO ligand is inert to substitution in complexes $[10-12]^{2+}$. For example, the corresponding aqua species of $[11]^{2+}$, $[Ru(OH_2)(phen)(cis-tach)]^{2+}$ is only observed in aqueous solution under ionisation conditions in ESI mass spectrometry; these complexes are inert to aquation, even when heated at reflux in water. This is reflected by the significantly slower solvolysis of $[Ru(DMSO-S)(bipy)(ttcn)]^{2+}$, which occurs over several days in comparison to the chlorido derivative $[RuCl(bipy)(ttcn)]^+$ which occurs within minutes.¹⁶¹

4.2.4 Conclusions

Reaction of [8]Cl with the *N,N*-chelating ligands bipy, phen and en results in the formation of the dimethylsulfoxide complexes [Ru(DMSO-*S*)(*N-N*)(*cis*-tach)](Cl)₂ [10–12](Cl)₂ that were characterised by NMR and IR spectroscopy, mass spectrometry and single crystal X-ray diffraction. The isolation of DMSO-*S* complexes opposed to the chlorido analogues with the *N,N*-chelates is accountable by the observations from the spectroscopic and crystallographic techniques employed. It is evident that the metal centre is electron rich in all three complexes, resulting in a strong ruthenium–DMSO bond and is therefore expected to be inert to substitution reactions. These complexes were still considered for *in vitro* biological evaluation.

4.3 *In Vitro* Biological Evaluation

The complex selected for biological evaluation by the MTT assay was [Ru(DMSO-*S*)(phen)(*cis*-tach)](Cl)₂ [11](Cl)₂ as it was successfully isolated with analytical purity. A modified procedure of that reported by Carmichael and co-workers was used, and [11](Cl)₂ was assessed for anti-proliferative (growth inhibition) activity with the A549 human lung adenocarcinoma cell line.^{228, 246} At concentrations up to 300 μM, [11](Cl)₂ was not found to inhibit the growth of tumour cells and was therefore considered inactive.

It is proposed that the poor activity of [11](Cl)₂ is due to the poorly labile DMSO ligand, and that aquation does not occur, not even when exposed to harsh conditions (e.g. boiling, *c.f.* synthesis). The DMSO ligand was observed to undergo substitution when reacted with guanosine (Guo), where the Ru-Guo adduct [Ru(Guo)(phen)(*cis*-tach)]²⁺ (*m/z* 347.2, 35%) was observed by ESI mass spectrometry. Only when subjected to the ionisation conditions of the ESI technique is the aqua-adduct [Ru(OH₂)(phen)(*cis*-tach)]²⁺ observed (*m/z* 214.6, 5%). The dominant ion in the mass spectrum is that of the starting complex, [11]²⁺ (*m/z* 244.6, 100%), suggesting poor affinity of guanosine to the complex.

A similar conclusion was made for the aquation-inert tacn complexes $[\text{Ru}(\text{DMSO-}S)(\text{N-N})(\text{tacn})](\text{Cl})_2$, (where N–N = en, dach), both of which were also inactive *in vitro*.¹⁶⁶ However, when N–N is bipy, exchange of DMSO with water (aquation) was observed, reaching equilibrium in approximately 6 days.¹⁶⁶ In contrast, the *cis*-tach analogue **[10]**(Cl)₂ is inert to exchange with the solvent in aqueous solutions, further highlighting the difference in reactivity of the ruthenium(II) *cis*-tach complexes and those of its isomer, tacn.

The complexes containing N–N chelating ligands presented within this chapter have been demonstrated, by the use of **[11]**²⁺ as an example, to be inactive in the inhibition of cancer cell growth. The DMSO ligand of this complex is resistant to exchange with water or Guo, hypothesised to be due to the strong Ru–S bond.

In an effort to obtain an active anti-cancer compound, a different design strategy must be employed. Principally, complexes with a chlorido leaving group are desired, where the chlorido concentration gradient from the plasma to the nucleus can be exploited to increase the activation of the compound within a cell and the nucleus. Furthermore, it is hoped that a chlorido ligand will act as a better leaving group, as suggested by the X-ray comparisons of the phosphane complexes (Section 2.3), enabling complexes which readily participate in ligand exchange reactions—both with the solvent and biomolecules.

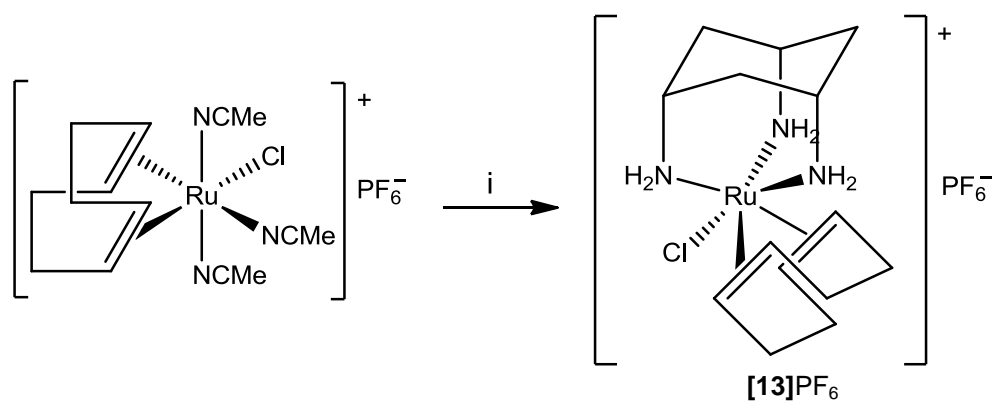
4.4 Attempted Preparation of Chlorido Analogues

Due to the resistance to substitution of the DMSO ligand in the complexes **[10–12]**²⁺, the chlorido analogues ($[\text{RuCl}(\text{N-N})(\textit{cis}\text{-tach})]^+$) were of interest. In order to prepare these complexes an alternative synthetic strategy is required. Modification of the reaction conditions in the preparation of **[10–12]**²⁺ is limited by solubility issues of **[8]**Cl. Therefore, alternative ruthenium(II) *cis*-tach complexes were developed to avoid use of the use of a DMSO precursor.

4.4.1 Use of η^4 -1,5-Cyclooctadiene Precursor Compounds

An alternative synthetic precursor to $[\text{RuCl}(\text{DMSO-}S)_2(\text{cis-tach})]\text{Cl}$ is potentially available by the use of a labile bidentate ligand. The η^4 -1,5-cyclooctadiene ligand is commonly used as a labile group in the ruthenium(II) synthetic chemistry of both η^5 -cyclopentadienyl and κ^3 -*tris*(pyrazolyl)borate.^{264, 265} An equivalent synthetic procedure with ruthenium(II) *cis-tach* complexes would permit the preparation of a variety of complexes containing chelating ligands, avoiding the use of the poorly labile DMSO ligands in **[8]**Cl. A potential ruthenium(II) precursor to use for the reaction with *cis-tach* is the polymeric Ru(II) η^4 -1,5-cyclooctadiene species, $[\text{RuCl}_2(\eta^4\text{-COD})]_n$. However, poor solubility of this compound in polar solvents was problematic in the preparation of target compounds. Therefore, the *tris*-acetonitrile derivative $[\text{mer-RuCl}(\text{NCMe})_3(\eta^4\text{-COD})]\text{PF}_6$ was employed. Use of this species not only has the advantage of greater solubility, but metathesis of the chlorido ligand has been previously performed. Displacement of the acetonitrile ligands with *cis-tach* was expected to yield $[\text{RuCl}(\eta^4\text{-COD})(\text{cis-tach})]\text{PF}_6$.

The successful coordination of *cis-tach* with $[\text{mer-RuCl}(\text{NCMe})_3(\eta^4\text{-COD})]^+$ was achieved by heating of the two reagents at reflux in ethanol and confirmed by the same methods employed for the previous complexes in this thesis. Amine resonances were observed in the ^1H NMR spectrum and were shifted downfield, resultant of electron donation to the metal. The absence of coordinated acetonitrile resonances coupled with those for a coordinated η^4 -COD ligand suggested the identity of this species is $[\text{RuCl}(\eta^4\text{-COD})(\text{cis-tach})]\text{PF}_6$, **[13]**PF₆. Furthermore, the *cis-tach* resonances demonstrated that the complex possessed C_s symmetry, in agreement with the η^4 -COD resonances. The proposed structure is shown in Scheme 4.4. Additionally, the ESI mass spectrum supported the assignment with a molecular ion observed in 100% abundance with m/z 374.0937 and corresponding isotope pattern. The only other ions observed were those resulting from the loss of a chlorido ligand.



Scheme 4.4: Preparation of $[\text{RuCl}(\eta^4\text{-COD})(\text{cis-tach})]\text{PF}_6$ (**[13]** PF_6) from the reaction of *cis-tach* with $[\text{mer-RuCl}(\text{NCMe})_3(\eta^4\text{-COD})]^+$. (i) *Reagents and conditions:* *cis-tach* (1 equiv.), solvent: ethanol, heated at reflux for 2 h.

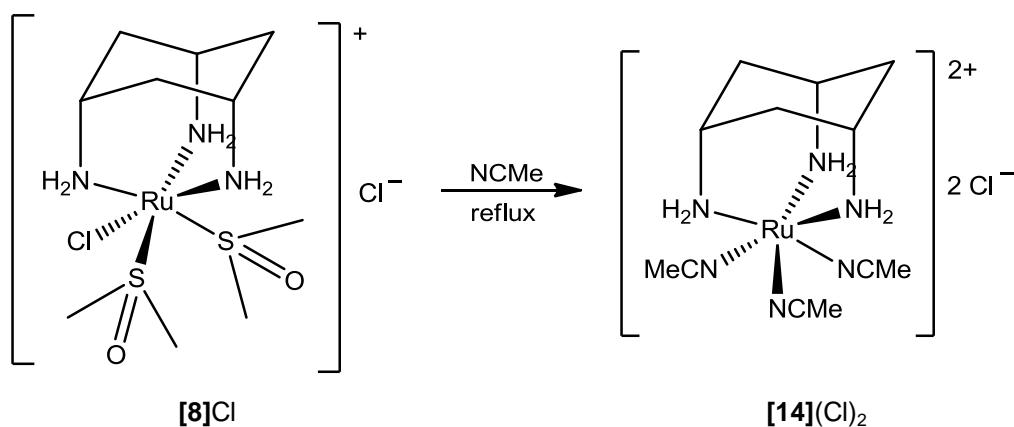
This complex could not to be isolated with analytical purity, nor were crystals suitable for X-ray diffraction analysis obtained. However, this species may offer alternative synthetic procedures to overcome the problems encountered with the use of the DMSO ligand previously, such as that of the hydrogen-bonding interactions with *cis-tach* which may alter the reactivity of the complex. This compound potentially expands the ruthenium(II) *cis-tach* synthetic precursors available for complex design and preparation.

The reaction of **[13]** PF_6 with 2,2'-bipyridine was monitored by ^1H NMR spectroscopy in CD_3OD and heated at 100°C in a sealed NMR tube. Although a colour change from yellow to orange was observed for the solution, no alteration to the ^1H NMR spectrum was recorded. Further heating for a week failed to alter the composition. Furthermore, dissolution of **[13]** PF_6 in d_6 -DMSO and heating at 90°C for 48 h revealed little change in the ^1H NMR spectrum. Therefore, the η^4 -1,5-cyclooctadiene ligand of $[\text{RuCl}(\eta^4\text{-COD})(\text{cis-tach})]^+$ appears to be inert towards substitution and is thus a poor precursor for further ruthenium (II) *cis-tach* complexes. Similar reactivity is observed for the equivalent Tp (*tris*(pyrazolyl)borate) complexes, in which the chloride ligand is readily labile.²⁶⁵ The η^4 -1,5-cyclooctadiene ligand in these complexes is relatively inert to substitution, requiring harsh conditions of heating under reflux in DMF for extended periods of time.²⁶⁵ An explanation for this observation in both systems is due to the

highly π -acidic nature of η^4 -COD, resulting in strong bonding with the electron rich ruthenium centre. On comparison to Tp, *cis*-tach is expected to act as a stronger σ -donor and therefore require even harsher conditions to displace the η^4 -COD ligand.

4.4.2 Use of Acetonitrile Precursor Compounds

In order to avoid highly π -acidic ligands, acetonitrile was employed. Successful preparation of a complex such as $[\text{RuCl}(\text{NCMe})_2(\textit{cis}\text{-tach})]^+$ would provide a convenient synthesis to the desired complexes by the displacement of the acetonitrile ligands. After initial dissolution in water, reaction of **[8]**Cl with acetonitrile whilst heating under reflux yielded $[\text{Ru}(\text{NCMe})_3(\textit{cis}\text{-tach})](\text{Cl})_2$ **[14]**(Cl)₂ (Scheme 4.5). This was evident from the ¹H NMR spectrum in D₂O where the *cis*-tach ligand exhibits C_{3v} symmetry, alongside a single resonance with integration corresponding to three acetonitrile ligands. The ESI mass spectrum supported the assignment with a molecular ion observed in 100% abundance with *m/z* 177.1 and corresponding isotope pattern for $[\text{M}]^{2+}$.



Scheme 4.5: Preparation of the complex $[\text{Ru}(\text{NCMe})_3(\textit{cis}\text{-tach})](\text{Cl})_2$ **[14]**(Cl)₂ by reaction of $[\text{RuCl}(\text{DMSO-S})_2(\textit{cis}\text{-tach})]\text{Cl}$ (**[8]**Cl) with acetonitrile and heating at reflux. **[8]**Cl required solvation in water and subsequent dilution with acetonitrile.

This species is structurally different to the desired complex, $[\text{RuCl}(\text{NCMe})_2(\textit{cis}\text{-tach})]^+$. The increased electron density located on the metal from a large number of nitrogen donor ligands has apparently increased the lability of the chlorido ligand. Alteration of the reaction conditions did not provide selectivity for a chlorido

complex. Although it was evident that dissociation of the chlorido ligand had occurred during the reaction, the synthetic scope of the compound was investigated with 2,2'-bipyridine. Unfortunately, the reaction in methanol did not provide a suitable single product, where it was evident that at least four 2,2'-bipyridine ruthenium (II) complexes were present in the reaction mixture.

4.4.3 Conclusions

It is apparent that the aim of preparing a chlorido complex following the general formula $[\text{RuCl}(\text{L})(\text{cis-tach})]\text{Cl}$, where L is a bidentate ligand is not without difficulty for *N,N*-chelating ligands. The strong σ -donor of *cis-tach* results in an electron-rich metal centre and is therefore stabilised by coordination of a π -acidic ligand. In the case of bipy, phen and en, the π -acidic nature of the ligands is insufficient to provide a suitable complex for application as an anti-cancer agent. Therefore, the identity of L, the chelating ligand, must be modified to compliment the properties of *cis-tach*.

4.5 Chapter Conclusions

The library of ruthenium *cis-tach* complexes has been extended to include the *N,N*-chelate complexes with bipy, phen and en, **[10]**(Cl)₂, **[11]**(Cl)₂ and **[12]**(Cl)₂ respectively. These complexes were isolated and shown to have retained a DMSO ligand from the starting complex **[8]**Cl, as evidenced by NMR and IR spectroscopy, ESI mass spectrometry and single crystal X-ray diffraction. IR spectroscopy and the structural determinations revealed the sulfoxide ligand in all complexes to adopt a greater degree of the $\text{Me}_2\text{S}^+-\text{O}^-$ resonance form. This has resulted in a shorter than average Ru–S bond, suggesting a poorly labile DMSO ligand and is reflected by the inability for displacement of the ligand with solvent while heated at reflux in water.

The complex $[\text{Ru}(\text{DMSO-}S)(\text{phen})(\text{cis-tach})](\text{Cl})_2$ (**[11]**{Cl})₂ was assessed for antiproliferative activity with the A549 human lung adenocarcinoma cell line where **[11]**(Cl)₂ was found to be inactive. The lack of activity was hypothesised to be due to the poor reactivity of the Ru–S bond, preventing the complex from coordination biomolecules.

In an attempt to obtain a biologically active species, the preparation of complexes following the formula $[\text{RuCl}(\text{N-N})(\text{cis-tach})]\text{Cl}$ was investigated. Two techniques were attempted to yield the desired compound. First, $[\text{RuCl}(\eta^4\text{-COD})(\text{cis-tach})]\text{PF}_6$ **[12]** PF_6 was employed, but the reaction with 2,2'-bipyridine failed to give the target species due to the poorly labile $\eta^4\text{-COD}$ ligand. This observation was also made with *tris*(pyrazolyl)-type ligands. Secondly, avoidance of the DMSO ligands was attempted *via* use of acetonitrile ligands, however reaction of **[8]** Cl gave the tris-acetonitrile species $[\text{Ru}(\text{NCMe})_3(\text{cis-tach})](\text{Cl})_2$ **[14]** $(\text{Cl})_2$. Further reactivity with 2,2-bipyridine did not yield a single clean product suitable for further investigation.

It is evident that the *N,N*-chelate complexes do not display suitable properties for the design and development of anti-cancer agents, and the identity of this ligand must be altered. Suitable modification principally concerns that of the donor atom of the chelating ligand, to those capable of complementing the hard σ donor that is *cis-tach*, providing successful synthesis of a chlorido complex. This forms the basis of the next chapter of this thesis.

Chapter 5. Ruthenium (II) *cis*-tach Complexes with P–P Chelating Ligands

5.1 Introduction

The preparation of ruthenium(II) *cis*-tach chlorido complexes with an N–N chelate (Chapter 4) proved difficult. Complexes with the DMSO ligand were exclusively obtained, and were found to be inert to substitution under physiologically relevant conditions. This led to the investigation of other chelating ligands which would alter the kinetic properties of the complex. The triphenylphosphane ligand-set (Chapter 2) allowed the preparation of chlorido complexes; furthermore, $[\text{RuCl}(\text{DMSO-}S)(\textit{cis}\text{-tach})(\text{PPh}_3)]\text{Cl}$ (**[4]**Cl) was weakly active in the inhibition of tumour cell growth. However, the lack of a chelating ligand in the system prevented adequate control of ligand exchange kinetics in a physiologically-relevant environment. The ruthenium(II) *cis*-tach precursor $[\text{RuCl}(\text{DMSO-}S)_2(\textit{cis}\text{-tach})]\text{Cl}$ (**[8]**Cl) provides a potential synthetic pathway for the preparation of complexes of the type $[\text{RuCl}(\text{P-P})(\textit{cis}\text{-tach})]\text{Cl}$.

The use of diphosphane ligands in anti-cancer complexes is already well-established. For example, incorporation of chelating diphosphanes into the gold(I) complex, $[\text{Au}(\text{dppe})_2]\text{Cl}$, provides kinetic stability and enhanced cytotoxicities over monodentate phosphanes.²⁶⁶ They have also been employed in ruthenium(II) half-sandwich complexes; Samuelson and co-workers demonstrated that the complexes $[\text{RuCl}(p\text{-cymene})(\text{P-P})]^+$ where P–P = dppm (Fig. 5.1) and dppe ($\text{IC}_{50} = 1.2$ and 1.4 μM respectively in H460, a lung large-cell carcinoma), are equipotent to cisplatin ($\text{IC}_{50} = 1.7$ μM).²⁶⁷ These complexes were also shown to bind DNA, inducing cell cycle arrest. The use of neutral $\kappa^3\text{-}N$ chelating ligands in the design of ruthenium anti-cancer compounds was first reported by Spivak and co-workers with the trispyrazolylmethane ligand (Tpm).²⁶⁸ These compounds incorporated a chelating diphosphane ligand, following the formula $[\text{RuCl}(\text{P-P})(\text{Tpm})]\text{Cl}$, where P–P = dppe or dppp (Fig. 5.1). The complexes were shown to be highly potent in the inhibition of tumour cell growth with IC_{50} values of 8.1 and 2.9 μM respectively for the MCF-7

cell line. The activity of these complexes surpassed that of cisplatin ($IC_{50} > 18 \mu\text{M}$ for MCF-7) in selected cell lines.²⁶⁸

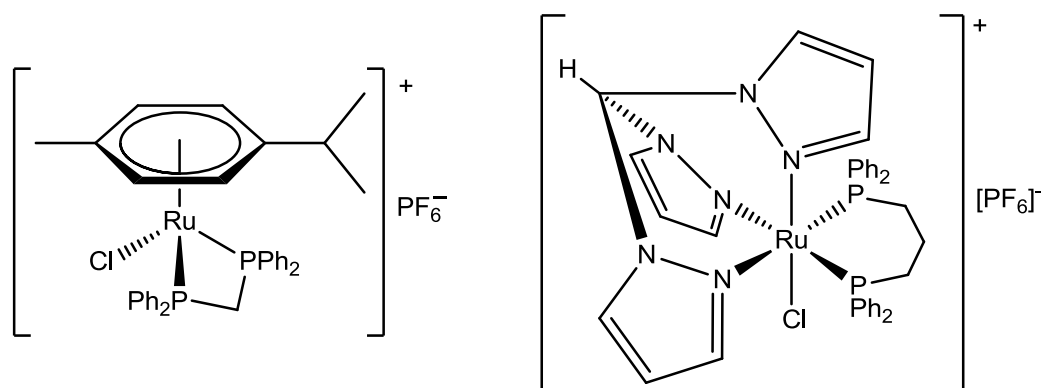


Figure 5.1: Structures of ruthenium(II) complexes with chelating diphosphane ligands assessed for anti-tumour activity *in vitro*: $[\text{RuCl}(p\text{-cymene})(\text{dppm})]\text{PF}_6$ (left) and $[\text{RuCl}(\text{dppp})(\text{Tpm})]\text{PF}_6$ (right).

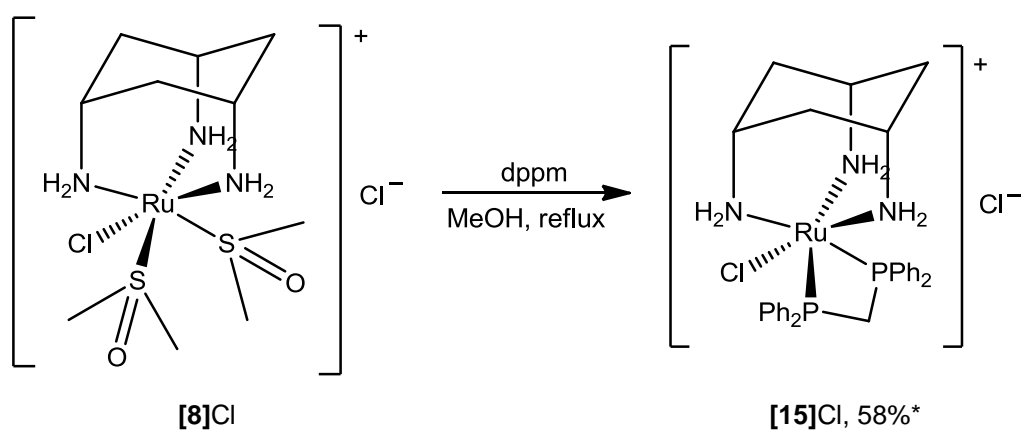
Based on the initial promising results of ruthenium(II) complexes with chelating diphosphane ligands, incorporation of these ligands within *cis-tach* complexes is desirable. Potentially, *cis-tach* may confer advantageous properties to the complex in comparison to the ruthenium(II) compounds previously reported in the literature, particularly though the inclusion of hydrogen-bond donors, allowing the preparation of freely water soluble compounds. The synthesis and characterisation of a series of *cis-tach* complexes containing diphosphane chelating ligands is described, followed by the discussion of X-ray crystal structures and NMR spectra. Finally, the assessment of the *in vitro* cytotoxicity of the compounds is provided and a structure-activity relationship is discussed.

5.2 Preparation of Complexes with P–P Chelating Ligands

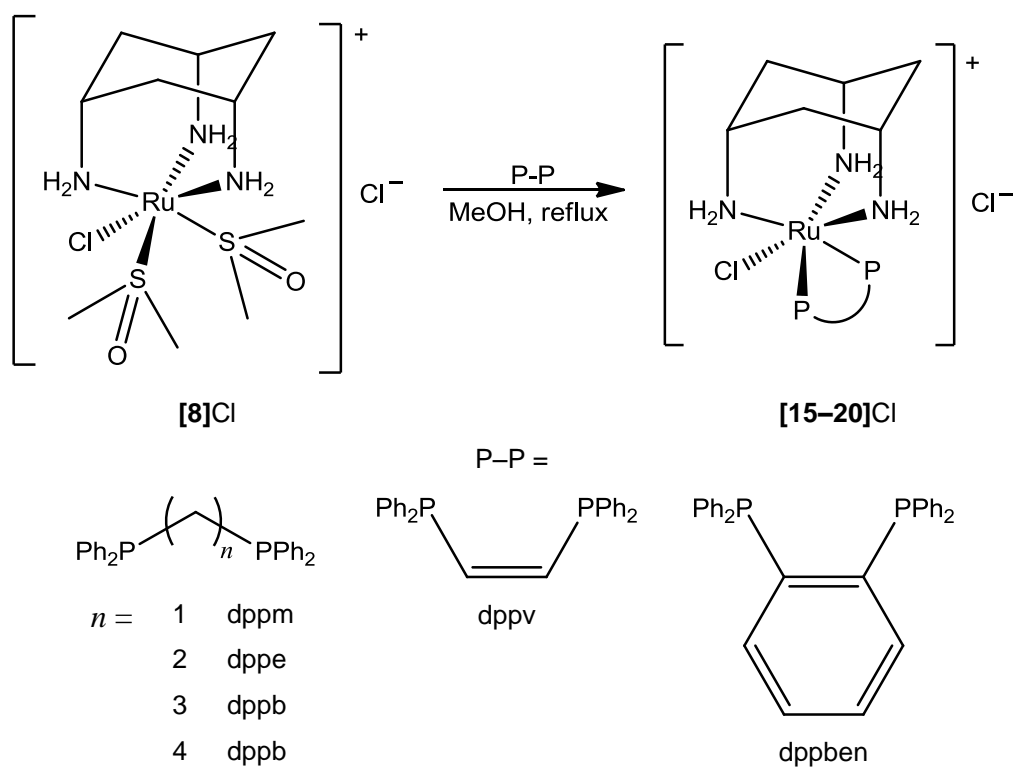
5.2.1 Synthesis and Characterisation

Initial investigations in the preparation of complexes of the type $[\text{RuCl}(\text{P-P})(\text{cis-tach})]\text{Cl}$ were performed with methylenebis(diphenylphosphane) (dppm). Reaction of **[8]Cl** with two equivalents of dppm, heated at reflux in methanol, resulted in the quantitative conversion (by ^1H NMR, based on **[8]Cl**) to a new species. After cooling, unreacted phosphane was removed by filtration and the solvent removed *in vacuo*. The complex was isolated by precipitation on addition of diethyl ether to a saturated dichloromethane solution ($\times 2$), giving a pale yellow powder in 58% yield.

Spectroscopic evidence demonstrated the successful coordination of the diphosphane in a κ^2 -fashion; the $^{31}\text{P}\{^1\text{H}\}$ NMR spectrum exhibited a single resonance for the two equivalent coordinated phosphorus nuclei at δ_{P} 10.1 ppm and the ^1H NMR spectrum indicated a C_s symmetry environment of *cis-tach*. The absence of a DMSO resonance in the ^1H NMR spectrum, coupled with the observation of solely the chlorido species, $[\text{RuCl}(\text{dppm})(\text{cis-tach})]^+$, in the mass spectrum (m/z 650.1213 and with expected isotope pattern) is indicative of the preference of the complex to retain a chlorido ligand rather than DMSO. All other experimental data were consistent with the identity of this species as $[\text{RuCl}(\text{dppm})(\text{cis-tach})]\text{Cl}$ (**[15]Cl**, Scheme 5.1).



Scheme 5.1: Reaction of **[8]Cl** with dppm to yield **[15]Cl**. * Isolated yield.



Scheme 5.2: Synthesis and proposed structures of the Ru(II) *cis*-tach complexes [15–20]Cl, which incorporate a chelating diphosphane ligand.

	P-P	Abbr.	δ_{P} (ppm)	$\delta_{\text{H}}(\text{N}^1)^a$ (ppm)	Yield ^b (%)
[15]Cl	Ph ₂ PCH ₂ PPh ₂	dppm	10.1	2.28	53
[16]Cl	Ph ₂ P(CH ₂) ₂ PPh ₂	dppe	78.3	1.14	93
[17]Cl	Ph ₂ P(CH ₂) ₃ PPh ₂	dppp	44.0	2.80	69
[18]Cl	Ph ₂ P(CH ₂) ₄ PPh ₂	dppb	46.8	2.55	55
[19]Cl	Ph ₂ PCH=CHPPh ₂	dppv	76.5	0.94	50
[20]Cl	Ph ₂ P(<i>o</i> -C ₆ H ₄)PPh ₂	dppben	72.9	1.39	69

Table 5.1: Selected data for the complexes [15–20]Cl of general formula [RuCl(P-P)(*cis*-tach)]Cl. *a*) N¹ = NH₂ resonance *trans*- to chlorido, *b*) Isolated yield as hydrate.

As observed for the previous ruthenium(II) *cis*-tach complexes, cationic species are readily obtained without chloride metathesis with weakly coordinating anions. The absence of these anions—such as hexafluorophosphate—aids the clinical preparation of these compounds and avoids incorporation of potentially toxic species.

To expand the range of available compounds of type $[\text{RuCl}(\text{P}-\text{P})(\textit{cis}\text{-tach})]\text{Cl}$, further complexes were developed by variation of the bridging group in the chelating diphosphane ligand (Scheme 5.2). Initially, the carbon chain length was extended, but the series was also expanded to include chelates with a vinyl and benzyl linker. Selected data for the complexes $[\mathbf{15}\text{--}\mathbf{20}]\text{Cl}$ is given in Table 5.1.

All of the complexes $[\mathbf{15}\text{--}\mathbf{20}]\text{Cl}$ were isolated with good yield (> 50%) and $[\text{RuCl}(\text{dppe})(\textit{cis}\text{-tach})]\text{Cl}$ $[\mathbf{16}]\text{Cl}$ with excellent yield (93%). All complexes were isolated with analytical purity (95%) with varying water composition, as determined by CHN analysis; the solvent composition was also verified by the ^1H NMR spectrum in anhydrous CD_2Cl_2 .

5.2.2 X-Ray Crystallography

Single crystals of $[\mathbf{15}]\text{PF}_6$ suitable for X-ray diffraction analysis were obtained by metathesis of the $[\mathbf{15}]\text{Cl}$ with sodium hexafluorophosphate in methanol followed by filtration and slow evaporation of the solvent. An ORTEP diagram and selected bond angles, lengths and torsions, as well as hydrogen-bond parameters are given in Fig. 5.2.

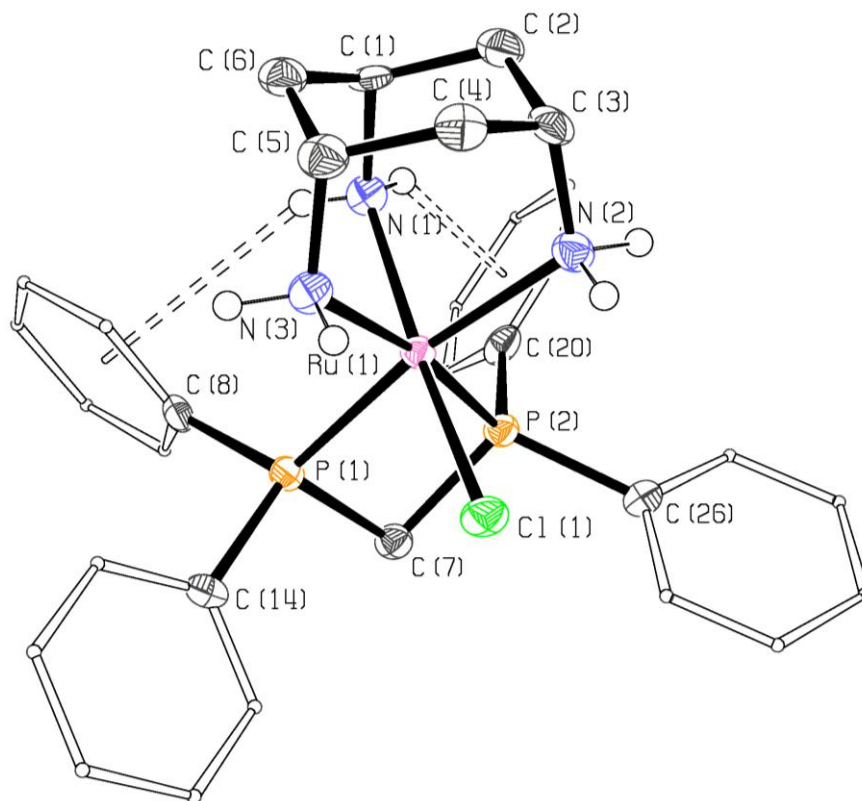


Figure 5.2: ORTEP (50% probability ellipsoids) diagram of one cation {Ru(1)} in the asymmetric unit of [15]PF₆. Hydrogen atoms (except for amino hydrogens) and the counter ion are omitted for clarity. Selected bond lengths (Å) and angles (°): Ru(1)–N(1) 2.119(4), Ru(1)–N(2) 2.171(4), Ru(1)–N(3) 2.162(4), Ru(1)–P(1) 2.2625(12), Ru(1)–P(2) 2.2610(12), Ru(1)–Cl(1) 2.4139(12), N(1)–Ru(1)–N(2) 87.65(16), N(1)–Ru(1)–N(3) 88.10(16), N(2)–Ru(1)–N(3) 87.84(16), P(1)–Ru(1)–P(2) 72.30(4), N(1)–Ru(1)–Cl(1) 168.19(12), P(1)–Ru(1)–Cl(1) 90.67(4), P(2)–Ru(1)–Cl(1) 94.49(4). Selected hydrogen-bond (D–H...A–X) lengths (Å) and angles (°) D...A, H...A, D–H...A, H...A–X, H...X (A = centroid and X = plane of respective phenyl ring of atom *): N(1)–H(1a)...C(20)* 4.00, 3.21, 147, 8.5, 2.41 (V); N(1)–H(1b)...C(8)* 4.25, 3.51, 152, 41.4, 2.35 (V). Malone hydrogen-bond type is given in parenthesis.²⁰⁶

As with the previous ruthenium *cis*-tach complexes, the structure is that of a distorted octahedron at the ruthenium centre. The ruthenium *cis*-tach adamantane moiety is also distorted and tilted in comparison to the octahedron. This is evident from the Ru–N bond lengths of 2.119(4) for the amine *trans*- to the chlorido ligand vs. 2.171(4) and 2.162(4) Å for those *trans*- to phosphane as a result of the different *trans*-influence of the two ligands. A small amount of disorder was present in the crystal structure with the hexafluorophosphate anions. The dpmm ligand forms a four-membered ring with the ruthenium centre, with a bite angle of 72.30(4)°, significantly smaller than the idealised 90°. The chelating phosphane is also angled away from the N(1) of *cis*-tach by approximately 20°, as a result of N–H... π hydrogen-bonds involving the amine. Therefore, the phenyl rings adjacent to the chlorido ligand are twisted apart, removing the bulky groups from the locality around any leaving group. The cations in [15]PF₆ also form linear hydrogen-bonded chains; this is shown in Fig. 5.3.

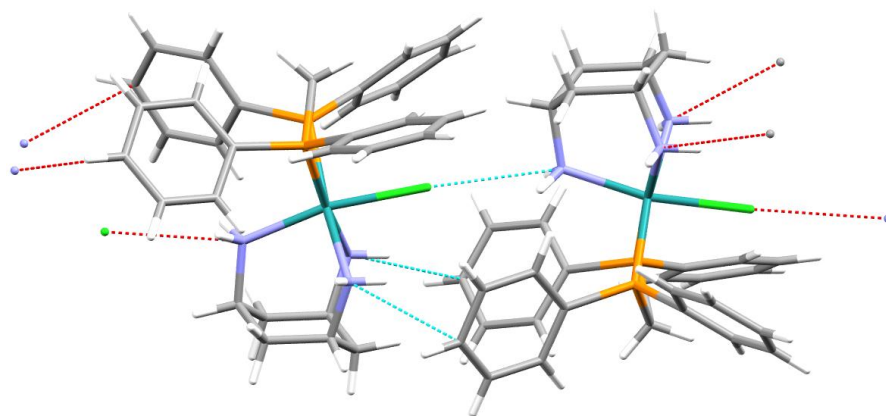


Figure 5.3: Diagram of the asymmetric unit and the intermolecular hydrogen-bonds within the linear chains of cations in [15]PF₆. The chains are separated by the PF₆ anions. Hydrogen-bonds are drawn as D...A, and in the case of the phenyl ring, to the closest carbon atom. Selected hydrogen-bond (D–H...A–X) lengths (Å) and angles (°) D...A, H...A, D–H...A, H...A–X: N(4)–H(4a)...Cl(1)–Ru(1) 3.180(4), 2.71(5), 113(4), 164(1); N(4)–H(4b)...Cl(1)–Ru(1) 3.180(4), 2.92(6), 102(5), 164(1). Selected hydrogen-bond (D–H...A–X) lengths (Å) and angles (°) D...A, H...A, D–H...A, H...A–X, H...X (A = centroid and X = plane of respective phenyl ring of atom *): N(2)–H(2d)...C(39)* 4.06, 3.30, 156, 50.6, 2.55 (V); N(3)–H(3b)...C(51)* 4.11, 3.27, 158, 51.8, 2.57 (V). Malone hydrogen-bond type is given in parenthesis.²⁰⁶

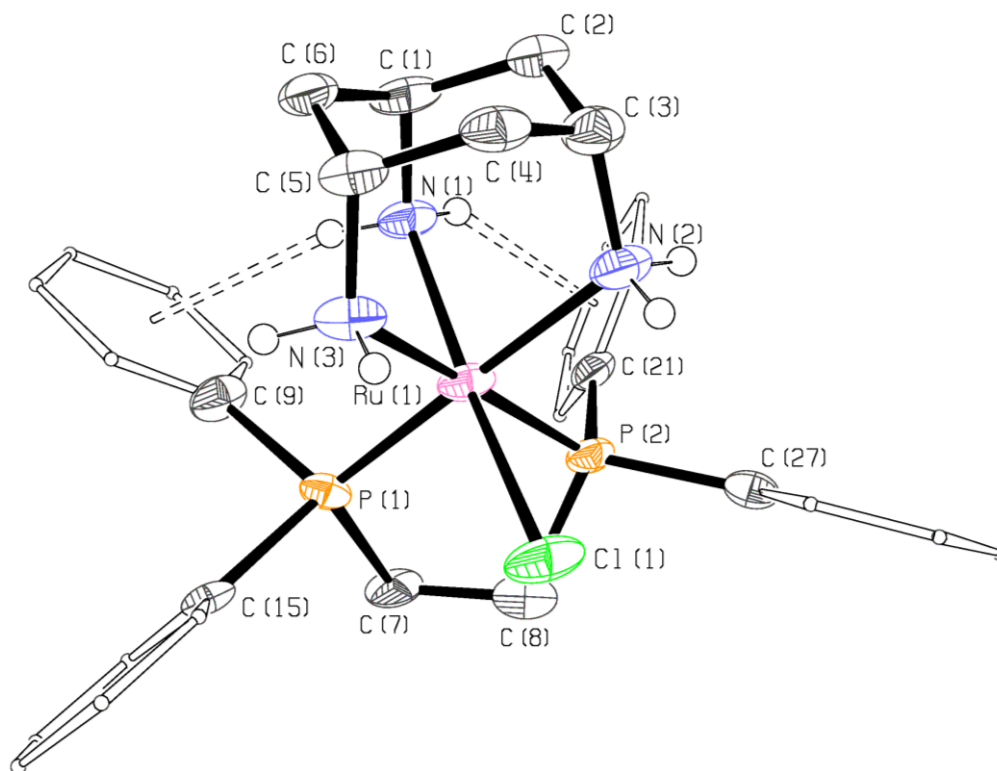


Figure 5.4: ORTEP (50% probability ellipsoids) diagram of **[16]PF₆**. Hydrogen atoms (except for amino hydrogens) and the counter ion are omitted for clarity. The crystal exhibited a diphosphane ligand disordered equally over two sites, diagram is given for one of the solutions. Selected bond lengths (\AA) and angles ($^\circ$): Ru(1)–N(1) 2.135(4), Ru(1)–N(2) 2.173(5), Ru(1)–N(3) 2.173(5), Ru(1)–P(1) 2.230(11), Ru(1)–P(2) 2.320(13), Ru(1)–Cl(1) 2.4431(14), N(1)–Ru(1)–N(2) 87.64(17), N(1)–Ru(1)–N(3) 87.61(18), N(2)–Ru(1)–N(3) 84.58(17), N(1)–Ru(1)–Cl(1) 170.35(13), N(2)–Ru(1)–P(1) 175.3(2), N(3)–Ru(1)–P(2) 174.0(2), P(1)–Ru(1)–P(2) 82.7(4), P(1)–Ru(1)–Cl(1) 96.9(2), P(2)–Ru(1)–Cl(1) 89.0(2). Selected hydrogen-bond (D–H...A–X) lengths (\AA) and angles ($^\circ$) D...A, H...A, D–H...A, H...A–X, H...X (A = centroid and X = plane of respective phenyl ring of atom *): N(1)–H(1a)...C(21)* 4.18, 3.33, 154, 42.6, 2.25 (V); N(1)–H(1b)...C(9)* 3.64, 2.72, 164, 59.0, 2.97 (V). Malone hydrogen-bond type is given in parenthesis.²⁰⁶

Single crystals of **[16]PF₆** suitable for X-ray diffraction analysis were obtained by metathesis of the **[16]Cl** with sodium hexafluorophosphate in methanol followed by filtration and slow evaporation. An ORTEP diagram and selected bond angles, lengths and torsions, as well as hydrogen-bond parameters are given in Fig. 5.4.

The cation in the solid state structure of **[16]⁺** exhibits similar octahedral and adamantane structures as **[15]⁺**. Increased flexibility of the chelating ring allows for disorder of the ligand over two positions with equal occupancy. The dppe ligand participates in a five-membered ring with the metal centre, with a bite angle of 82.7(4)°; although larger than the respective angle in **[15]⁺**, the angle remains smaller than the idealised 90° for an octahedron.

The two ruthenium–phosphane bond lengths in the cation **[16]⁺**, unlike the other complexes in this chapter, are not equal; the primary coordination sphere of the complex does not adopt a true *C_s* symmetry in the solid state, resulting from the geometrical constraints of the chelating ligand. Although it is evident from the structure that the rotation of P(1) allows for maximum overlap of the σ*(P-C) and ruthenium 4d orbitals compared to P(2), resulting in the shorter bond length, differing σ-donation of the phosphanes to the metal centre may additionally influence the bond lengths.

The crystals of **[16]PF₆** grew in the trigonal space group P3c1, resulting in hexagonally-shaped crystals. This observation was reflected by the long-range structure of the crystals, as shown in Fig. 5.5. The cations of **[16]⁺** form trigonal and hexagonal motifs around the hexafluorophosphate anions, located on special positions. A single anion and the dppe ligand are disordered across two sites in the structural solution. A hydrophobic solvent channel is present around one of the anions, but it did not prove to be possible to model the solvent channel, therefore the SQUEEZE algorithm was employed.^{207, 208}

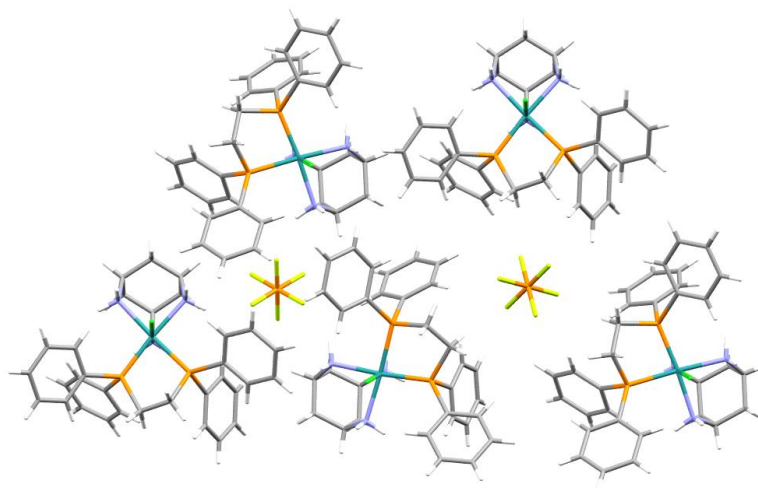


Figure 5.5: Diagram of the trigonal structures in **[16]PF₆**. Three cations surround each hexafluorophosphate anion, and *vice versa*. The PF₆[−] molecules occupy special positions of the asymmetric unit.

Single crystals of **[17]Cl** were obtained by slow evaporation of a methanol solution, and **[18]Cl** by the standing of an aqueous solution. ORTEP diagrams are given in Fig. 5.6 and selected bond angles and lengths, as well as hydrogen-bond parameters are given in Appendix I.

As for the two previous structures, the cations of both **[17]⁺** and **[18]⁺** are that of a distorted octahedron and a Ru-*cis*-tach adamantane motif. The increased size of the chelate ring to incorporate a total of six and seven members respectively has resulted in a P(1)–Ru(1)–P(2) angle close to the idealised 90° of an octahedron, of 89.481(17)° and 92.98(5) for **[17]⁺** and **[18]⁺** respectively. Furthermore, the six-membered Ru-phosphane ring of **[17]⁺** adopts a chair conformation. Due to the increased flexibility of the diphosphane chelate in both complexes, there is reduced hydrogen-bonding interactions between N(1) and the mutually *cis*-phosphane, with preference for hydrogen-bonds with the other amines. Both complexes do not exhibit strong hydrogen-bonding interactions between the cations within the solid state structure; intermolecular interactions are largely dominated by solvent-cation hydrogen-bonding interactions.

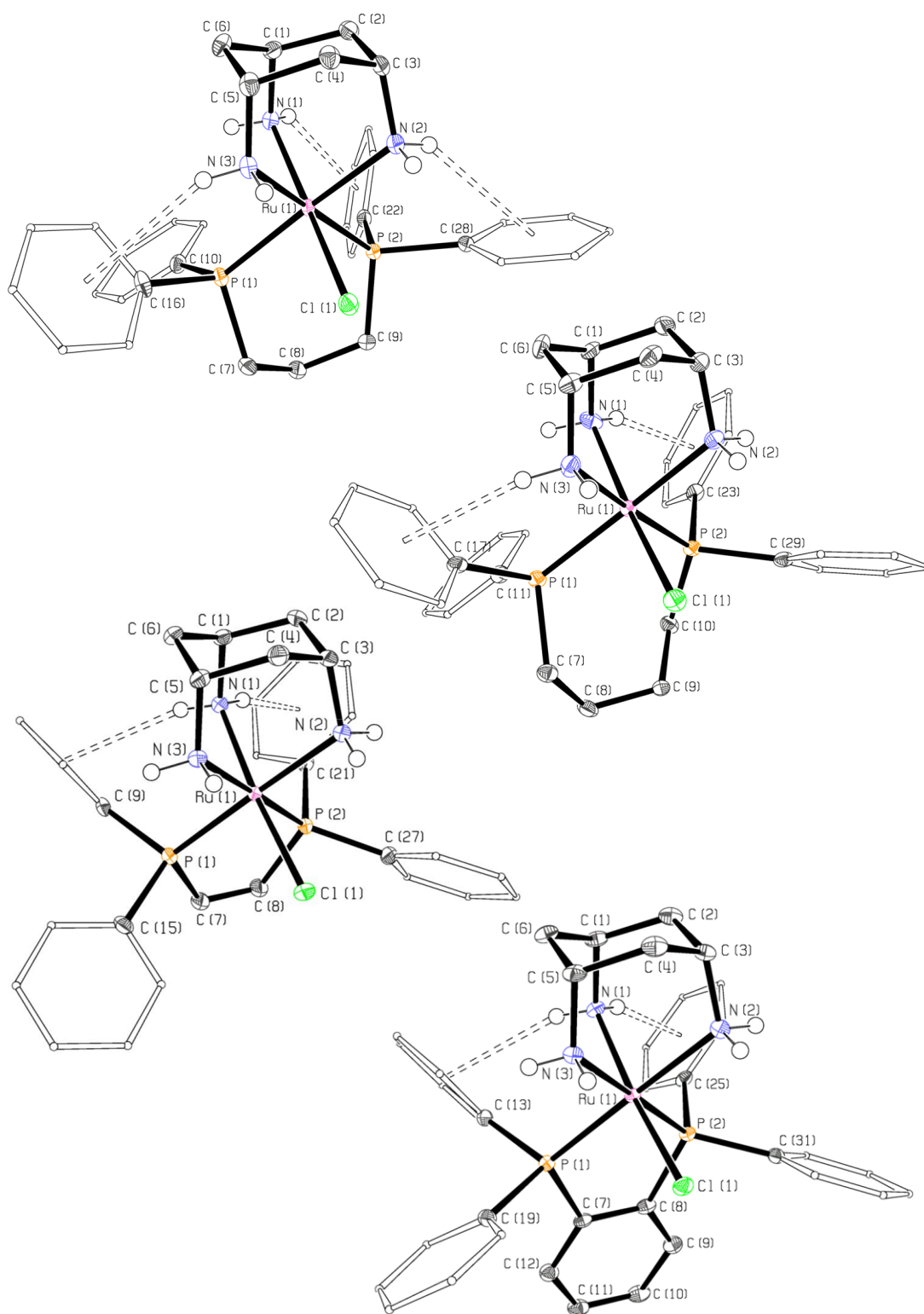


Figure 5.6: ORTEP (50% probability ellipsoids) diagrams of [17–20]Cl. Hydrogen atoms (except for amino hydrogens) and the counter ion are omitted for clarity. Selected bond and hydrogen-bond lengths and angles are given in Appendix I.

Single crystals of [19]Cl and [20]Cl were obtained by slow diffusion of diethyl ether into a methanol solution. ORTEP diagrams are given in Fig. 5.6 and selected bond angles and lengths, as well as hydrogen-bond parameters are given in Appendix I.

The structural solutions of [19]⁺ and [20]⁺ are again similar to the previous structures of chelating diphosphane complexes with distorted adamantane and octahedral structures. As with [15]⁺, the phosphane is tilted towards the chlorido ligand, resulting from the hydrogen-bonding interactions between the phenyl rings and N(1). The tilt angles are approximately 11 and 18° for [19]⁺ and [20]⁺ respectively. Both complexes do not exhibit strong hydrogen-bonding interactions between the cations; the solid state structure is largely dominated by solvent-cation hydrogen-bonding interactions.

5.2.3 Discussion

5.2.3.1 Preference for Chlorido Ligand

In contrast to the complexes incorporating N–N chelating ligands, all complexes were isolated with a chlorido ligand in preference to DMSO. This is proposed to result not only from the increased steric hindrance around the applicable coordination site favouring the smaller chlorido ligand, but also the electronic properties conferred by the metal from the phosphanes. As phosphanes are capable of acting as good π -acceptor ligands, less π -back donation would be involved in the metal-DMSO bond. Therefore the DMSO ligand is expected to be more labile than in the complexes with N–N chelating ligands and may be readily exchanged for a chloride, forming a stable chlorido complex.

5.2.3.2 ³¹P{¹H} NMR Chemical Shifts

In the ³¹P{¹H} NMR spectra of [15–20]Cl, the chemical shift of the phosphanes are between 10 and 80 ppm. It is expected that the chemical shift will reflect the electron donation from the metal complex to the phosphane, where a greater electron density located on the phosphorus nuclei will result in increased shielding and an up-field resonance. This is assumed to be most influenced by the *trans*-amine and

therefore the overlap between the Ru–P and Ru–N orbitals. The chemical shifts and *trans*-phosphorus-nitrogen bond angles are given in Table 5.2.

Complex	Bond angle (°)		Average <i>trans</i> - N–Ru–P angle (°)	$\Delta\delta_p^a$ (ppm)
	P(1)–Ru(1)–P(2)	N(2)–Ru(1)–N(3)		
[15] ⁺	72.30(4)	87.84(16)	171.0(2)	+31.9
[16] ⁺	82.7(4)	84.58(17)	174.7(3)	+90.3
[17] ⁺	89.48(2)	82.11(7)	172.74(7)	+60.8
[18] ⁺	92.98(5)	82.67(17)	173.8(2)	+62.3
[19] ⁺	83.21(2)	83.51(6)	177.97(7)	+99.1
[20] ⁺	84.00(2)	84.43(8)	179.11(8)	+86.2

Table 5.2: Selected bond angles and $^{31}\text{P}\{^1\text{H}\}$ NMR chemical shifts for [15–20]⁺. *a)* $\Delta\delta_p = \delta_p(\text{complex}) - \delta_p(\text{free phosphane})$; $\delta_p(\text{free phosphane}) (\text{CDCl}_3) = -21.8$ (dppm), -12.0 (dppe), -16.9 (dppp), -15.5 (dppb), -22.6 (dppv), -13.3 (dppben).

The geometrically constrained dppm ligand of [15]⁺ deviates from the ideal octahedron more than the other complexes in the *trans*-P–Ru–N bond, at 171°, therefore reducing the *trans*-influence of *cis*-tach; This is reflected in the up-field resonance of δ_p 10.1 ppm. Of the remaining complexes, [20]⁺ has the optimum overlap of 178°, followed by [16]⁺ at 175°. Both of these complexes contain five-membered diphosphane rings and exhibit the most downfield resonances in the series with [19]⁺ of δ_p 70–80 ppm. Furthermore, the diphosphane bite angle mirrors the corresponding *cis*-tach bite angle *trans*- to the chelate in these three complexes to a greater extent than the others. Finally, the extended chelating ligands of [17]⁺ and [18]⁺ are located between the latter two sets of ligands with angles of 173–174° and is mirrored in the $^{31}\text{P}\{^1\text{H}\}$ spectra with δ_p 44–47 ppm.

5.2.3.3 ^1H NMR Chemical Shift of Amine Groups

The ^1H NMR chemical shift of the amine group *trans*- to the chlorido ligand for the complexes $[\mathbf{16}]^+$, $[\mathbf{19}]^+$ and $[\mathbf{20}]^+$ are observed at approximately δ_{H} 1 ppm, opposed to those for all other complexes, which are typically present between 2–5 ppm. Although amine chemical shifts in this region are suggestive of a non-coordinated nitrogen group, an NOE cross peak between the NH_2 resonance and the adjacent phenyl rings were observed in CD_3OD solution (Fig. 5.7) suggesting the amine is within the coordination sphere of the metal.

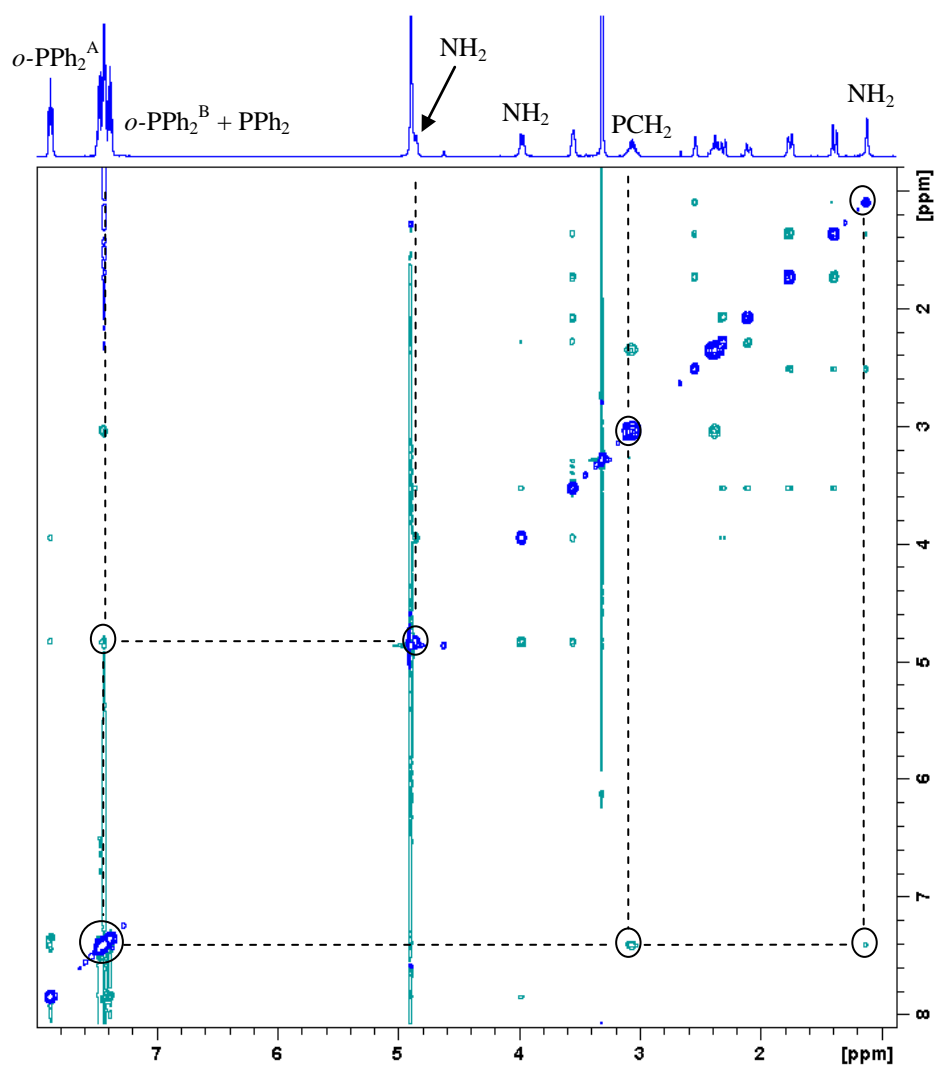


Figure 5.7: ^1H - ^1H NOESY NMR spectrum of $[\text{RuCl}(\text{dppe})(\text{cis-tach})]\text{Cl}$ ($[\mathbf{16}]\text{Cl}$) in CD_3OD .

The *ortho* proton of the adjacent phenyl ring shares a NOE cross peak with the ethylene linker group, although obscured by coincidental resonances in the 1D spectrum. In addition to the NOESY spectrum, the assigned cyclohexane conformation of [16]Cl was supported by the 1D ^1H NMR spectrum from the observation of cyclohexane ring *J*-coupling of an all-axial configuration corresponding with all other κ^3 -species observed. It is proposed that upfield-shifted amine resonances of [16]Cl, [19]Cl and [20]Cl result from the shielding cone of the nearby aromatic systems of the diphosphane ligand. This is seen in the structural solutions obtained by single crystal X-ray diffraction, where the adjacent phosphane phenyl rings in [16]PF₆, [19]Cl and [20]Cl are located close to the N(1) NH₂ protons, with an average NH...centroid stance of 3.0(4), 2.7(2) and 3.0(1) Å respectively. This is in contrast to 4.0(6) Å for [15]Cl, the only other solid state structure with a similar hydrogen-bonding motif; this provides a rationale for the upfield NH₂ resonance in the ^1H NMR of these complexes.

5.2.3.4 Ruthenium–Chlorido Bond Lengths

A structural parameter relevant to the reactivity of these complexes is the Ru–Cl bond length, as ligand exchange reactions are expected to occur at this coordination site. A similar (within error) Ru–Cl bond length was obtained for [16–20]⁺. However the Ru–Cl bond in [15]PF₆ is shorter than in [16–20]⁺ by almost 0.03 Å. Assuming these complexes inhibit the growth of tumour cells by coordination of biomolecules to the coordination site occupied by the chlorido ligand, it would be expected that the activity of [15]Cl will be greatly compromised in comparison to the other complexes. The Ru–Cl bond lengths in the crystal structures of [15–18]⁺ and analogous complexes are presented in Table 5.3.

<i>fac</i> -ligand	r(Ru–Cl) (Å), L =			
	dppm	dppe	dppp	dppb
$\eta^5\text{-C}_5\text{H}_5$	2.4302(6) ²⁶⁹	2.4466(7) ²⁶⁹		2.4404(4) ²⁷⁰
<i>cis</i>-tach	2.4139(12)	2.4431(14)	2.4404(4)	2.4379(12)
$\eta^6\text{-}p\text{-cymene}$	2.397(2) ²⁷¹	2.430(1) ²⁷¹		
Tpm		2.397(3) ¹⁹²	2.4056(9) ²⁶⁸	
$\eta^6\text{-toluene}$		-		2.399(2) ²⁷²
Tp ^{iPr}		2.352(2) ²⁷³		

Table 5.3: Comparison of Ru–Cl bond lengths from the X-ray crystal structures of complexes following the formula $[\text{Ru}^{\text{II}}\text{Cl}(\text{L})(\textit{fac}\text{-ligand})]^{n+}$. *cis*-tach complexes: **[15]**PF₆ (dppm), **[16]**PF₆ (dppe), **[17]**Cl (dppp), **[18]**Cl (dppb).

The Ru–Cl bond lengths in the crystal structures of **[15–18]**⁺ reflect those of the triphenylphosphane complexes detailed in Section 2.3; *cis*-tach confers similar effects to the ruthenium-chlorido bond as the anionic $\eta^5\text{-C}_5\text{H}_5$ ligand, with bond lengths identical (within error) for the dppe and dppp complexes. The *cis*-tach ligand in all four structures generally results in a longer metal–halide bond in comparison to the neutral *fac*-ligands, including the cytotoxic complexes $[\text{RuCl}(\text{dppm})(\eta^6\text{-}p\text{-cymene})]\text{PF}_6$ and $[\text{RuCl}(\text{dppp})(\text{Tpm})]\text{PF}_6$. This observation also extends to other ruthenium(II) *fac*-ligand compounds, such as $[\text{RuCl}(\eta^6\text{-benzene})(\text{phen})]^+$ (2.4132(5) Å),²⁷⁴ $[\text{RuCl}(\eta^6\text{-}p\text{-cymene})(\text{acac})]$ (2.4199(6) Å),²⁷⁵ and the promising anti-cancer complex $[\text{RuCl}(\eta^6\text{-bip})(\text{en})]^+$ (2.4080(15) Å).⁷⁸ This observation mirrors that of the triphenylphosphane complexes, where the *trans*-influence of the electron rich *cis*-tach ligand promotes the weakening of the ruthenium–chlorido bond in comparison to other *fac*-ligands such as the $\eta^6\text{-arenes}$. Although the *in vitro* activity cannot be compared to this parameter, the differences in Ru–Cl bond lengths may be manifested in the ligand exchange reactions of these complexes, where favourable kinetics or equilibria may result. However, other physical parameters may also influence these properties, such as mechanism of ligand exchange and the stability of transition states or products; therefore the effect of the Ru–Cl bond length on the aquation reaction or *in vitro* activity of these complexes cannot be predicted.

5.2.4 Conclusions

A series of six *cis*-tach ruthenium(II) complexes incorporating chelating diphosphane ligands was prepared in good to excellent yields with analytical purity. The structures of the complexes are ideal for application as cytotoxic agents. The phenyl rings provide a degree of hydrophobicity to the complexes, which could aid diffusion across cell membranes; the rings also have the potential to interact with biologically relevant molecules through π -stacking interactions. Additionally, the other amine groups of the tach are located adjacent to the chlorido ligand and may have a role in strengthening interactions with an exogenous ligand through hydrogen-bonding. For these reasons, it is believed these compounds will exhibit some potency in the *in vitro* inhibition of tumour cell proliferation.

5.3 *In Vitro* Biological Evaluation

All six diphosphane chelate ruthenium(II) *cis*-tach complexes, [15–20]Cl, were selected for assessment of antiproliferative activity by growth inhibition assay with the colorimetric MTT assay.²²⁸ Compounds were tested against the A549 human lung adenocarcinoma and the cisplatin-sensitive A2780 human ovarian carcinoma cell lines. Importantly for the biological aspect of this study, analytically pure samples of [15–20]Cl are freely soluble in water up to mM levels of concentrations, and soluble in media to at least 500 μ M, well in excess of that needed for therapy.

5.3.1 Antiproliferative Activity

Media with cells was seeded in a 96-well plate 24 h prior to the addition of the compound to be tested. Cell viability was assessed after 72 h exposure to the compound by metabolisation of MTT to the insoluble formazan product. The relative amount of MTT-formazan per well was determined by the absorbance at 540 nm after aspiration of the media dissolution in DMSO. Cell viability was calculated as a function of the positive (no cells, 0% viability) and negative (no drug added, 100% viability) controls.

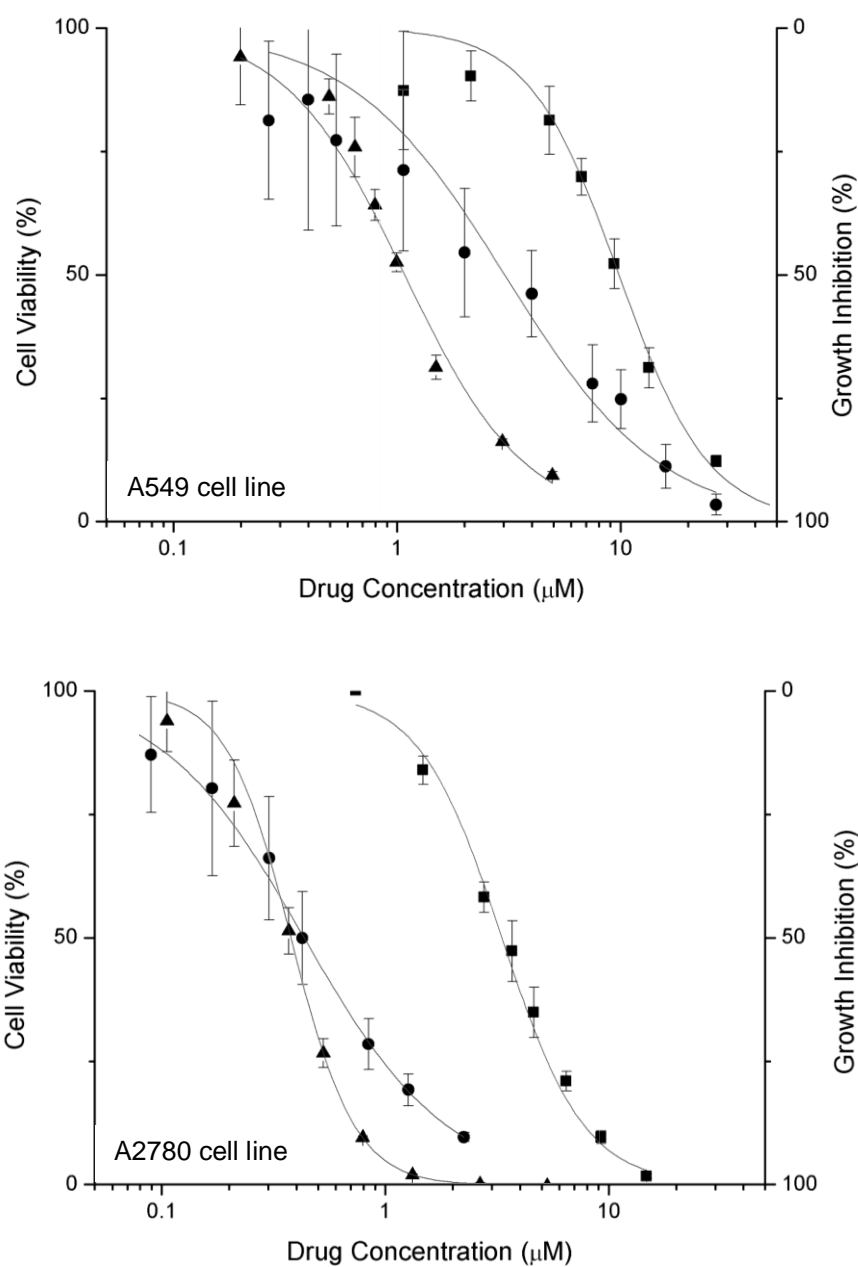


Figure 5.8: Logarithmic dose-response curves for ● cisplatin, ■ [16]Cl and ▲ [17]Cl in the A549 (top) and A2780 (bottom) cell lines. Solid lines represent the calculated best-fit to the dose response curve (Eqn. 5.1).

For the compounds cisplatin, [16]Cl and [17]Cl, logarithmic dose-response curves of a single experiment performed in octuplicate with the A549 and A2780 cell lines are shown in Figs. 5.8. The resulting IC₅₀ values were calculated as the concentration required to inhibit growth by 50%. The ability for a drug to act on a tumour cell to inhibit growth over a wide concentration range is described in the dose-response curve by the gradient of the slope, determined by the *power* value (*p*) in Eqn. 5.1.

$$y = \frac{100}{1+(x/IC_{50})^p} \quad \text{Equation 5.1}$$

The IC₅₀ and *power* values for all complexes in the A549 and A2780 cell lines are given in Table 5.4. All values given are the average of three experiments, each performed in octuplicate.

Compound	A549		A2780	
	IC ₅₀ (μM)	<i>power</i>	IC ₅₀ (μM)	<i>power</i>
cisplatin	2.70(5)	0.92(5)	0.43(1)	1.36(3)
[15]Cl	41.7(10)	1.87(8)	12.4(2)	1.63(4)
[16]Cl	9.88(4)	2.06(6)	3.39(12)	2.54(9)
[17]Cl	1.02(3)	1.74(7)	0.35(1)	2.80(4)
[18]Cl	1.15(2)	1.76(3)	0.39(1)	2.27(4)
[19]Cl	25.1(4)	1.92(6)	7.47(17)	2.14(9)
[20]Cl	2.73(11)	2.30(13)	1.14(4)	2.99(20)

Table 5.4: IC₅₀ and slope values (*power*, see Eqn. 5.1) for cisplatin and compounds [15–20]Cl in both A549 and A2780 cell lines. Cells were exposed to the selected compound for 72 h and cell viability was determined by MTT assay. Standard deviations are given in parenthesis.

In both the A549 and A2780 cell lines, the complexes display a wide range of cytotoxicity from moderate to excellent in comparison to cisplatin. In particular, [17]Cl and [18]Cl possess potent activity, exceeding that of cisplatin in the A549 cell line by two- to three-fold. In A2780, these compounds are at least equipotent to the clinical drug. Good activity is also achieved with the complexes [16]Cl and [20]Cl.

The success of cisplatin as a clinical drug is evident here, where the gradient of its dose response curve for both cell lines is shallow; therefore the range of concentrations of which the drug inhibits growth is broad. A similar shallow gradient is only observed with [15]Cl in the A2780 cell line, but it is poorly active compared to cisplatin. The ruthenium *cis*-tach complexes with activity close to or surpassing that of cisplatin are not active over a similarly wide range. Despite the importance of this characteristic of a drug, and ultimately, the ability for a physician to moderate a dose, it is rarely reported in literature for complexes which have been assessed for *in vitro* antiproliferative activity. Therefore, comparison with established ruthenium anti-tumour complexes is not possible.

The difference in absolute activity between the two cell lines is the product of different biological processes within each system, whereby selected biological pathways and cell defence mechanisms vary. Furthermore, due to the different growth characteristics of the cell lines, different conditions were employed. Therefore, one cannot perform a direct comparison between the two cell lines used.

Compared to other ruthenium(II) complexes, [17]Cl and [18]Cl are among the most active, mono-nuclear and freely water-soluble candidates under study. The complexes [17]Cl and [18]Cl are equipotent to cisplatin. Similar activity (compared to cisplatin) was observed with HC11, [RuCl(η^6 -tha)(en)]PF₆—a lead compound from the Sadler laboratory—with the A2780 cell line, but a different method was used (24 h drug exposure).⁸⁰ These complexes have similar cytotoxicities to the previously reported diphosphane complexes [RuCl(η^6 -*p*-cymene)(P–P)]⁺ and [RuCl(P–P)(Tpm)]⁺ (compared to cisplatin). However, the *cis*-tach ligand is believed to significantly enhance water solubility, with solubility of >10 mM for [16]Cl and [17]Cl, without assistance from other solvents (e.g. initial preparation of a stock solution in DMSO). These complexes are promising candidates for future studies and developments. It should be noted that several *fac*-ligand ruthenium(II) complexes exhibit sub-micromolar cytotoxicities, several times greater than cisplatin. However, these are dominated by dinuclear species, such as [$\{(\eta^6$ -*p*-cymene)Ru₂(*p*-SC₆H₄Me)₃}]Cl (IC₅₀ = 0.13 μ M in A2780), and these complexes are not reported to be freely water soluble, requiring DMSO to assist in solvation for growth inhibition assays.²⁷⁶

5.3.2 Structure-Activity Relationship

Significant research has focused on the structural properties of anti-cancer compounds to provide crucial insights into the vital features for antiproliferative activity by structure activity relationships (SARs). For example, the activities of cisplatin (highly potent) vs. transplatin (inactive) is accounted for by differing ligand exchange kinetics and the geometrical constraints of cross-linking DNA.²⁷⁷ Knowledge of the SAR allows informative design of new candidates with the aim of increasing activity or reducing unwanted side effects. Although comprehensive SARs require many tens of compounds, analysis of the activities of the ruthenium (II) *cis*-tach complexes presented here may highlight key features for future development of these compounds.

Antiproliferative activity was only observed in ruthenium(II) *cis*-tach complexes with a phosphane ligand. The phosphane provides two benefits; a relatively stable yet reactive chlorido complex can be prepared and the phenyl groups provide increased lipophilicity. At least one of these factors is absent in [RuCl(DMSO-*S*)₂(*cis*-tach)]Cl and [Ru(DMSO-*S*)(phen)(*cis*-tach)](Cl)₂, possibly accounting for the poor activity. Inclusion of two phosphane donors, in the diphosphane complexes, significantly increased activity to surpass that of cisplatin. This correlates with the observations of Sadler and co-workers, where extended and larger arene ligands results in improved activity.⁸²

The possibility of the activity of these complexes arising as a consequence of phosphane dissociation must be considered. Under physiologically relevant conditions, no evidence was obtained to suggest displacement of the chelating phosphane. In chapter 2, it was hypothesised that the Ru–P bonds have a large degree of π -back bonding character using crystallographic data from **[1]**PF₆ and **[2]**. Therefore, the Ru–P bond is expected to be relatively strong. Assuming activity originated from the free phosphane ligand, one may expect for activity to correlate with the ability for the phosphane to be potentially displaced, with the geometrically constrained complexes more readily releasing phosphane. The observed *in vitro* activities of these complexes do not correlate, with the most constrained exhibiting

poorest activity. Furthermore, $[\text{RuCl}(\text{DMSO-}S)(\text{cis-tach})(\text{PPh}_3)]\text{Cl}$ [4]Cl, which features a mono-dentate phosphane is over two orders of magnitude less active than [17]Cl, suggesting that phosphane dissociation may not be occurring in the conditions of the MTT assays. It is therefore proposed that phosphane de-coordination does not occur and that the Ru(II) phosphane complex is responsible for the growth inhibition observed.

The solid state structures of all the diphosphane chelate complexes provide potential insight into the successful *in vitro* activity. The phenyl rings are capable of forming hydrogen-bonds to the amine groups, thereby protecting the hydrogen-bond donor groups when in an apolar environment such as that of the cell membrane, aiding transfer into the cell. The phenyl rings are also able to extend outward, past the chlorido ligand to create steric bulk around the reactive coordination site of the complex or form hydrophobic interactions with coordinated biomolecules (Fig. 5.9). The ligand as a whole also forms a large hydrophobic face to the complex and in conjunction with the *cis-tach* cyclohexane ring; the majority of the hydrophilic properties of the *cis-tach* ligand is hidden. Only a strongly hydrophilic region (the exposed amine groups) is present around the chlorido ligand, capable of forming non-covalent interactions with coordinated biomolecules (Fig. 5.9).

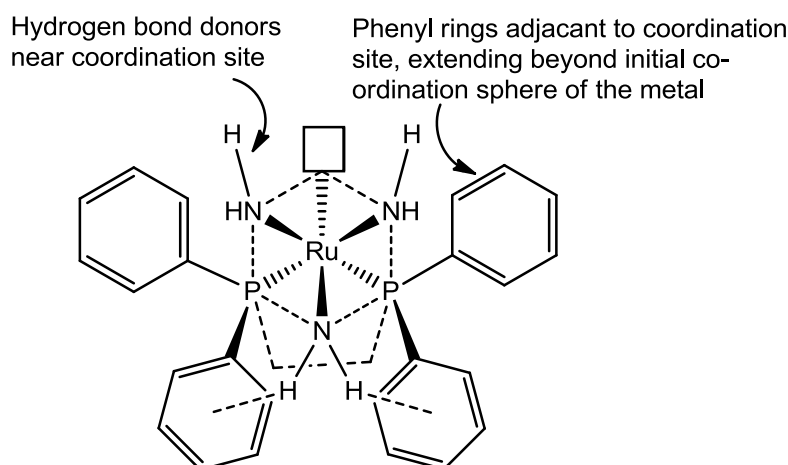


Figure 5.9: Schematic representation of the diphosphane complexes showing possible sites of interactions when coordinated to biomolecules by substitution of the chlorido ligand.

For compounds of type $[\text{RuCl}(\text{Ph}_2\text{P}\{\text{CH}_2\}_n\text{PPh}_2)(\text{cis-tach})]\text{Cl}$, the activity increases upon extension of the chelate chain length in both cell lines, up to the case where $n = 3$, **[17]Cl**, which exhibits the highest activity of all compounds tested in both cell lines. However, further extension of the chain results in little change to the activity. From the solid state structures of complexes **[15–18]⁺**, the Ru(1)–Cl(1) bond length in **[15]Cl** is shorter than those with a longer chelating chain at 2.4139(12) vs. approximately 2.441(2) Å. This could result in a less reactive ruthenium-chlorido bond, and therefore reduced potency, but this does not extend to **[16–20]Cl**.

The three structural factors which vary between the complexes are the phosphane bite angle, flexibility and lipophilicity/hydrophobicity. Hydrophobicity is an important influence in the potency of a compound; it has been previously demonstrated that increased hydrophobicity improves the uptake of a compound into the cell, resulting in greater activities.^{82, 89, 113, 131} The complexes **[19]Cl** and **[20]Cl** share a similar coordination sphere around the metal centre, with only variation in the size of the hydrophobic chelating diphosphane. Extension of the chelate from dppv (**[19]Cl**) to dppben (**[20]Cl**), results in an increase of activity, as expected, by almost an order of magnitude. Further studies into calculation of the water/octan-1-ol partition coefficient, $\log P$ will prove informative to the link between hydrophobicity and potency.

The trend of activity of complexes following the formula $[\text{RuCl}(\text{cis-tach})]\text{Cl}$ does show some correlation to the bite angle of the chelating ligand, with angles of 72.30(4), 82.7(4), 89.98(5) and 92.98(5)° for **[15]⁺**, **[16]⁺**, **[17]⁺** and **[18]⁺** respectively. However, this does not account for the reduced activity in **[19]⁺**, with bite angle of 83.207(17)°. A structural trend which follows *in vitro* activity is the reduced strain and therefore flexibility of the chelate ring. The flexibility of the complexes is expected to follow the trend of $\text{dppb} \geq \text{dppp} > \text{dppe} > \text{dppv}$ and dppm . This trend appears to breakdown when a fully flexible ligand is employed—such as dppb—and activity no longer increases. The flexibility may enhance activity by either providing greater protection of the *cis-tach* amine groups when passing through the cell membrane, or for selective protection of the effective “vacant” coordination site (from loss of the chlorido ligand). The flexible phenyl groups could mask this coordination site to prevent side reactions from occurring, but also

rotate or move to aid in the formation of stronger interactions with biomolecules. For the continued development of these complexes, it is proposed that both the flexibility and lipophilicity of the chelating diphosphane ligand are important factors towards the activity of the complex, as well inclusion of a sufficiently labile chlorido ligand. Therefore these factors should be exploited, although other properties of the complexes may also contribute to the observed trends.

5.3.3 Conclusions

The ruthenium(II) *cis*-tach complexes in this chapter are highly active in the inhibition of tumour cell growth, with two compounds surpassing that of cisplatin in the A549 cell line. All the compounds are freely water soluble in at least mM concentrations and do not require use of a potentially toxic counter-ions. The activities obtained are among the best obtained for ruthenium(II) complexes currently being studied for their cytotoxic capabilities, and present an important class of compounds warranting further investigations.

5.4 Chapter Conclusions

The family of ruthenium(II) *cis*-tach compounds has been expanded to include the chelating diphosphane complexes [15-20]Cl. The complexes are obtained in moderate to high yield by the reaction of the respective phosphane and [8]Cl. Six complexes were prepared, characterised and assessed for their antiproliferative activity by *in vitro* technique using the MTT assay. All compounds were obtained with analytical purity and characterised further by single crystal X-Ray diffraction. Employment of a chelating diphosphane gives the respective chlorido complex. Additionally, all complexes were isolated as the chloride salt, and did not require use of weakly coordinating anions for synthesis.

Use of the chelating diphosphane ligand gave complexes which are highly active in growth inhibition of both A549 and A2780 cell lines, two of which surpassed the activity of the clinical drug cisplatin in the A549 line. Furthermore, the activity of ruthenium(II) *cis*-tach complexes is among the highest obtained for mono-nuclear ruthenium compounds. It is believed this activity is a consequence of the

diphosphane coupled with *cis*-tach. Although potent diphosphane complexes with *facially*-coordinating ligands have been previously reported, *cis*-tach may provide additional advantages, such as potential hydrogen-bonding interactions between the amine groups and biological target, and improved water solubility. An initial analysis of the structure-activity relationship (SAR) suggests that activity may be related to both the lipophilicity of the complex and the flexibility of the chelating ligand; further studies are required to form a comprehensive SAR.

However, there are further questions to be answered to understand the cause for the excellent potency *in vitro* of ruthenium *cis*-tach complexes. It remains unclear the chemical processes these compounds undergo in aqueous media, or the biological molecules the compounds target. These questions form the basis of the final chapter of this thesis.

Chapter 6. Aquation and Biomolecule Interactions of Ruthenium(II) *cis*-tach Diphosphane Complexes

6.1 Introduction

Given the promising anti-proliferative activity of ruthenium(II) *cis*-tach complexes, the chemical processes which may occur within a cell were of interest. The mechanism by which cisplatin activates a cellular response, which results in apoptosis, has been extensively studied.^{8, 14, 21} The universally accepted hypothesis is that cisplatin forms cross links between the *N7* atoms of the guanine or adenine bases in DNA, resulting in distortion of the secondary structure.^{19, 24} Prior to interaction with DNA, aquation is required to generate the more reactive aqua complex $[\text{PtCl}(\text{NH}_3)_2(\text{OH}_2)]^+$ (subsequent aquation and hydrolysis may also occur).¹⁹ It has been shown that many ruthenium(II) η^6 -arene complexes that exhibit promising anti-tumour activity also generate a reactive aqua species when exposed to conditions similar to that within a cell. For example, the complexes of type $[\text{RuCl}(\eta^6\text{-arene})(\text{en})]^+$ are hypothesised to undergo rapid aquation on entering the cell prior to binding to DNA selectively *via* a single covalent bond to the *N7* of guanine.^{96, 99} Computational studies of this complex with DNA, as well as crystallographic studies of small molecular models have shown that the hydrogen-bonding groups of the en ligand assist in strengthening the interaction, thus increasing the structural distortion of DNA.^{90, 103}

The aqueous chemistry of ruthenium(II) *cis*-tach chelating diphosphane complexes is herein described. The aquation of the chlorido species is investigated in detail and the resulting aqua complexes characterised in solution. A kinetic study was performed to provide information regarding the transformation these complexes may undergo in a biologically-relevant environment, as well as the mechanism of aquation. The reaction equilibrium was also determined to give insight into the proportion of each species in various biological conditions. The potential of DNA as a biological target for these complexes was investigated by reaction with the DNA model compounds 9-ethyl guanine and guanosine monophosphate, as well as

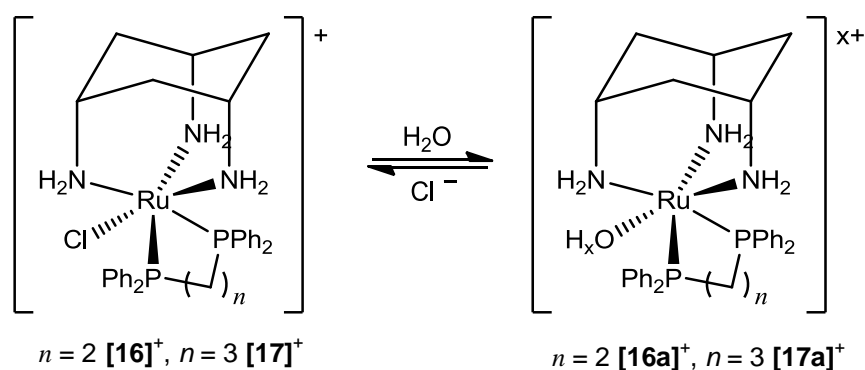
electrophoretic mobility shift assays to assess the ability of the complexes to alter the tertiary structure of plasmid DNA.

6.2 Identity of Aquation Products

The aqueous chemistry of the diphosphane complexes was investigated in detail with focus on [16]Cl and [17]Cl. These two compounds were selected as [17]Cl exhibited the highest *in vitro* activity, whereas [16]Cl displayed good activity coupled with excellent water solubility. Furthermore, the results of the investigation may provide information to the differing *in vitro* activity of these two complexes.

6.2.1 Aquation of [16]Cl and [17]Cl

The $^{31}\text{P}\{^1\text{H}\}$ NMR spectra of [16]Cl or [17]Cl at $\sim 300\ \mu\text{M}$ were obtained in H_2O solution, with 10 mM sodium phosphate buffer (pH 7.4) and 1.6% CD_3OD to provide a lock signal. The spectrum for both complexes consisted of two singlet resonances (Fig. 6.1). It is proposed that one of these signals is that of the starting chlorido complex ($[\mathbf{16}]^+ / [\mathbf{17}]^+$) and the other a new species, hypothesised as the aqua/hydroxy complex, $[\text{Ru}(\text{OH}_x)(\text{P}-\text{P})(\text{cis-tach})]^{x+}$ ($[\mathbf{16a}]^{x+} / [\mathbf{17a}]^{x+}$), which results from exchange of the chlorido ligand with the solvent (Scheme 6.1). Both complexes co-exist in an equilibrium mixture, which had fully established within the time of obtaining the spectrum.



Scheme 6.1: The complexes [16]Cl and [17]Cl aquate rapidly in aqueous solution, giving an aqua/hydroxy complexes [16a]^{x+} and [17a]^{x+}.

The identity of each resonance in the $^{31}\text{P}\{^1\text{H}\}$ NMR spectra was assigned based on the relative change of its integration on addition of sodium chloride to the aqueous solution (Fig. 6.1).

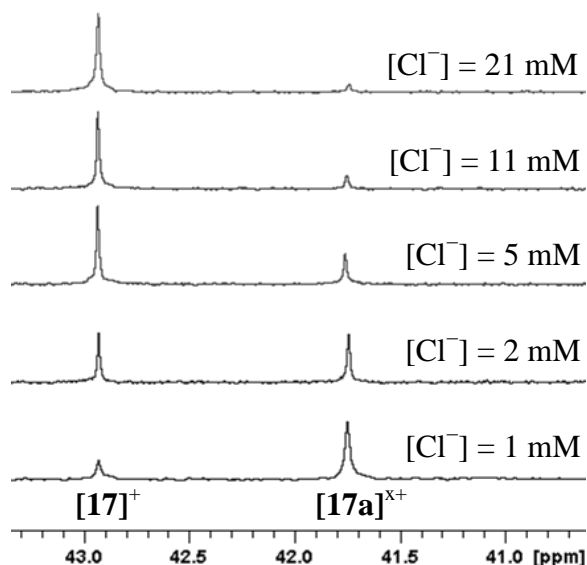


Figure 6.1: $^{31}\text{P}\{^1\text{H}\}$ NMR spectra of a 500 μM solution (pH 7.4) of $[\mathbf{17}]\text{Cl}$ with various chloride concentrations (NaCl) to assign the two resonances. $[\text{Cl}^-] = [\text{NaCl}] + [\text{Cl}^-]_{\text{Ru}}$ where $[\text{Cl}^-]_{\text{Ru}} = [\text{Cl}^-]$ inherent from ruthenium species.

The $^{31}\text{P}\{^1\text{H}\}$ NMR and ESI-MS data for the chlorido and aqua species are given in Table 6.1. It is evident from the $^{31}\text{P}\{^1\text{H}\}$ NMR integrations that the aquated species is in significantly greater abundance for $[\mathbf{16}]\text{Cl}$ than in the case of $[\mathbf{17}]\text{Cl}$. It is therefore expected that the equilibrium constant for the aquation reaction will be higher for $[\mathbf{16}]\text{Cl}$ than $[\mathbf{17}]\text{Cl}$. ESI mass spectrometry of $[\mathbf{16}]\text{Cl}$ and $[\mathbf{17}]\text{Cl}$ in 75% $\text{H}_2\text{O}/25\%$ MeOH supported the proposed new species as being the aqua/hydroxy complex, with mass and isotope patterns corresponding to the $[\text{M}-\text{Cl}+\text{OH}]^+$ ion for both complexes.

	P-P	L	$\delta_P / \text{ppm (J)}$	$m/z (\%)$
[16] ⁺	dppe	Cl	76.2 (5)	664.0 (10)
[16a] ^{x+}	dppe	OH _x	74.6 (100)	646.1 (100) ^a
[17] ⁺	dppp	Cl	42.9 (100)	678.1 (100)
[17a] ^{x+}	dppp	OH _x	41.7 (30)	660.1 (20) ^a

Table 6.1: ³¹P{¹H} NMR spectroscopy and ESI mass spectrometry data for [Ru(L)(P-P)(*cis*-tach)]^{x+}, where L = Cl or OH_x. [Ru] = 500 μM, pH 7.4 (10 mM sodium phosphate). a) Only the hydroxo species [Ru(OH)(P-P)(*cis*-tach)]⁺ was observed.

Both of the aqua/hydroxy complexes **[16a]**^{x+} and **[17a]**^{x+} were characterised by ¹H and ³¹P{¹H} NMR spectroscopy by preparation of solutions of the triflate salts by chloride metathesis with two equivalents of silver triflate. All *cis*-tach resonances were observed, with the exception of a single NH₂ environment in **[16a]**^{x+}. The resonance for the corresponding proton in the chlorido complex is within 0.1 ppm of the water signal in CD₃OD, and is assumed to have a similar chemical shift in **[16a]**^{x+}. Therefore, it is proposed that this resonance has been suppressed by the solvent suppression pulse sequence. Additionally, due to rapid exchange with the solvent, the aqua/hydroxy protons are not observed in the ¹H NMR spectra. The ¹H NMR spectra for all complexes correlate with that expected for a κ³-*cis*-tach ligand in a C_s symmetry environment.

Aquation of **[10]**Cl in D₂O showed evidence for the selective deuteration of *trans*-chlorido amine groups, hypothesised as the product of a conjugate base mechanism (chapter 3). Therefore, the incorporation of deuterium into the diphosphane complexes was studied by ESI mass spectrometry in 75% D₂O/25% CD₃OD solution. No deuteration of the *cis*-tach amine protons were observed, with the only deuterium-containing signals corresponding to [M-Cl+OD]⁺ at m/z 647.2 and 661.1 for **[16a]**⁺ and **[17a]**⁺ respectively. Therefore, it is proposed that the aquation of these two complexes does not proceed *via* an S_N1CB type mechanism. It is expected that aquation occurs by either a concerted I_A or I_D mechanism; a true dissociative mechanism is not expected, as exchange has not been observed with solvents other

than water. Given the relatively long Ru–Cl bonds in the crystal structures of the chlorido complexes (*cf.* Chapter 5), it is hypothesised the aquation mechanism will have a large dissociative character, suggesting an I_D mechanism.

6.2.2 Coordination of Buffer

On further inspection of the NMR spectra obtained from the aquation of $[17]Cl$, a third species was present in solution, with a characteristic singlet in the $^{31}P\{^1H\}$ spectrum at δ_P 44.8 ppm. This species was only observed in sodium phosphate buffered solutions and therefore its identity was proposed to be the ruthenium–phosphate adduct $[Ru(PO_4-O)(dppp)(cis-tach)]^{x+}$ $[17b]^{x+}$. 1H NMR spectra were recorded with sodium phosphate concentrations of 0, 10 and 20 mM with 300 μM of ruthenium complex at pH 7.4 (Fig. 6.2).

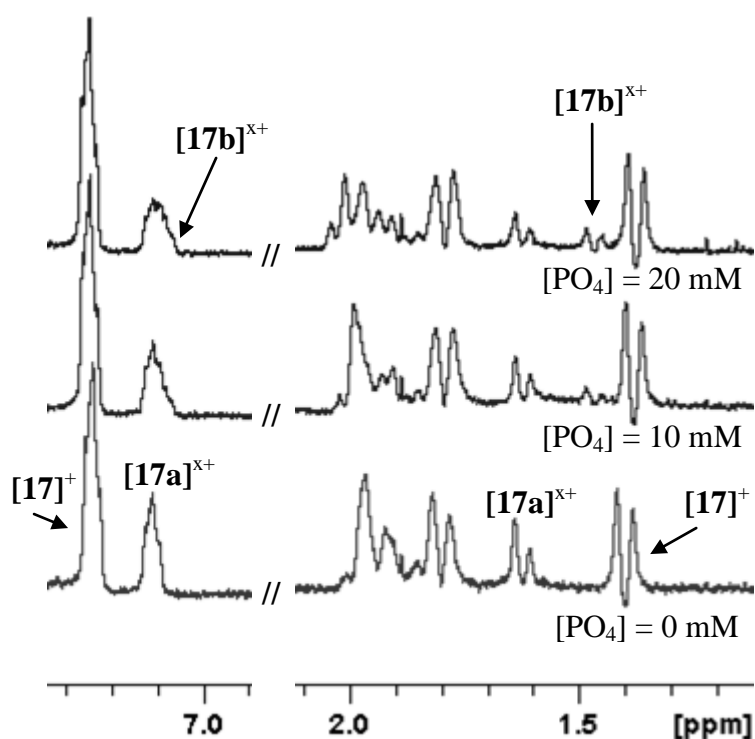


Figure 6.2: 1H NMR spectra of $[17]Cl$ in H_2O with 1.6% CD_3OD and 0 (bottom), 10 (middle) or 20 (top) mM sodium phosphate at pH 7.4.

The resonances for the ruthenium-phosphate species are most prominent at δ_H 1.5 ppm where a resonance for the CH_2 groups was observed. Additionally, the

phosphate complex contributes to the resonance for a phenyl proton in the chlorido complex at δ_{H} 7.1 ppm, where the profile of the multiplet is clearly distorted when the concentration of sodium phosphate is increased. It is not possible to identify other resonances from $[\mathbf{17b}]^{\text{x}+}$ due to coincidental or overlapping signals with the chlorido and aqua complexes. The relative proportion of this resonance to those for the aqua/hydroxy species was dependent on the concentration of sodium phosphate added to the solution.

The relative integration of the phosphate in the ^1H NMR spectrum is approximately 10% of the resonance corresponding to the aqua/hydroxy complex at 10 mM sodium phosphate, and therefore believed to be a minor constituent of the reaction mixture. This process was also observed in the aquation of $[\mathbf{16}]\text{Cl}$ giving the phosphate complex $[\text{Ru}(\text{PO}_4\text{-O})(\text{dppe})(\text{cis-tach})]^{\text{x}+}$ $[\mathbf{16b}]^{\text{x}+}$, but to a lesser extent of 2–3%. The protonation state of the phosphate ligand in both $[\mathbf{16b}]^{\text{x}+}$ and $[\mathbf{17b}]^{\text{x}+}$ remains unknown. The interaction of the aquated complex with the phosphate anions are of interest, given that the complexes may form adducts with phosphate-rich species, such as the DNA.

6.2.3 Aquation at Physiologically-Relevant Concentrations

The concentrations employed for analysis of the aquation reactions here are over two orders of magnitude greater than concentrations used for *in vitro* biological evaluation (300 μM vs. 0.5–10 μM). It has been demonstrated that osmium en complexes may undergo different aquation processes at physiologically-relevant concentrations than those typically employed in the laboratory.^{94, 111} For this reason, it was of interest to identify the species present in aqueous solution at concentrations close to the IC_{50} values obtained. The ^1H NMR spectrum of $[\mathbf{16}]\text{Cl}$ in 10% $\text{D}_2\text{O}/90\%$ H_2O buffered with 10 mM sodium phosphate at pH 7.4 was also recorded at 200 and 50 μM . Both spectra are identical. The phenyl regions of the ^1H NMR spectra obtained are shown in Fig. 6.3.

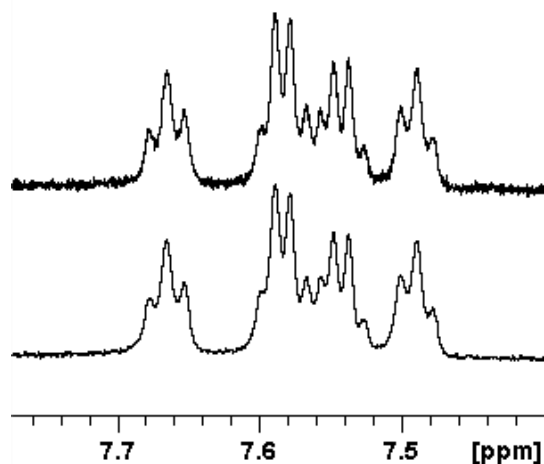


Figure 6.3: Phenyl region of the ^1H NMR spectra of [16]Cl at 200 (top) and 50 μM (bottom) in 10% $\text{D}_2\text{O}/90\%$ H_2O .

The ^1H NMR spectrum of a 10 μM aqueous solution of [17]Cl was recorded after 4 h at 37°C and is shown in Fig. 6.4. The resulting ^1H NMR spectrum between δ_{H} 7 and 8 ppm is identical to that of a 300 μM solution of [17]Cl. The *cis*-tach resonances were too weak to provide suitable comparison due to few protons in each chemical environment (1–2 protons) compared to the phenyl groups (4–8 protons).

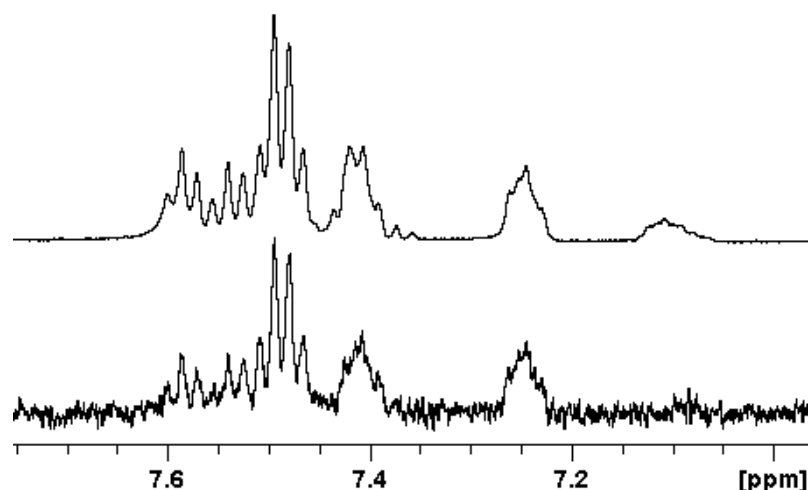


Figure 6.4: Phenyl region of the ^1H NMR spectra of [17]Cl in H_2O at 300 (top) and 10 μM (bottom) in H_2O with 1.6% CD_3OD and 10 mM sodium phosphate at pH 7.4.

For both compounds, there was no evidence of degradation of the aquated species at near physiological concentrations compared to those suitable for NMR analysis. Therefore, it is assumed that the solutions studied at 300 to 500 μM are representative of those in biological application in terms of speciation.

6.2.4 Stability of Aquation Products with Time

Both compounds were found to be relatively stable for the duration of a typical MTT assay experiment. Over a two week period at 37°C , the ^1H NMR spectrum of **[16]Cl** in 10% $\text{D}_2\text{O}/90\%$ H_2O did not change. However, a sample of **[17]Cl** in H_2O was observed to undergo a small change after 48 h. A new set of phenyl signals corresponding to approximately 5% of the phenyl resonance intensity was observed in the ^1H NMR spectrum alongside those of the chlorido and aqua/hydroxy complexes, shown in Fig. 6.5.

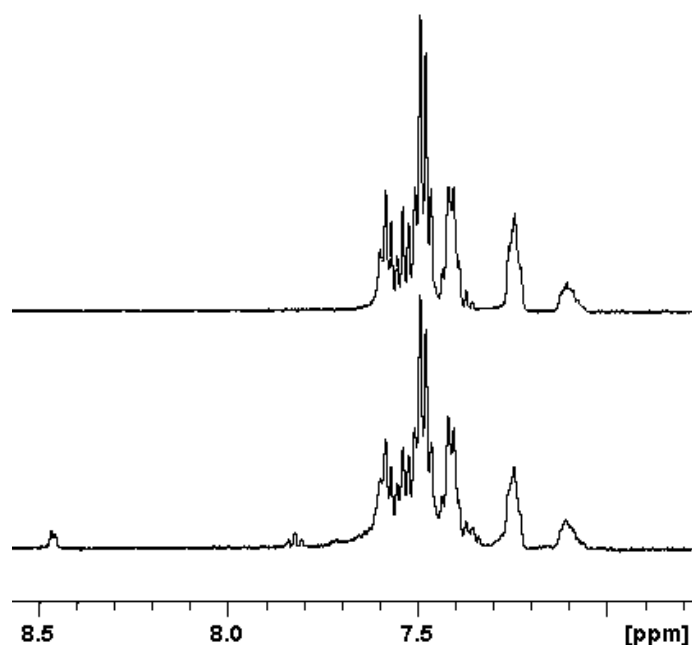


Figure 6.5: ^1H NMR of the phenyl region of **[17]Cl** in H_2O after 1 (top) and 48 h (bottom) at 37°C .

The species could not be identified, although no liberated *cis*-tach or phosphane were observed in the NMR spectra, therefore it is believed that the ruthenium *cis*-tach diphosphane moiety has not degraded. Unfortunately, it remains unknown if this species is innocent in the biological activity as a deactivation product or acts as the active species responsible for the antiproliferative nature of [17]Cl.

6.2.5 Influence of Salts to Moderate Ionic Strength

Attempts to match the ionic strength of aqueous solutions of [16]Cl and [17]Cl to physiologically-relevant conditions (~ 0.15 M) were met with difficulty. Use of weakly coordinating anions, including perchlorate, hexafluorophosphate and triflate resulted in the formation of a precipitate when exposed to ruthenium *cis*-tach complexes. Employment of other anions including nitrate and acetate resulted in significant coordination of the anion to the ruthenium complex. Therefore, the only suitable salts for moderation of the ionic strength are chlorides; but these suppress the aquation reaction, hindering its study.

6.2.6 Conclusions

The dissolution of [16]Cl and [17]Cl resulted in the aquation of the ruthenium chlorido bond to give the aqua/hydroxy species [16a]^{x+} and [17a]^{x+}. The aquation of [16]⁺ was seen to complete to a greater extent in comparison to the more cytotoxic [17]⁺. These species are stable at low concentrations and over 48 h, therefore these solutions are believed to be representative of those employed in the MTT assays for biological evaluation. Both aqua/hydroxy complexes are capable of binding phosphate, but only [17a]^{x+} binds phosphate to a significant extent. The identity of the ligand which occupies the coordination site provided by displacement of the chlorido ligand remains unclear and identification of the protonation of this group is of interest.

6.3 Determination of the pK_a of the Aqua Ligand in $[16a]^{x+}$ and $[17a]^{x+}$.

Characterisation of the aqua ligand is important in the understanding of the reactivity of $[16]Cl$ and $[17]Cl$. It has previously been observed with metal-based cytotoxic compounds that the protonation state of the aqua ligand may influence the reactivity of the complex. For example, the hydroxy derivative of RAen complexes, which is formed at high pH, was observed to have reduced reactivity compared to the aqua complex at physiological pH, mirroring the reactivity of cisplatin.^{96, 97, 278} Such an observation is expected for coordination of biological targets to the ruthenium-aqua coordination site, through the aqua ligand's better ability to act as a leaving group in comparison to hydroxy. Thus, the pK_a of metal complexes form the basis of a structure-activity relationship study, and it has been hypothesised that resulting aqua complexes with higher pK_a values exhibit greater potency *in vitro*.¹⁵⁷ Therefore, it is of interest to ascertain the protonation state of ruthenium(II) *cis*-tach complexes under physiologically-relevant conditions, in an effort to fully characterise these complexes.

6.3.1 UV/Vis pH Titrations

Aqueous solutions of $[16a](OTf)_x$ and $[17a](OTf)_x$ were obtained by reaction of a 500 μM solution of $[16]Cl$ or $[17]Cl$ with two equivalents of silver trifluoromethanesulfonate (triflate) while shielded from light. Complete chloride metathesis was confirmed by $^{31}P\{^1H\}$ NMR spectroscopy (with addition of 1.6% CD_3OD), where the only resonance observed was that of the aqua/hydroxy species. The UV/Visible spectrum was recorded at various intervals between pH 4/2 and 12 at 298 K, with the assumption that the observed spectrum is the weighted average according to the populations of the protonated and deprotonated species. The initial data was fitted to the Henderson-Hasselbalch equation which gave pK_a values of 10.80 ± 0.06 and 10.42 ± 0.15 for $[16a]^{x+}$ and $[17a]^{x+}$ respectively (Fig. 6.6). It is proposed that these acid-dissociation constants correspond to the deprotonation of the aqua ligand in $[16a]^{x+}$ and $[17a]^{x+}$.

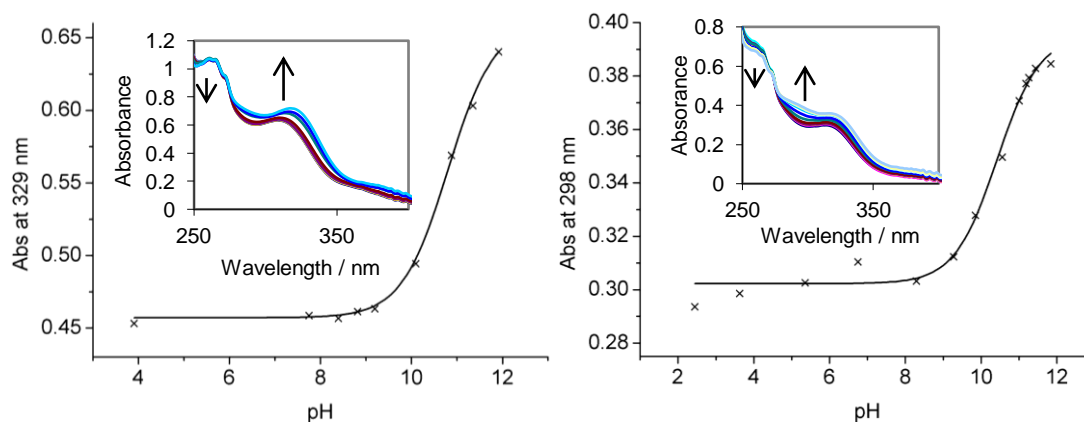


Figure 6.6: UV/Vis pH titration for $[16a]^{x+}$ (left) and $[17a]^{x+}$ (right) from pH 2 to 12. The plot of absorbance at 329 ($[16a]^{x+}$) or 298 nm ($[17a]^{x+}$) vs. pH is given as well as the change of the UV/Vis spectrum between 250 and 400 nm during the experiment. It is assumed that the spectrum is the weighted average according to the populations of the protonated and deprotonated species. Calculated pK_a s: $[16a]^{x+} = 10.80 \pm 0.06$; $[17a]^{x+} = 10.42 \pm 0.15$.

The process was demonstrated as reversible as the original spectrum was obtained on returning the solution to pH 2. Additionally, the ESI mass spectrum of this solution at pH 11 corresponds to the previously obtained spectra of the aqueous solutions, but with the hydroxy complex observed at 100% intensity. During the experiments, chloride leeching occurred from the pH electrode, evident from the pH titration of $[17a](OTf)_x$, where a non-level baseline was obtained. Therefore, it was necessary to employ a technique able to distinguish between the chlorido and aqua/hydroxy complexes, such as NMR spectroscopy.

6.3.2 1H NMR pH Titrations

It is common practice to perform 1H NMR pD titrations in D_2O , with the assumption that the observed chemical shifts are weighted averages according to the populations of the protonated and deprotonated species. The experimental pK_a values obtained in D_2O , pK_a^* , can then be converted to the corresponding pK_a in H_2O by the equation $pK_a = 0.929pK_a^* + 0.42$, suggested by Krezel and Bal.²⁷⁹ Reliable data from NMR measurements are obtained in the range $2 \leq pH \leq 12$ for compounds with $3 \leq pK_a \leq 11$.²⁸⁰ From translation of the pK_a data obtained from the UV/Vis pH titration, the

pK_a^* values would be expected to be 11.17 and 10.76 for $[16a]^{x+}$ and $[17a]^{x+}$ respectively. Thus, NMR pH titrations were performed in H_2O with 1.6% CD_3OD to provide a lock signal at 298 K. The effect of < 0.5% HOD was not factored into calculations. Methanol, with a pK_a of 15.5,²⁸¹ will not be deprotonated during the experiments and the small quantity of it is assumed not to alter the solution properties significantly. Additionally, these conditions replicate the other aquation experiments performed studying these two complexes in this chapter. An ionic strength buffer is often employed in pK_a determination. However, increasing the ionic strength of the solution will result in the stabilisation of the doubly cationic aqua complex, thereby further increasing the pK_a . For this reason and the previously highlighted complications associated with weakly coordinating anions and these complexes, the ionic strength of the solutions was not fixed by the addition of salts.

Preparation of aqueous solution of $[16a](OTf)_x$ and $[17a](OTf)_x$ was repeated as for the previous UV/Vis titration, but the resulting solutions were supplemented with 1.6% CD_3OD as a lock solvent after removal of silver chloride by filtration. The pH of the solutions was varied from pH 2–12 and 1H NMR spectra recorded at various intervals. Selected resonances were fitted to the Henderson-Hasselbalch equation with the assumption that the observed chemical shifts are weighted averages according to the populations of the protonated and deprotonated species (Fig. 6.7).

The resulting pK_a values from the 1H NMR titration of 10.85 ± 0.02 and 10.54 ± 0.02 for $[16a]^{x+}$ and $[17a]^{x+}$ respectively are in accordance with the initial data obtained from UV/Vis spectroscopy. Calculation of the ratio of protonated to deprotonated species at pH 7.4 is over 1000:1, therefore both complexes can be considered to exist exclusively as the aqua species, $[16a]^{2+}$ and $[17a]^{2+}$. For these complexes the hydrolysis and subsequent deactivation of the aqua species is suppressed under physiological conditions, potentially reducing deactivation.

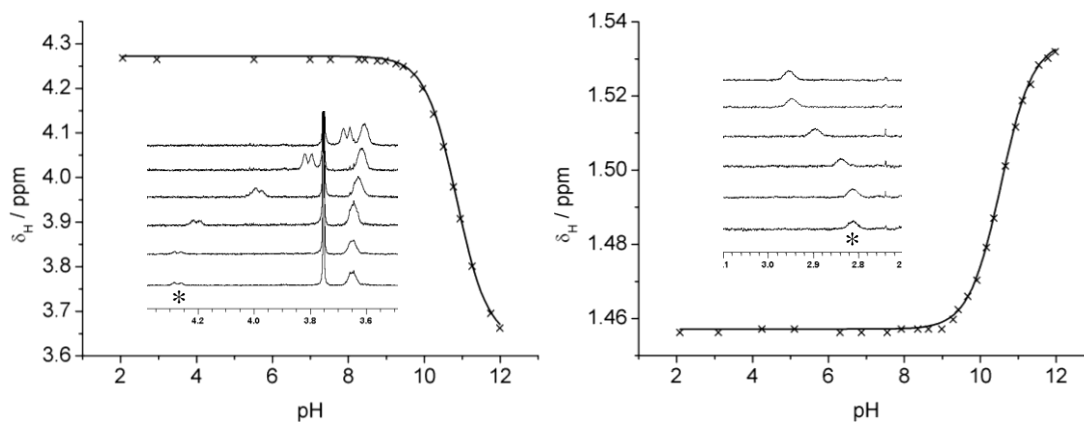


Figure 6.7: ^1H NMR pH titration of $[\mathbf{16a}]^{\text{x}+}$ and $[\mathbf{17a}]^{\text{x}+}$ from pH 2 to 12. One of three selected resonances is shown for $[\mathbf{16a}]^{\text{x}+}$ (left, NH_2 , $\text{p}K_{\text{a}}$ 10.85 ± 0.01) and $[\mathbf{17a}]^{\text{x}+}$ (right, CH , $\text{p}K_{\text{a}}$ 10.53 ± 0.01). The inset shows the shift of the resonance in NMR spectrum during the experiment.

The acid-dissociation constants of these complexes are higher than those commonly obtained for ruthenium(II) η^6 -arene complexes, including $[\text{Ru}(\text{OH}_2)(\eta^6\text{-bip})(\text{en})]^{2+}$ (7.71 ± 0.01) $[\text{Ru}(\text{OH}_2)(\eta^6\text{-tha})(\text{en})]^{2+}$ (8.01 ± 0.03), and $[\text{RuCl}(\text{OH}_2)(\eta^6\text{-C}_6\text{H}_6)(\text{PTA})]^{2+}$ (9.2).^{97, 282} The highest $\text{p}K_{\text{a}}$ values are typically obtained for *O,O*-chelates, such as $[\text{Ru}(\text{OH}_2)(\eta^6\text{-}p\text{-cym})(\text{mal})]^+$ (9.23 ± 0.02) and $[\text{Ru}(\text{OH}_2)(\eta^6\text{-}p\text{-cym})(\text{acac})]^+$ (9.41 ± 0.01).^{111, 275}

6.3.3 Conclusions

The acid-dissociation constants of the aqua complexes $[\mathbf{16a}]^{2+}$ and $[\mathbf{17a}]^{2+}$ were determined by ^1H NMR pH titration; the $\text{p}K_{\text{a}}$ of both complexes were physiologically inaccessible by over 3 pH units. Therefore, aquation affords exclusively the aqua adduct. It is hypothesised that formation of the aqua complex is important in the activation of the chlorido complexes, allowing reactivity with biomolecules. Deprotonation to give the hydroxo species is not expected to occur under physiological conditions, and therefore the potential deactivation of the aqua species by this mechanism is not considered.

6.4 Kinetics of Aquation

The importance of the rate at which the aquation process occurs is somewhat mixed. The RAen complexes $[\text{RuCl}(\eta^6\text{-arene})(\text{en})]\text{PF}_6$ aquate relatively rapidly (arene = bip, $t_{1/2} = 3$ min),⁹⁷ but the Os analogues aquate much slower (arene = bip, $t_{1/2} = 6.4$ h),⁹⁴ yet both display similar *in vitro* cytotoxicities, with the biphenyl complexes equipotent to carboplatin.^{78, 85} Furthermore, the aquation-resistant azopyridine complexes $[\text{RuI}(\eta^6\text{-arene})(\text{Azpy})]$ are also highly active.¹⁴² The kinetics of aquation and anation of ruthenium *cis*-tach complexes were investigated with the aim of providing further insight into structure-activity relationships of the diphosphane series of complexes.

6.4.1 Kinetics of Aquation and Anation of [16]Cl

The rate of aqua adduct $[\mathbf{16a}]^+$ formation was studied by UV/Visible spectroscopy, with the extent of the reaction at completion determined by ^1H or $^{31}\text{P}\{^1\text{H}\}$ NMR spectroscopy. A selected region of the time-evolution difference spectrum of the aquation of a 300 μM solution of $[\mathbf{16}]\text{Cl}$ at pH 7.4 (10 mM sodium phosphate buffer) is provided in Fig. 6.8. The phosphate acted as both pH and ionic strength buffer ($I \approx 25$ mM). The ionic strength was unable to be easily elevated to physiologically-relevant conditions due to coordination of the anion or formation of a precipitate (Section 6.2). The $\text{p}K_a$ of the complex (10.85 ± 0.02) indicates that only the aqua species is obtained as hydrolysis is suppressed at pH 7.4. The presence of isosbestic points at 325, 335 and 368 nm suggests the reaction involves a single step mechanism in the formation of the aqua derivative from the chlorido complexes. The small quantity of ruthenium – phosphate complex formed in the reaction was not taken into account in analysis.

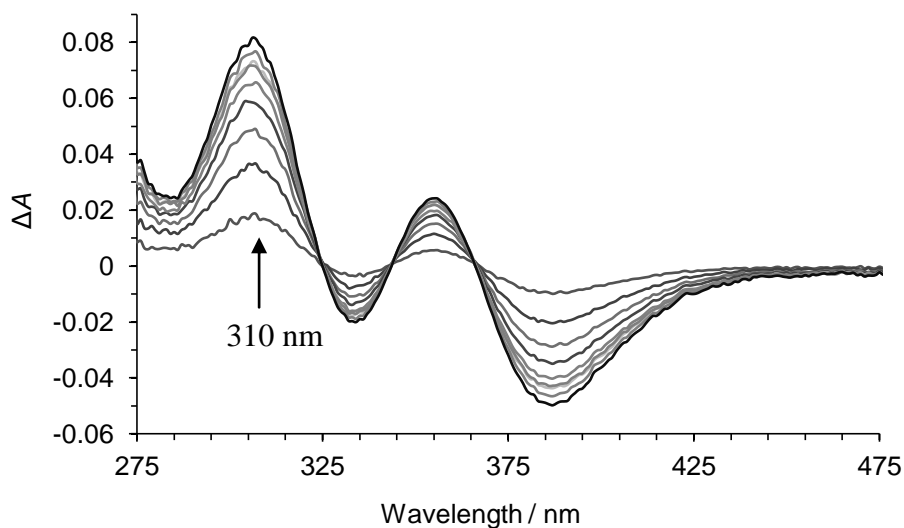


Figure 6.8: Time-evolution of UV/Vis difference spectra for the aquation of 300 μM [16]Cl in aqueous solution buffered at pH 7.4 (10 mM sodium phosphate) with 1.6% MeOH at 298 K, $I \approx 25$ mM. Plots are given for minutes 1 to 9. $\Delta A = A_t - A_0$, where A_t = absorbance at time t and $A_0 = A$ at $t = 22$ seconds.

The $(\Delta A)_{\text{max}}$ for [16]Cl occurred at 310 nm and was used in the kinetic study of this complex. The change of absorbance at this wavelength was monitored at 298 K as shown in Fig. 6.9.

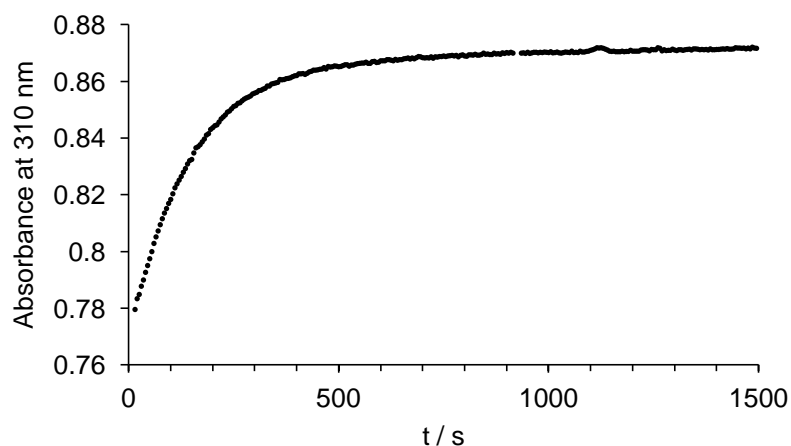


Figure 6.9: Time-dependence of the absorbance at 310 nm in the aquation of a [16]Cl (300 μM) aqueous solution, buffered at pH 7.4 (10 mM sodium phosphate) with 1.6% MeOH at 298 K. $I \approx 25$ mM.

The time dependence of the absorbance at 310 nm followed first order kinetics and indicated that the reaction had reached equilibrium within 15 minutes at 298 K. The equilibrium constant K was calculated from the ratio of integrations of the ruthenium *cis-tach* species in the ^1H NMR spectrum and the expected chloride concentration for the given distribution of complexes. The rate of aquation, k , was determined using DynaFit kinetic fit analysis and the rate of anation, k' , was calculated using Eqn. 6.1. The half life, $t_{1/2}$ for a first order reaction was determined using Eqn. 6.2.

$$K = \frac{k}{k'} \quad \text{Equation 6.1}$$

$$t_{1/2} = \frac{\ln 2}{k} \quad \text{Equation 6.2}$$

The range of temperatures was extended to include 288, 293, 303 and 310 K, for which the rate and equilibrium constants are provided in Table 6.2.

T (K)	k (10^{-3} s^{-1})	$t_{1/2}$ (s)	k' ($\text{M}^{-1} \text{ s}^{-1}$)	K (10^{-3} M)
288	2.09±0.02	331±3	0.128±0.002	16.4±0.1
293	3.60±0.08	192±5	0.232±0.008	15.6±0.4
298	6.55±0.06	106±1	0.430±0.005	15.3±0.1
303	10.7±0.2	65.1±1.4	0.718±0.021	14.8±0.3
310	21.0±0.7	32.9±1.1	1.51±0.07	14.0±0.5

Table 6.2: Rate and equilibrium constants for the aquation of [16]Cl at various temperatures. pH 7.4, $I \approx 25$ mM.

The rates of reaction at 298 and 310 K are of particular interest. The rate of reaction at 310 K correlates to a half life of only 33 seconds under physiological conditions. Therefore, the rate of aquation is not a significant factor in the *in vitro* activity of the complex as aquation occurs extremely rapidly in comparison to cell proliferation (typically 24 h). The kinetic parameters at 298 K allow for meaningful comparison of the kinetics of aquation with $[\text{RuCl}(\eta^6\text{-arene})(\text{en})]^+$ due to similar ionic strengths (25 mM for [16]Cl and 15 mM for $[\text{RuCl}(\eta^6\text{-arene})(\text{en})]^+$). The rate of aquation of the *cis-tach* complex is over five times faster than the η^6 -biphenyl complex

($1.28 \pm 0.01 \times 10^{-3} \text{ s}^{-1}$) and over twice as fast as the η^6 -tha complex ($2.36 \pm 0.02 \times 10^{-3}$), with half lives of five minutes and greater.⁹⁷ The aquation rate constant of the η^6 -arene complexes was not observed to change with ionic strength. The equilibrium constant for **[16]Cl** is up to twice that of the η^6 -arene complexes. Analysis of the biological implications of the equilibrium constants for both **[16]**⁺ and **[17]**⁺ are discussed in Section 6.5. The difference in k between the *cis*-tach and RAen complexes mirrors the Ru–Cl bond lengths. The Ru(1)–Cl(1) bond length of **[16]Cl** (2.4431(14) Å) is significantly longer than that of the RAen complexes (2.405(6)–2.408(15) Å). This is proposed as a result of the trans-influence of the strong *cis*-tach amine donor atoms, thus weakening the bond and increasing the kinetics of aquation.

The reaction rates for aquation and anation allowed the determination of the Arrhenius activation energy (E_a), activation enthalpy (ΔH^\ddagger) and activation entropy (ΔS^\ddagger) using rearrangements of the Arrhenius (Eqn. 6.3) and Eyring (Eqn. 6.4) equations.

$$\ln\left(\frac{k}{T}\right) = \frac{-\Delta H^\ddagger}{RT} + \ln\left(\frac{k_B}{h}\right) + \frac{\Delta S^\ddagger}{R} \quad \text{Equation 6.3}$$

$$\ln(k) = \frac{-E_a}{RT} + \ln(A) \quad \text{Equation 6.4}$$

A plot of $\ln(k/T)$ versus $1/T$ gives a straight line with slope of $-(\Delta H^\ddagger/R)$ and intercept of $\ln(k_B/h) + (\Delta S^\ddagger/R)$, and plot of $\ln(k)$ versus $1/T$ gives a straight line with gradient $-(E_a/R)$. All plots for the aquation and anation reactions are given in Fig. 6.10. Data analysis was performed using OriginPro8.

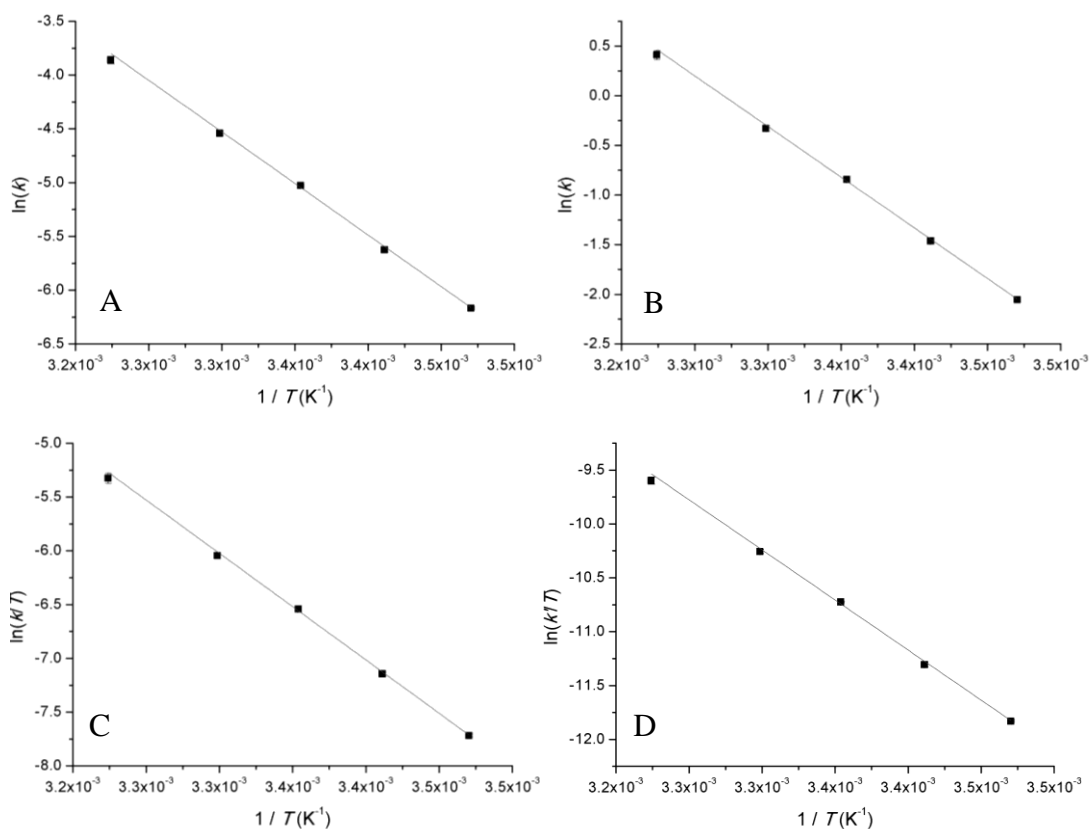


Figure 6.10: A and B: Arrhenius plots (Eqn. 6.3) for the aquation and anation reactions of $[16]Cl$ respectively; C and D: Eyring plots (Eqn. 6.4) for the aquation and anation reactions of $[16]Cl$ respectively.

	E_a (kJ mol ⁻¹)	ΔH^\ddagger (kJ mol ⁻¹)	ΔS^\ddagger (J K ⁻¹ mol ⁻¹)
$[16]^+$	79.8±0.7	77.3±0.7	-27.6±4.8
$[16a]^{2+}$	84.9±1.0	82.4±1.0	24.4±3.4

Table 6.3: Arrhenius activation energy (E_a), activation enthalpy (ΔH^\ddagger) and activation entropy (ΔS^\ddagger) for the aquation and anation of $[16]^+$ and $[16a]^{2+}$. pH 7.4, $I \approx 25$ mM.

The activation energy and enthalpy of activation for the aquation reaction are similar to those reported for RAen complexes.⁹⁷ The difference arises with a smaller negative entropy of activation, ΔS^\ddagger . This could suggest some association (I_A) in the substitution mechanism, which is in contrast to the hypothesised I_D mechanism, but the small value of ΔS^\ddagger possibly eliminates a true associative or dissociative type mechanism. The anation reaction has a small positive value of ΔS^\ddagger and may correspond to a degree of dissociation (I_D) in the mechanism. However, due to the small ΔS^\ddagger values, little can be concluded as to the type of concerted mechanism responsible for either ligand exchange processes. This may be accounted for by the effects of solvent reordering or changes to the conformation of the complex during the activation step.

6.4.2 Kinetics of Aquation and Anation of [17]Cl

To complement the kinetic analysis of [16]Cl, the corresponding aquation reaction of [17]Cl was monitored by UV/Visible spectroscopy at 298 K under identical conditions. The greatest absorbance change for [17]Cl occurred at 300 nm and was used in the kinetic study of this complex. The change of absorbance at this wavelength was monitored at 298 K as shown in Fig. 6.11.

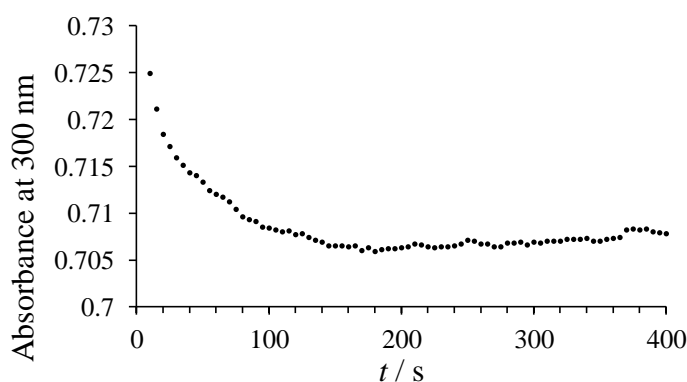


Figure 6.11: Time-dependence of the absorbance at 300 nm for the aquation of 300 μ M of [17]Cl in aqueous solution buffered at pH 7.4 (10 mM sodium phosphate) with 1.6% MeOH at 298 K, $I \approx 25$ mM.

The end-point of the reaction was determined by ^1H and $^{31}\text{P}\{^1\text{H}\}$ NMR spectroscopy. Analysis by the same method as employed for **[16]Cl** gave parameters of $k = (63.9 \pm 6.0) \times 10^{-3} \text{ s}^{-1}$, $k' = 32.3 \pm 7.4 \text{ M}^{-1} \text{ s}^{-1}$ and $K = (1.98 \pm 0.49) \times 10^{-3} \text{ M}$. The rate of aquation for **[17]Cl** is an order of magnitude faster than **[16]Cl**. However, the rate of the reverse reaction, forming **[17]⁺** is comparatively faster, by almost two orders of magnitude greater than for **[16]⁺**. The difference in reaction rate does not correlate with the Ru–Cl bond lengths. The bond lengths in **[16]Cl** (2.4431(14) Å) and **[17]Cl** (2.4404(4) Å) are identical, within error. Therefore the reactions are most likely dictated by the thermodynamic stability of the aqua products. Although full analysis was not possible, it is evident that the equilibria for the aquation/anation reaction of both **[16]Cl** and **[17]Cl** are almost an order of magnitude in difference.

The half life of the reaction was calculated as $t_{1/2} = 10.8 \pm 1.0 \text{ s}$ and the reaction reached equilibrium within 180 seconds. As the first recorded measurement was only possible from approximately 20 seconds to allow turbidity to subside, two half lives have already occurred before the first measurement was obtained. The reaction at 310 K was observed to have reached completion within 30 s; therefore kinetic analysis was not possible. Furthermore, the small measured change in Abs ($\Delta A = 0.01\text{--}0.02$) throughout the reaction increases the error of the calculated rate constants, giving parameters with little certainty. A small amount of bubble formation on the inside of the cell also resulted in a change of Abs with time to a level comparable to ΔA (Fig. 6.11). As a result, full kinetic analysis was not performed.

6.4.3 Discussion and Conclusions

The rates for the aquation and anation reactions of the ruthenium(II) *cis*-tach complex **[16]Cl** were determined and activation parameters calculated. The rate of aquation was found to be up to five times faster than the established RAen complexes. Initial investigation into the aquation of **[17]Cl** found that it has a rate of aquation an order of magnitude greater than **[16]Cl**, and almost 50 times that of $[\text{RuCl}(\eta^6\text{-bip})(\text{en})]^+$. However, the quick rate of aquation at 310 K prevented determination of the reaction rate, as equilibrium was reached shortly after

commencing measurement. The rates of aquation for both complexes are unlikely to provide further evidence regarding the development of structure-activity relationships, as both reactions occur rapidly, reaching completion within minutes.

Although the conditions employed were not directly physiologically relevant, as the ionic strength within a cell is higher than the experimental conditions used, it is assumed that both the aquation and anation reaction still occur readily at these ionic strengths. The kinetic studies of Sadler and co-workers show that for the RAen complexes only the rate of the reverse reaction changes with ionic strength and therefore the equilibrium.⁹⁷ This correlates with an associative mechanism for the aquation reactions for both the *cis*-tach and RAen complexes.

It is proposed that the *in vitro* activities of these complexes are more dependent on the ability of the complexes to bind potential biological targets and the equilibrium between the chlorido and aquated species, dictating the proportion of activated species within the cell. The equilibrium constants obtained from the kinetic analysis for the two species are different by almost an order of magnitude, which is expected to be reflected in the proportions of chlorido and aqua species in a given environment. The determination of the equilibrium mixture at physiologically-relevant conditions forms the basis of the proceeding section.

6.5 Equilibrium of Aquation/Anation

As shown in the kinetic analysis, the rate of aquation is not believed to be an important factor for the *in vitro* activity of the ruthenium(II) *cis*-tach complexes as both [16]Cl and [17]Cl aquate rapidly at 310 K, reaching equilibrium within minutes. Therefore, it is of interest to understand the extent to which these complexes aquate within a cell or nucleus to predict the composition of species present in a given environment. Although equilibrium constants were calculated in the kinetic analyses, these were not obtained under physiologically-relevant conditions due to the difference in ionic strength of the solution; a relevant ionic strength, I , is of the order of 10^{-1} M.

Rearrangement of the equilibrium Eqn. 6.5 permits the calculation of K by variation of chloride concentration and the determination of the concentrations of the ruthenium species present in the solution.

$$\text{For a given } I: \quad \frac{[\text{chlorido}]}{[\text{aqua}]} = \frac{[\text{Cl}^-]}{K} \quad \text{Equation 6.5}$$

However, I cannot be maintained constant throughout the chloride concentration range employed due to the difficulties discussed in Section 6.2 of either coordination of the anion or precipitation. Therefore, a plot of $[\text{chloro}]/[\text{aqua}]$ vs. $[\text{Cl}^-]$ will not result in a linear correlation and Eqn. 6.1 cannot be used to calculate K . Estimation of K is still possible for a given condition from the ratio of species for the corresponding point on the fitted curve. The plot will not only improve the confidence of the calculated value, but also reveal the variation of K between physiologically-relevant conditions and those employed for the kinetic studies.

6.5.1 Results

Aqueous solutions of the appropriate complex (500 μM) and sodium chloride (0 to 100 mM) at pH 7.4 (10 mM sodium phosphate) with 1.6% CD_3OD were heated at 37°C for 2 h before the ^1H ([**16**]Cl) or ^1H and $^{31}\text{P}\{^1\text{H}\}$ ([**17**]Cl) NMR spectra were recorded at 37°C. Deprotonation of the aqua ligand is not expected to occur at pH 7.4 and therefore to not affect any speciation observed. Relative integrations of the chlorido and aqua species were calculated for each chloride concentration, the plots of which are given in Fig. 6.12. The ruthenium-phosphate adduct, although present, was not accounted for in the analysis. The chloride concentration was calculated accounting for the chloride originating from the ruthenium complexes.

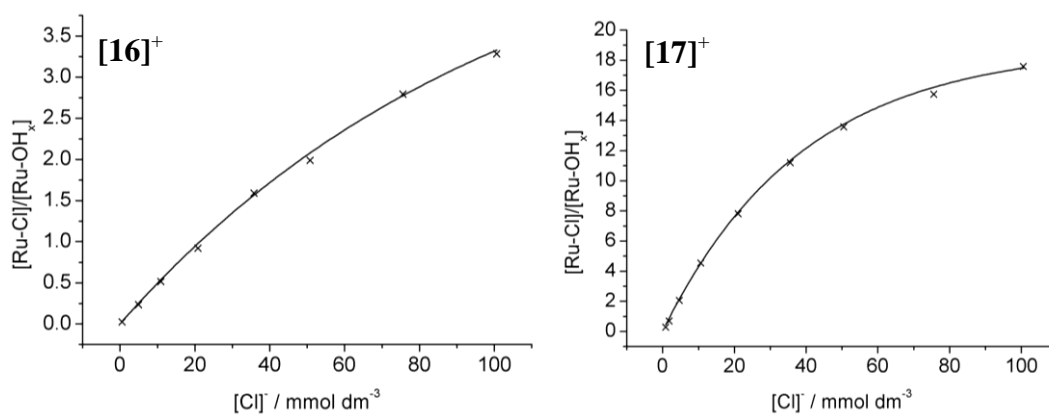


Figure 6.12: Plots of the fraction of chlorido/aquated species and $[\text{Cl}^-]$ for $[\mathbf{16}]^+$ (left) and $[\mathbf{17}]^+$ (right) vs. chloride concentration at pH 7.4 (10 mM sodium phosphate) and 37°C . $I_x \approx [\text{Cl}^-]_x + 25 \text{ mM}$. Curves were fitted using the equation $y = a(1-b^x)$ in OriginPro 8. $[\mathbf{16}]^+$ $a = 5.34 \pm 0.29$, $b = 0.990 \pm 0.001$; $[\mathbf{17}]^+$ $a = 18.9 \pm 0.3$, $b = 0.975 \pm 0.001$.

For both complexes, K increases with ionic strength, evident from the curve trending downwards in the $1/K$ relationship. The equilibrium constant for the aquation-anation of $[\mathbf{17}]\text{Cl}$ undergoes a greater increase with ionic strength than $[\mathbf{16}]\text{Cl}$. The variation with I is as expected, as the higher ionic strengths promotes the formation of the doubly charged aqua species as opposed to the mono-cationic chlorido complex. This is resultant from either an enhanced rate of aquation or a reduction in the rate of anation. This observation supports the assumption that the kinetics of aquation at higher ionic strengths is *at least* comparable to those observed in the kinetic analysis ($I_x \approx 25 \text{ mM}$). It is proposed that the anation reaction is unfavoured at higher ionic strengths, as observed with the complexes $[\text{RuCl}(\eta^6\text{-arene})(\text{en})]^+$, providing the largest contribution to the variation in K .⁹⁷ Therefore the rate of aquation and anation is thought not to be of significance to the activity of the complexes, but to the equilibrium between the chlorido and aqua complexes.

6.5.2 Calculated Distribution of Species in Biological Environments

The equilibrium constant K was calculated from the fitted curve for the aquation of each complex at an ionic strength of approximately 130 mM, corresponding to 104 mM sodium chloride and 10 mM sodium phosphate at pH 7.4. The values are

(30.6 ± 1.7) $\times 10^{-3}$ and (5.90 ± 0.08) $\times 10^{-3}$ M for complexes [16]Cl and [17]Cl respectively. The two complexes are evidently very different to the degree at which aquation occurs within a given environment. In order to illustrate the physiological relevance of the equilibrium constant, the predicted distribution of chlorido and aqua species are given in Table 6.4 for the blood, cytoplasm and cell nucleus. These are calculated based on the chloride concentrations reported for these environments.^{97, 247}

	K (10^{-3} M)	pK_a^b	Predicted % Aqua ^a (Ru–OH ₂) at pH 7.4		
			Blood ^c	Cytoplasm ^d	Nucleus ^e
[16]Cl	30.6 ± 1.7^f	10.85 ± 0.02	22.8 ± 1.2	48.6 ± 3.2	88.5 ± 4.9
[17]Cl	5.90 ± 0.08^f	10.54 ± 0.02	5.4 ± 0.1	20.7 ± 0.3	59.6 ± 0.8
RM175 ^{g 97}	9.1 ± 0.9^h	7.71 ± 0.01	5.2^i	18.6^i	45.2^i
HC11 ^{j97}	11.7 ± 0.7^h	8.01 ± 0.03	8.8^i	29.7^i	65.2^i
RAPTA-C ¹¹⁸	3.8 ± 0.2^k	$9.2^{282i,l}$	<i>m</i>	<i>m</i>	<i>m</i>
[PtCl ₂ (en)] ²⁸³	<i>n</i>	6.53^i	2.7^i	<i>m</i>	42^i

Table 6.4: Equilibrium constants and proportion of ruthenium species aquated under various physiologically-relevant conditions. Values of K for [16]Cl and [17]Cl were calculated for a pH 7.4 10 mM sodium phosphate solution, $I = 130$ mM at 37°C. Equilibrium constant used was calculated for 104 mM NaCl. \pm values are one standard deviation. *a*) predicted, based on K , *b*) $T = 298$ K, values given for first aqua deprotonation only (if applicable), *c*) 104 mM, *d*) 22.7 mM, *e*) 4 mM NaCl, *f*) $T = 310$ K, $I = 130$ mM, *g*) [RuCl(η^6 -bip)(en)]PF₆, *h*) $T = 310$ K, $I = 100$ mM, *i*) No standard deviations reported; remainder of species made up of both chlorido and hydroxy species, *j*) [RuCl(η^6 -tha)(en)]PF₆, *k*) $T = 298$ K, $I = 150$ mM, *l*) Calculated pK_a for [RuCl(OH₂)(η^6 -C₆H₆)(PTA)]⁺, *m*) no speciation reported, *n*) 296 K, $I = 200$ mM.

It is believed the activity of cisplatin and the ruthenium(II) η^6 -arene complexes is resultant from the formation of the aqua species within the cell. Formation of hydroxo-complexes causes inactivation due to the poor lability of the hydroxide compared to the aqua ligand.^{21, 96, 278} Therefore, only the percentage of aqua

complex provides an indication of the active species, which is dependent upon both K and pK_a .

The equilibrium constants for the two *cis*-tach complexes are remarkably different from each other. The equilibrium constant for the aquation of [16]Cl is significantly greater than [17]Cl and results in a considerable difference in speciation. The two equilibrium constants encompass those of the RAen complexes. Unfortunately, the equilibrium constant for the aquation of [16]Cl is not desirable, as it results in the formation of the aqua species in all environments, leading to a greater possibility for deactivation reactions to occur. For example, cisplatin is deactivated by glutathione binding prior to reaching the nucleus;¹⁸ a similar process may account for the poor activity of this complex compared to [17]Cl.

The combination of both a lower equilibrium constant of aquation and pK_a of the aqua species has resulted in a favourable proportion of [17a]²⁺ formed under each environment. The equilibrium constant is not too low that aquation does not occur to a significant extent, plus deprotonation to form the potentially inactive hydroxo species is inhibited by the high pK_a . This might result in a low proportion of aqua species in the blood, but a high percentage in the nucleus in comparison to the RAen complexes. Therefore, the proportion of aqua species across the physiologically-relevant chloride concentrations is more greatly exaggerated than the other complexes presented. This gives an ideal balance between protection of the complex outside the cell and a relative higher degree of activation inside the cell. As demonstrated by the kinetic study, the rate at which the complex is aquated once in the cell is very rapid and is not a factor in the speciation.

6.5.3 Conclusions

Both [16]Cl and [17]Cl undergo rapid aquation in water, which is suppressed by the addition of chloride. The formation of the aqua species [16a]²⁺ is not suppressed by chloride concentrations comparable to the blood to the same extent as for established cytotoxic compounds, with > 20% [16a]²⁺ present. Furthermore, a much higher proportion of [16a]⁺ is also present at concentrations relevant to the cell and nucleus. In contrast, [17]Cl aquates to a lesser extent under all conditions, despite kinetics of

aquation an order of magnitude faster. This results in a low proportion of the aqua complex in conditions similar to blood and the cytoplasm. The lower equilibrium constant combined with the high pK_a of the *cis*-tach ruthenium(II) complexes results in a greater proportion of the aquated species in the nucleus than the promising RAen complexes. This complex is predicted to possess an effective balance between the protection from deactivation while in the blood and to an extent, the cytoplasm, whilst allowing abundant activation in the nucleus.

6.6 Interactions of [16]Cl and [17]Cl with Nucleosides

The *cis*-tach ligand for ruthenium(II) anti-cancer complexes was chosen to replicate the DNA-binding characteristics of the existing compounds, $[\text{RuCl}(\eta^6\text{-arene})(\text{en})]^+$. These complexes form strong covalent adducts with DNA, with a preference to the *N7* of guanine.^{90, 96, 103} This is further strengthened by hydrogen-bonding interactions between the amine groups of the en ligand and the *O6* of an adjacent guanine residue. Therefore, the interactions with ruthenium(II) *cis*-tach complexes with DNA, particularly the guanine base, were of interest.

9-Ethyl guanine (EtG, Fig. 6.13) and guanosine monophosphate (GMP, Fig. 6.13) were selected as small molecular models of DNA for NMR spectroscopy experiments to determine the capability for the *cis*-tach complexes to react with purine bases. EtG is advantageous for use in NMR spectroscopy experiments over guanine and guanosine, as it displays good solubility in neutral solutions and lacks a chiral centre, reducing the complexity of resulting resonances. It has been commonly used with ruthenium compounds in the investigation of metal-DNA interactions *via* the *N7* of guanine.^{90, 108, 157, 284} In order to also provide a model compound closer to the molecular structure of DNA, GMP was employed. It was of interest to use a model with the phosphate incorporated due to the potential interactions of this group with the complexes, either by coordination or hydrogen-bond interactions.

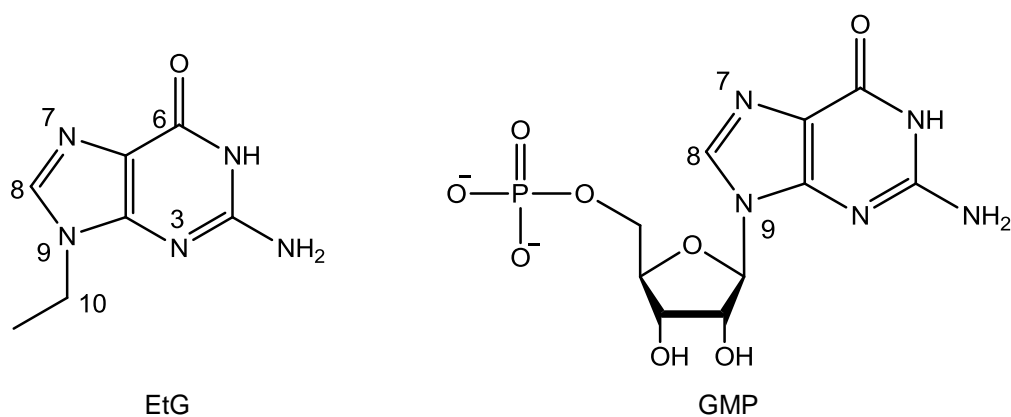


Figure 6.13: Structure and numbering scheme of 9-ethyl guanine (EtG, left) and Guanosine monophosphate (GMP, right).

6.6.1 Interaction of [16]Cl with DNA Model Complexes

In order to evaluate the potential for [16]Cl to form covalent bonds to the *N*7 of a guanine residue, the complex was heated at 310 K for 24 h with one equivalent of EtG or GMP (1 mM) in H₂O. The solutions were characterised by ¹H and ³¹P{¹H} NMR spectroscopy, supplemented with 1.6% CD₃OD as a lock solvent.

The reaction with EtG resulted in a new guanine containing species in the ¹H NMR spectrum, evident from a new H8 resonance ($\Delta\delta_{\text{H}}(\text{H}8) = -1.93$ ppm), shown in Fig. 6.14. Approximately 25% of the aquated species [16a]⁺ reacted with EtG under the conditions employed. The proposed coordination site of the guanine residue is the *N*7 position, resulting in [Ru(EtG-*N*⁷)(dppe)(*cis*-tach)]²⁺ [16c]²⁺. A similar species is also observed in the reaction of [16]Cl with guanosine monophosphate with $\Delta\delta_{\text{H}}(\text{H}8) = -1.87$ ppm for [Ru(GMP-*N*⁷)(dppe)(*cis*-tach)] [16d], but to a lesser extent (~15%).

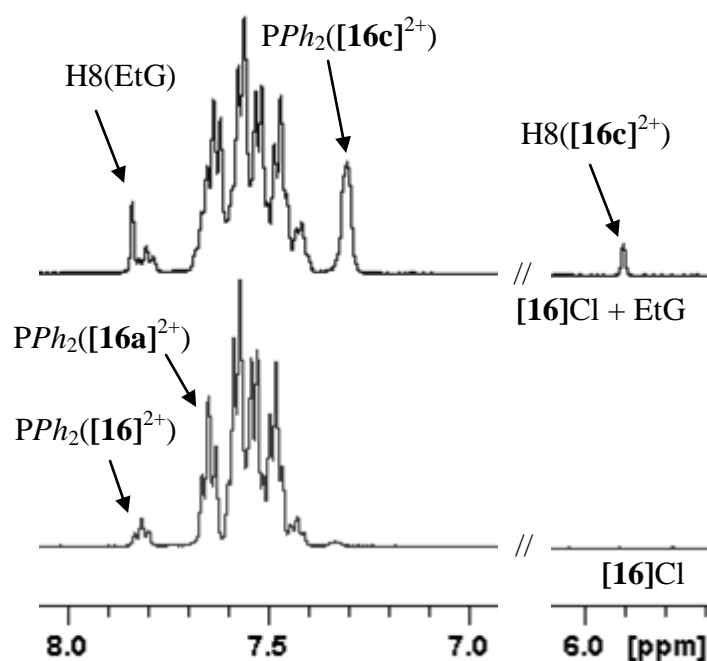


Figure 6.14: Guanosine H8 and phenyl region of the ^1H NMR spectra for **[16]Cl** (1 mM, bottom) and the reaction of **[16]Cl** (1 mM) with EtG (1 mM, top) after 24 h at 310 K.

Displacement of the chlorido ligand by a guanine derivative was demonstrated by the reaction of **[16]Cl** (1 mM) with guanosine (Guo, 2 eq.) after incubation at 37°C for 24 h in water. The solution was diluted to 0.1 mM with 50% methanol in water and the ESI mass spectrum recorded. An ion with mass and isotope pattern corresponding to $[\text{M}-\text{Cl}+\text{Guo}-\text{H}]^+$ (30%) and $[\text{M}-\text{Cl}+\text{Guo}]^{2+}$ (30%) was observed at m/z 911.1 and 456.2 respectively along with chlorido (100%) and hydroxy (30%) species.

For both complexes, resonances corresponding to *cis*-tach with C_s symmetry are present in the ^1H NMR spectra (Fig. 6.15). However, in the case of **[16d]^{x+}**, protons localised near the GMP ligand reflect its chiral nature with slight inequivalence of atoms related by symmetry.

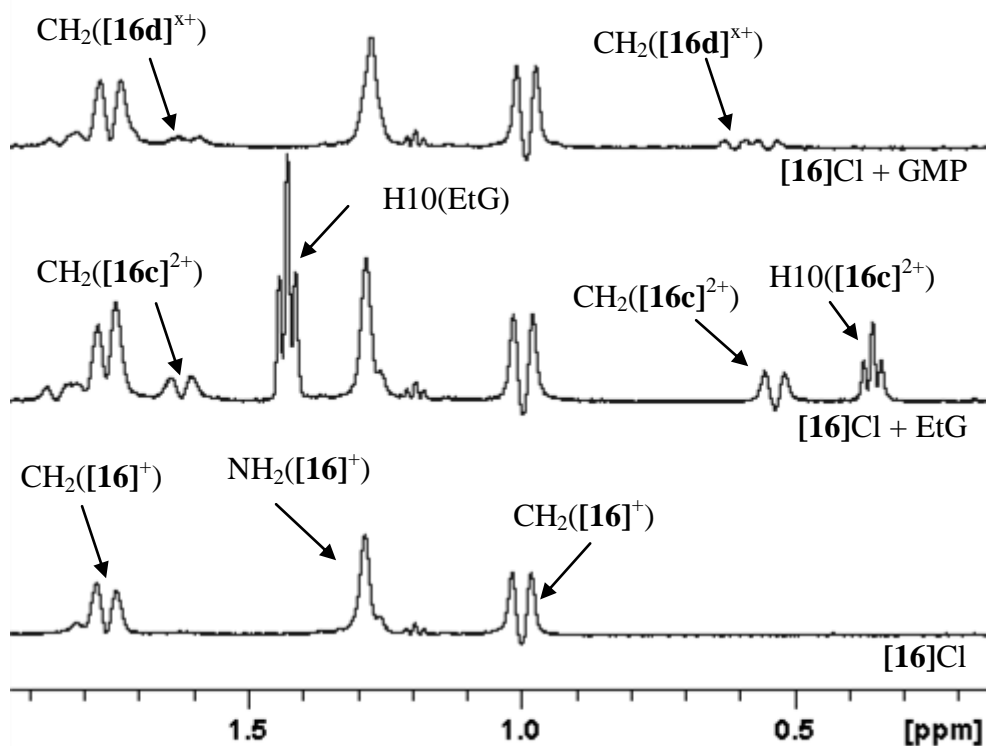


Figure 6.15: *cis*-tach CH₂ region of the ¹H NMR spectra for [16]Cl (1 mM, bottom) and the reaction of [16]Cl (1 mM) with EtG (1 mM, middle) and GMP (1 mM, top) after 24 h at 310 K.

The ³¹P{¹H} NMR spectra mirror the ¹H NMR experiments with signals corresponding to [16]⁺ and [16a]²⁺ present in both reactions (δ_P 76.2 and 74.6 ppm respectively) as well as the guanine adducts. The model guanine adduct complexes are both upfield to the aqua species at δ_P 72.9 for [16c]²⁺ and 72.6 and 71.5 ppm for [16d], where the two phosphorus nuclei are also inequivalent, as seen with the *cis*-tach protons. The ²J_{PP} coupling was unable to be observed due to weak signals.

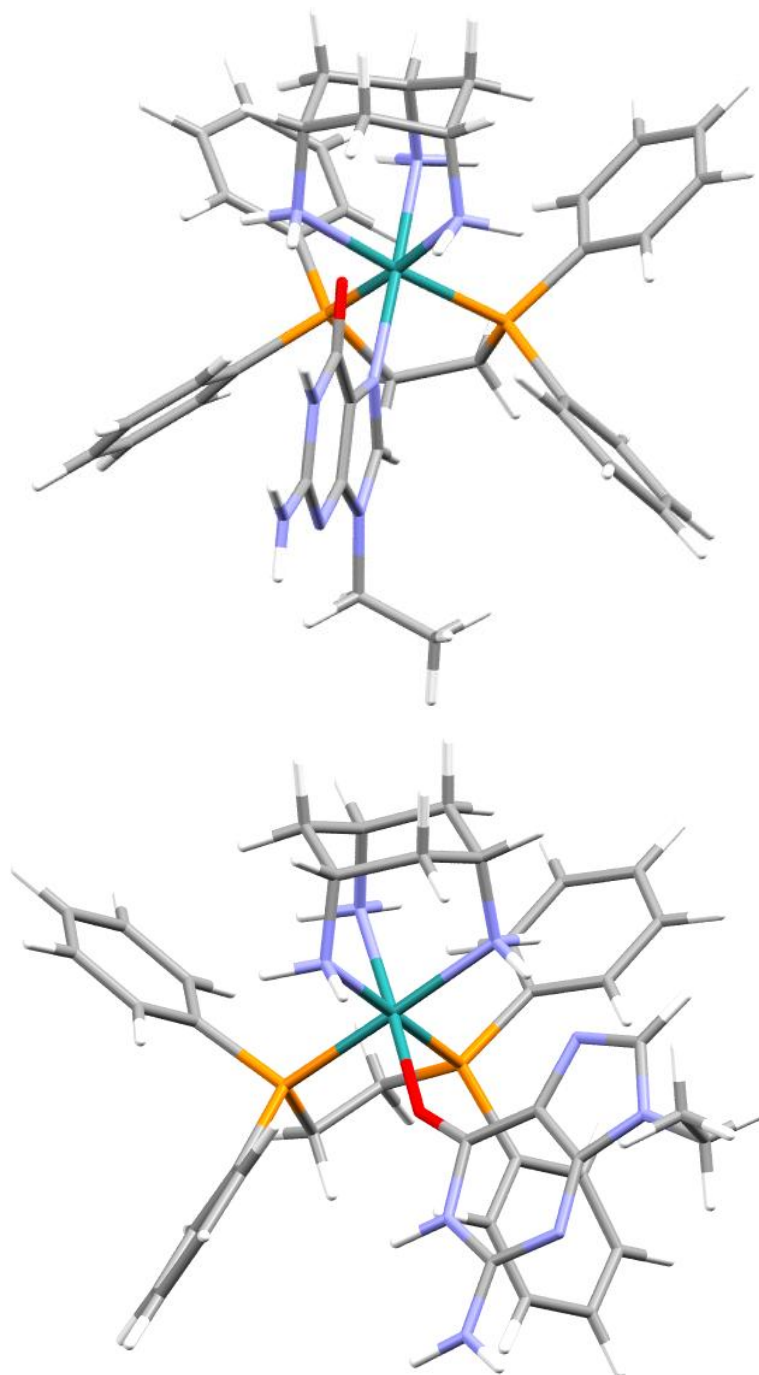


Figure 6.16: Top: Geometry optimised structure of $[\text{Ru}(\text{EtG-}N^7)(\text{dppe})(\text{cis-tach})]^{2+}$, obtained by DFT calculations. The O6 of guanine is rotated to participate in hydrogen-bond interactions with two *cis-tach* amine groups. Bottom: Geometry optimised structure of $[\text{Ru}(\text{EtG-}O^6)(\text{dppe})(\text{cis-tach})]^{2+}$, obtained by DFT calculations. The N7 is involved in a hydrogen-bond with *cis-tach*.

The large upfield shift of the H8 proton is in contrast to the observations of Sadler and co-workers, where only a comparatively small downfield shift ($+0.3 < \Delta\delta_{\text{H}}(\text{H8}) < +1.0$ ppm) was seen in the ^1H NMR of the complexes $[\text{Ru}(\eta^6\text{-arene})(\text{en})(\text{EtG-N7})]^{2+}$.⁹⁰ The chemical shift for the RAen complexes is as expected, where coordination results in a down-field shift due to electron donation from the purine ring system to the metal centre. It was initially hypothesised that the large difference in chemical shift was due to the H8 proton being rotated towards a phenyl ring from the geometrical constraints of a hydrogen-bonding interaction between the O6 and *cis*-tach.

In order to probe the 3D-structure of $[\mathbf{16c}]^{2+}$, DFT calculations on complexes $[\text{Ru}(\text{EtG-N}^7)(\text{dppe})(\textit{cis}\text{-tach})]^{2+}$ and $[\text{Ru}(\text{EtG-O}^6)(\text{dppe})(\textit{cis}\text{-tach})]^{2+}$ were performed at the (RI-)PBE0/def2-TZVPP/(RI-)BP86/SV(P)²⁹⁹ level using TURBOMOLE 5.10²⁹⁹ by Dr Jason Lynam (unpublished work, University of York, 2012). The geometry optimised structures are given in Fig. 6.16.

The energies of the two EtG-*N*⁷ complexes were compared, with the *N*7 coordination mode 14 (enthalpy) and 12 (free energy at 298 K) kJmol^{-1} lower in energy than the O6 complex. A structure was not able to be obtained for an *N*3-bound EtG complex. Although calculations were performed for the gaseous state, they agree with the postulated coordination mode of the EtG ligand in $[\mathbf{16c}]^{2+}$ in solution. The EtG-*N*7 ligand is rotated perpendicular to the *cis*-tach ligand to participate in hydrogen-bonding interactions with two amine groups of *cis*-tach and does not direct the H8 towards an adjacent phenyl ring. Therefore, the upfield shift of the H8 resonance may be due to electron back-donation from the metal to the EtG purine ring.

6.6.2 Interaction of $[\mathbf{17}]\text{Cl}$ with DNA Model Complexes

In contrast to the case of $[\mathbf{16}]\text{Cl}$, the reaction of $[\mathbf{17}]\text{Cl}$ with EtG failed to provide an observable product in the ^1H NMR spectrum after 24 h at 310 K. Therefore, it is plausible that coordination of $[\mathbf{17}]^+$ the N7 of guanine is not involved in the mechanism by which the complex inhibits proliferation. However, reaction of $[\mathbf{17}]\text{Cl}$ with GMP resulted in a small quantity of new species after 24 h, observed as a new guanine H8 resonance in the ^1H NMR spectrum (Fig. 6.17).

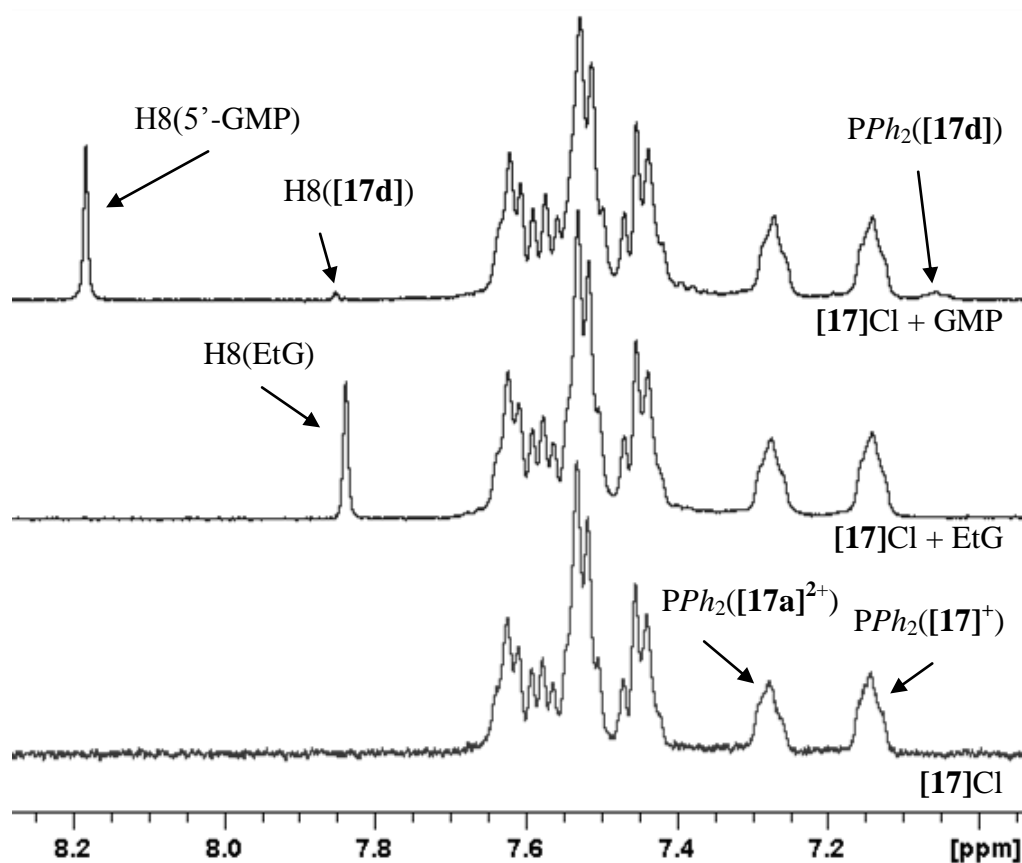


Figure 6.17: Guanine H8 and phenyl region of the ^1H NMR spectra for $[\mathbf{17}]\text{Cl}$ (1 mM, bottom) and the reaction of $[\mathbf{17}]\text{Cl}$ (1 mM) with EtG (1 mM, middle) and GMP (1 mM, top) after 24 h at 310 K.

The small upfield alteration of the chemical shift of H8 ($\Delta\delta_{\text{H}}(\text{H8}) = -0.33$ ppm) in the proposed product $[\text{Ru}(\text{GMP})(\text{dppp})(\text{cis-tach})]^{x+}$ $[\mathbf{17d}]$, would suggest a minor alteration in the environment of the H8 proton upon coordination. However, the identity of the coordination mode of the 5'-GMP cannot be determined. A $\text{PO}_4\text{-O}$ coordination mode is plausible, given that coordination was only achieved with inclusion of the phosphate-ribose group and it was observed in the aquation studies (Section 6.2.2) that phosphate is capable of coordinating to $[\mathbf{17}]\text{Cl}$. However, the possibility of an *N7*-coordination must not be overlooked, given a similar—but to a lesser extent—up-field shift of the H8 resonance on coordination. Again, this may result from close proximity to the phenyl rings of the diphosphane ligands, but with greater flexibility in the chelate ring allowing reduced geometrical constraint. The inclusion of the charged group may also assist in coordination by salt formation.

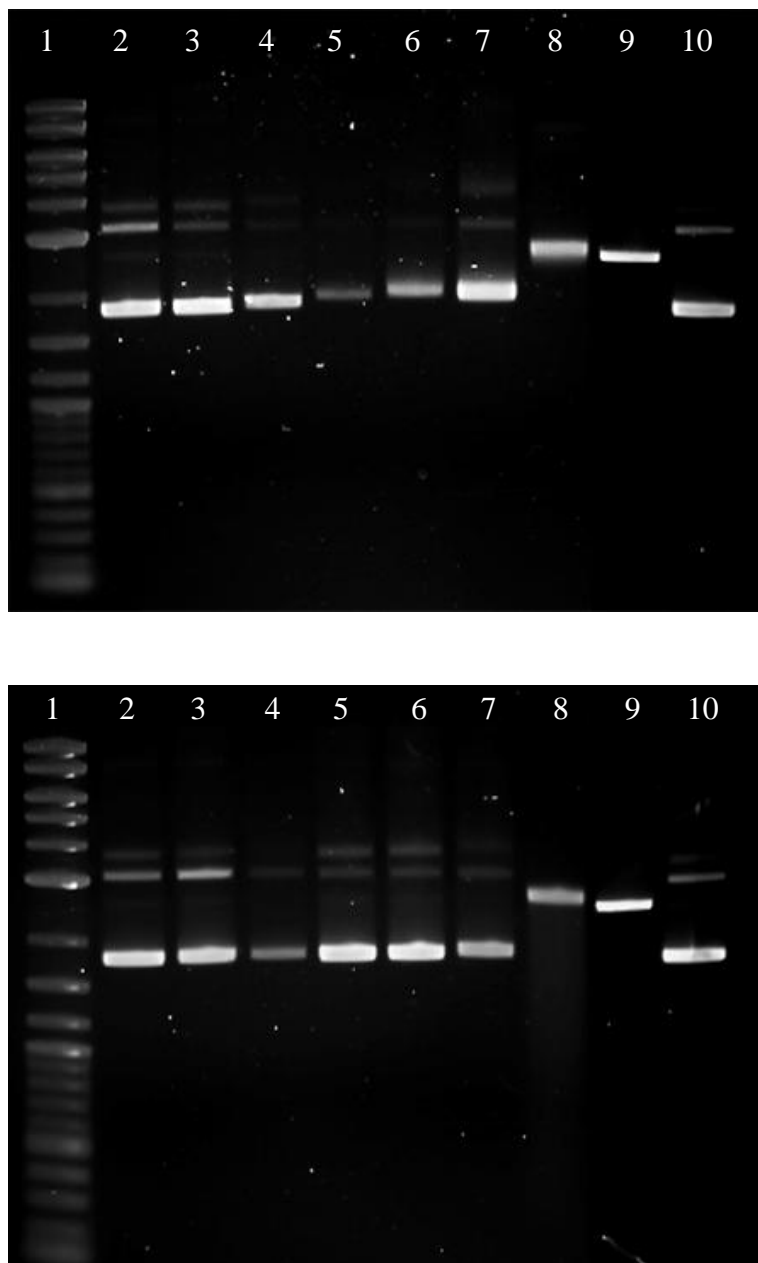


Figure 6.18: GEMSA of [16]Cl (top) and [17]Cl (bottom) with pUC18 plasmid DNA after 20 h at 37°C. Lanes: Molecular marker (1); pUC18 (2 and 10); pUC18 + [17]Cl (% bpe), 2.5 (3), 10 (4), 25 (5), 50 (6), 100 (7); pUC18 + 10% bpe cisplatin (8); pUC18 linearised by single cut with SmaI (9). bpe = base pair equivalents.

After 48 h, the reaction mixture was observed to contain multiple products in the $^{31}\text{P}\{^1\text{H}\}$ NMR spectrum, possibly from degradation of the aqua species, as discussed in Section 6.2.4. Despite an interaction, it is not of the magnitude one would expect to result in the inhibition of cell proliferation by coordination of the complex with DNA. Based on integrations from the ^1H NMR spectrum, only 10% of the aqua complex has reacted with GMP. Therefore, it is not expected that [17]Cl will significantly modify the structure of DNA.

6.6.3 Interaction of [16]Cl and [17]Cl with Plasmid DNA

The interaction of [16]Cl and [17]Cl with plasmid DNA was investigated with gel electrophoretic mobility shift assays (GEMSA), where the mobility of the open coil (OC) and super-coiled (CCC) form of plasmid DNA is altered by modifications of the tertiary structure. GEMSA experiments were performed with pUC18 plasmid DNA with varying concentrations of [16]Cl and [17]Cl and the results are shown in Fig. 6.18.

Under the conditions employed, [16]Cl alters the mobility of the OC or CCC forms of pUC18 DNA to a limited extent. Only at, and above, 25% bpe (base pair equivalents), a small shift is observed which increases with concentration of the complex. These correlate with the results from the NMR experiments, where a small degree of binding to GMP was observed. At the same concentration (10% bpe), [16]Cl does not alter the tertiary structure of DNA to the extent of which cisplatin does, where the platinated OC and CCC forms have the same mobility; this is in contrast to only a minor change to the mobility of the two plasmid forms with [16]Cl.

Across the entire concentration range used, [17]Cl does not cause any effect either in the mobility of the OC or CCC plasmid forms under the conditions employed. As with [16]Cl, this observation mirrors those from the NMR experiments with 9-ethyl guanine and guanosine monophosphate, where little interaction was observed.

From the GEMSA experiments with [16]Cl and [17]Cl, it is unclear as to whether DNA is involved in the mechanism by which these complexes inhibit proliferation.

However, it is evident that the DNA interactions of these compounds are different to cisplatin. Therefore, is it hypothesised that these complexes inhibit cell growth by an alternative mechanism, which most likely does not involve DNA.

6.6.4 Conclusions

The ruthenium(II) *cis*-tach complexes [16]Cl and [17]Cl have exhibited limited reactivity towards the DNA model compounds 9-ethyl guanine and 5'-guanosine monophosphate. A greater degree of coordination of EtG is observed with [16]Cl, with [17]Cl showing no reactivity on the mM level after 24 h at 37°C. This was mirrored in the gel electrophoresis assays with pUC18 DNA, where [17]Cl—with the greatest *in vitro* activity—did not alter the mobility of either the OC or CCC forms of the plasmid under the conditions employed. It is evident that these complexes have different reactivity with DNA than cisplatin.

Furthermore, these findings are in contrast to those of the complex [RuCl(*p*-cymene)(dppm)]PF₆, which was demonstrated to unwind supercoiled DNA,²⁶⁷ and the [RuCp(dppm)(L)]⁺ (L = 4-methyl pyridine) which is hypothesised to intercalate into DNA.²⁵⁰ The biological activity of these *cis*-tach and organometallic half-sandwich complexes cannot be attributed to the presence of a diphosphane ligand alone, as it is clear these complexes have significantly different reactivities. The possible absence of DNA in the mechanism of action of the *cis*-tach complexes is potentially advantageous by the avoidance of drug-resistance mechanisms, such as platinated-DNA repair.

However, it remains unclear if DNA is involved in the inhibition of cell growth by these complexes. A weak or dynamic binding may be present, thereby undetectable in the GEMSA experiments as dissociation could be promoted in the gel environment. Alternatively, the ruthenium–DNA interactions may have failed to alter the tertiary structure, despite successful coordination. Further investigations are required to determine the potential role of DNA in the mechanism of activity, such as circular dichromism which is able to provide information regarding the secondary structure of DNA in the presence of [16]Cl and [17]Cl.

6.7 Interaction of [16]Cl and [17]Cl with a Protein Model: Glutathione

The coordination of sulfur-containing residues to metallo-based anti-cancer compounds has often been associated with negative side effects and the development of resistance mechanisms.^{18, 109} The tripeptide glutathione (GSH) is an abundant intracellular biological nucleophile and is involved in the detoxification of cisplatin.²⁸⁵ GSH is also involved in the cleavage of ruthenium–ubiquitin bonds in RAPTA-C, resulting in detoxification.¹²⁶ However, competitive reactions of cyclic guanosine monophosphate (cGMP) and glutathione with RM175, $[\text{RuCl}(\eta^6\text{-bip})(\text{en})]^+$, showed that GSH may play an important role in the ruthenation of DNA *via* glutathione-*S* complexes.¹⁰⁸ The complex was ultimately able to bind cGMP *via* a ruthenium–GSH adduct, even in the presence of a 250 fold excess of the tripeptide. Although GSH is not required for the binding of the complex to DNA, it may act as a delivery system to protect the complex until it reaches the cell nucleus.

GSH is not only of a physiological concern to the mode of action of cytotoxic transition metal complexes, but it may also be employed as a model compound for the assessment of the interactions of [16]Cl and [17]Cl with proteins. Glutathione (Fig. 6.19) was specifically chosen for its simplicity and its inclusion of a cysteine residue. It has four potential donors for coordination to a transition metal complex in a mono-dentate fashion: the two terminal carboxylic acid groups, the amine group of glutamic acid and the thiol side chain of cysteine.

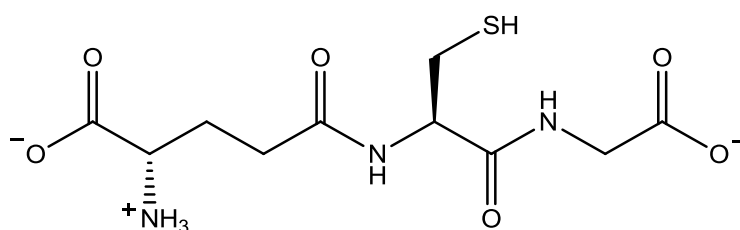


Figure 6.19: Structure of the tripeptide γ -L-Glutamyl-L-cysteinylglycine, glutathione (GSH) in aqueous solution at pH 7. GSH was employed as a simple model for the initial investigation of the ability for [16]Cl and [17]Cl to bind peptides or proteins.

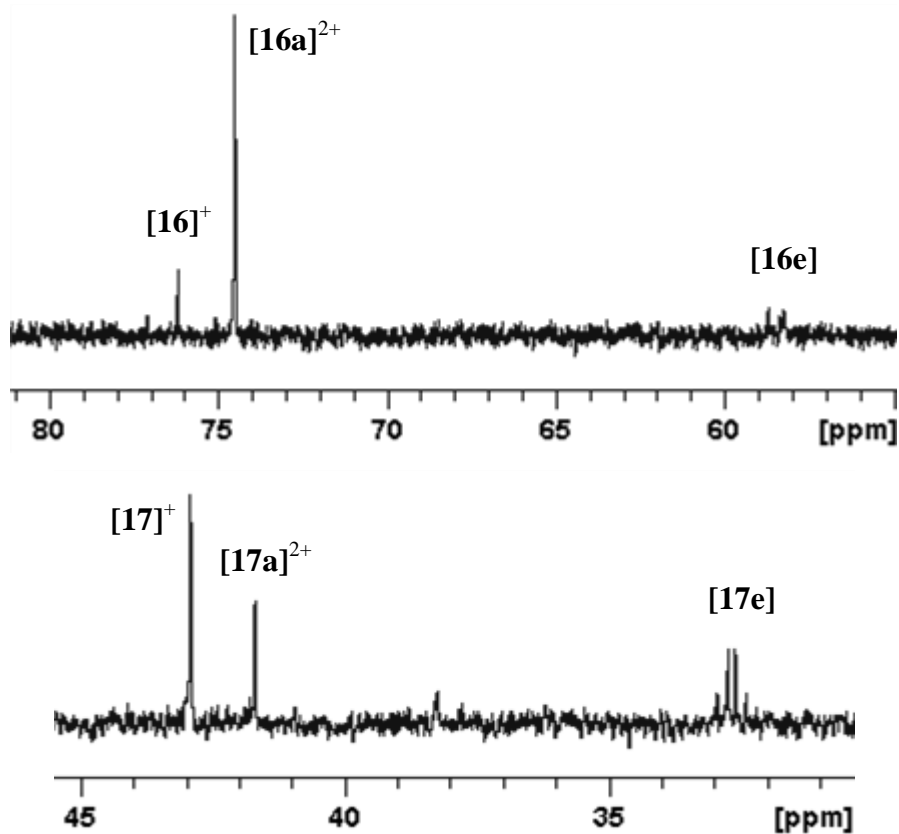


Figure 6.20: $^{31}\text{P}\{^1\text{H}\}$ NMR spectra of the reaction between GSH and $[\mathbf{16}]\text{Cl}$ (top) or $[\mathbf{17}]\text{Cl}$ (bottom).

Solutions of $[\mathbf{16}]\text{Cl}$ and $[\mathbf{17}]\text{Cl}$ (1 μM) were exposed to an equimolar amount of GSH at 310 K. After 24 h, new ruthenium(II) *cis*-tach species, $[\mathbf{16e}]$ and $[\mathbf{17e}]$, were observed in the resulting $^{31}\text{P}\{^1\text{H}\}$ NMR spectra for both compounds, shown in Fig. 6.20. The resonances for the new species were characteristic of inequivalent phosphorus nuclei from the coordination of the chiral glutathione ligand (GS) to the complex.

The extent of both reactions could not be determined by ^1H NMR spectroscopy due to a large number of overlapping resonances of the *cis*-tach and phosphane protons of the chlorido, aqua and glutathione complexes as well as those of GSH, both free and coordinated. It was also not possible to determine the coordination mode of glutathione from the ^1H NMR spectrum. It is evident that $[\mathbf{17}]^+$ may have a greater affinity than $[\mathbf{16}]^+$ for glutathione based on $^{31}\text{P}\{^1\text{H}\}$ signal intensities; competitive reactions may provide further information. Given the previously observed

preference for ruthenium(II) *cis*-tach compounds to coordinate soft donor ligands such as sulfur and phosphorus, it is hypothesised that the glutathione ligand may be coordinated *via* the *S*-donor of cysteine, [Ru(GS-*S*)(L)(*cis*-tach)] (L = dppe [16e] or dppp [17e]).

The role of glutathione coordination in the mechanism of [16]Cl or [17]Cl remains unknown, and has differing roles in the biological activity of other inorganic compounds, including the detoxification of cisplatin.^{18, 108, 126} It could suggest that a plausible biomolecular target for these compounds may be that of a protein *via* the thiol of a cysteine residue in a protein, possibly inhibiting its function. The role of ruthenium-protein interactions should be considered for future experiments to determine the mechanism of action for the *cis*-tach ruthenium(II) complexes.

6.8 Chapter Conclusions

The highly active cytotoxic complexes [16]Cl and [17]Cl have been demonstrated by NMR spectroscopy and mass spectrometry to aquate when in aqueous solution. It is proposed—as in the case of cisplatin and other cytotoxic ruthenium(II) chlorido complexes—that this reaction is the initial activation step in the mechanism by which these species inhibit tumour cell growth. The resulting aqua complexes [16a]Cl and [17a]Cl were characterised by NMR spectroscopy by the preparation of the triflate salts; these complexes exist in the protonated aqua form at physiological pH with hydrolysis unable to occur. Both of these species were stable at physiologically-relevant concentrations, with [16]Cl stable to degradation over 72 h in aqueous solution, whilst [17]Cl showed only a small degree of degradation over the time period used for the MTT assays.

The kinetics of aquation and anation of [16]Cl were studied; the rate of the forward reaction is over five times faster than cisplatin and the established RAen complexes. Initial analysis of the ligand exchange kinetics with [17]Cl showed the reaction had reached equilibrium within thirty seconds at 310 K and it is therefore proposed that the kinetics of aquation is not a major influence in the *in vitro* activity of these complexes.

To understand speciation under physiologically-relevant conditions further experimental work was conducted. It is proposed that a greater proportion of the aqua species $[16a]^{2+}$ will be observed in the blood than other ruthenium complexes and cisplatin, indicating activation before the complex has entered the cell. The combination of aquation and hydrolysis equilibria for $[17]^+$ result in a greater contrast between the speciation in the blood and the cell nucleus than that observed for cisplatin and the RAen complexes, with a suitable balance between activation of the complex and deactivation before it has reached its target.

NMR experiments have shown that EtG does not coordinate to $[17]^+$ or $[17a]^+$ under physiologically-relevant conditions, therefore suggesting that the *N7* of guanine is not involved in the mechanism of action. Furthermore, the complexes $[17]Cl$ and $[18]Cl$ did not alter the mobility of plasmid DNA, suggesting that the tertiary structure of DNA is unaffected by this complex, unlike half-sandwich organometallic analogues. Further studies showed that these complexes do have an affinity to glutathione; therefore proteins may be involved in the mechanism of anti-proliferative activity.

The experimental evidence obtained for the complexes presented here suggest their activity originates from a different mechanism to cisplatin and the RAen complexes. Further investigations are required to identify biomolecules which may be involved in the mode of action and if nucleic acids, proteins, enzymes or other biomolecules are responsible for the potency of the ruthenium *cis*-tach complexes presented in this thesis.

Chapter 7. Conclusions and Future Work

7.1 Thesis Conclusions

This thesis was set out to achieve three key aims: to establish the preparation of ruthenium(II) *cis*-tach complexes; to develop a general-purpose precursor complex, allowing the synthesis of a wide range of compounds; and finally to evaluate these compounds for their *in vitro* activity in the inhibition of tumour cell growth.

The first preparation of ruthenium(II) *cis*-tach complexes was achieved by the reaction of the ligand with $[\text{RuCl}_2(\text{PPh}_3)_3]$ in DCM, rapidly forming the cationic complex $[\text{RuCl}(\textit{cis}\text{-tach})(\text{PPh}_3)_2]\text{Cl}$ [**1**] Cl . Charge neutralisation occurs much slower, affording $[\text{RuCl}_2(\textit{cis}\text{-tach})(\text{PPh}_3)_2]$ [**2**]. Solvent complexes were prepared, but these complexes provided limited scope in the design of new complexes, with displacement of the triphenylphosphane ligand difficult. The DMSO complex $[\text{RuCl}(\text{DMSO-}S)(\textit{cis}\text{-tach})(\text{PPh}_3)]\text{Cl}$ [**4**] Cl proved weakly cytotoxic against the A549 and A2780 cell lines.

Reaction of $[\textit{cis}\text{-RuCl}_2(\text{DMSO})_4]$ with *cis*-tach in DMSO at elevated temperatures yielded the solvent complex $[\text{RuCl}(\text{DMSO-}S)_2(\textit{cis}\text{-tach})]\text{Cl}$ [**8**] Cl . This complex was able to be employed as a precursor to complexes containing N–N and P–P chelating ligands. Complexes of type $[\text{Ru}(\text{DMSO-}S)(\text{N-N})(\textit{cis}\text{-tach})](\text{Cl})_2$ were obtained by reaction of [**8**] Cl with bipy, phen and en. The DMSO ligand in these complexes is inert to substitution by water, but the DMSO ligand was shown to exchange with guanine to a limited extent. This complex was inactive against the A549 cell line, hypothesised to be due to poor hydrophobicity, possibly reducing cellular uptake and poor reactivity of the ruthenium-DMSO bond.

Reaction of P–P chelating ligands with [**8**] Cl afforded chlorido complexes with the formula $[\text{RuCl}(\text{P-P})(\textit{cis}\text{-tach})]\text{Cl}$. All complexes were isolated with analytical purity as the chloride salt, with good water solubility. These compounds displayed good to excellent *in vitro* cytotoxicity, with two complexes (P–P = dppp [**17**] Cl and dppb [**18**] Cl) twice as active as the clinical drug cisplatin in A549 and equipotent in

A2780. The inclusion of a reactive chlorido ligand and improved lipophilicity from the phosphane ligands is proposed to account for the improved activity compared to the N–N chelates.

The aqueous chemistry of two diphosphane complexes, [16]Cl and [17]Cl (P–P = dppe and dppp) was investigated, selected for the high water solubility and excellent *in vitro* activity respectively. Both complexes aquate extremely rapidly with $t_{1/2} = 106$ and 10.8 s, respectively at 298 K yielding the corresponding aqua species; therefore the rate of aquation is considered to be insignificant in comparison to the cell cycle. It is hypothesised that the aqua species is responsible for reacting with biomolecules, with the chlorido complex inactive. Deprotonation of the aqua ligand is inaccessible under physiological conditions, resulting in exclusively the aqua product. A key difference between these two species is the extent of aquation in the plasma, cytoplasm and nucleus, where [16]Cl aquates to a greater extent than [17]Cl. This may result in decreased deactivation of [17]Cl by protection as the chlorido complex, providing a rationale for the increased antiproliferative activity.

Studies with DNA model compounds revealed the poor affinity for these complexes with guanine. Of the two complexes studied, [17]Cl displayed the least binding to guanine, in contrast with the *in vitro* activities. The same observations were made with mobility shift assays, where [17]Cl did not inhibit the mobility of plasmid DNA, with [16]Cl only affecting it to a small extent. Therefore, it is hypothesised that DNA is not the target for these complexes in their anti tumour activity and is by a novel mechanism. The lack of evidence for strong interactions with DNA is in contrast with many ruthenium(II) half-sandwich complexes which aquate, where many highly active compounds (including RAen and RAPTA) have been shown to bind DNA. Initial studies with glutathione suggested that ruthenium-protein interactions should not be overlooked, and may form the basis of future studies.

This thesis has described the use of *cis*-tach as a new *facially*-coordinating ligand for water-soluble ruthenium(II) half-sandwich type compounds. A series of complexes based on this ligand have been prepared, with several complexes highly active in the inhibition of tumour cell growth and are believed to act by a novel non-classical

mechanism. The ruthenium(II) *cis*-tach complexes presented in this thesis are highly promising and exciting, certainly warranting further investigations.

7.2 Future Work

The potential scope for the development and further study of ruthenium(II) *cis*-tach compounds is extensive. Structure-activity relationships may be continued to further explore possible new cytotoxic complexes, exploring new chelating ligands, tethering to other anti-tumour complexes or biologically active ligands, or the development of multinuclear complexes. Complexes with phosphane ligands have shown exciting activity and properties, where further variation of these ligands should logically form the core of further studies. A phosphane of particular interest is *S,S*- and *R,R*-chiraphos (Fig. 7.1), where their possibly differing reactivity with biomolecules and *in vitro* activities may provide clues to the mechanism of action.

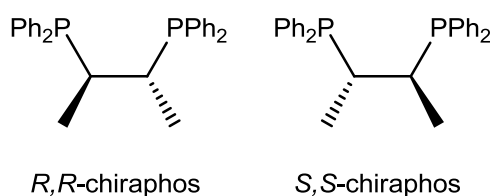


Figure 7.1: Structure of *R,R*- and *S,S*-chiraphos, chiral phosphanes based on dppe.

The complexes presented in this thesis have only been screened against two selected cell lines by *in vitro* technique. This study should not only be expanded to other tumour types, but to drug-resistant variants such as A2780cis and A2780^{AD}. This will provide further information in the mode of the ruthenium *cis*-tach complexes, whereby similar mechanisms of action can be identified. Screening against a large range of cell lines is required before these complexes can be considered for *in vivo* experiments. Other *in vitro* studies may include apoptosis assays/determination.

Finally, this thesis began to look at what happens to the *cis*-tach diphosphane complexes when introduced to cell, although little is known on the cellular uptake or interactions with biomolecules. Such experiments to expand understanding would include determination of the partition coefficient, $\log P$ and investigations into *in*

vitro cellular uptake. Finally, the mechanism by which these complexes disrupt the cell cycle remains unknown, therefore the attention of future experiments must be directed towards the interactions with biomolecules. Further DNA binding studies are required—for example circular dichroism to investigate the alteration of DNA secondary structure by these complexes—before DNA can be excluded as a target, as well as investigating the interactions with other biomolecules, such as proteins.

Computational methods, such as density functional theory (DFT) and molecular dynamics (MD) may also be employed to probe the interaction of ruthenium(II) *cis*-*tach* complexes with biomolecules. Such studies include assessing the DNA bases and amino acids, which may feature side-chains with carboxylate, amine, hydroxyl and imidazole groups which are capable of coordinating to a metal.

Chapter 8. Experimental

8.1 General

All chemicals used were purchased from Sigma-Aldrich UK and solvents from Fisher Scientific, with the exception of *cis-cis*-1,3,5-Cyclohexanetricarboxylic acid (TCI UK) ruthenium trichloride hydrate (Precious Metals Online), methylenebis(diphenylphosphane) (Acros Organics), propane-1,3-diylbis(diphenylphosphane) (Strem Chemicals) and butane-1,4-diylbis(diphenylphosphane) (Lancaster Synthesis). *Cis,cis*-1,3,5-triaminocyclohexane (*cis*-tach),^{167, 168} dichloridotris(triphenylphosphane)ruthenium(II)¹⁹⁵, dichlorido[*fac*-tris(dimethylsulfoxide- κ S)](dimethylsulfoxide- κ O)ruthenium(II)²⁸⁶ and *mer*-chloro-trisacetonitrile(η^4 -cycloocta-1,5-diene)ruthenium(II) hexafluorophosphate²⁸⁷ were prepared according to literature procedures. Di- μ -chloro(η^4 -1,5-cyclooctadiene)ruthenium(II) was synthesised by the Lynam research group according to the literature procedure²⁸⁷.

NMR spectra were obtained using either a Jeol ECS 400, Jeol EXC 400 (^1H 399.78 MHz, ^{31}P 161.83, ^{13}C 100.52) at 293 K or a Bruker Avance 500 spectrometer (^1H 500.23 MHz, ^{31}P 202.50, ^{13}C 125.78) at 295 K. ^{31}P and ^{13}C spectra were recorded with proton decoupling. The CD_2Cl_2 used for NMR experiments was dried over CaH_2 and degassed with three freeze-pump-thaw cycles. All other solvents were used as received. IR spectra were recorded on a Unicam (Research Series) FTIR using SensIR Technologies ATR equipment. High resolution mass spectrometry was performed by the University of York mass spectrometry service using the ESI technique on a Bruker Daltonic microTOF instrument. Elemental analyses (CHN) were performed using an Exeter Analytical Inc. CE-440 analyser. Residual solvent in analyses were confirmed by ^1H NMR spectroscopy in anhydrous solvent (CD_2Cl_2). Specific experimental details for each chapter can be found at the beginning of each corresponding section. pH measurements were recorded using a MeterLab ION 450 calibrated with Aldrich standard solutions of pH 4, 7 and 10. For NMR samples in 10% D_2O /90% H_2O , no correction was applied for the effect of deuterium on the glass electrode.

8.1.1 X-Ray Crystallography

All data collection and structural solutions were obtained by Dr Adrian Whitwood and Dr Robert Thatcher (University of York Crystallography service) and Dr Jason Lynam.

8.1.1.1 Bruker Smart Apex

Diffraction data were collected at 110 (2) K on a Bruker Smart Apex diffractometer with Mo-K α radiation ($\lambda = 0.71073 \text{ \AA}$) using a SMART CCD camera. Diffractometer control, data collection and initial unit cell determination was performed using SMART.²⁹² Frame integration and unit-cell refinement was carried out with SAINT+.²⁹³ Absorption corrections were applied by SADABS.²⁹⁴ Structures were solved by direct methods using SHELXS-97 (Sheldrick, 1997)²⁹⁴ and refined by full-matrix least squares using SHELXL-97 (Sheldrick, 1997).²⁹⁴ All non-hydrogen atoms were refined anisotropically. Hydrogen atoms were placed using a “riding model” and included in the refinement at calculated positions.

8.1.1.2 Oxford Diffraction SuperNova

Diffraction data were collected at 110.0 K on an Oxford Diffraction SuperNova diffractometer with Mo-K α radiation ($\lambda = 0.71073 \text{ \AA}$) using an EOS CCD camera. The crystal was cooled with an Oxford Instruments Cryojet. Diffractometer control, data collection, initial unit cell determination, frame integration and unit-cell refinement was carried out with CrysAlis.²⁹⁵ Face-indexed absorption corrections were applied using spherical harmonics, implemented in SCALE3 ABSPACK scaling algorithm.²⁹⁶ OLEX2²⁹⁷ was used for overall structure solution, refinement and preparation of computer graphics and publication data. Within OLEX2, the algorithms used for structure solution were direct methods using the XS (Sheldrick, 2008).²⁹⁴ Refinement by full-matrix least-squares used the SHELXL-97²⁹⁸ algorithm within OLEX2.²⁹⁷ All non-hydrogen atoms were refined anisotropically. Hydrogen atoms were placed using a “riding model” and included in the refinement at calculated positions.

8.1.2 *In Vitro* Biological Evaluation

The A549 cell line was kindly donated by The Bioscience Technology Facility, Department of Biology, University of York. The A2780 cell line was purchased from the ECACC. Cell cultures were maintained in a 90% humidified atmosphere of CO₂ at 37°C, in DMEM (A549) or RPMI 1640 (A2780) medium supplemented with 2 mM glutamine and 10% Foetal Bovine Serum. Sub-confluent cultures (70-80%) were split at a seeding of 1:3 to 1:6 using 0.25% Trypsin/EDTA. Culture medium and FBS were obtained from Invitrogen/Gibco and all other materials from Sigma.

Growth inhibition assays were performed using the MTT (3-(4,5-Dimethylthiazol-2-yl)-2,5-diphenyltetrazolium bromide) assay, with a modified procedure of Carmichael *et al.*²²⁸ Suitable seeding density of cells was determined prior to experiments to ensure logarithmic phase of growth and prevention of over-confluent culture at the end of the assay, and that optical density of the metabolised MTT formazan measured was within the linearity limits of the plate reader.

Cells were seeded at a density of 1,000 (A549) or 2,500 (A2780) cells per well in 100 µL of their respective culture medium in a 96 well plate, with positive (columns 1 and 11) and negative (columns 2 and 12) controls located at each end of the plate. Positive controls consisted of culture medium with no cells, representative of 100% inhibition of MTT metabolism, and negative controls consisted of untreated cells, representative of 0% inhibition. Cells were allowed to adhere to the plate surface by incubating for 24 h before addition of compound to be tested. 100 µL of culture medium was added to each control well, and 100 µL of a 2x solution of the compound to be tested in culture medium to the remaining wells. A total of eight concentrations were tested, performed in octuplicate and typically between 300 µM and 0.1 µM, with the eight concentrations selected to fall on the dose-response curve for the compound.

The cells were incubated with the drug for 72 h before addition of MTT (50 µL, 2 mg/mL) in PBS and incubated for a further 2 h, over which MTT was metabolized to insoluble formazan crystals. The plates were centrifuged at 500 g for 10 minutes and 220 µL of the culture medium in each well was removed. The formazan was

solubilised by addition of DMSO (150 μ L). The plate was shaken to ensure complete dissolution of the formazan, and absorbance at 540 nm recorded using a Hidex Plate Chameleon V plate reader. The value for each concentration of drug was plotted graphically as a percentage of the negative control compared to the positive. The data was fitted using a dose-response function and the concentration of drug to cause 50% reduction of the absorbance (compared to control values) was calculated as the IC₅₀ value. Statistical calculations were performed using Origin v8.5. IC₅₀ values were calculated as the average of three independent experiments as the weighted mean.

8.1.3 ¹H and ¹³C{¹H} NMR Assignments

The resonances in ¹H and ¹³C{¹H} NMR spectra are assigned using a code scheme. The schemes used are given in Figs 9.1 to 9.4.

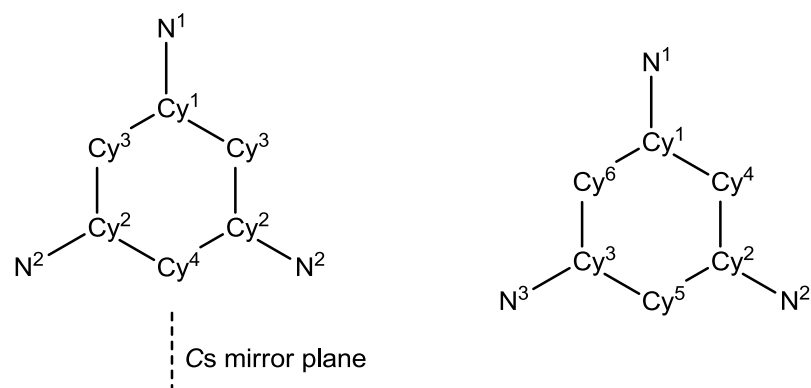


Figure 8.1: *cis*-tach ¹H and ¹³C{¹H} NMR assignments for C_s (left) and C₁ (right) symmetry environments used in characterisation.

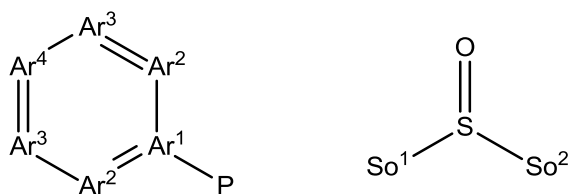


Figure 8.2: Triphenylphosphane and asymmetrical-DMSO-S ^1H and $^{13}\text{C}\{^1\text{H}\}$ NMR assignments used in characterisation. Triphenylphosphane assignments apply to all three phenyl rings of the phosphane.

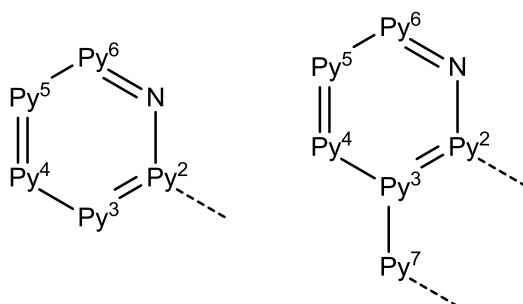


Figure 8.3: 2,2'-bipyridyl and 1,10-phenanthroline ^1H and $^{13}\text{C}\{^1\text{H}\}$ NMR assignments used in characterisation.

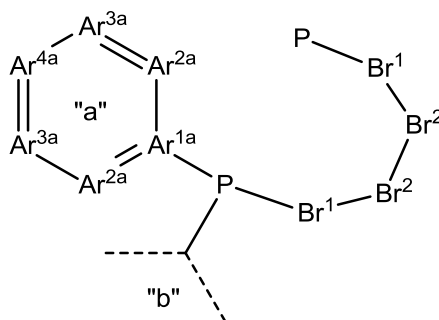


Figure 8.4: Diphospane ^1H and $^{13}\text{C}\{^1\text{H}\}$ NMR assignments used in characterisation. The bridging alkyl chain is numbered Br^n , where n = number of bonds to nearest phosphorus. The dppb ligand is used as an example. Of the two phenyl ring environments as shown, “a” and “b” correlate between ^1H and $^{13}\text{C}\{^1\text{H}\}$ NMR spectra.

8.1.4 Synthesis of *cis*-tach

8.1.4.1 *cis,cis*-1,3,5-Cyclohexanetrakis(benzyl carbamate)

The literature procedure was followed.¹⁶⁷ Triethylamine (9.65 g, 69.5 mmol) and diphenylphosphorlyazide (15 ml, 69.5 mmol) were added to a mixture of *cis-cis*-1,3,5-cyclohexanetricarboxylic acid (5 g, 23.2 mmol) and benzene (125 ml). The suspension was refluxed until all solid had dissolved. Benzyl alcohol (7.2 ml, 69.5 mmol) was added to the solution, and was heated under reflux for 16 h. The cream precipitate was collected by vacuum filtration. The filtrate was washed with small amounts of chilled diethyl ether and dried *in vacuo*. Yield: 6.43 g (51%, 11.7 mmol). ¹H NMR ((CD₃)₂SO, 399.8 MHz, 293K): δ 7.35 (m, 15H, Ar-*H*), 5.01 (s, 6H, -CO₂CH₂Ph), 3.36 (m, 3H, CR₂*H*), 1.89 (d, ³J_{HH} = 12.3 Hz, 3H, CH(*H*_{eq})), 1.07 (q, ³J_{HH} = 12.3 Hz, ²J_{HH} = 12.3, 3H, CH(*H*_{ax})).

8.1.4.2 *Cis,cis*-1,3,5-triaminocyclohexane trihydrobromide

The literature procedure was followed.¹⁶⁷ Hydrogen bromide (50 ml of 30% by weight in acetic acid) was added to *cis,cis*-1,3,5-cyclohexanetrakis(benzyl carbamate) (3.46 g, 7.07 mmol) and stirred for 16 h. Ethanol (100 ml) was added and stirred for 24 h. The precipitate was isolated by filtration, washed with small amounts of chilled ethanol and dried *in vacuo*. Yield: 1.90 g (72.3%, 5.11 mmol of *cis*-tach.3HBr). ¹H NMR (D₂O, 399.8 MHz, 293K): δ 3.51 (tt, ³J_{HH} = 11.7 Hz, ³J_{HH} = 3.7, 3H, CR₂*H*), 2.46 (dt, ²J_{HH} = 11.7 Hz, ³J_{HH} = 3.7, 3H, CH(*H*_{eq})), 1.65 (q, ³J_{HH} = 11.7 Hz, ²J_{HH} = 11.7, 3H, CH(*H*_{ax})).

8.1.4.3 *Cis,cis*-1,3,5-triaminocyclohexane (*cis*-tach)

The literature procedure was followed.¹⁶⁸ *Cis,cis*-1,3,5-triaminocyclohexane trihydrobromide (1.00 g, 2.68 mmol) was dissolved in the minimum amount of water and loaded on to a Dowex 1X4-50 (300 g) anion exchange column, which was pre-rinsed with water, hydrochloric acid (1 M), sodium hydroxide (1 M) and finally water until washings were neutral. The basic fractions were collected and the solvent removed by rotary evaporation. The solid was sublimed at 10⁻² mbar at 70

°C onto a cold finger at 77 K. Yield: 0.295 g (85.1%, 2.28 mmol of *cis*-tach). ^1H NMR (CD_2Cl_2 , 500.2 MHz, 295K): δ 2.67 (tt, $J = 11.3, 3.9$ Hz, 3H, CHNH_2) 1.89 (dm, $J = 11.8$ Hz, 3H, CH_{ax}H) 1.04 (s, 6H, NH_2) 0.76 (q, $J = 11.6$, 3H, CHH_{eq}); $^{13}\text{C}\{^1\text{H}\}$ NMR (CD_2Cl_2 , 125.8 MHz, 295K): δ 48.5 (s, CHNH_2) 47.5 (s, CH_2).

8.2 Chapter 2 Experimental

All reactions were performed under an atmosphere of dry nitrogen using standard Schlenk line and glove box techniques. Dichloromethane, acetonitrile and pentane were purified with an Innovative Technologies anhydrous solvent engineering system. Diethyl ether was dried over sodium, and d_2 -dichloromethane over calcium hydride and vacuum transferred prior to use. All other chemicals were purchased from Sigma-Aldrich UK.

8.2.1 Reaction of $[\text{RuCl}_2(\text{PPh}_3)]$ with *cis*-tach.

cis-cis-1,3,5-triaminocyclohexane (3 mg, 0.023 mmol) was added to a CD_2Cl_2 solution of dichlorido^1\text{H} and ^{31}P NMR spectra were recorded. The NMR features observed were similar to those reported for $[\mathbf{1}]\text{PF}_6$. After standing for one week, the NMR features were similar to those reported for $[\mathbf{2}]$. In both cases, a resonance for additional triphenylphosphane was observed.

8.2.2 $[\text{RuCl}(\text{PPh}_3)_2(\textit{cis}\text{-tach})]\text{PF}_6$, $[\mathbf{1}]\text{PF}_6$

cis-cis-1,3,5-triaminocyclohexane (13 mg, 0.1 mmol) was added to a Schlenk tube charged with dichlorido

pentane into a dichloromethane solution. [1]PF₆ was unable to be isolated pure as a solid. ¹H NMR (CD₂Cl₂, 399.8 MHz, 293 K) δ 7.43 (*app. t*, ²J_{HP} = 10 Hz, ³J_{HH} = 7.5 Hz, ⁴J_{HH} = 1.5 Hz, 12H, PPh₃, Ar²), 7.37 (m, 6H, PPh₃, Ar⁴), 7.25 (tt, ³J_{HH} = 7.6 Hz, ⁴J_{HH} = 1.5 Hz, 12H, PPh₃, Ar³), 3.57 (d, ²J_{HH} = 11.8 Hz, 2H, NH₂, N²), 3.44 (d, ²J_{HH} = 11.8 Hz, 2H, NH₂, N²), 3.27 (s, 2H, CH, Cy²), 2.96 (s, 1H, CH, Cy¹), 2.15 (s, 2H, NH₂, N¹), 1.97 (d, ²J_{HH} = 15.7 Hz, 1H, CH₂, Cy⁴), 1.91 (d, ²J_{HH} = 15.7 Hz, 1H, CH₂, Cy⁴), 1.77 (d, ²J_{HH} = 15.0 Hz, 2H, CH₂, Cy³), 1.42 (d, ²J_{HH} = 15.0 Hz, 2H, CH₂, Cy³); ³¹P{¹H} NMR (CD₂Cl₂, 161.8 MHz, 293 K) δ 47.3 (s, 2P, PPh₃) -144.67 (septet, ¹J_{PF} = 710.5 0Hz, 1P, PF₆); ¹³C{¹H} NMR (CD₂Cl₂, 100.5 MHz, 293 K) δ 134.5 (t, |²J_{PC} + ⁴J_{PC}| = 9.5 Hz, PPh₃, Ar²), 133.1 (t, |¹J_{PC} + ³J_{PC}| = 37.0 Hz, PPh₃, Ar¹), 130.7 (s, PPh₃, Ar⁴), 129.3 (t, |³J_{PC} + ⁵J_{PC}| = 8.8 Hz, PPh₃, Ar³), 43.0 (s, CH, Cy²), 42.8 (s, CH, Cy¹), 35.0 (s, CH₂, Cy⁴), 33.3 (s, CH₂, Cy³). **ESI-MS:** *m/z* 941.2051 ([1-Cl+NCMe+PF₆]⁺, Calc. for C₄₄H₄₈F₆N₄P₃Ru⁺: 941.2039, 10%), 790.1826 ([1]⁺, C₄₂H₄₅ClN₃P₂Ru⁺: 790.1815, 100). Crystals suitable for X-ray diffraction analysis were obtained by the slow diffusion of n-pentane into a saturated dichloromethane solution of [1]PF₆.

8.2.3 [RuCl₂(PPh₃)(*cis-tach*)], [2]

cis-cis-1,3,5-triaminocyclohexane (30.0 mg, 0.232 mmol) was added to an ampoule charged with dichloridotris(triphenylphosphane)ruthenium(II) (196 mg, 0.204 mmol) dissolved in dichloromethane (20 mL), causing an instant colour change from black to orange. The solution was stirred at 50 °C for 4 days in the sealed vessel, during which time the solution changed colour to yellow and a white precipitate formed. The precipitate was removed by filtration and the filtrate reduced in volume to approximately 1 mL *in vacuo*. The product was precipitated by addition of pentane (20 mL) as an orange powder, and washed twice with pentane (20 mL). Yield: 115 mg (87%, 0.177 mmol of [RuCl₂(*cis-tach*)(PPh₃)]·CH₂Cl₂). Found: C 46.25; H 4.92; N 6.43%. Calcd for C₂₄H₃₀Cl₂N₃PRu(CH₂Cl₂): C 46.31; H 4.97; N 6.48%. ¹H NMR (CD₂Cl₂, 399.8 MHz, 293 K) δ 7.85 (*app t*, ³J_{HH} = 7.5 Hz, ²J_{HP} = 5.8 Hz, ⁴J_{HH} = 1.5 Hz, 6H, PPh₃, Ar²), 7.36 (m, 9H, PPh₃, Ar³ + Ar⁴), 4.77 (s, 2H, NH₂, N¹), 3.90 (bs, 1H, CH, Cy¹), 2.92 (s, 2H, CH, Cy²), 2.65 (d, ²J_{HH} = 10.6 Hz, 2H, NH₂, N²), 1.92 (s, 4H, CH₂, Cy³), 1.85 (d, ²J_{HH} = 10.6 Hz, 2H, NH₂, N²), 1.62 (d, ²J_{HH} = 15.3 Hz, 1H, CH₂, Cy⁴), 1.00 (d, ²J_{HH} = 15.3 Hz, 1H, CH₂, Cy⁴); ³¹P{¹H} NMR (CD₂Cl₂,

161.8 MHz, 293 K) δ 66.0 (s, 1P, *PPh*₃); ¹³C{¹H} NMR (CD₂Cl₂, 100.5 MHz, 293 K) δ 136.2 (d, ¹J_{PC} = 36.0 Hz, *PPh*₃, Ar¹), 134.2 (d, ²J_{PC} = 10.1 Hz, *PPh*₃, Ar²), 129.5 (d, ⁴J_{PC} = 1.9 Hz, *PPh*₃, Ar⁴), 128.8 (d, ³J_{PC} = 8.7 Hz, *PPh*₃, Ar³), 44.0 (s, CH, Cy¹), 43.8 (s, CH, Cy²), 35.0 (s, CH₂, Cy³), 33.6 (s, CH₂, Cy⁴). **ESI-MS**: *m/z* 569.1186 ([**2**-Cl+NCMe]⁺, Calc for C₂₆H₃₃ClN₄PRu⁺: 569.1173, 100%), 528.0919 ([**2**-Cl]⁺, C₂₄H₃₀ClN₃PRu⁺: 528.0907, 25), 246.5607 ([**2**-2Cl]²⁺, C₂₄H₃₀N₃PRu²⁺: 246.5608, 10). **ATR-IR** (cm⁻¹): 3462, 3283, 3240, 3050, 2888, 1649, 1588, 1480, 1432 (P-Ph), 1367, 1346, 1270, 1211, 1183, 1156, 1089, 1027, 968, 905. Crystals suitable for X-ray diffraction analysis were obtained by the slow diffusion of diethylether into a saturated dichloromethane solution of [**2**].

8.2.4 [{RuCl(*cis*-tach)}₂(μ -Cl)]BPh₄, [**3**]BPh₄

Sodium tetraphenylborate (44.2 mg, 0.129 mmol) was added to a solution of [**2**].CH₂Cl₂ (65.5 mg, 0.101 mmol) in dichloromethane (20 mL) and allowed to stir for 6 h. The precipitate was removed by filtration and the product crystallised by slow diffusion of pentane (100 mL). The crystals were isolated by filtration and dried *in vacuo*. Yield: 43.2 mg (56%, 0.014 mmol of [{RuCl(*cis*-tach)(*PPh*₃)₂(μ -Cl)]BPh₄.1½CH₂Cl₂). Found: C 57.72; H 5.51; N 5.38%. Calcd for C₇₂H₈₀BCl₃N₆P₂Ru₂(1½ CH₂Cl₂): C 57.40; H 5.43; N 5.46%. ¹H NMR (CD₂Cl₂, 399.8 MHz, 293 K) δ 7.70 (m, 12H, *PPh*₃), 7.29 (m, 26H, *PPh*₃, BPh₄), 7.00 (m, 8H, BPh₄), 6.85 (m, 4H, BPh₄), 6.73 (d, ²J_{HH} = 10.5 Hz, 2H, NH₂, N¹), 4.24 (d, ²J_{HH} = 10.5 Hz, 2H, NH₂, N¹), 3.93 (m, 2H, CH, Cy¹), 2.90 (s, 2H, CH, Cy²), 2.67 (d, ²J_{HH} = 11.6 Hz, 2H, NH₂, N²), 2.62 (s, 2H, CH, Cy³), 2.39 (d, ²J_{HH} = 11.6 Hz, 2H, NH₂, N²), 1.96 (m, 8H, CH₂, Cy⁴ + Cy⁶), 1.87 (d, ²J_{HH} = 10.7 Hz, 2H, NH₂, N³), 1.52 (d, ²J_{HH} = 15.8 Hz, 2H, CH₂, Cy⁵), 0.80 (d, ²J_{HH} = 10.7 Hz, 2H, NH₂, N³), 0.70 (d, ²J_{HH} = 15.8 Hz, 2H, CH₂, Cy⁵); ³¹P{¹H} NMR (CD₂Cl₂, 161.8 MHz, 293 K) δ 60.3 (s, 2P, *PPh*₃); ¹³C{¹H} NMR (CD₂Cl₂, 100.5 MHz, 293 K) δ 136.4 (s, BPh₄), 135.2 (d, ¹J_{PC} = 35.5 Hz, *PPh*₃, Ar¹), 133.6 (d, ²J_{PC} = 9.8 Hz, *PPh*₃, Ar²), 130.0 (s, *PPh*₃, Ar⁴), 129.0 (d, ³J_{PC} = 8.6 Hz, *PPh*₃, Ar³), 126.1 (m, BPh₄), 122.3 (s, BPh₄), 43.9 (s, CH, Cy¹), 43.65 (s, CH, Cy³), 43.6 (s, CH, Cy²), 35.1 (s, CH₂), 34.2 (s, CH₂), 33.0 (s, CH₂). **ESI-MS**: *m/z* 1091.1496 ([**3**]⁺, Calc. for C₄₈H₆₀Cl₃N₆P₂Ru₂⁺: 1091.1502, < 1%), 569.1175 ([RuCl(NCMe)(*cis*-tach)(*PPh*₃)]⁺, C₂₆H₃₃ClN₄PRu⁺: 569.1173, 100), 528.0896 ([RuCl(*cis*-tach)(*PPh*₃)]⁺, C₂₄H₃₀ClN₃PRu⁺: 528.0907, 20). **ATR-IR**

(cm^{-1}): 3281, 3237, 3137, 3049, 2896, 1590, 1480, 1434 (P–Ph), 1265, 1158, 1092, 1027, 903. Crystals suitable for X-ray diffraction analysis were obtained by the slow diffusion of n-pentane into a saturated dichloromethane solution of [3]BPh₄.

8.2.5 [{RuCl(PPh₃)(*cis*-tach)}₂(μ -Cl)]PF₆, [3]PF₆

Preparation is identical to [3]BPh₄, however sodium hexafluorophosphate (0.129 mmol) was used opposed to sodium tetraphenylborate. ¹H NMR (CD₂Cl₂, 399.8 MHz, 293 K) δ 7.84 (m, 4H, PPh₃), 7.71 (m, 8H, PPh₃), 7.35 (m, 10H, PPh₃), 7.26 (m, 8H, PPh₃), 6.74 (d, J = 10.1 Hz, 2H, NH₂), 4.27 (d, J = 10.1 Hz, 2H, NH₂), 3.96 (bs, 2H, CH), 3.00 (s, 2H, CH), 2.73 (d, J = 11.8 Hz, 2H, NH₂), 2.67 (s, 2H, CH), 2.45 (d, J = 11.8 Hz, 2H, NH₂), 1.98 (m, 12H, CH₂), 1.61 (d, J = 15.3 Hz, 2H, NH₂), 0.77 (d, J = 15.3 Hz, 2H, NH₂); ³¹P{¹H} NMR (CD₂Cl₂, 161.8 MHz, 293 K) δ 60.2 (s, 2P, PPh₃), -144.6 (septet, ¹J_{PF} = 710.5 0Hz, 1P, PF₆);

8.2.6 Dissolution of [2] in *d*₆-DMSO

[2].CH₂Cl₂ was dissolved in *d*₆-DMSO and the ¹H and ³¹P{¹H} NMR spectra recorded. ¹H NMR ((CD₃)₂SO, 399.8 MHz, 293 K) δ 7.86 (m, 6H PPh₃), 7.46 m (m, 8H PPh₃), 4.97 (d, 1H, ²J_{HH} = 11.7 Hz, NH₂), 4.28 (d, 1H, ²J_{HH} = 12.1 Hz, NH₂), 3.83 (d, 1H, ²J_{HH} = 11.7 Hz, NH₂), 3.71 (d, 1H, ²J_{HH} = 12.1 Hz, NH₂), 3.58 (d, 1H, ²J_{HH} = 11.8 Hz, NH₂), 3.35 (s, 1H, CH, obscured by δ 3.33), 3.33 (H₂O), 3.06 (s, 1H, CH), 2.56 (s, 1H, CH), 1.99 (d, 1H, ²J_{HH} = 14.6 Hz, CH₂), 1.80 (d, 1H, ²J_{HH} = 14.6 Hz, CH₂), 1.67 (d, 1H, ²J_{HH} = 15.2 Hz, CH₂), 1.59 (d, 1H, ²J_{HH} = 15.2 Hz, CH₂), 1.53 (d, 1H, ²J_{HH} = 15.9 Hz, CH₂), 1.25 (d, 1H, ²J_{HH} = 14.9 Hz, CH₂), 1.16 (d, 1H, ²J_{HH} = 11.8 Hz, NH₂); ³¹P{¹H} NMR (CD₂Cl₂, 161.8 MHz, 293 K) δ 49.7 (s, 1P, PPh₃).

8.2.7 [RuCl(DMSO-*S*)(PPh₃)(*cis*-tach)]Cl, [4]Cl

An orange mixture of [2].CH₂Cl₂ (56.4 mg, 0.0870 mmol) in methanol (10 mL) was heated at reflux with dimethylsulfoxide (6.5 μ L, 0.095 mmol) for 3 h. The pale yellow solution was allowed to cool to room temperature, and the solvent removed *in vacuo*. The product was washed with pentane (2 x 10 mL) and dried *in vacuo*.

Yield 42.8 mg (87%, 0.0613 mmol of [RuCl(DMSO-*S*)(*cis*-tach)(PPh₃)]Cl·H₂O·½(C₂H₆SO)). Found: C 46.48; H 5.87; N 5.92%. Calcd for C₂₆H₃₆Cl₂N₃OPRuS(H₂O)(½ C₂H₆SO): C 46.44; H 5.87; N 6.02%. ¹H NMR (CD₃OD, 399.8 MHz, 293 K) δ 7.93 (m, 6H, PPh₃, Ar²), 7.50 (m, 9H, PPh₃, Ar³ + Ar⁴), 5.10 (d, 1H, ²J_{HH} = 10.9 Hz, NH₂, N¹), 4.38 (d, 1H, ²J_{HH} = 12.2 Hz, NH₂, N²), 4.03 (d, 1H, ²J_{HH} = 10.9 Hz, NH₂, N¹), 3.77 (d, 1H, ²J_{HH} = 12.2 Hz, NH₂, N²), 3.65 (d, 1H, ²J_{HH} = 11.5 Hz, NH₂, N³), 3.49 (m, 1H, CH, Cy¹), 3.20 (m, 4H: 3H, (CH₃)₂SO, So¹; 1H, CH, Cy³), 2.69 (m, 4H: 3H, (CH₃)₂SO, So²; 1H, CH, Cy²), 2.09 (d, ²J_{HH} = 15.2 Hz, 1H, CH₂, Cy⁶), 1.98 (d, ²J_{HH} = 15.2 Hz, 1H, CH₂, Cy⁶), 1.82 (m, 2H, CH₂, Cy⁴), 1.72 (m, 1H CH₂, Cy⁵), 1.34 (m, 3H: 1H, CH₂, Cy⁵; 1H, NH₂, N³); ³¹P{¹H} NMR (CD₃OD, 161.8 MHz, 293 K) δ 48.8 (s, 1P, PPh₃); ¹³C{¹H} NMR (CD₃OD, 399.8 MHz, 293 K) δ 134.65 (d, ¹J_{PC} = 39.5 Hz, PPh₃, Ar¹), 134.6 (d, ²J_{PC} = 9.5 Hz, PPh₃, Ar²), 131.6 (d, ⁴J_{PC} = 2.5 Hz, PPh₃, Ar⁴), 130.3 (d, ³J_{PC} = 9.5 Hz, PPh₃, Ar³), 48.9 (s, (CH₃)₂SO, So²), 45.4 (s, (CH₃)₂SO, So¹), 44.15 (s, CH, Cy³), 44.1 (s, CH, Cy²), 43.8 (s, CH, Cy¹), 34.9 (s, CH₂, Cy⁶), 33.8 (s, CH₂, Cy⁴), 33.4 (s, CH₂, Cy⁵). ESI-MS: *m/z* 606.1062 ([4]⁺, Calc. for C₂₆H₃₆ClN₃OPRuS⁺: 606.1046, 100%).

8.2.8 [RuCl(NCMe)(PPh₃)(*cis*-tach)]PF₆, [5]PF₆

To a mixture of [2]·CH₂Cl₂ (55.5 mg 0.085 mmol) in acetonitrile (20 mL) was added sodium hexafluorophosphate (18.0 mg, 0.107 mmol). The resulting pale yellow solution was stirred for 30 mins until all the solid had dissolved. The solvent was then removed *in vacuo*, and the residue taken up in dichloromethane (10 mL). The insoluble salts were removed by filtration, and the pale cream product precipitated by addition of diethyl ether (50 mL). The product was isolated by filtration and washed a further time with diethyl ether (20 mL). Yield: 48.3 mg (71%, 0.060 mmol of [RuCl(NCMe)(*cis*-tach)(PPh₃)]PF₆). Found: C 43.39; H 4.61; N 6.61%. Calcd for C₂₆H₃₃ClF₆N₄P₂Ru(½CH₂Cl₂)(½Et₂O): C 43.14; H 4.95; N 7.06%. ¹H NMR (CD₂Cl₂, 399.8 MHz, 293 K) δ 7.75 (m, 6H, PPh₃, Ar²), 7.45 (m, 9H, PPh₃, Ar³ + Ar⁴), 4.12 (m, 2H, NH₂, N¹), 3.77 (m, 1H, CH, Cy¹), 3.12 (s, 1H, CH, Cy²), 3.05 (d, ²J_{HH} = 12.0 Hz, 1H, NH₂, N²), 2.89 (s, 1H, CH, Cy³), 2.85 (d, ²J_{HH} = 12.0 Hz, 1H, NH₂, N³), 2.49 (d, ²J_{HH} = 12.2 Hz, 1H, NH₂, N²), 2.29 (s, 3H, CH₃CN), 2.15 (d, ²J_{HH} = 15.5 Hz, 1H, CH₂, Cy⁶), 1.96 (m, 2H, CH₂, Cy⁴), 1.85 (d, ²J_{HH} = 15.5 Hz, 1H, CH₂

Cy⁶), 1.68 (d, ²J_{HH} = 15.4. 2.0 Hz, 1H, CH₂, Cy⁵), 1.30 (d, ²J_{HH} = 12.1 Hz, 1H, NH₂, N³), 1.00 (d, ²J_{HH} = 15.4. 2.0 Hz, 1H, CH₂, Cy⁵); ³¹P{¹H} NMR (CD₂Cl₂, 161.8 MHz, 293 K) δ 60.6 (s, 1P, PPh₃), -144.67 (septet, 1P, PF₆); ¹³C{¹H} NMR (CD₂Cl₂, 100.5 MHz, 293 K) δ 133.8 (d, ¹J_{PC} = 38.7 Hz, PPh₃, Ar¹), 133.7 (d, ²J_{PC} = 9.9 Hz, PPh₃, Ar²), 130.5 (d, ⁴J_{PC} = 2.1 Hz, PPh₃, Ar⁴), 129.5 (d, ³J_{PC} = 8.8 Hz, PPh₃, Ar³), 126.4 (s, NCCH₃), 43.8 (s, CH, Cy¹), 43.6 (s, CH, Cy³), 43.4 (s, CH, Cy²), 34.8 (s, CH₂, Cy⁴), 33.5 (s, CH₂, Cy⁵ + Cy⁶), 4.7 (s, NCCH₃). **ESI-MS**: *m/z* 720.1416 ([**5**-Cl+NCMe+PF₆])⁺, Calc for C₂₈H₃₆F₆N₅P₂Ru⁺: 720.1393, 2%), 569.1167 ([**5**]⁺, C₂₆H₃₃ClN₄PRu⁺: 569.1173, 100), 528.0909 ([**5**-NCMe]⁺, C₂₄H₃₀ClN₃PRu⁺: 528.0907, 5), 287.5866 ([**5**-Cl+NCMe]²⁺, C₂₈H₃₆N₅PRu: 287.5874²⁺, 25), 267.0733 ([**5**-Cl]²⁺, C₂₆H₃₃N₄PRu²⁺: 267.0741, 35), 246.5603 ([**5**-Cl-NCMe]²⁺, C₂₄H₃₀N₃PRu²⁺: 246.5608, 25). **ATR-IR** (cm⁻¹): 2249 (C≡N), 1596, 1482, 1436 (P-Ph), 1367, 1270, 1174, 1140, 1118, 1009, 915, 838 (PF₆⁻).

8.2.9 [Ru(NCMe)₂(PPh₃)(*cis*-tach)](PF₆)₂, [**6**](PF₆)₂

A mixture of sodium hexafluorophosphate (37.8 mg, 0.225 mmol) and [**2**].CH₂Cl₂ (56.1 mg, 0.086 mmol) were heated under reflux in acetonitrile for 4 h. After, the solvent was removed *in vacuo*, and the product extracted in dichloromethane (40 mL). The insoluble salt was removed by filtration, and the filtrate concentrated to 10 mL. The white product was precipitated out by addition of diethyl ether (50 mL), collected by filtration, washed with diethyl ether (20 mL) and dried *in vacuo*. Yield: 38.1 mg (51%, 0.044 mmol of of [RuCl(NCMe)₂(*cis*-tach)(PPh₃)](PF₆)₂.) ¹H NMR (CD₂Cl₂, 399.8 MHz, 293 K) δ 7.53 (m, 15H, PPh₃, Ar² + Ar³ + Ar⁴), 3.82 (s, 2H, NH₂, N¹), 3.74 (s, 1H, CH, Cy¹), 3.36 (d, ²J_{HH} = 12.5 Hz, 2H, NH₂, N²), 3.06 (s, 2H, CH, Cy²), 2.40 (s, 3H, CH₃CN), 2.21 (d, ²J_{HH} = 15.2 Hz, 2H, NH₂, N²), 1.92 (m, 4H, Cy³), 1.70 (d, ²J_{HH} = 15.6 Hz, 1H, CH₂, Cy⁴), 0.85 (d, ²J_{HH} = 15.6 Hz, 1H, CH₂, Cy⁴); ³¹P{¹H} NMR (CD₂Cl₂, 161.8 MHz, 293 K) δ 55.9 (s, 1P, PPh₃), -144.67 (septet, 2P, PF₆); ¹³C{¹H} NMR* (CD₂Cl₂, 100.5 MHz, 293 K) δ 133.2 (d, ²J_{PC} = 10.1 Hz, PPh₃, Ar²), 131.6 (d, ⁴J_{PC} = 2.4 Hz, PPh₃, Ar⁴), 131.5 (d, ¹J_{PC} = 42.6 Hz, PPh₃, Ar¹), 130.2 (d, ³J_{PC} = 9.3 Hz, PPh₃, Ar³), 43.9 (s, CH, Cy¹), 43.2 (s, CH, Cy²), 33.4 (s, CH₂, Cy⁴), 33.2 (s, CH₂, Cy³), 4.8 (s, NCCH₃). **ESI-MS**: *m/z* 720.1372 ([**6**+PF₆])⁺, Calc for C₂₈H₃₆F₆N₅P₂Ru⁺: 720.1395, 100%). * The NCCH₃ signal was not observed.

8.2.10 Reaction of [5]PF₆ with dppm

Methylenebis(diphenylphosphane) (5 mg, 0.01 mmol) was added to a CD₂Cl₂ solution of [5]PF₆ (5mg, 0.01 mmol) in an NMR tube fitted with a Teflon tap. The solution was heated at 50 °C for 45 minutes and the ³¹P{¹H} NMR spectrum was recorded. Data is provided for [RuCl(η¹-dppm)(*cis*-tach)(PPh₃)]PF₆, [8]PF₆ from this spectrum. ³¹P{¹H} NMR (CD₂Cl₂, 161.8 MHz, 293 K) δ 48.2 (d, ²J_{PP} = 30.0 Hz, PPh₃), 45.1 (dd, ²J_{PP} = 33.5, ²J_{PP} = 30.0 Hz, RuPPh₂), -28.1 (d, ²J_{PP} = 33.4 Hz, *pend*-PPh₂). The ¹H and ³¹P{¹H} NMR spectra were recorded after a further 16 h of heating, however no identifiable signals were present due to degradation.

8.3 Chapter 3 Experimental

8.3.1 [RuCl(DMSO-*S*)₂(*cis*-tach)]Cl, [8]Cl

Cis-tach (65.0 mg, 0.503 mmol) was added to a solution of dichloro[*fac*-tris(dimethylsulfoxide-κ*S*)](dimethylsulfoxide-κ*O*)ruthenium(II) (243.0 mg, 0.501 mmol) in dimethylsulfoxide (20 mL). The resulting yellow suspension was heated at 130°C for 30 minutes. The pale yellow solution was allowed to cool, and the product was precipitated out by addition of 200 mL of ethyl acetate. The mixture was chilled to -20°C for 18 hours, forming more precipitate, which was isolated by filtration under reduced pressure, washed with ethyl acetate (2 x 20 mL) and dried *in vacuo*. Yield: 200.1 mg (92%, 0.461 mmol of [RuCl(DMSO-*S*)₂(*cis*-tach)]Cl). Found: C 26.33; H 5.83; N 8.96%. Calcd for C₁₀H₂₇Cl₂N₃O₂RuS₂: C 26.26; H 5.95; N 9.19%. ¹H NMR (D₂O, 399.8 MHz, 293K): δ 4.52 (d, ²J_{HH} = 11.6 Hz, 2H, NH₂, N²), 4.23 (d, ²J_{HH} = 11.6 Hz, 2H, NH₂, N²), 3.88 (s, 2H, NH₂, N¹), 3.53 (s, 2H, CH, C²), 3.36 (s, 6H, (CH₃)₂SO), 3.27 (s, 1H, CH, Cy¹), 2.14 (d, ²J_{HH} = 15.5 Hz, 1H, CH₂, Cy⁴), 2.07 (d, ²J_{HH} = 15.5 Hz, 2H, CH₂, Cy³), 2.04 (d, ²J_{HH} = 15.5 Hz, 1H, CH₂, Cy⁴), 1.84 (d, ²J_{HH} = 15.5 Hz, 2H, CH₂, Cy³); ¹³C{¹H} NMR (D₂O 100.5 MHz, 293K): δ 44.2 (s, (CH₃)₂SO), 43.1 (s, CH, Cy¹), 42.4 (s, CH, Cy²), 33.4 (s, CH₂, Cy⁴), 32.5 (s, CH₂, Cy³). ESI-MS: *m/z* 422.0271 ([8]⁺, Calc for C₁₀H₂₇ClN₃O₂RuS₂⁺: 422.0269, 100%). ATR-IR (cm⁻¹): 3261 (w), 2089 (m), 1595 (m), 1359 (m), 1223 (m), 1174 (w), 1061 (s, S-O), 909 (m), 682 (m). Crystals of

[8]PF₆ suitable for X-ray diffraction analysis were obtained by the addition of 1.5 equivalents of potassium hexafluorophosphate to a methanol solution followed by filtration and slow evaporation.

8.3.2 [RuCl₂(DMSO-*S*)(*cis*-tach)], [9]

Crystals of [RuCl₂(DMSO-*S*)(*cis*-tach)] [9] were obtained from an attempted crystallisation of [15]PF₆ by slow evaporation.

8.3.3 Aquation of [8]Cl: Mass Spectrometry

An aqueous solution of [8]Cl (1 mM, 10 mL) was heated at 40°C for 18 hours. The solution was diluted to 100 μM with 50% H₂O/50% MeOH and the ESI mass spectrum recorded using a Bruker Esquire instrument. Selected peaks:

m/z	Ion	Calc. for	Calc.	Height (%)
422.0	[8] ⁺	C ₁₀ H ₂₇ ClN ₃ O ₂ RuS ₂ ⁺	422.0	5
362.0	[8-DMSO+H ₂ O] ⁺	C ₈ H ₂₃ ClN ₃ O ₂ RuS ⁺	362.0	10
344.0	[8-DMSO] ⁺	C ₈ H ₂₁ ClN ₃ ORuS ⁺	344.0	10
232.5	[8-Cl+DMSO] ²⁺	C ₁₂ H ₃₃ N ₃ O ₃ RuS ₃ ²⁺	232.5	100
202.5	[8-Cl+H ₂ O] ²⁺	C ₁₀ H ₂₉ N ₃ O ₃ RuS ₂ ²⁺	202.5	50
193.6	[8-Cl] ²⁺	C ₁₀ H ₂₇ N ₃ O ₂ RuS ₂ ²⁺	193.5	60
163.6	[8-DMSO-Cl+H ₂ O] ²⁺ ,	C ₈ H ₂₃ N ₃ O ₂ RuS ²⁺	163.5	30
154.6	[8-DMSO-Cl] ²⁺	C ₈ H ₂₁ N ₃ ORuS ²⁺	154.5	10

Table 8.1: ESI-MS data for the aquation of [8]Cl

8.3.4 Aquation of [8]Cl: NMR Kinetics

A solution of [8]Cl (10.8 mM) in D₂O, (0.5 mL) with ethyl acetate (1 equiv.) was prepared under a dinitrogen atmosphere in an NMR tube fitted with a Teflon tap at 40°C. The sample was loaded into a thermally equilibrated Bruker AV500 NMR spectrometer, where ¹H NMR spectra were recorded at 20 minute intervals for 14

hours. Kinetic analysis of integrations relative to ethyl acetate were performed using DynaFit with the mechanisms $[\mathbf{8}]\text{Cl} \rightarrow [\mathbf{8a}]^{\text{n}+} + \text{DMSO}$ and $[\mathbf{8}]\text{Cl} \rightarrow [\mathbf{8b}]^{\text{n}+} + \text{DMSO} + \text{Cl}^-$.²⁴⁹

8.3.5 Aquation of $[\mathbf{8}]\text{Cl}$: pH Study

A solution of $[\mathbf{8}]\text{Cl}$ (10 mM) was prepared in 10% $\text{D}_2\text{O}/90\%$ H_2O (20 mL) with 10 mM sodium phosphate and the pH adjusted to 6.4, 7.4 or 8.2 under an atmosphere of dinitrogen. An aliquot (0.5 mL) was transferred into an NMR tube fitted with a Teflon tap under a dinitrogen atmosphere. The solution was heated at 40°C for 18 hours, after which the ^1H NMR spectrum was recorded using a Bruker AV500 spectrometer.

8.3.6 Reaction of $[\mathbf{8}]\text{Cl}$ with Nucleosides

An aqueous solution of $[\mathbf{8}]\text{Cl}$ (5 mM, 25 mL) was heated at 40°C for 18 hours with two equivalents of guanosine or adenosine. The resulting solution was diluted to 100 μM with 50% $\text{H}_2\text{O}/50\%$ MeOH and the ESI mass spectrum recorded on a Bruker Esquire instrument.

m/z	Ion	Calc. for	Calc.	Height (%)
627.1	$[\mathbf{8}\text{-DMSO+Guo}]^+$	$\text{C}_{18}\text{H}_{34}\text{ClN}_8\text{O}_6\text{RuS}^+$	627.1	5
591.1	$[\mathbf{8}\text{-DMSO-Cl+Guo-H}]^+$	$\text{C}_{18}\text{H}_{33}\text{N}_8\text{O}_6\text{RuS}^+$	591.2	100
422.0	$[\mathbf{8}]^+$	$\text{C}_{10}\text{H}_{27}\text{ClN}_3\text{O}_2\text{RuS}_2^+$	422.0	5
398.6	$[\mathbf{8}\text{-2DMSO-Cl+2Guo}]^{2+}$	$\text{C}_{26}\text{H}_{41}\text{N}_{13}\text{O}_{10}\text{Ru}^{2+}$	398.6	25
296.1	$[\mathbf{8}\text{-DMSO-Cl+Guo}]^{2+}$	$\text{C}_{18}\text{H}_{34}\text{N}_8\text{O}_6\text{RuS}^{2+}$	296.1	10
230.1	$[\mathbf{8}\text{-DMSO-Cl+Guo-ribose}]^{2+}$	$\text{C}_{13}\text{H}_{26}\text{N}_8\text{O}_2\text{RuS}^{2+}$	230.0	25
575.1	$[\mathbf{8}\text{-DMSO-Cl+Ado-H}]^+$	$\text{C}_{18}\text{H}_{33}\text{N}_8\text{O}_5\text{RuS}^+$	575.2	100

Table 8.2: ESI-MS data for the reaction of $[\mathbf{8}]^+$ and Guo (top) and Ado (bottom).

8.4 Chapter 4 Experimental

8.4.1 [Ru(bipy)(DMSO-*S*)(*cis*-tach)](Cl)₂, [10](Cl)₂

[8]Cl (45.7 mg, 0.0999 mmol) and 2,2'-bipyridine (18.7 mg, 0.120 mmol) were heated at 120°C in water (5 mL) for 20 minutes, resulting in a deep red solution. Once cooled, the solution was washed with dichloromethane (3 x 10 mL) and dried *in vacuo*, giving a dark red residue. This was dissolved in methanol (5 mL) and dried *in vacuo*, giving an orange powder. Yield: 42.7 mg (80%, 0.0797 mmol of [Ru(bipy)(DMSO-*S*)(*cis*-tach)](Cl)₂). ¹H NMR (D₂O, 399.8 MHz, 293K) δ 8.95 (dd, ³J_{HH} = 5.8 Hz, ⁴J_{HH} = 1.2, 2H, bipy, Py⁶), 8.43 (dd, ³J_{HH} = 8.3 Hz, ⁴J_{HH} = 1.3, 2H, bipy, Py³), 8.14 (td, ³J_{HH} = 7.8 Hz, ⁴J_{HH} = 1.2, 2H, bipy, Py⁴), 7.70 (ddd, ³J_{HH} = 7.8 Hz, ³J_{HH} = 5.8 Hz, ⁴J_{HH} = 1.3, 2H, bipy, Py⁵), 4.33 (d, ²J_{HH} = 12.5 Hz, 2H, NH₂, N²), 4.16 (d, ²J_{HH} = 12.5 Hz, 2H, NH₂, N²), 4.01 (s, 2H, NH₂, N¹), 3.49 (s, 2H, CH, Cy²), 3.24 (s, 1H, CH, Cy¹), 2.63 (s, 6H, (CH₃)₂SO), 2.03 (m, 3H, CH₂; 2H Cy³ + 1H Cy⁴), 1.83 (m, 3H, CH₂; 2H Cy³ + 1H Cy⁴); ¹³C{¹H} NMR (D₂O, 100.5 MHz, 293K) δ 157.7 (s, bipy, Py²), 151.5 (s, bipy, Py⁶), 138.6 (s, bipy, Py⁴), 127.3 (s, bipy, Py⁵), 125.5 (s, bipy, Py³), 43.5 (s, CH, Cy²), 43.1 (s, (CH₃)₂SO), 42.0 (s, CH, Cy¹), 33.2 (s, CH₂, Cy⁴), 32.8 (s, CH₂, Cy³). ESI-MS: *m/z* 464.1064 ([10-H]⁺, Calc. for C₁₈H₂₈N₅ORuS⁺: 464.1056, 5%), 232.5573 ([10]²⁺, C₁₈H₂₉N₅ORuS²⁺: 232.5568, 100). ATR-IR (cm⁻¹): 3383, 3211, 3101, 2919, 1602, 1444, 1369, 1226, 1127, 1066, 1050, 1015 (s, S-O), 910. Crystals of [10](PF₆)₂ suitable for X-ray diffraction were obtained by the addition of 3 equivalents of potassium hexafluorophosphate to a methanol solution of [10](Cl)₂ followed by filtration and slow evaporation.

8.4.2 [Ru(DMSO-*S*)(phen)(*cis*-tach)](Cl)₂, [11](Cl)₂

[8]Cl (45.8 mg, 0.100 mmol) and 1,10-phenanthroline (21.6 mg, 0.120 mmol) were heated at 120°C in water (5 mL) for 20 minutes, resulting in a deep red solution. Once cooled, the solution was washed with dichloromethane (3 x 10 mL) and dried *in vacuo* giving a dark red residue. This was dissolved in methanol (5 mL) and dried *in vacuo*, giving an orange powder. Yield: 35.9 mg (64%, 0.641 mmol of [Ru(DMSO-*S*)(phen)(*cis*-tach)](Cl)₂). Found: C 40.79; H 5.55; N 11.29%. Calcd

for $C_{20}H_{29}Cl_2N_5ORuS(2 H_2O)$: C 40.34; H 5.58; N 11.75%. 1H NMR (D_2O , 399.8 MHz, 293K) δ 9.36 (dd, $^3J_{HH} = 5.3$ Hz, $^4J_{HH} = 1.1$, 2H, phen, Py⁶), 8.71 (dd, $^3J_{HH} = 8.25$ Hz, $^4J_{HH} = 1.1$, 2H, phen, Py⁴), 8.16 (s, 2H, phen, Py⁷), 8.03 (dd, $^3J_{HH} = 8.25$ Hz, $^3J_{HH} = 5.3$, 2H, phen, Py⁵), 4.54 (d, $^2J_{HH} = 12.4$ Hz, 2H, NH_2 , N²), 4.31 (d, $^2J_{HH} = 12.4$ Hz, 2H, NH_2 , N²), 3.90 (s, 2H, NH_2 , N¹), 3.55 (s, 2H, CH, Cy²), 3.20 (s, 1H, CH, Cy¹), 2.52 (s, 6H, $(CH_3)_2SO$), 2.07 (m, 3H, CH_2 ; 2H Cy³ + 1H Cy⁴), 1.89 (m, 3H, CH_2 ; 2H Cy³ + 1H Cy⁴); $^{13}C\{^1H\}$ NMR (D_2O , 100.5 MHz, 293K) δ 152.3 (s, phen, Py⁶), 148.2 (s, phen, Py²), 137.9 (s, phen, Py⁴), 131.2 (s, phen, Py³), 128.0 (s, phen, Py⁷), 125.6 (s, phen, Py⁵), 43.5 (s, CH, Cy²), 42.9 (s, $(CH_3)_2SO$), 42.0 (s, CH, Cy¹), 33.2 (s, CH_2 , Cy⁴), 32.9 (s, CH_2 , Cy³). **ESI-MS**: m/z 244.5570 ($[11]^{2+}$, Calc. for $C_{20}H_{29}N_5ORuS^{2+}$: 244.5565, 100%). **ATR-IR** (cm^{-1}): 3374, 3251, 4149, 2922, 1602, 1432, 1226, 1126, 1016 (s, S–O), 912. Crystals of $[11](PF_6)_2$ suitable for X-ray diffraction were obtained by the addition of 3 equivalents of potassium hexafluorophosphate to a methanol solution of $[11](Cl)_2$ followed by filtration and slow evaporation.

8.4.3 $[Ru(DMSO-S)(en)(cis-tach)](Cl)_2$, $[12](Cl)_2$

$[8]Cl$ (45.8 mg, 0.100 mmol) and 1,2-diaminoethane (7.2 mg, 8.0 μ L, 0.12 mmol) were heated at 120°C in water (5 mL) for 20 minutes, resulting in a deep red solution. Once cooled, the solution was washed with dichloromethane (3 x 10 mL) and dried *in vacuo* giving an orange residue. This was dissolved in methanol (5 mL) and dried *in vacuo*, giving an orange powder. Yield: 29.7 mg (68%, 0.0676 mmol of $[Ru(DMSO-S)(en)(cis-tach)](Cl)_2$). 1H NMR (D_2O , 399.8 MHz, 293K) δ 4.66 (s, 2H, NH_2 , N¹), 4.10 (d, $^2J_{HH} = 12.0$ Hz, 2H, NH_2 , N²), 3.71 (s, 1H, CH, Cy¹), 3.60 (d, 2H, $^2J_{HH} = 11.1$ Hz, en- NH_2), 3.48 (d, 2H, $^2J_{HH} = 11.1$ Hz, en- NH_2), 3.37 (d, $^2J_{HH} = 12.0$ Hz, 2H, NH_2 , N²), 3.34 (s, 6H, $(CH_3)_2SO$), 3.31 (s, 2H, CH, Cy²), 2.52 (s, 2H, en- CH_2), 2.07 (d, $^2J_{HH} = 15.2$ Hz, 2H, CH_2 , Cy³), 1.95 (d, $^2J_{HH} = 15.2$ Hz, 2H, CH_2 , Cy³), 1.91 (d, $^2J_{HH} = 15.4$ Hz, 2H, CH_2 , Cy⁴), 1.57 (d, $^2J_{HH} = 15.4$ Hz, 2H, CH_2 , Cy⁴); $^{13}C\{^1H\}$ NMR (CD_3OD , 100.5 MHz, 293K) δ 45.3 (s, 6H, $(CH_3)_2SO$), 44.6 (s, en- CH_2), 43.2 (s, CH, C¹), 42.9 (s, CH, C²), 33.1 (s, CH_2 , C³), 32.6 (s, CH_2 , C⁴). **ESI-MS**: m/z 368.1045 ($[12-H]^+$, Calc. for $C_{10}H_{28}N_5ORuS^+$: 368.1057, 5%), 184.5553 ($[12]^{2+}$, $C_{10}H_{29}N_5ORuS^{2+}$: 184.5568, 100). **ATR-IR** (cm^{-1}): 3220 (m), 3150 (vbr, s), 3108 (m), 2874 (w), 1609 (m), 1454 (m), 1329 (w), 1215 (w), 1129

(m), 1034 (s, S–O), 911 (m). Crystals of [12](Cl)(PF₆) suitable for X-ray diffraction were obtained by the addition of 3 equivalents of potassium hexafluorophosphate to a methanol solution of [12](Cl)₂ followed by filtration and slow evaporation.

8.4.4 Reaction of [11](Cl)₂ with Guanosine

An aqueous solution of [11](Cl)₂ (5 mM, 25 mL) was heated at 40°C for 18 h with guanosine (2 eq). The resulting solution was diluted to 100 μM with 50% H₂O/50% MeOH and the ESI mass spectrum recorded on a Bruker Esquire instrument

m/z	Ion	Calc. for	Calc.	Height (%)
693.2	[11–DMSO+Guo–H] ⁺	C ₂₈ H ₃₆ N ₁₀ O ₅ Ru ⁺	693.2	15
347.2	[11–DMSO+Guo] ²⁺	C ₂₈ H ₃₇ N ₁₀ O ₅ Ru ²⁺	347.1	100
244.6	[11] ²⁺	C ₂₀ H ₂₉ N ₅ ORuS ²⁺	244.6	50
214.6	[11–DMSO+H ₂ O] ²⁺	C ₁₈ H ₂₅ N ₅ ORu ²⁺	214.6	25

Table 8.3: ESI-MS data for reaction of [11]²⁺ with Guo.

8.4.5 [RuCl(η⁴-COD)(*cis*-tach)]PF₆, [13]PF₆

A solution of *mer*-tris(acetonitrile)chloro(η⁴-1,5-cyclooctadiene)ruthenium(II) hexafluorophosphate (51.3 mg, 0.100 mmol) and *cis*-tach (13.0 mg, 0.101 mmol) in deoxygenated ethanol (10 mL) was heated at reflux for 2 h. The orange solution was allowed to cool to room temperature, and the volume reduced by half *in vacuo* and diethyl ether (30 mL) added. The resulting precipitate was collected by filtration and washed with diethyl ether (2 x 10 mL) and dried *in vacuo*. Yield: 35.0 mg (64%, 0.0637 mmol of [RuCl(η⁴-COD)(*cis*-tach)]PF₆). ¹H NMR (CD₃OD, 399.8 MHz, 293K) δ 5.13 (s, 2H, NH₂, N¹), 4.20 (d, 2H, ²J_{HH} = 11.2 Hz, NH₂, N²), 3.97 (m, 2H, COD-CH), 3.73 (m, 4H: 2H, COD-CH; 2H, NH₂, N²), 3.36 (s, 2H, CH, Cy²), 3.18 (m, 1H, CH, Cy¹), 2.50 (m, 2H, COD-CH₂), 2.35 (m, 2H, COD-CH₂), 2.16 (m, 2H, CH₂, Cy³), 2.03 (m, 6H: 2H, CH₂, Cy⁴; 4H, COD-CH₂), 1.89 (d, 2H, ²J_{HH} = 14.9 Hz, CH₂, Cy³); ¹³C{¹H} NMR (CD₃OD, 100.5 MHz, 293K): 91.7 (s, COD-CH), 88.4 (s, COD-CH), 43.6 (s, CH, Cy²), 43.4 (s, CH, Cy¹), 34.0 (s, CH₂, Cy³), 33.5 (s, CH₂, Cy⁴), 31.1 (s, COD-CH₂), 29.5 (s, COD-CH₂). **ESI-MS:** *m/z* 374.0937 ([13]⁺, Calc.

for $C_{14}H_{27}ClN_3Ru^+$: 374.0932, 100%), 169.5588 ($[13-Cl]^+$, $C_{14}H_{27}N_3Ru$: 169.5624, 25).

8.4.6 Reaction of $[13]PF_6$ with 2,2'-bipyridine

A solution of $[13]PF_6$ (5.0 mg) and 2,2'-bipyridine (2 eq) in CD_3OD (0.5 mL) was heated at $100^\circ C$ for 24 h in an NMR tube fitted with a Teflon tap under nitrogen. Although a colour change had occurred to red, the 1H NMR spectrum was identical to that of $[13]PF_6$. No significant reaction was observed after one week of further heating.

8.4.7 $Ru(NCMe)_3(cis-tach)(Cl)_2$, $[14](Cl)_2$

All synthetic procedures were performed under deoxygenated conditions with an argon atmosphere. $[8]Cl$ (25.0 mg, 0.547 mmol) was taken up in the minimum volume of water ($\sim 1/2$ mL), and acetonitrile (7 mL) added. The solution was heated under reflux for 6 h and the solvent removed *in vacuo*. The residue was taken up in the minimum volume of methanol, and addition of diethyl ether (50 mL) resulted in precipitation of the product, which was collected by filtration and dried *in vacuo*. Yield: 15.9 mg (69% of $[Ru(NCCH_3)_3(cis-tach)](Cl)_2$). 1H NMR (D_2O , 399.8 MHz, 293K) δ 3.91 (s, 6H, NH_2), 3.30 (s, 3H, CH), 2.41 (s, 9H, CH_3CN), 1.92 (d, $^2J_{HH} = 15.2$ Hz, 3H, CH_2), 1.70 (d, $^2J_{HH} = 15.2$ Hz, 3H, CH_2); $^{13}C\{^1H\}$ NMR (D_2O , 100.5 MHz, 293K) δ 123.9 (s, CH_3CN), 42.9 (s, CH), 32.7 (s, CH_2), 3.2 (CH_3CN). **ESI-MS**: m/z 177.1 ($[14]^{2+}$, Calc for $C_{12}H_{24}N_6Ru^{2+}$: 177.1, 100%), 165.5 ($[14-NCMe+H_2O]^{2+}$, $C_{10}H_{23}N_5ORu^{2+}$: 165.5, 60), 156.6 ($[14-NCMe]^{2+}$, $C_{10}H_{21}N_5Ru^{2+}$: 156.5, 30), 145.1 ($[14-2NCMe+H_2O]^{2+}$, $C_8H_{20}N_4ORu^{2+}$: 145.0, 5). **ATR-IR** (cm^{-1}): 3345 (br, m), 3221 (br, m), 3168 (m), 3118 (m), 2911 (w), 2266 (m, $C\equiv N$), 1619 (s), 1365 (m), 1228 (m), 1185 (m), 1129 (w), 1033 (w), 916 (m).

8.4.8 Reaction of $[14](Cl)_2$ with 2,2'-bipyridine

A solution of $[14](Cl)_2$ (5 mg, 0.01 mmol) and 2,2'-bipyridyl (2 eq, 0.02 mmol) in CD_3OD (0.5 mL) was heated at $100^\circ C$ for 30 minutes, after which the 1H NMR spectrum was recorded. Selected resonances: 1H NMR (CD_3OD , 399.8 MHz,

293K) 9.45 (d), 9.33(d), 9.23(d) 9.17 (d), 8.66 (d), 8.57 (d), 8.47 (d), 8.37(d), 8.31 (d), 8.19 (td), 8.01 (td), 7.96 (td), 7.81 (td), 7.77 (td), 7.63 (ddd), 7.51 (ddd), 7.45 (ddd). Further heating provided no change.

8.5 Chapter 5 Experimental

8.5.1 [RuCl(dppm)(cis-tach)]Cl, [15]Cl

A solution of [8]Cl (50.1 mg, 0.109 mmol) in methanol (10 mL) was heated under reflux with methylenebis(diphenylphosphane) (76.9 mg, 0.200 mmol) for 18 h. The solution was filtered to remove unreacted phosphane, and the solvent removed *in vacuo*. The residue was taken up in dichloromethane (1 mL), followed by addition of diethyl ether (10 mL), resulting in precipitation. The product was collected by filtration, and the process repeated. The pale cream product was dried *in vacuo*. Yield: 41.0 mg (58%, 0.0631 mmol of [RuCl(dppm)(cis-tach)]Cl.1½H₂O). Found: C 52.40; H 5.26; N 5.85%. Calcd for C₃₁H₃₇N₃P₂Cl₂Ru(1½ H₂O): C 52.25; H 5.66; N 5.89%. ¹H NMR (CD₃OD, 500.23 MHz, 300K) δ 7.74 (dd, ³J_{HP} = 11.5 Hz, ³J_{HH} = 7.5 Hz, ⁴J_{HH} = 1.5 Hz, 4H, PPh₂, Ar^{2a}), 7.67 (dd, ³J_{HP} = 11.5 Hz, ³J_{HH} = 7.5 Hz, ⁴J_{HH} = 1.5 Hz, 4H, PPh₂, Ar^{2b}), 7.50 (t, ³J_{HH} = 7.5 Hz, 4H, PPh₂, Ar^{3a}), 7.43 (t, ³J_{HH} = 7.5 Hz, ⁴J_{HH} = 1.5 Hz, 2H, PPh₂, Ar^{4a}), 7.34 (m, 6H, PPh₂, Ar^{3b} + Ar^{4b}), 5.79 (dt, ²J_{HH} = 15.8 Hz, ²J_{HP} = 10.6 Hz, 1H, PCH₂, Br¹), 5.17 (d, ²J_{HH} = 11.0 Hz, 2H, NH₂, N²), 3.99 (dt, ²J_{HH} = 15.8 Hz, ²J_{HP} = 11.4 Hz, 1H, PCH₂, Br¹), 3.72 (d, ²J_{HH} = 11.0 Hz, 2H, NH₂, N²), 3.60 (s, 2H, CH, Cy²), 2.95 (s, 1H, CH, Cy¹), 2.30 (d, ²J_{HH} = 14.9 Hz, 1H, CH₂, Cy⁴), 2.28 (s, 2H NH₂, N¹), 2.17 (d, ²J_{HH} = 14.9 Hz, 1H, CH₂, Cy⁴), 1.95 (d, ²J_{HH} = 14.9 Hz, 2H, CH₂, Cy³), 1.72 (d, ²J_{HH} = 14.9 Hz, 2H, CH₂, Cy³); ³¹P{¹H} NMR (CD₃OD, 202.5 MHz, 295K) δ 10.1 (s, 2P, PPh₂); ¹³C{¹H} NMR (CD₃OD, 125.8 MHz, 295K) δ 136.12 (vt, |¹J_{PC} + ³J_{P'C}| = 40 Hz, PPh₂, Ar^{1b}), 133.9 (vt, |²J_{PC} + ⁴J_{P'C}| = 10 Hz, PPh₂, Ar^{2b}), 133.4 (vt, |¹J_{PC} + ³J_{P'C}| = 33 Hz, PPh₂, Ar^{1a}), 132.2 (vt, |²J_{PC} + ⁴J_{P'C}| = 10 Hz, PPh₂, Ar^{2a}), 131.2 (s, PPh₂, Ar^{4a}), 131.1 (s, PPh₂, Ar^{4b}), 130.8 (vt, |³J_{PC} + ⁵J_{P'C}| = 9 Hz, PPh₂, Ar^{3a}), 129.1 (vt, |³J_{PC} + ⁵J_{P'C}| = 9 Hz, PPh₂, Ar^{3b}), 48.7 (m, PCH₂, Br¹), 44.8 (s, CH, C²), 44.7 (s, CH, C¹), 35.5 (s, CH₂, C⁴), 34.7 (s, CH₂, C³). ESI-MS: *m/z* 650.1213 ([15]⁺, Calc. for C₃₁H₃₇N₃P₂ClRu⁺: 650.1194, 100%). ATR-IR (cm⁻¹): 3290 (br, w), 3121 (br, w), 2913 (br, w), 1609 (br, m), 1433

(m, P-Ph), 1368 (w), 1160 (m), 1098 (m), 901 (m), 726 (s), 705 (s). Crystals of [15]PF₆ suitable for X-ray crystallography were obtained by the addition of 1.5 equivalents of potassium hexafluorophosphate to a methanol solution of [15]Cl followed by filtration and slow evaporation.

8.5.2 [RuCl(dppe)(cis-tach)]Cl, [16]Cl

A solution of [8]Cl (50.0 mg, 0.109 mmol) in methanol (10 mL) was heated under reflux with ethane-1,2-diylbis(diphenylphosphane) (85.0 mg, 0.213 mmol) for 18 h. The solution was filtered to remove unreacted phosphane, and the solvent removed *in vacuo*. Ethanol (1 mL) was added to the residue, followed by diethyl ether (10 mL) and the product collected by filtration, and the process repeated. The pale cream product was dried *in vacuo*. Yield: 76.6 mg (93%, 0.102 mmol of [RuCl(dppe)(cis-tach)]Cl·3H₂O). Found: C 50.88; H 5.66; N 5.65%. Calcd for C₃₂H₃₉N₃P₂Cl₂Ru(3 H₂O): C 50.99; H 6.02; N 5.58%. ¹H NMR (CD₃OD, 500.2 MHz, 295K) δ 7.87 (ddd, 4H, ³J_{HP} = 8.8 Hz, ³J_{HH} = 7.5 Hz, ⁴J_{HH} = 1.2 Hz, PPh₂, Ar^{2a}), 7.48 (t, 4H, ³J_{HH} = 7.7 Hz, PPh₂, Ar^{3b}), 7.43 (m, 8H, PPh₂, Ar^{2b} + Ar^{4a} + Ar^{4b}), 7.30 (td, 4H, ³J_{HH} = 7.5 Hz, ⁴J_{HH} = 1.2 Hz, PPh₂, Ar^{3a}), 4.82 (d, ²J_{HH} = 11.5 Hz, 2H, NH₂, N²), 3.98 (d, ²J_{HH} = 11.5 Hz, 2H, NH₂, N²), 3.58 (br. s, 2H, CH, Cy²), 3.06 (m, ΣJ_{HH,HP} = 61.3 Hz, ²J_{HH} = 16.1 Hz, ³J_{HH} = 7.7 Hz, 2H, PCH₂, Br¹), 2.55 (s, 1H, CH, Cy¹), 2.38 (m, ΣJ_{HH,HP} = 60.0 Hz, ²J_{HH} = 16.1 Hz, ³J_{HH} = 7.7 Hz, 2H, PCH₂, Br¹), 2.30 (d, ²J_{HH} = 15.8 Hz, 1H, CH₂, Cy⁴), 2.10 (d, ²J_{HH} = 15.8 Hz, 1H, CH₂, Cy⁴), 1.76 (d, ²J_{HH} = 15.4 Hz, 2H, CH₂, Cy³), 1.38 (d, ²J_{HH} = 15.4 Hz, 2H, CH₂, Cy³), 1.14 (s, 2H NH₂, N¹); ³¹P{¹H} NMR (CD₃OD, 202.5 MHz, 295K) δ 78.3 (s, 2P, PPh₂); ¹³C{¹H} NMR (CD₃OD, 125.8 MHz, 295K) δ 136.2 (d, |¹J_{PC} + ³J_{P'Cl}| = 40 Hz, PPh₂, Ar^{1a}), 135.6 (vquint., |²J_{PC} + ⁴J_{P'Cl}| = 20 Hz, PPh₂, Ar^{2a}), 135.3 (d, |¹J_{PC} + ³J_{P'Cl}| = 40 Hz, PPh₂, Ar^{1b}), 132.1 (s, PPh₂, Ar^{4a}), 131.3 (s, PPh₂, Ar^{4b}), 130.9 (vquint., |²J_{PC} + ⁴J_{P'Cl}| = 20 Hz, PPh₂, Ar^{2b}), 130.7 (vquint., |³J_{PC} + ⁵J_{P'Cl}| = 20 Hz, PPh₂, Ar^{3b}), 129.2 (vquint., |³J_{PC} + ⁵J_{P'Cl}| = 20 Hz, PPh₂, Ar^{3a}), 44.6 (s, CH, Cy²), 44.0 (s, CH, Cy¹), 35.5 (s, CH₂, Cy³), 34.3 (s, CH₂, Cy⁴), 29.7 (m, |²J_{PC} + ⁴J_{P'Cl}| = 45 Hz, PCH₂, Br¹). ESI-MS: *m/z* 664.1356 ([16]⁺, Calc. for C₃₂H₃₉N₃P₂ClRu⁺: 664.1351, 100%). ATR-IR (cm⁻¹): 3395 (br, w), 3283 (br, w), 3145 (br, w), 2913 (br, w), 1604 (br, m), 1432 (m, P-Ph), 1168 (m), 1131 (w), 1095 (m), 902 (m), 751 (m), 702 (s). Crystals of [16]PF₆ suitable for X-ray diffraction were obtained by the addition of 1.5

equivalents of potassium hexafluorophosphate to a methanol solution of [16]Cl followed by filtration and slow evaporation.

8.5.3 [RuCl(dppp)(cis-tach)]Cl, [17]Cl

A solution of [8]Cl (53.9 mg, 0.117 mmol) in methanol (10 mL) was heated under reflux with propane-1,3-diylbis(diphenylphosphane) (97.3 mg, 0.236 mmol) for 18 h. The solvent was removed *in vacuo*, recrystallised three times in dichloromethane/diethyl ether, collected by filtration and the pale cream product dried *in vacuo*. Yield: 60.1 mg (69%, 0.0802 mmol of [RuCl(dppp)(cis-tach)]Cl.2H₂O). Found: C 52.65; H 5.80; N 5.39%. Calcd for C₃₃H₄₁N₃P₂Cl₂Ru(2H₂O): C 52.87; H 6.05; N 5.61%. ¹H NMR (CD₃OD, 500.2 MHz, 295K) δ 7.66 (br. s, 4H, PPh₂, Ar^{2b}), 7.54 (t, ³J_{HH} = 7.5 Hz, 2H, PPh₂, Ar^{4a}), 7.47 (m, 6H, PPh₂, Ar^{4b} + Ar^{3b}), 7.44 (t, ³J_{HH} = 7.5 Hz, 4H, PPh₂, Ar^{3a}), 7.12 (app. t, ³J_{HP} = 9.2 Hz, ³J_{HH} = 7.5 Hz, 4H, PPh₂, Ar^{2a}), 3.61 (d, 2H, ²J_{HH} = 11.8 Hz, NH₂, N²), 3.29 (s, 2H, CH, Cy²), 3.20 (d, 2H, ²J_{HH} = 11.8 Hz, NH₂, N²), 3.02 (s, 1H, CH, Cy¹), 2.82 (m, 2H, PCH₂, Br¹), 2.80 (s, 2H NH₂, N¹), 2.34 (m, 2H, PCH₂ Br¹), 2.28 (m, 1H, PCH₂CH₂, Br²), 2.00 (d, 1H, ²J_{HH} = 15.0 Hz, CH₂, Cy⁴), 1.90 (d, 1H, ²J_{HH} = 15.0 Hz, CH₂, Cy⁴), 1.83 (d, 2H, ²J_{HH} = 15.3 Hz, CH₂, Cy³), 1.74 (d, 2H, ²J_{HH} = 15.3 Hz, CH₂, Cy³), 1.60 (m, ΣJ_{HH,HP} = 60.0 Hz, ²J_{HH} = 13.6, ³J_{HH} = 13.6 1H, PCH₂CH₂, Br²); ³¹P{¹H} NMR (CD₃OD, 202.5 MHz, 295K) δ 44.0 (s, 2P, PPh₂); ¹³C{¹H} NMR (CD₃OD, 125.8 MHz, 295K) δ 136.4 (t, |¹J_{PC} + ³J_{P'Cl}| = 37 Hz, PPh₂, Ar^{1a}), 134.5 (t, |¹J_{PC} + ³J_{P'Cl}| = 35 Hz, PPh₂, Ar^{1b}), 134.3 (t, |²J_{PC} + ⁴J_{P'Cl}| = 5 Hz, PPh₂, Ar^{2a}), 133.7 (t, |²J_{PC} + ⁴J_{P'Cl}| = 4 Hz, PPh₂, Ar^{2b}), 131.4 (s, PPh₂, Ar^{4a}), 130.9 (s, PPh₂, Ar^{4b}), 130.5 (t, |³J_{PC} + ⁵J_{P'Cl}| = 8.5 Hz, PPh₂, Ar^{3a}), 129.9 (t, |³J_{PC} + ⁵J_{P'Cl}| = 8.5 Hz, PPh₂, Ar^{3b}), 44.5 (s, CH, Cy²), 44.3 (s, CH, Cy¹), 35.2 (s, CH₂, Cy⁴), 34.4 (s, CH₂, Cy³), 29.3 (t, |¹J_{PC} + ³J_{P'Cl}| = 35 Hz, PCH₂, Br¹), 20.9 (s, PCH₂CH₂, Br²). ESI-MS: *m/z* 678.1505 ([17]⁺, Calc. for C₃₃H₄₁N₃P₂ClRu⁺: 678.1508, 100%). ATR-IR (cm⁻¹): 3399 (vbr, s), 3290 (w), 3158 (w), 3052 (br, w), 2916 (br, w), 1587 (br, m), 1483 (w), 1433 (m, P-Ph), 1370 (w), 1133 (m, br), 1094 (m), 902 (m), 747 (m), 699 (s). Crystals of [17][Cl] suitable for X-ray diffraction were obtained by the slow evaporation of a saturated methanol solution.

8.5.4 [RuCl(dppb)(cis-tach)]Cl, [18]Cl

A solution of [8]Cl (50.0 mg, 0.109 mmol) in methanol (10 mL) was heated under reflux with butane-1,4-diylbis(diphenylphosphane) (90.1 mg, 0.211 mmol) for 18 h. The solvent was removed *in vacuo*, and the residue recrystallised twice in dichloromethane/diethyl ether, and the product was dried *in vacuo*. Yield: 45.2 mg (55%, 0.0599 mmol of [RuCl(dppb)(cis-tach)]Cl·1½H₂O). Found: C 54.16; H 6.01; N 5.84%. Calcd for C₃₄H₄₃N₃P₂Cl₂Ru(1½ H₂O): C 54.11; H 6.14; N 5.56%. ¹H NMR (CD₃OD, 500.2 MHz, 295K) δ 7.67 (ddd, ³J_{HP} = 12.0 Hz ³J_{HH} = 7.3, ⁴J_{HH} = 1.5, 4H, PPh₂, Ar^{2a}), 7.61 (m, 6H, PPh₂, Ar^{3b} + Ar^{4b}), 7.47 (m, ³J_{HP} = 9.6 Hz ³J_{HH} = 7.0, ⁴J_{HH} = 1.5, 4H, PPh₂, Ar^{2b}), 7.42 (m, 6H, PPh₂, Ar^{3a} + Ar^{4a}), 3.70 (d, 2H, ²J_{HH} = 11.8 Hz, NH₂, N²), 3.33 (d, 2H, ²J_{HH} = 11.8 Hz, NH₂, N²), 3.21 (m, 4H: 2H, CH, Cy²; 2H, PCH₂, Br¹), 2.65 (s, 1H, CH, Cy¹), 2.55 (s, 2H, NH₂, N¹), 2.34 (m, ΣJ_{HH,HP} = 30.5 Hz, ²J_{HH} = 13.6, ²J_{HH} = 5.3, PCH₂, Br¹), 2.00 (d, 1H, ²J_{HH} = 15.0 Hz, CH₂, Cy⁴), 1.93 (m, 2H, PCH₂CH₂, Br²), 1.88 (d, 1H, ²J_{HH} = 15.0 Hz, CH₂, Cy⁴), 1.67 (d, 2H, ²J_{HH} = 15.0 Hz, CH₂, Cy³), 1.49 (d, 2H, ²J_{HH} = 15.0 Hz, CH₂, Cy³), 1.35 (vquint, ΣJ_{HH,HP} = 49.0 Hz, ²J_{HH} = ³J_{HH} = 12.0, 2H, PCH₂CH₂, Br²); ³¹P{¹H} NMR (CD₃OD, 202.5 MHz, 295K) δ 46.8 (s, 2P, PPh₂); ¹³C{¹H} NMR (CD₃OD, 125.8 MHz, 295K) δ 139.1 (t, |¹J_{PC} + ³J_{P'C}| = 36 Hz, PPh₂, Ar^{1a}), 135.8 (t, |¹J_{PC} + ³J_{P'C}| = 34 Hz, PPh₂, Ar^{1b}), 135.0 (t, |²J_{PC} + ⁴J_{P'C}| = 9 Hz, PPh₂, Ar^{2b}), 134.4 (t, |²J_{PC} + ⁴J_{P'C}| = 9 Hz, PPh₂, Ar^{2a}), 131.8 (s, PPh₂, Ar^{4b}), 130.8 (s, PPh₂, Ar^{4a}), 130.1 (t, |³J_{PC} + ⁵J_{P'C}| = 8 Hz, PPh₂, Ar^{3b}), 129.7 (t, |³J_{PC} + ⁵J_{P'C}| = 8.5 Hz, PPh₂, Ar^{3a}), 44.3 (s, CH, Cy²), 44.0 (s, CH, Cy¹), 35.5 (s, CH₂, Cy⁴), 33.6 (s, CH₂, Cy³), 33.1 (t, |¹J_{PC} + ³J_{P'C}| = 30 Hz, PCH₂, Br¹), 23.9 (s, PCH₂CH₂, Br²). ESI-MS: *m/z* 692.1662 ([18]⁺, Calc. for C₃₄H₄₃N₃P₂ClRu⁺: 692.1665, 100%). ATR-IR (cm⁻¹): 3270 (vbr, s), 2925 (m), 2856 (w), 1599 (br, m), 1483 (w), 1433 (m, P-Ph), 1352 (w), 1228 (w), 1176 (m), 1144 (m), 1092 (m), 1006 (w), 903 (s), 815 (s), 700 (s). Crystals of [18]Cl suitable for X-ray diffraction were obtained from the standing on an aqueous solution of [18]Cl.

8.5.5 [RuCl(dppv)(cis-tach)]Cl, [19]Cl

A solution of [8]Cl (50.0 mg, 0.109 mmol) in methanol (5 mL) was heated under reflux with (*Z*)-ethylene-1,2-bis(diphenylphosphane) (80.0 mg, 0.202 mmol) under an argon atmosphere for 24 h, resulting in an orange solution. The solution was

allowed to cool, the insoluble phosphane was removed by filtration, and diethyl ether (50 mL) added, forming a pale yellow precipitate. The product was collected by filtration and dried *in vacuo*. Yield: 39.5 mg (50%, 0.0545 mmol of [RuCl(dppv)(*cis*-tach)]Cl·H₂O). Found: C 53.70; H 5.48; N 5.89%. Calcd for C₃₂H₃₇N₃P₂Cl₂Ru(H₂O): C 53.71; H 5.49; N 5.87%. ¹H NMR (CD₃OD, 500.2 MHz, 295K) δ 7.99 (t, ³J_{HP} = 10.9 Hz, ³J_{HH} = 7.6, ⁴J_{HH} = 1.5, 4H, PPh₂, Ar^{2a}), 7.94 (vd, |²J_{PH} + ³J_{P'H}| = 60.7 Hz, 2H, PCH=CHP, Br¹), 7.52 (t, ³J_{HP} = 10.1 Hz, ³J_{HH} = 7.6, ⁴J_{HH} = 1.5, 4H, PPh₂, Ar^{2b}), 7.47 (t, ³J_{HH} = 7.5 Hz, 4H, PPh₂, Ar^{3a}), 7.43 (m, 8H, PPh₂, Ar^{3b} + Ar^{4a} + Ar^{4b}), 5.17 (d, 2H, ²J_{HH} = 11.4 Hz, NH₂, N²), 3.99 (d, 2H, ²J_{HH} = 11.4 Hz, NH₂, N²), 3.59 (s, 2H, CH, Cy²), 2.46 (s, 1H, CH, Cy¹), 2.32 (d, 1H, ²J_{HH} = 15.1 Hz, CH₂, Cy⁴), 2.13 (d, 1H, ²J_{HH} = 15.1 Hz, CH₂, Cy⁴), 1.77 (d, 2H, ²J_{HH} = 15.0 Hz, CH₂, Cy³), 1.40 (d, 2H, ²J_{HH} = 15.0 Hz, CH₂, Cy³), 0.94 (s, 2H, NH₂, N¹); ³¹P{¹H} NMR (CD₃OD, 202.5 MHz, 295K) δ 76.5 (s, 2P, PPh₂); ¹³C{¹H} NMR (CD₃OD, 125.8 MHz, 295K) δ 152.4 (vd, |¹J_{PC} + ²J_{P'C}| = 69.5 Hz, PCH=CHP, Br¹), 136.0 (vquint., |²J_{PC} + ⁴J_{P'C}| = 18 Hz, PPh₂, Ar^{2a}), 135.7 (vd, |¹J_{PC} + ³J_{P'C}| = 43 Hz, PPh₂, Ar^{1a}), 133.6 (vd, |¹J_{PC} + ³J_{P'C}| = 43 Hz, PPh₂, Ar^{1b}), 132.4 (vquint., |²J_{PC} + ⁴J_{P'C}| = 17.5 Hz, PPh₂, Ar^{2b}), 131.5 (s, PPh₂, Ar^{4a}), 131.3 (s, PPh₂, Ar^{4b}), 130.7 (vquint., |³J_{PC} + ⁵J_{P'C}| = 17.5 Hz, PPh₂, Ar^{3a}), 129.4 (vquint., |³J_{PC} + ⁵J_{P'C}| = 18 Hz, PPh₂, Ar^{3b}), 44.6 (s, CH, Cy²), 44.1 (s, CH, Cy¹), 35.6 (s, CH₂, Cy⁴), 34.3 (s, CH₂, Cy³). ESI-MS: *m/z* 662.1195 ([19]⁺, Calc. for C₃₂H₃₇N₃P₂ClRu⁺: 622.1194, 100%). ATR-IR (cm⁻¹): 3462 (br, w), 3284 (m), 3245 (m), 3144 (br, w), 2934 (br, w), 1647 (w), 1596 (w), 1481 (w), 1435 (m P-Ph), 1372 (w), 1176 (m), 1129 (w), 1093 (m), 998 (w), 902 (m), 755 (s), 701 (s). Crystals of [19]Cl suitable for X-ray diffraction analysis were obtained from the slow diffusion of diethyl ether into a methanol solution of [19]Cl.

8.5.6 [RuCl(dppben)(*cis*-tach)]Cl, [20]Cl

A solution of [8]Cl (50.0 mg, 0.109 mmol) in methanol (5 mL) with phenylene-1,2-bis(diphenylphosphane) (80 mg, 0.179 mmol) was heated at 90 °C in sealed ampoule under argon for 48 h. The deep orange solution was allowed to cool, over which a white precipitate formed. The unreacted phosphane precipitate was removed by filtration and diethyl ether (90 mL) added to the solution, forming a cream precipitate. The mixture was cooled to -20 °C for 2 h, the product isolated by

filtration and dried *in vacuo*. Yield: 58.6 mg (69%, 0.0748 mmol of [RuCl(dppben)(*cis*-tach)]Cl·2H₂O). Found: C 55.50; H 5.44; N 5.33%. Calcd for C₃₆H₃₉N₃P₂Cl₂Ru(2 H₂O): C 55.18; H 5.53; N 5.36%. **¹H NMR** (CD₃OD, 500.2 MHz, 295K) δ 8.07 (ddd, ³J_{HP} = 11.0 Hz, ³J_{HH} = 7.5 Hz, ⁴J_{HH} = 1.2 Hz, 4H, PPh₂, Ar^{2a}), 7.52 (m, 6H: 2H, PPh₂, Ar^{4a}; 4H, PC₆H₄P, Br² + Br³), 7.44 (t, ³J_{HH} = 7.5 Hz, 4H, PPh₂, Ar^{3a}), 7.39 (dd, ³J_{HH} = 7.4 Hz, ³J_{HH} = 7.2 Hz, 4H, PPh₂, Ar^{3b}), 7.34 (td, ³J_{HH} = 7.2 Hz, ⁴J_{HH} = 1.4 Hz, 4H, PPh₂, Ar^{4b}), 7.34 (ddd, ³J_{HP} = 10.0 Hz, ³J_{HH} = 7.4 Hz, ⁴J_{HH} = 1.4 Hz, 4H, PPh₂, Ar^{4b}), 4.93 (d, ²J_{HH} = 11.8 Hz, 2H, NH₂, N²), 3.87 (d, ²J_{HH} = 11.8 Hz, 2H, NH₂, N²), 3.56 (s, 2H, CH, Cy²), 2.72 (s, 1H, CH, Cy¹), 2.30 (d, ²J_{HH} = 15.4 Hz, 1H, CH₂, Cy⁴), 2.14 (d, ²J_{HH} = 15.4 Hz, 1H, CH₂, Cy⁴), 1.86 (d, ²J_{HH} = 15.2 Hz, 2H, CH₂, Cy³), 1.74 (d, ²J_{HH} = 15.2 Hz, 2H, CH₂, Cy³), 1.39 (s, 2H, NH₂, N²); **³¹P{¹H} NMR** (CD₃OD, 202.5 MHz, 295K) δ 72.9 (s, 2P, PPh₂); **¹³C{¹H} NMR** (CD₃OD, 125.8 MHz, 295K) δ 145.6 (vt, |¹J_{PC} + ²J_{P'C}| = 82 Hz, PC₆H₄P, Br¹), 139.9 (t, |²J_{PC} + ⁴J_{P'C}| = 10 Hz, PPh₂, Ar^{2a}), 133.6 (m, PPh₂, Ar^{1a} + Ar^{1b}), 133.5 (t, |²J_{PC} + ³J_{P'C}| = 17 Hz, PC₆H₄P, Br²), 133.0 (t, |²J_{PC} + ⁴J_{P'C}| = 9 Hz, PPh₂, Ar^{2b}), 131.8 (s, PC₆H₄P, Br³; s, PPh₂, Ar^{4a}), 131.1 (s, PPh₂, Ar^{4b}), 130.5 (t, |³J_{PC} + ⁵J_{P'C}| = 9 Hz, PPh₂, Ar^{3b}), 129.5 (t, |³J_{PC} + ⁵J_{P'C}| = 9 Hz, PPh₂, Ar^{3a}), 44.7 (s, CH, Cy²), 44.4 (s, CH, Cy¹), 35.6 (s, CH₂, Cy⁴), 34.3 (s, CH₂, Cy³). **ESI-MS**: *m/z* 712.1372 ([**20**]⁺, Calc. for C₃₆H₃₉N₃P₂ClRu: 712.1352⁺, 100%). **IR (ATR)** (cm⁻¹): 3646 (br, w), 3282 (w), 3241 (w), 3110 (vbr, m), 3069 (br, w), 2914 (br, w), 1611 (br, m), 1482 (w), 1431 (m, P-Ph), 1368 (w), 1170 (s), 1127 (w), 1091 (s), 902 (m), 754 (s), 701 (s). Crystals of [**20**]Cl suitable for X-ray diffraction analysis were obtained from the slow diffusion of diethyl ether into a methanol solution of [**20**]Cl.

8.6 Chapter 6 Experimental

8.6.1 NMR Spectroscopy

NMR experiments were performed using a Bruker AV 500 spectrometer operating at 500.23 MHz (¹H) and 202.50 (³¹P). ¹H NMR experiments using solvent suppression techniques used the zgesgp pulse program with 1D excitation sculpting (using 180° water-selective pulses). Quantitative phosphorus experiments were performed using the zgig pulse program with a relaxation delay (D1) of 10 s. Unless otherwise stated,

all NMR experiments were performed at in H₂O supplemented with 1.6% CD₃OD as a lock solvent and solvent suppression techniques employed.

8.6.2 Mass Spectrometry of Aquation Products

A solution of [16]Cl or [17]Cl (300 μM) in H₂O or D₂O (5 mL) was heated at 310 K for 2 h. The solution was diluted to 15 mL with H₂O or D₂O and 5 mL CH₃OH or CD₃OD added, giving a final concentration of approximately 75 μM. The ESI mass spectrum was recorded on a Bruker Esquire instrument.

	Solvent	[M] ⁺ (calc, %)	[M-Cl+OH] ⁺ ^a (calc, %)	[M-Cl] ²⁺ (calc, %)
[16]Cl	H ₂ O	664.0 (664.1, 10)	646.1 (646.2, 50)	314.6 (314.6, 100)
[16]Cl	D ₂ O	664.1 (664.1, 60)	647.2 (647.1, 100)	314.7 (314.6, 75)
[17]Cl	H ₂ O	678.1 (678.2, 100)	660.1 (660.2, 20)	321.6 (321.6, 60)
[17]Cl	D ₂ O	678.1 (678.1, 100)	661.2 (661.2, 60)	321.6 (321.6, 40)

Table 8.4: ESI-MS data for aquation of [16]Cl and [17]Cl in H₂O and D₂O. ^a) [M-Cl+OD]⁺ when in D₂O.

8.6.3 [Ru(OH₂)(dppe)(cis-tach)](OTf)₂, [16a](OTf)₂

A solution of [16]Cl (500 μM) and silver triflate (2 equiv) in H₂O (25 mL) was stirred for 18 h, shielded from light. The resulting suspension was filtered over celite to remove the insoluble silver chloride. 1,4-dioxane (1 equiv, reference at δ_H 3.75) and CD₃OD (1.6%) were added to the solution. NMR spectra were recorded on a Bruker Avance AV500 spectrometer at 310 K using solvent suppression techniques and CD₃OD as deuterium lock. ¹H NMR (H₂O, 500.2 MHz, 298K) δ 7.62 (t, *J* = 8.6 Hz, 4H, PPh₂), 7.50 (m, 16H, PPh₂), 4.27 (d, ²J_{HH} = 12.5 Hz, 2H, NH₂, N^{2*}), 3.37 (s, 2H, CH, Cy²), 3.12 (m, 2H, PCH₂), 2.68 (m, 2H, PCH₂), 2.38 (s, 1H, CH, Cy¹), 2.27 (d, ²J_{HH} = 14.8 Hz, 1H, CH₂, Cy⁴), 2.18(d, ²J_{HH} = 14.8 Hz, 1H, CH₂, Cy⁴), 1.74 (d, ²J_{HH} = 17.7 Hz, 2H, CH₂, Cy³), 1.26 (s, 2H, NH₂, N¹), 0.99 (d, ²J_{HH} = 17.7 Hz, 2H, CH₂, Cy³); ³¹P{¹H} NMR (H₂O, 202.5 MHz, 295K) δ 74.6 (s, 2P, PPh₂). *

Integration suppressed and geminal resonance not observed due to solvent suppression technique.

8.6.4 [Ru(OH₂)(dppp)(cis-tach)](OTf)₂, [17a](OTf)₂

A solution of [17]Cl (500 μM) and silver triflate (2 equiv) in H₂O (25 mL) was stirred for 18 h, shielded from light. The resulting suspension was filtered over celite to remove the insoluble silver chloride. 1,4-dioxane (1 equiv, reference at δ_H 3.75) and CD₃OD (1.6%) were added to the solution. NMR spectra were recorded on a Bruker Avance AV500 spectrometer at 310 K using solvent suppression techniques and CD₃OD as deuterium lock. ¹H NMR (H₂O, 500.2 MHz, 298K) δ 7.59 (*app* q, *J* = 7.4 Hz, 2H, PPh₂), 7.54 (d, *J* = 7.6 Hz, 2H, PPh₂), 7.50 (t, *J* = 7.4 Hz, 8H, PPh₂), 7.42 (t, *J* = 7.6 Hz, 4H, PPh₂), 7.25 (t, *J* = 7.4 Hz, 4H, PPh₂), 3.78 (d, ²J_{HH} = 15.3 Hz, NH₂, N²), 3.35 (m, 4H; 2H, NH₂, N²; 2H CH*, Cy²), 2.90 (s, 1H, CH, Cy¹), 2.64 (m, 2H, PCH₂), 2.45 (m, 4H; 2H, PCH₂; 2H NH₂*, N¹), 2.27 (m, 1H, PCH₂CH₂), 1.99 (*app.* s, 2H; CH₂, Cy⁴), 1.92 (m, 1H, PCH₂CH₂), 1.82 (d, ²J_{HH} = 17.5 Hz, 2H, CH₂, Cy³), 1.46 (d, ²J_{HH} = 17.5 Hz, 2H, CH₂, Cy³); ³¹P{¹H} NMR (H₂O, 202.5 MHz, 295K) δ 41.7 (s, 2P, PPh₂). * Unable to unequivocally assign resonances without ¹H/¹³C 2D correlation spectrum.

8.6.5 NMR Sample Preparation – Aqueation Experiments

Sodium phosphate solutions were prepared prior to addition of ruthenium complex. Desired salts (where stated, e.g. NaCl, 4–100 mM) were added to NaH₂PO₄ and Na₂HPO₄ solutions (10 mM) in Millipore water. The Na₂HPO₄ solution was titrated to pH 7.4 using the NaH₂PO₄ solution at 310 K. Solutions were stored in the dark in a sealed vessel prior to use.

A stock solution of [16]Cl or [17]Cl (50 μL, 20 mM) in CD₃OD was added to the sodium phosphate solution (3 mL) giving a final concentration of approximately 300 μM. The solutions were heated at 310 K for 2 h prior to loading in the spectrometer. ¹H and/or ³¹P{¹H} NMR spectra were recorded on a Bruker Avance AV500 spectrometer at 310 K using solvent suppression techniques and CD₃OD as deuterium lock.

Determination of Phosphate Complex

Procedure for NMR sample preparation was followed; however sodium phosphate solutions used were 0, 10 and 20 mM concentrations.

Low Concentration NMR Studies

For [16]Cl, a 50 μM solution was prepared in 10% $\text{D}_2\text{O}/90\%$ H_2O and heated at 310 K for 2 h. The ^1H NMR spectrum was recorded on a Bruker Avance AV 700 spectrometer at 310 K. For [17]Cl, the NMR sample preparation was followed, however the solution was diluted with 1.6% $\text{CD}_3\text{OD}/\text{H}_2\text{O}$ to 10 μM and the ^1H NMR spectrum recorded on a Bruker Avance AV 500.

Stability Studies

The NMR sample preparation was followed, however ^1H NMR spectra were recorded after 1, 24 and 48 h of heating at 310 K.

8.6.6 pH Titrations

Solutions of the aqua complexes [16a](OTf)₂ and [17a](OTf)₂ were prepared by the addition of silver triflate (2 equiv) to a solution of [16]Cl and [16]Cl (500 μM) in H_2O (25 mL). The solutions were stirred for 18 h, shielded from light. The resulting suspension was filtered over celite, and 1,4-dioxane (1 equiv) and CD_3OD (1.6%) added. pH values were adjusted using triflic acid (0.1 M) or sodium hydroxide (0.01, 0.1 and 1 M) supplemented with 1.6% CD_3OD to between pH 2 and 12. A small amount of leakage of Cl^- ions from the electrode occurred into the solutions, as evident in the UV/Vis titration of [17a]²⁺. UV/Vis spectra were recorded on an Agilent Technologies UV-Vis Diode Array spectrometer, and ^1H NMR spectra on a Bruker Avance AV500 spectrometer using solvent suppression techniques and CD_3OD as deuterium lock. Solutions were maintained at 298 K throughout the experiment. Selected resonances were fitted to the Henderson-Hasselbalch equation with the assumption that the observed chemical shifts are weighted averages according to the populations of the protonated and deprotonated species.

8.6.7 Kinetics of Aquation

Sodium phosphate solutions were prepared prior to addition of ruthenium complex. NaH_2PO_4 and Na_2HPO_4 solutions (10 mM) were prepared in Millipore water and the Na_2HPO_4 solution was titrated to pH 7.4 using the NaH_2PO_4 solution at the temperature to be used (288 – 310 K). Solutions were stored in the dark in a sealed vessel prior to use.

A stock solution of [16]Cl or [17]Cl (50 μL , 20 mM) in CD_3OD was added to a sodium phosphate solution (3 mL, pH 7.4, no added salts) giving a final concentration of approx. 300 μM *in situ*. The absorbance was recorded at 5 (single wavelength, $\lambda = 310/300$ nm for [16]Cl/[17]Cl) or 20 s (diode array) intervals at $T = 288\text{--}310$ K. After the reaction was complete (no change in absorbance was observed), the ^1H NMR spectrum was recorded using a Bruker Avance AV500 spectrometer at the required temperature (288 – 310 K) using solvent suppression techniques and CD_3OD as deuterium lock. The proportions of the aqua and chlorido species were obtained from ^1H NMR integrations and the equilibrium constant, K , calculated by Eqn. 9.1.

$$K = \frac{[\text{aqua}][\text{Cl}^-]}{[\text{chlorido}]}$$

Equation 8.1: Calculation of the equilibrium constant, K , for the aquation of [16]Cl and [19]Cl. The concentration of Cl^- was calculated from those of the ruthenium complexes.

The initial and final absorbance values for the kinetic profile was calculated using DynaFit,²⁴⁹ and the absorption coefficients for the chlorido and aqua species calculated using Eqn. 9.2, assuming no contribution to the absorbance from the minor amounts of phosphate complex (< 2.5%)

$$Abs = \varepsilon_{aqua}[aqua] + \varepsilon_{chlorido}[chlorido]$$

Equation 8.2: Calculation of the absorption coefficients for the aqua and chlorido complexes.

The absorbance coefficients were applied to the Dynafit script and the time-absorbance data fitted to first order reaction $[X]^+ \rightarrow [Y]^{2+} + Cl^-$, giving the first order rate constant (k). The anation rate constant (k') was calculated using the equation $k' = k / K$.

Full kinetic analysis of [17]Cl was not performed due to limitations of the reaction. However, analysis was performed at 298 K using the same technique as for [16]Cl, but the absorbance was measured at 300 nm (for [17]Cl).

8.6.8 Equilibrium Constants

NMR Samples were prepared in the same manner as *Kinetics of Aquation* (Section 8.6.7), however with addition of NaCl (0 to 100 mM) to the buffer solution prior to titration to pH 7.4. Samples were heated at 310 K for 2 h. 1H NMR spectra were recorded on a Bruker Avance AV500 spectrometer at 310 K using solvent suppression techniques and CD_3OD as deuterium lock. $^{31}P\{^1H\}$ NMR spectra were recorded on a Bruker Avance AV500 spectrometer at 310 K using CD_3OD as deuterium lock and the zgig pulse sequence ($d1 = 10$ s).

8.6.9 NMR Sample Preparation – Guanine and GSH Experiments

A solution of [16]Cl or [17]Cl (1 mM) and 9-EtG, GMP or GSH (1 mM) in H_2O (5 mL) with CD_3OD (85 μ L, 1.6%) was heated at 310 K for 24 h. 1H and $^{31}P\{^1H\}$ NMR spectra were recorded on a Bruker Avance AV500 spectrometer at 310 K using solvent suppression techniques and CD_3OD as deuterium lock. NMR spectra of a negative control for each complex (complex only, 1 mM, without 9-EtG, GMP or GSH) was also obtained after 24 h at 310 K.

8.6.10 Mass Spectroscopy of [16]Cl with Guo

A solution of [16]Cl (1 mM) and Guo (2 mM) in H₂O (5 mL) 310 K for 24 h. 50% methanol was added to an aliquot of the solution and the ESI mass spectrum recorded on a Bruker Esquire instrument.

m/z	Ion	Calc. for	Calc.	Height (%)
911.1	[16-Cl+Guo] ⁺		911.3	30
664.1	[16] ⁺		664.1	100
646.2	[16-Cl+OH] ⁺		646.2	30
456.2	[16-Cl+Guo] ²⁺		456.1	30
314.7	[16-Cl] ²⁺		314.6	70

Table 8.5: ESI-MS data for the reaction of [16]Cl with Guo.

8.6.11 Interaction of Ruthenium Complexes with pUC18 Plasmid DNA

Aliquots (10 μL) of pUC18 plasmid DNA (105 ng, 161 μM bp) were incubated at 37°C for 20 h with between 0.025 and 1.0 bpe (base pair equivalents) of the ruthenium complexes [16]Cl or [17]Cl. After incubation, gel loading buffer (3 μL) was added to the samples, and separated by electrophoresis in 1% agarose gel for 1 h at 100 V, 400 mA using Tris-acetate-EDTA buffer (TAE). The gel was stained with ethidium bromide solution for 5 minutes and imaged by UV. Cisplatin (0.1 bpe) and pUC18 linearised by a single cut with SmaI were employed as controls.

8.6.12 DFT Calculations

Initial optimisations were performed at the (RI-)BP86/SV(P) level, followed by frequency calculations at the same level. All minima were confirmed as such by the absence of imaginary frequencies and all transition states were identified by the presence of only one imaginary frequency.

Single-point calculations on the (RI-)BP86/SV(P) optimised geometries were performed using the hybrid PBE0 functional and the flexible def2-TZVPP basis set. The (RI-)PBE0/def2-TZVPP SCF energies were corrected for their zero point energies, thermal energies and entropies (obtained from the (RI-)BP86/SV(P)-level frequency calculations). In all calculations, a 28 electron quasi-relativistic ECP replaced the core electrons of Ru. No symmetry constraints were applied during optimisations. All calculations were performed using the TURBOMOLE V5.10 package using the resolution of identity (RI) approximation.²⁹⁹

Appendix I. ORTEP Diagrams of [17–20]Cl

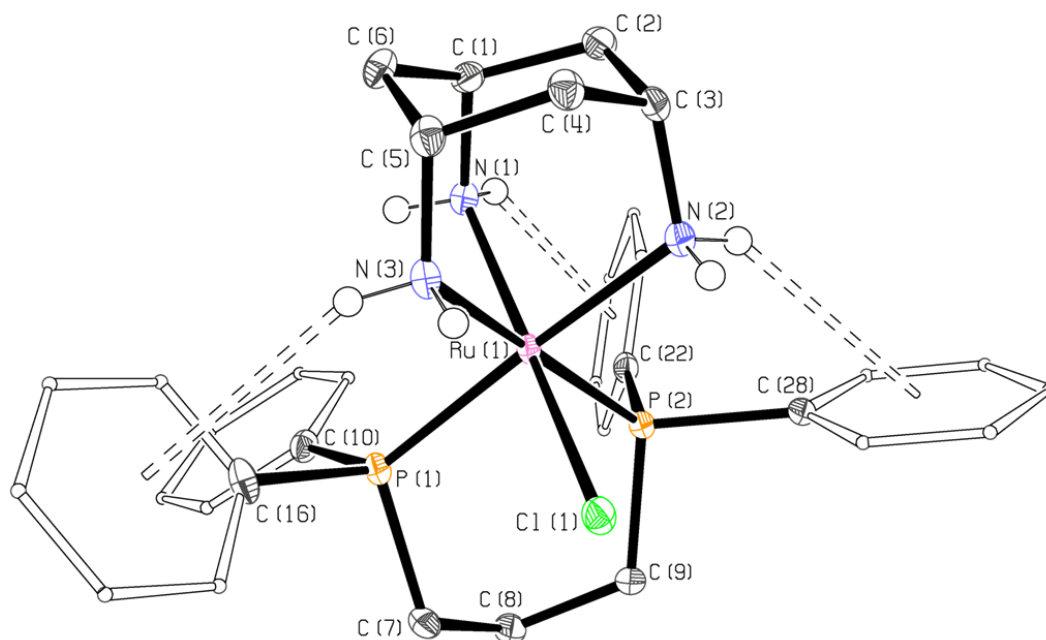


Figure I.1: ORTEP (50% probability ellipsoids) diagram of [17]Cl(H₂O)_{2.15}.MeOH. Hydrogen atoms (except for amino hydrogens), counter ion and solvent of crystallisation are omitted for clarity. Selected bond lengths (Å) and angles (°): Ru(1)–N(1) 2.133(2), Ru(1)–N(2) 2.182(2), Ru(1)–N(3) 2.185(2), Ru(1)–P(1) 2.2721(1), Ru(1)–P(2) 2.2836(1), Ru(1)–Cl(1) 2.4404(1), N(1)–Ru(1)–N(2) 90.77(6), N(1)–Ru(1)–N(3) 87.28(6), N(2)–Ru(1)–N(3) 82.11(7), N(1)–Ru(1)–Cl(1) 169.78(4), N(2)–Ru(1)–P(1) 173.01(5), N(3)–Ru(1)–P(2) 172.47(5), P(1)–Ru(1)–P(2) 89.481(17), P(1)–Ru(1)–Cl(1) 88.939(17), P(2)–Ru(1)–Cl(1) 90.332(16). Selected hydrogen-bond (D–H...A–X) lengths (Å) and angles (°) D...A, H...A, D–H...A, H...A–X, H...X (A = centroid and X = plane of respective phenyl ring of atom *): N(1)–H(1a)...C(22)* 4.29, 3.53, 147, 35.7, 2.06 (V); N(2)–H(2d)...C(28)* 3.99, 3.28, 147, 48.2, 2.44 (V); N(3)–H(3b)...C(16)* 3.77, 2.99, 156, 52.1, 3.26 (V). Malone hydrogen-bond type is given in parenthesis.²⁰⁶

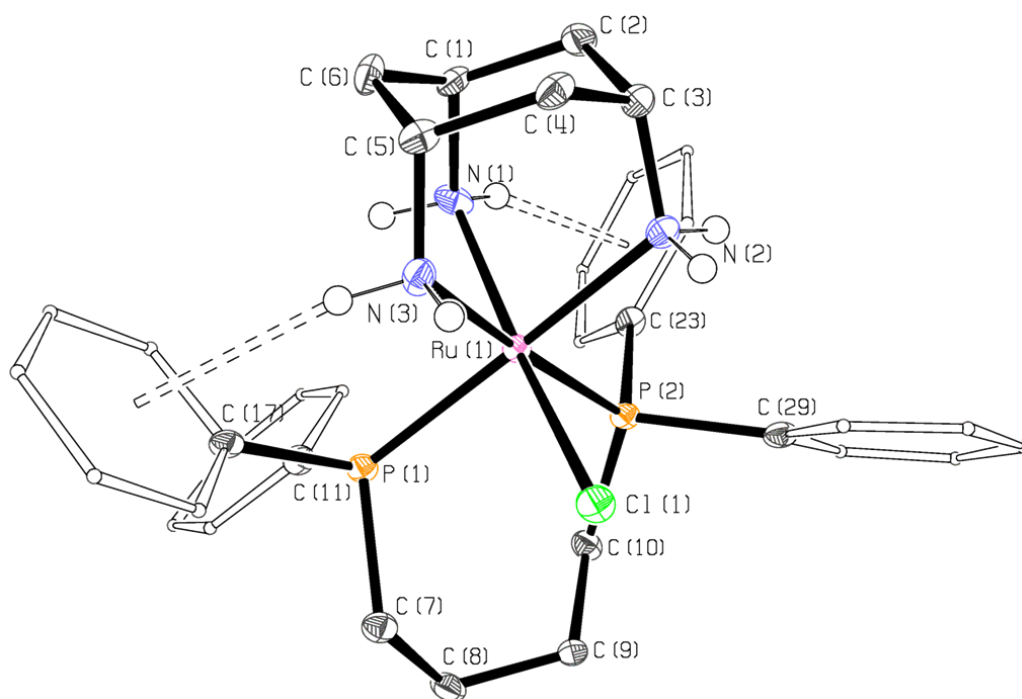


Figure I.2: ORTEP (50% probability ellipsoids) diagram of **[18]Cl(H₂O)₄**. Hydrogen atoms (except for amino hydrogens), counter ion and solvent of crystallisation are omitted for clarity. Selected bond lengths (Å) and angles (°): Ru(1)–N(1) 2.139(4), Ru(1)–N(2) 2.172(4), Ru(1)–N(3) 2.174(5), Ru(1)–P(1) 2.2872(13), Ru(1)–P(2) 2.2860(14), Ru(1)–Cl(1) 2.4379(12), N(1)–Ru(1)–N(2) 86.67(16), N(1)–Ru(1)–N(3) 87.22(16), N(2)–Ru(1)–N(3) 82.67(17), N(1)–Ru(1)–Cl(1) 168.19(12), N(2)–Ru(1)–P(1) 173.32(12), N(3)–Ru(1)–P(2) 174.30(12), P(1)–Ru(1)–P(2) 92.98(5), P(1)–Ru(1)–Cl(1) 90.44(4), P(2)–Ru(1)–Cl(1) 93.48(5). Selected hydrogen-bond (D–H...A–X) lengths (Å) and angles (°) D...A, H...A, D–H...A, H...A–X, H...X (A = centroid and X = plane of respective phenyl ring of atom *): N(1)–H(1a)...C(23)* 3.87, 3.00, 164, 55.9, 2.43 (V); N(3)–H(3a)...C(17)* 3.47, 2.58, 169, 63.5, 2.31 (V). Malone hydrogen-bond type is given in parenthesis.²⁰⁶

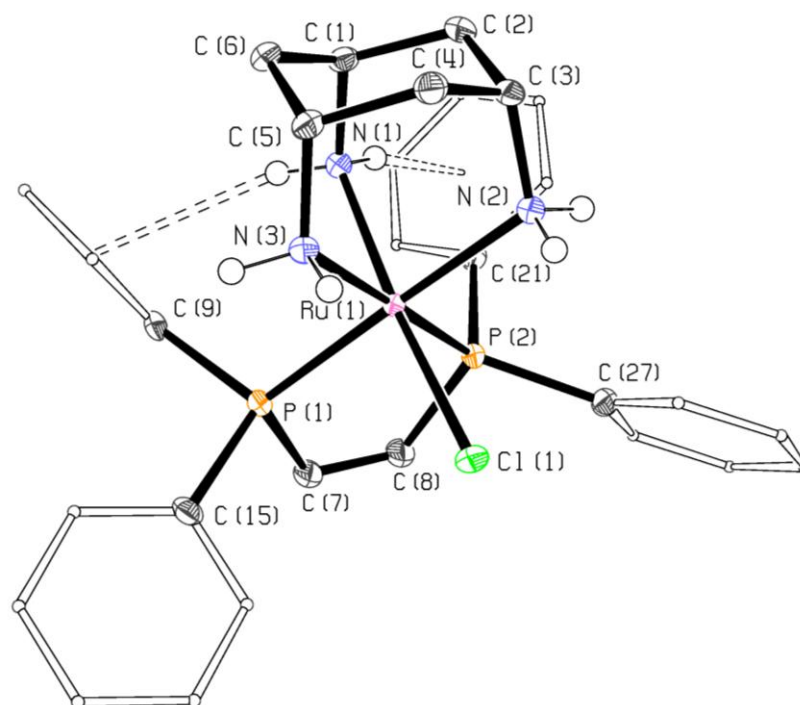


Figure I.3: ORTEP (50% probability ellipsoids) diagram of $[19]Cl(H_2O)_{1.5}$. Hydrogen atoms (except for amino hydrogens), counter ion and solvent of crystallisation are omitted for clarity. Selected bond lengths (\AA) and angles ($^\circ$): Ru(1)–N(1) 2.1266(15), Ru(1)–N(2) 2.1932(15), Ru(1)–N(3) 2.2003(15), Ru(1)–P(1) 2.2661(5), Ru(1)–P(2) 2.2699(5), Ru(1)–Cl(1) 2.4415(4), N(1)–Ru(1)–N(2) 88.84(6), N(1)–Ru(1)–N(3) 87.18(6), N(2)–Ru(1)–N(3) 83.50(6), N(1)–Ru(1)–Cl(1) 172.04(4), N(2)–Ru(1)–P(1) 177.59(5), N(3)–Ru(1)–P(2) 178.34(4), P(1)–Ru(1)–P(2) 83.207(17), P(1)–Ru(1)–Cl(1) 93.562(16), P(2)–Ru(1)–Cl(1) 92.982(16). Selected hydrogen-bond (D–H...A–X) lengths (\AA) and angles ($^\circ$) D...A, H...A, D–H...A, H...A–X, H...X (A = centroid and X = plane of respective phenyl ring of atom *): N(1)–H(1a)...C(21)* 3.51, 2.61, 160, 64.2, 2.35 (II); N(1)–H(1b)...C(9)* 3.69, 2.87, 165, 59.4, 2.48 (V). Malone hydrogen-bond type is given in parenthesis.²⁰⁶

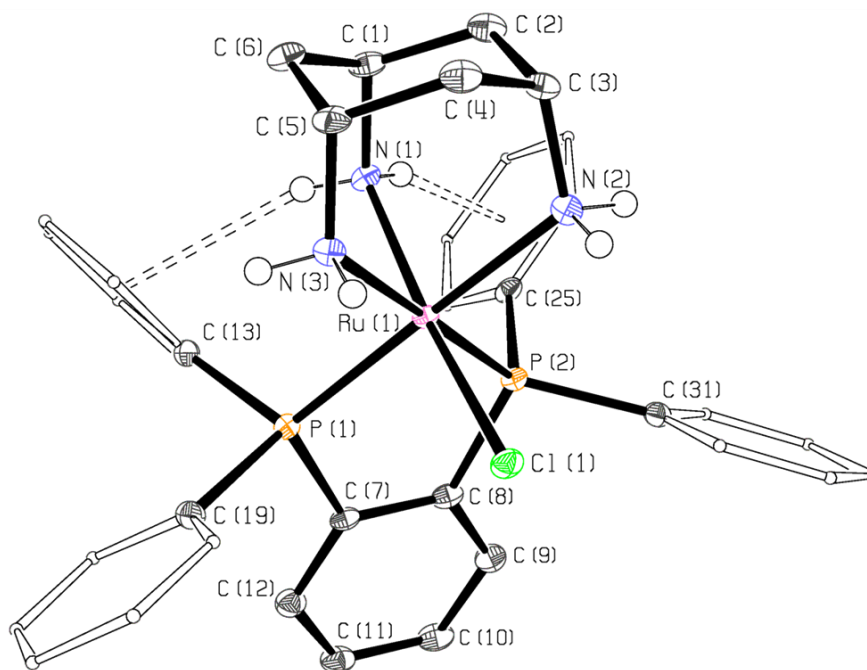


Figure I.4: ORTEP (50% probability ellipsoids) diagram of $[20]Cl(CH_3OH)_3$. Hydrogen atoms (except for amino hydrogens), counter ion and solvent of crystallisation are omitted for clarity. Selected bond lengths (\AA) and angles ($^\circ$): Ru(1)–N(1) 2.124(2), Ru(1)–N(2) 2.181(2), Ru(1)–N(3) 2.182(2), Ru(1)–P(1) 2.2756(6), Ru(1)–P(2) 2.2657(6), Ru(1)–Cl(1) 2.4426(6), N(1)–Ru(1)–N(2) 88.37(8), N(1)–Ru(1)–N(3) 87.37(8), N(2)–Ru(1)–N(3) 84.43(8), N(1)–Ru(1)–Cl(1) 169.11(6), N(2)–Ru(1)–P(1) 178.69(6), N(3)–Ru(1)–P(2) 179.52(6), P(1)–Ru(1)–P(2) 84.00(2), P(1)–Ru(1)–Cl(1) 95.21(2), P(2)–Ru(1)–Cl(1) 95.16(2). Selected hydrogen-bond (D–H...A–X) lengths (\AA) and angles ($^\circ$) D...A, H...A, D–H...A, H...A–X, H...X (A = centroid and X = plane of respective phenyl ring of atom *): N(1)–H(1a)...C(25)* 3.78, 3.005, 164, 53.9, 2.43 (II); N(1)–H(1b)...C(13)* 3.73, 2.95, 161, 54.8, 2.41 (V). Malone hydrogen-bond type is given in parenthesis.²⁰⁶

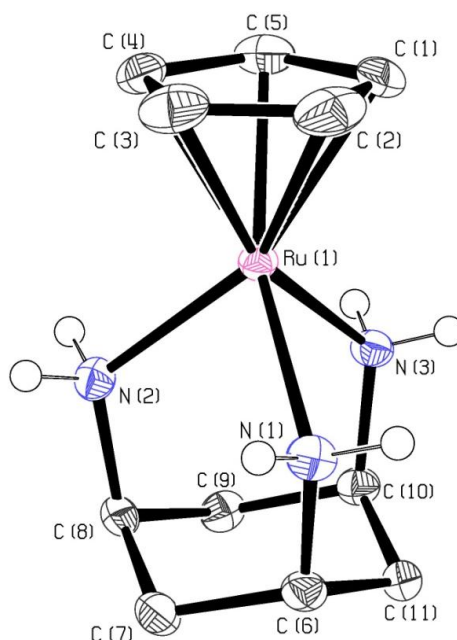


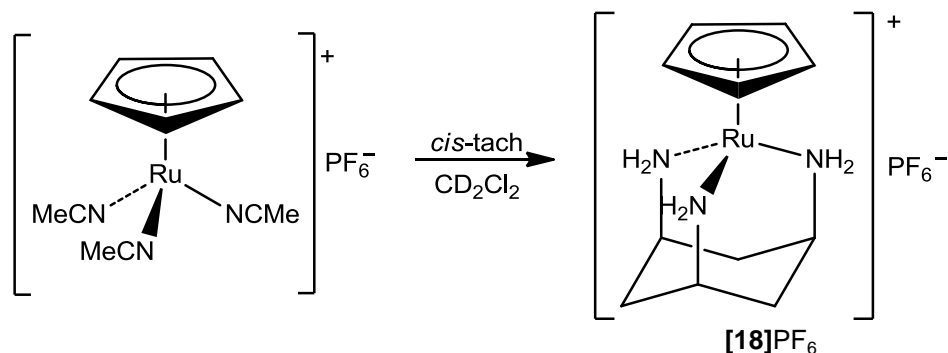
Figure II.1: ORTEP (50 % probability ellipsoids) diagram of the asymmetrical unit of [18]PF₆. Hydrogen atoms (except for amino hydrogens), solvent of crystallisation and counter ion are omitted for clarity. Selected bond lengths (Å) and angles (°): Ru(1)–N(1) 2.1842(14), Ru(1)–N(2) 2.1798(15), Ru(1)–N(3) 2.1801(15), Ru(1)–C(1) 2.1378(17), Ru(1)–C(2) 2.134(2), Ru(1)–C(3) 2.147(2), Ru(1)–C(4) 2.134(2), Ru(1)–C(5) 2.143(2), Ru(1)...*c* 1.76, N(1)–Ru(1)–N(2) 85.28(5), N(2)–Ru(1)–N(3) 84.40(6), N(1)–Ru(1)–N(3) 84.75(6), N(1)–Ru(1)...*c* 130, N(2)–Ru(1)...*c* 129, N(3)–Ru(1)...*c* 128, *Cis*-tach cone 126.5(10), Cp cone 101.5(3). *c* = centroid of Cp ring.

	average	
	ref	r(Ru–C) (Å) Cone Angle (°)
[Ru(η ⁵ -C ₅ H ₅)(NCMe) ₃] ⁺	²⁸⁸	2.135(3)
[Ru(η ⁵ -C ₅ H ₅)(<i>cis</i> -tach)] ⁺		2.138(1) 126.5(10)
[Ru(η ⁵ -C ₅ H ₅)(κ ³ -Tp)]	²⁸⁹	2.153(3) 169(1)
[Ru(η ⁵ -C ₅ H ₅) ₂]	²⁹⁰	2.202(2) 101.5(3)
[Ru(η ⁵ -C ₅ H ₅)(η ⁶ -C ₆ H ₆)] ⁺	²⁹¹	2.208(2) 108.56(2)

Table II.1: Comparison of average Ru–C bond lengths of the RuCp fragment in various complexes. Averages calculated as the weighted mean.²²⁰ Cone angles were calculated as the average of the outermost centroid...Ru...H angles.

Appendix II. Preparation of a Metallocene Analogue

The acetonitrile precursor compound $[\text{Ru}(\eta^5\text{-C}_5\text{H}_5)(\text{NCMe})_3]\text{PF}_6$ provides a structural template for the preparation of a ruthenocene analogue with *cis*-tach. The reaction of $[\text{Ru}(\eta^5\text{-C}_5\text{H}_5)(\text{NCMe})_3]\text{PF}_6$ with *cis*-tach in CD_2Cl_2 occurs rapidly, giving $[\text{Ru}(\eta^5\text{-C}_5\text{H}_5)(\textit{cis}\text{-tach})]\text{PF}_6$ (Scheme II.1).*



Scheme II.1: Preparation of the ruthenocene analogue $[\mathbf{18}]\text{PF}_6$ from $[\text{Ru}(\eta^5\text{-C}_5\text{H}_5)(\text{NCMe})_3]\text{PF}_6$ and *cis*-tach.

On standing, single crystals suitable for X-ray diffraction analysis slowly formed from the reaction mixture. An ORTEP diagram and selected bond lengths and angles are given in Fig. II.1. Most interestingly the cone angle of *cis*-tach when participating in κ^3 coordination to ruthenium can be calculated (Table II.1). This is aided by the absence of bulky co-ligands or significant hydrogen-bonding, coupled with the geometrical freedom incurred by the Cp ligand. The cone angle was calculated as $126.5(10)^\circ$, which is between that of the small carbon donor (Cp, η^6 -benzene) ligands the bulky pyrazolyl-based ligands (Tp). In comparison, the average ruthenium carbon bond lengths (Table II.1) for the $\eta^5\text{-C}_5\text{H}_5$ ligand of $2.138(1) \text{ \AA}$ are significantly shorter for $[\mathbf{9}]\text{PF}_6$ than in analogous organometallic and Tp complexes. This observation is accounted for by the increased π -acceptor character of these ligands, whereas *cis*-tach has no suitable orbitals.

***Experimental Data:** $[\text{Ru}(\eta^5\text{-C}_5\text{H}_5)(\text{NCMe})_3]\text{PF}_6$ (4 mg 0.015 mmol) and *cis*-tach (2mg 0.015 mmol) were taken up in CD_2Cl_2 (0.5 mL) and allowed to mix for 5 minutes. The solution was left to stand for 24 h, over which crystals suitable for X-ray diffraction has formed. $^1\text{H NMR}$ (CD_2Cl_2 , 399.8 MHz, 293 K) δ 3.95 (br. s, 6H, NH_2), 3.72 (s, 5H, Cp), 3.54 (br. s, 3H, CH), 1.81 (m, 6H, CH_2); $^{13}\text{C}\{^1\text{H}\}$ NMR (CD_2Cl_2 , 399.8 MHz, 293 K) δ 63.4 (s, Cp), 43.5 (s, CH), 34.6 (s, CH_2).

Appendix III. X-Ray Crystallography Data

	[1]PF ₆
Identification code	jml0928a
Empirical formula	C ₄₂ H ₄₅ ClF ₆ N ₃ P ₃ Ru
Formula weight	935.24
Temperature / K	110(2)
Wavelength / Å	0.71073
Crystal system	Orthorhombic
Space group	Pca2 ₁
<i>a</i> / Å, <i>b</i> / Å, <i>c</i> / Å	24.817(2), 10.1230(9), 31.819(3)
α / °, β / °, γ / °	90, 90, 90
Volume / Å ³	7993.7(12)
<i>Z</i>	8
Density (calculated) / Mg/m ⁻³	1.554
Absorption coefficient / mm ⁻¹	0.643
<i>F</i> (000)	3824
Crystal size / mm ³	0.34 × 0.33 × 0.07
θ range for data collection / °	1.64 to 28.30
Index ranges	-33 ≤ <i>h</i> ≤ 33, -13 ≤ <i>k</i> ≤ 13, -42 ≤ <i>l</i> ≤ 42
Reflections collected	77522
Independent reflections	19871 [<i>R</i> _{int} = 0.0737]
Completeness to θ	99.9% (θ = 28.30°)
Max. and min. transmission	1.000 and 0.696
Data / restraints / parameters	19871 / 7 / 1058
Goodness-of-fit on <i>F</i> ²	1.049
Final <i>R</i> indices [<i>I</i> > 2σ(<i>I</i>)]	<i>R</i> ₁ = 0.0528, <i>wR</i> ₂ = 0.1101
<i>R</i> indices (all data)	<i>R</i> ₁ = 0.0706, <i>wR</i> ₂ = 0.1177
Largest diff. peak and hole / e Å ⁻³	1.639 and -1.520
Absolute structure parameter	0.00(6)

[2]CH ₂ Cl ₂	[3]BPh ₄ (CH ₂ Cl ₂) _{1.5}
jml0927m	jml0930a
C ₄₉ H ₆₂ Cl ₆ N ₆ P ₂ Ru ₂	C _{73.5} H ₈₃ BCl ₆ N ₆ P ₂ Ru ₂
1211.83	1538.05
110(2)	110(2)
0.71073	0.71073
Monoclinic	Triclinic
P2 ₁ /c	P-1
16.1501(13), 18.0454(14), 18.5649(14)	13.7095(15), 16.0447(17), 16.4533(17)
90, 90.148(2), 90	90.061(2), 100.534(2), 92.488(2)
5410.4(7)	3554.6(7)
4	2
1.488	1.437
0.953	0.742
2472	1582.0
0.16 × 0.15 × 0.07	0.34 × 0.29 × 0.03
1.26 to 30.01	1.26 to 30.07
-22 ≤ h ≤ 22, -25 ≤ k ≤ 25, -26 ≤ l ≤ 25	-19 ≤ h ≤ 19, -22 ≤ k ≤ 22, -22 ≤ l ≤ 22
59492	39610
15557 [<i>R</i> _{int} = 0.0429]	19832 [<i>R</i> _{int} = 0.0342]
98.5% (θ = 30.01°)	99.7% (θ = 30.07°)
0.935 and 0.740	1.000 and 0.714
15557 / 4 / 616	19832 / 2 / 845
1.130	1.083
<i>R</i> ₁ = 0.0748, <i>wR</i> ₂ = 0.2272	<i>R</i> ₁ = 0.0482, <i>wR</i> ₂ = 0.1209
<i>R</i> ₁ = 0.0903, <i>wR</i> ₂ = 0.2470	<i>R</i> ₁ = 0.0693, <i>wR</i> ₂ = 0.1364
3.183 and -2.418	2.25 and -1.19

	[8]PF ₆
Identification code	jml1003a
Empirical formula	C ₁₀ H ₂₇ ClF ₆ N ₃ O ₂ PRuS ₂
Formula weight	566.96
Temperature / K	110
Wavelength / Å	0.71073
Crystal system	Orthorhombic
Space group	Aba2
<i>a</i> / Å, <i>b</i> / Å, <i>c</i> / Å	14.7124(6), 15.6131(7), 17.1848(7)
α / °, β / °, γ / °	90, 90, 90
Volume / Å ³	3947.5(3)
<i>Z</i>	8
Density (calculated) / Mg/m ⁻³	1.908
Absorption coefficient / mm ⁻¹	1.288
<i>F</i> (000)	2288
Crystal size / mm ³	0.21 × 0.16 × 0.15
θ range for data collection / °	2.24 to 28.30
Index ranges	-19 ≤ <i>h</i> ≤ 19, -20 ≤ <i>k</i> ≤ 20, -22 ≤ <i>l</i> ≤ 22
Reflections collected	19637
Independent reflections	4902 [<i>R</i> _{int} = 0.0340]
Completeness to θ	100% (θ = 28.30°)
Max. and min. transmission	0.824 and 0.648
Data / restraints / parameters	4902 / 22 / 306
Goodness-of-fit on <i>F</i> ²	1.055
Final <i>R</i> indices [<i>I</i> > 2σ(<i>I</i>)]	<i>R</i> ₁ = 0.0236, <i>wR</i> ₂ = 0.0588
<i>R</i> indices (all data)	<i>R</i> ₁ = 0.0239, <i>wR</i> ₂ = 0.0590
Largest diff. peak and hole / e Å ⁻³	2.352 and -0.610
Absolute structure parameter	-0.01(2)

[9]	[10](PF₆)₂
jml1004m	phw1001a
C ₈ H ₂₁ Cl ₂ N ₃ ORuS	C ₁₈ H ₂₉ F ₁₂ N ₅ OP ₂ RuS
379.31	754.53
110(2)	110(2)
0.71073	0.71073
Monoclinic	Monoclinic
P2 ₁ /n	P2 ₁ /c
7.9097(16), 9.753(2), 17.456(4)	17.934(3), 10.6572(16), 13.783(2)
90, 93.394(4), 90	90, 90.055(4), 90
1344.3(5)	2634.2(7)
4	4
1.874	1.903
1.703	0.906
768	1512
0.15 × 0.15 × 0.10	0.16 × 0.13 × 0.07
2.34 to 28.40	2.22 to 28.32
-10 ≤ h ≤ 10, -12 ≤ k ≤ 12, -23 ≤ l ≤ 23	-23 ≤ h ≤ 23, -14 ≤ k ≤ 13, -18 ≤ l ≤ 18
13148	26643
3341 [<i>R</i> _{int} = 0.0387]	6527 [<i>R</i> _{int} = 0.0546]
98.9% (θ = 28.40°)	99.3% (θ = 28.32°)
1.000 and 0.764	0.9393 and 0.8686
3341 / 33 / 219	6527 / 0 / 388
1.079	1.024
<i>R</i> ₁ = 0.0365, <i>wR</i> ₂ = 0.0820	<i>R</i> ₁ = 0.0407, <i>wR</i> ₂ = 0.0905
<i>R</i> ₁ = 0.0492, <i>wR</i> ₂ = 0.0876	<i>R</i> ₁ = 0.0580, <i>wR</i> ₂ = 0.0997
1.336 and -0.870	0.999 and -0.784

	[11](PF ₆) ₂ .MeOH
Identification code	jml1001m
Empirical formula	C ₂₁ H ₃₃ F ₁₂ N ₅ O ₂ P ₂ RuS
Formula weight	810.59
Temperature / K	110(2)
Wavelength / Å	0.71073
Crystal system	Triclinic
Space group	P-1
<i>a</i> / Å, <i>b</i> / Å, <i>c</i> / Å	9.947(4), 10.678(4), 6.409(6)
α / °, β / °, γ / °	93.116(7), 107.140(7), 114.478(7)
Volume / Å ³	1484.2(10)
<i>Z</i>	2
Density (calculated) / Mg/m ⁻³	1.814
Absorption coefficient / mm ⁻¹	0.813
<i>F</i> (000)	816
Crystal size / mm ³	0.25 × 0.18 × 0.16
θ range for data collection / °	2.14 to 28.40
Index ranges	-13 ≤ <i>h</i> ≤ 13, -14 ≤ <i>k</i> ≤ 14, -21 ≤ <i>l</i> ≤ 21
Reflections collected	15239
Independent reflections	7276 [<i>R</i> _{int} = 0.0234]
Completeness to θ	97.8% (θ = 28.30°)
Max. and min. transmission	0.878 and 0.663
Data / restraints / parameters	7276 / 6 / 468
Goodness-of-fit on <i>F</i> ²	1.056
Final <i>R</i> indices [<i>I</i> > 2σ(<i>I</i>)]	<i>R</i> ₁ = 0.0285, <i>wR</i> ₂ = 0.0746
<i>R</i> indices (all data)	<i>R</i> ₁ = 0.0313, <i>wR</i> ₂ = 0.0767
Largest diff. peak and hole / e Å ⁻³	0.832 and -0.677

[12] Cl.PF ₆	[15] PF ₆
jml1006m	jml1007m
C ₁₀ H ₂₉ ClF ₆ N ₅ OPRuS	C ₃₁ H ₃₇ ClF ₆ N ₃ P ₃ Ru
548.93	795.07
110(2)	130(2)
0.71073	0.71073
Monoclinic	Triclinic
P2 ₁ /c	P-1
9.5843(8), 11.4320(10), 18.2955(16)	11.2999(13), 15.1247(17), 20.609(2)
90, 90.604(2), 90	79.083(3), 89.207(2), 69.075(2)
2004.5(3)	3224.9(6)
4	4
1.819	1.638
1.164	0.781
1112	1616
0.40 × 0.19 × 0.08	0.10 × 0.09 × 0.08
2.10 to 28.29	1.01 to 25.06
-12 ≤ h ≤ 12, -15 ≤ k ≤ 15, -24 ≤ l ≤ 24	-13 ≤ h ≤ 13, -18 ≤ k ≤ 17, -24 ≤ l ≤ 24
20281	26296
4979 [R _{int} = 0.0206]	11364 [R _{int} = 0.0419]
99.9% (θ = 28.29°)	99.4% (θ = 25.06°)
0.911 and 0.771	0.939 and 0.745
4979 / 0 / 277	11364 / 54 / 899
1.064	1.040
R ₁ = 0.0213, wR ₂ = 0.0517	R ₁ = 0.0435, wR ₂ = 0.1024
R ₁ = 0.0234, wR ₂ = 0.0529	R ₁ = 0.0684, wR ₂ = 0.1130
0.627 and -0.395	1.504 and -0.655

	[16]PF₆
Identification code	phw1012
Empirical formula	C ₃₂ H ₃₉ ClF ₆ N ₃ P ₃ Ru
Formula weight	809.09
Temperature / K	110(2)
Wavelength / Å	0.7107
Crystal system	Trigonal
Space group	P3c1
<i>a</i> / Å, <i>b</i> / Å, <i>c</i> / Å	18.9550(7), 18.9550(7), 16.9765(6)
α / °, β / °, γ / °	90, 90, 90
Volume / Å ³	5282.3(5)
<i>Z</i>	6
Density (calculated) / Mg/m ⁻³	1.526
Absorption coefficient / mm ⁻¹	0.717
<i>F</i> (000)	2472
Crystal size / mm ³	0.1754 × 0.099 × 0.0707
θ range for data collection / °	3.22 to 29.00
Index ranges	-21 ≤ <i>h</i> ≤ 16, -23 ≤ <i>k</i> ≤ 25, -12 ≤ <i>l</i> ≤ 23
Reflections collected	11946
Independent reflections	5256 [<i>R</i> _{int} = 0.0334]
Completeness to θ	99.6% (θ = 29.00°)
Max. and min. transmission	1.000 and 0.925
Data / restraints / parameters	5256 / 13 / 511
Goodness-of-fit on <i>F</i> ²	1.044
Final <i>R</i> indices [<i>I</i> > 2σ(<i>I</i>)]	<i>R</i> ₁ = 0.0417, w <i>R</i> ₂ = 0.0987
<i>R</i> indices (all data)	<i>R</i> ₁ = 0.0486, w <i>R</i> ₂ = 0.1040
Largest diff. peak and hole / e Å ⁻³	0.844 and -0.487

[17] Cl(H ₂ O) _{2.15} ·MeOH	[18] Cl(H ₂ O) ₄
jml1134	jml1147_twin1_hklf4
C ₃₄ H ₄₇ Cl ₂ N ₃ O _{3.15} P ₂ Ru	C ₃₄ H ₅₁ Cl ₂ N ₃ O ₄ P ₂ Ru
782.10	799.69
110.0	110.00(10)
0.7107	0.7107
Monoclinic	Triclinic
P2 ₁ /n	P-1
9.70362(19), 20.1181(4), 17.9253(4)	8.8119(7), 10.6377(9), 20.0033(13)
90, 94.431(2), 90	75.110(7), 88.833(6), 78.932(7)
3488.89(13)	1777.6(2)
4	2
1.489	1.494
0.733	0.723
1621	832.0
0.1919 × 0.132 × 0.1156	0.2867 × 0.1014 × 0.0562
2.92 to 32.15	2.79 to 31.76
-13 ≤ h ≤ 12, -21 ≤ k ≤ 29, -12 ≤ l ≤ 26	-13 ≤ h ≤ 13, -15 ≤ k ≤ 15, -28 ≤ l ≤ 29
18989	12956
10808 [R _{int} = 0.0267]	12956 [R _{int} = 0.0000]
99.8% (θ = 32.15°)	99.0% (θ = 31.76°)
0.986 and 0.979	1.000 and 0.100
10808 / 0 / 451	12956 / 0 / 428
1.034	1.084
R ₁ = 0.0344, wR ₂ = 0.0761	R ₁ = 0.0666, wR ₂ = 0.1943
R ₁ = 0.0442, wR ₂ = 0.0813	R ₁ = 0.0734, wR ₂ = 0.2037
0.582 and -0.913	3.36 and -3.61

	[19](H₃O)_{0.5}(Cl)_{1.5}.H₂O
Identification code	jml1149
Empirical formula	C ₃₂ H _{40.5} Cl ₂ N ₃ O _{1.5} P ₂ Ru
Formula weight	724.58
Temperature / K	110.00(10)
Wavelength / Å	0.7107
Crystal system	Monoclinic
Space group	P2 ₁ /a
<i>a</i> / Å, <i>b</i> / Å, <i>c</i> / Å	16.9554(3), 9.90919(14), 20.2316(5)
α / °, β / °, γ / °	90.00, 113.859(3), 90.00
Volume / Å ³	3108.72(11)
<i>Z</i>	4
Density (calculated) / Mg/m ⁻³	1.548
Absorption coefficient / mm ⁻¹	0.813
<i>F</i> (000)	1494.0
Crystal size / mm ³	0.2954 × 0.2458 × 0.0541
θ range for data collection / °	6.02 to 64.22
Index ranges	-25 ≤ <i>h</i> ≤ 16, -14 ≤ <i>k</i> ≤ 13, -28 ≤ <i>l</i> ≤ 30
Reflections collected	17028
Independent reflections	9680 [<i>R</i> (int) = 0.0244]
Completeness to θ	99.34% (θ = 64.22°)
Max. and min. transmission	1.000 and 0.709
Data / restraints / parameters	9680 / 9 / 445
Goodness-of-fit on <i>F</i> ²	1.073
Final <i>R</i> indices [<i>I</i> > 2σ(<i>I</i>)]	<i>R</i> ₁ = 0.0314, <i>wR</i> ₂ = 0.0689
<i>R</i> indices (all data)	<i>R</i> ₁ = 0.0403, <i>wR</i> ₂ = 0.0737
Largest diff. peak and hole / e Å ⁻³	0.83 and -0.84
Absolute structure parameter	

[20] Cl(CH ₃ OH) ₃	[21] PF ₆ .CH ₂ Cl ₂
jml1137	jml0929a
C ₃₉ H ₅₁ Cl ₂ N ₃ O ₃ P ₂ Ru	C ₁₂ H ₂₂ Cl ₂ F ₆ N ₃ PRu
843.74	525.27
110.0	110(2)
0.7107	0.71073
Monoclinic	Orthorhombic
Cc	Pna2 ₁
18.3263(7), 8.5294(2), 26.4162(13)	15.4931(12), 11.9225(9), 10.0452(8)
90, 109.141(5), 90	90, 90, 90
3900.9(3)	1855.5(2)
4	4
1.437	1.880
0.662	1.277
1752	1048.0
0.1549 × 0.1457 × 0.0797	0.16 × 0.15 × 0.12
2.90 to 30.05	2.16 to 29.98
-25 ≤ h ≤ 25, -11 ≤ k ≤ 12, -34 ≤ l ≤ 34	-21 ≤ h ≤ 21, -16 ≤ k ≤ 16, -13 ≤ l ≤ 13
22702	20007
9763 [<i>R</i> _{int} = 0.0336]	5332 [<i>R</i> _{int} = 0.0173]
99.8% (θ = 30.05°)	99.3% (θ = 29.98°)
0.989 and 0.981	1.000 and 0.865
9763 / 2 / 484	5332 / 1 / 250
1.035	1.055
<i>R</i> ₁ = 0.0283, <i>wR</i> ₂ = 0.0570	<i>R</i> ₁ = 0.0174, <i>wR</i> ₂ = 0.0428
<i>R</i> ₁ = 0.0305, <i>wR</i> ₂ = 0.0585	<i>R</i> ₁ = 0.0181, <i>wR</i> ₂ = 0.0432
0.410 and -0.402	0.60 and -0.41
	0(10)

Compound Codes

[RuCl(tach)(PPh ₃) ₂]Cl	[1]Cl
[RuCl ₂ (tach)(PPh ₃)]Cl	[2]
[{RuCl(PPh ₃)(<i>cis</i> -tach)} ₂ (μ-Cl)]BPh ₄	[3]BPh ₄
[RuCl(DMSO- <i>S</i>)(<i>cis</i> -tach)(PPh ₃)]Cl	[4]Cl
[RuCl(NCMe)(<i>cis</i> -tach)(PPh ₃)]PF ₆	[5]PF ₆
[Ru(NCMe) ₂ (<i>cis</i> -tach)(PPh ₃)](PF ₆) ₂	[6](PF ₆) ₂
[RuCl(κ ¹ -dppm)(<i>cis</i> -tach)(PPh ₃)]PF ₆	[7]PF ₆
[RuCl(DMSO- <i>S</i>) ₂ (<i>cis</i> -tach)]Cl	[8]Cl
[Ru(OH _x) ₂ (DMSO- <i>S</i>)(<i>cis</i> -tach)] ^{(2-2x)+} ,	[8a] ⁿ⁺
[RuCl(OH _x)(DMSO- <i>S</i>)(<i>cis</i> -tach)] ⁿ⁺	[8b] ⁿ⁺
[RuCl ₂ (DMSO- <i>S</i>)(<i>cis</i> -tach)]	[9]
[Ru(bipy)(DMSO- <i>S</i>)(<i>cis</i> -tach)](Cl) ₂	[10](Cl) ₂
[Ru(DMSO- <i>S</i>)(phen)(<i>cis</i> -tach)](Cl) ₂	[11](Cl) ₂
[Ru(DMSO- <i>S</i>)(en)(<i>cis</i> -tach)](Cl) ₂	[12](Cl) ₂
[RuCl(COD)(<i>cis</i> -tach)]PF ₆	[13]PF ₆
[Ru(NCMe) ₃ (<i>cis</i> -tach)](Cl) ₂	[14](Cl) ₂
[RuCl(dppm)(<i>cis</i> -tach)]Cl	[15]Cl
[RuCl(dppe)(<i>cis</i> -tach)]Cl	[16]Cl
[RuCl(dppp)(<i>cis</i> -tach)]Cl	[17]Cl
[RuCl(dppb)(<i>cis</i> -tach)]Cl	[18]Cl
[RuCl(dppv)(<i>cis</i> -tach)]Cl	[19]Cl
[RuCl(dppben)(<i>cis</i> -tach)]Cl	[20]Cl
[Ru(OH _x)(dppe)(<i>cis</i> -tach)] ⁿ⁺	[16a] ^{x+}
[Ru(OH _x)(dppp)(<i>cis</i> -tach)] ⁿ⁺	[17a] ^{x+}
[Ru(OH ₂)(dppe)(<i>cis</i> -tach)] ⁿ⁺	[16a] ²⁺
[Ru(OH ₂)(dppp)(<i>cis</i> -tach)] ⁿ⁺	[17a] ²⁺
[Ru(PO ₄ - <i>O</i>)(dppe)(<i>cis</i> -tach)] ⁿ⁺	[16b] ^{x+}
[Ru(PO ₄ - <i>O</i>)(dppp)(<i>cis</i> -tach)] ⁿ⁺	[17b] ^{x+}
[Ru(dppe)(EtG)(<i>cis</i> -tach)] ²⁺	[16c] ²⁺

$[\text{Ru}(\text{dppp})(\text{EtG})(\text{cis-tach})]^{2+}$	[17c] ²⁺
$[\text{Ru}(\text{dppe})(\text{GMP})(\text{cis-tach})]^{2+}$	[16d] ⁿ⁺
$[\text{Ru}(\text{dppp})(\text{GMP})(\text{cis-tach})]^{2+}$	[17d] ⁿ⁺
$[\text{Ru}(\text{dppe})(\text{GSH})(\text{cis-tach})]^{2+}$	[16e] ⁿ⁺
$[\text{Ru}(\text{dppp})(\text{GSH})(\text{cis-tach})]^{2+}$	[17e] ⁿ⁺
$[\text{RuCp}(\text{cis-tach})]\text{PF}_6$	[21] PF ₆

Abbreviations

A	absorbance
Ado	adenosine
acac	acetyl acetate
Ar	aryl group (NMR assignment)
ATR	Attenuated Total Reflectance
ax	axial
bip	biphenyl
bipy	2,2'-bipyridyl
Bn	benzyl
bpe	base-pair equivalents
br	broad
Br	bridging group (NMR assignment)
^t Bu	<i>tert</i> -butyl
Calc.	calculated
CCC	covalently closed circular
cGMP	cyclic 5'-guanosine monophosphate
COD	1,4-cyclooctadiene
COSY	Correlation spectroscopy
Cp	η ⁵ -cyclopentadienyl
Cp*	η ⁵ -pentamethylcyclopentadienyl
Cy	cyclohexyl
d	doublet
dab	1,2-diaminobenzene
dach	trans-1,2-diaminocyclohexane

DCM	dichloromethane
dha	9,10-dihydroanthracene
DMSO	dimethylsulfoxide
DNA	deoxyribonucleic acid
DPPA	Diphenylphosphoryl azide
dppb	butane-1,4-diylbis(diphenylphosphane); 1,4-bis(diphenylphosphino)butane
dppben	phenylene-1,2-bis(diphenylphosphane); 1,2-bis(diphenylphosphino)benzene
dppe	ethane-1,2-diylbis(diphenylphosphane); 1,2-bis(diphenylphosphino)ethane
dppm	methylenebis(diphenylphosphane); bis(diphenylphosphino)methane
dppp	propane-1,3-diylbis(diphenylphosphane); 1,3-bis(diphenylphosphino)propane
dppv	(<i>Z</i>)-ethylene-1,2-bis(diphenylphosphane); <i>cis</i> -1,2-bis(diphenylphosphino)ethylene
EtG	9-ethyl guanine
en	1,2-ethylenediamine
eq	equatorial
Eqn.	Equation
ESI	electrospray ionisation
Et	ethyl
<i>fac</i>	<i>facial</i>
Fig.	Figure
G	guanine
GEMSA	Gel electrophoretic mobility shift assay
gly	glycine
Guo	guanosine
GMP	5'-guanosine monophosphate
GS	glutathione, <i>S</i> -deprotonated
GSH	glutathione
h	hour(s)
HC11	[RuCl(η^6 -tha)(en)]PF ₆
HSQC	Heteronuclear single quantum coherence

imi	imidazole
ind	indazole
IR	infra-red
L	ligand
LUMO	Lowest unoccupied molecular orbital
m	multiplet (NMR)
m	medium (IR)
<i>m</i>	<i>meta</i>
mal	maltolato
Me	methyl
<i>mer</i>	<i>meridinal</i>
min	minute(s)
MS	mass spectrometry
MTT	(3-(4,5-dimethylthiazol-2-yl)-2,5-diphenyltetrazolium bromide
N	amine (NMR assignment)
NMR	nuclear magnetic resonance
NOESY	Nuclear overhauser effect spectroscopy
<i>o</i>	<i>ortho</i>
OC	Open Circular
ORTEP	Oak Ridge Thermal Ellipsoid Program
OTf	Trifluoromethanesulfonate
<i>p</i>	<i>para</i>
PBS	Phosphate Buffered Saline
Ph	phenyl
phen	1,10-phenanthroline
pico	picolinate
ppm	parts per million
Pr	propyl
ppt	1-(2-picolyl)-4-phenyl-1 <i>H</i> -1,2,3-triazole
PTA	1,3,5-triaza-7-phosphaadamantane
py	pyridine
q	quartet
RAen	Ruthenium(II) η^6 -arene en (complex)
RAPTA	Ruthenium(II) η^6 -arene PTA (complex)

RM175	[RuCl(η^6 -bip)(en)]PF ₆
RT	Room/ambient Temperature
s	singlet (NMR)
s	strong (IR)
SAR	Structure-Activity Relationship
t	triplet
$t_{1/2}$	half-life
<i>cis</i> -tach	<i>cis,cis</i> -1,3,5-triaminocyclohexane
tachpyr	<i>cis,cis</i> -1,3,5- <i>N,N',N''</i> -tris(2-pyridylmethylene)triaminocyclohexane
taen	1,4,7-triazacyclononane
tha	1,4,9,10-tetrahydroanthracene
Tp	hydrogen trispyrazolylborate
Tp ^{iPr}	hydrogen tris(3,5-di-isopropylpyrazolyl)borate
Tpm	trispyrazolylmethane
tten	1,4,7-trithiacyclononane
UV	ultra-violet
v	virtual (NMR)
v	very (IR)
Vis	visible
w	weak (IR)

References

1. Cancer Research UK: Cancer Statistics, <http://info.cancerresearchuk.org/cancerstats/reports/>, Accessed 1st July, 2012.
2. B. Alberts, A. Johnson, J. Lewis, M. Raff, K. Roberts and P. Walter, in *Molecular Biology of the Cell*, Garland Science, 2002, pp. 1313-1362.
3. J. D. Martinez, M. Taylor Parker, K. E. Fultz, N. A. Ignatenko and E. W. Gerner, in *Burger's Medicinal Chemistry and Drug Discovery*, ed. D. J. Abraham, John Wiley & Sons, Inc., 2003, pp. 1-50.
4. D. Hanahan and R. A. Weinberg, *Cell*, 2011, **144**, 646-674.
5. A. L. Harris, *Nature Reviews Cancer*, 2002, **2**, 38-47.
6. L. A. Liotta, P. S. Steeg and W. G. Stetlerstevenson, *Cell*, 1991, **64**, 327-336.
7. W. H. Ang and P. J. Dyson, *European Journal of Inorganic Chemistry*, 2006, 4003-4018.
8. N. J. Wheate, S. Walker, G. E. Craig and R. Oun, *Dalton Transactions*, 2010, **39**, 8113-8127.
9. Rosenberg, B, L. Vancamp and T. Krigas, *Nature*, 1965, **205**, 698-699.
10. Rosenberg, B, L. Vancamp, J. E. Trosko and V. H. Mansour, *Nature*, 1969, **222**, 385-386.
11. D. J. Higby, H. J. Wallace, D. J. Albert and J. F. Holland, *Cancer*, 1974, **33**, 1219-1225.
12. Y. Jung and S. J. Lippard, *Chemical Reviews*, 2007, **107**, 1387-1407.
13. S. E. Miller and D. A. House, *Inorganica Chimica Acta*, 1989, **161**, 131-137.
14. K. Wang, J. F. Lu and R. C. Li, *Coordination Chemistry Reviews*, 1996, **151**, 53-88.
15. A. I. Ivanov, J. Christodoulou, J. A. Parkinson, K. J. Barnham, A. Tucker, J. Woodrow and P. J. Sadler, *Journal of Biological Chemistry*, 1998, **273**, 14721-14730.
16. C. A. Puckett, R. J. Ernst and J. K. Barton, *Dalton Transactions*, 2010, **39**, 1159-1170.
17. S. J. Bernersprice, T. A. Frenkiel, U. Frey, J. D. Ranford and P. J. Sadler, *Journal of the Chemical Society-Chemical Communications*, 1992, 789-791.

18. A. K. Godwin, A. Meister, P. J. Odwyer, C. S. Huang, T. C. Hamilton and M. E. Anderson, *Proceedings of the National Academy of Sciences of the United States of America*, 1992, **89**, 3070-3074.
19. L. Kelland, *Nature Reviews Cancer*, 2007, **7**, 573-584.
20. S. Mansy, G. Y. H. Chu, R. E. Duncan and R. S. Tobias, *Journal of the American Chemical Society*, 1978, **100**, 607-616.
21. S. E. Sherman and S. J. Lippard, *Chemical Reviews*, 1987, **87**, 1153-1181.
22. A. M. J. Fichtingerschepman, J. L. Vanderveer, J. H. J. Denhartog, P. H. M. Lohman and J. Reedijk, *Biochemistry*, 1985, **24**, 707-713.
23. R. C. Todd and S. J. Lippard, *Metallomics*, 2009, **1**, 280-291.
24. E. R. Jamieson and S. J. Lippard, *Chemical Reviews*, 1999, **99**, 2467-2498.
25. Z. H. Siddik, *Oncogene*, 2003, **22**, 7265-7279.
26. M. J. Cleare and J. D. Hoeschele, *Platinum Metals Review*, 1973, **17**, 2-13.
27. S. M. Aris and N. P. Farrell, *European Journal of Inorganic Chemistry*, 2009, 1293-1302.
28. K. Chvalova, V. Brabec and J. Kasparkova, *Nucleic Acids Research*, 2007, **35**, 1812-1821.
29. E. G. Chapman and V. J. DeRose, *Journal of the American Chemical Society*, 2010, **132**, 1946-1952.
30. A. Basu and S. Krishnamurthy, *J Nucleic Acids*, 2010, **2010**, 201367.
31. E. Wong and C. M. Giandomenico, *Chemical Reviews*, 1999, **99**, 2451-2466.
32. A. H. Calvert, S. J. Harland, D. R. Newell, Z. H. Siddik, A. C. Jones, T. J. McElwain, S. Raju, E. Wiltshaw, I. E. Smith, J. M. Baker, M. J. Peckham and K. R. Harrap, *Cancer Chemotherapy and Pharmacology*, 1982, **9**, 140-147.
33. U. Frey, J. D. Ranford and P. J. Sadler, *Inorganic Chemistry*, 1993, **32**, 1333-1340.
34. M. E. Gore, I. Fryatt, E. Wiltshaw, T. Dawson, B. A. Robinson and A. H. Calvert, *British Journal of Cancer*, 1989, **60**, 767-769.
35. J. D. Page, I. Husain, A. Sancar and S. G. Chaney, *Biochemistry*, 1990, **29**, 1016-1024.
36. E. Raymond, S. G. Chaney, A. Taamma and E. Cvitkovic, *Annals of Oncology*, 1998, **9**, 1053-1071.

37. J. Kasparikova, M. Vojtiskova, G. Natile and V. Brabec, *Chemistry-a European Journal*, 2008, **14**, 1330-1341.
38. L. R. Kelland, G. Abel, M. J. McKeage, M. Jones, P. M. Goddard, M. Valenti, B. A. Murrer and K. R. Harrap, *Cancer Research*, 1993, **53**, 2581-2586.
39. J. Reedijk, *European Journal of Inorganic Chemistry*, 2009, 1303-1312.
40. P. Heffeter, U. Jungwirth, M. Jakupec, C. Hartinger, M. Galanski, L. Elbling, M. Micksche, B. Keppler and W. Berger, *Drug Resistance Updates*, 2008, **11**, 1-16.
41. I. Ott and R. Gust, *Archiv Der Pharmazie*, 2007, **340**, 117-126.
42. S. H. van Rijt and P. J. Sadler, *Drug Discovery Today*, 2009, **14**, 1089-1097.
43. L. Ronconi and P. J. Sadler, *Coordination Chemistry Reviews*, 2007, **251**, 1633-1648.
44. G. Sava and A. Bergamo, *International Journal of Oncology*, 2000, **17**, 353-365.
45. M. Galanski, V. B. Arion, M. A. Jakupec and B. K. Keppler, *Current Pharmaceutical Design*, 2003, **9**, 2078-2089.
46. I. Kostova, *Current Medicinal Chemistry*, 2006, **13**, 1085-1107.
47. G. Sava and A. Bergamo, *Platinum and Other Heavy Metal Compounds in Cancer Chemotherapy*, 2009, 57-66.
48. J. Reedijk, *Platinum Metals Review*, 2008, **52**, 2-11.
49. C. G. Hartinger, S. Zorbas-Seifried, M. A. Jakupec, B. Kynast, H. Zorbas and B. K. Keppler, *Journal of Inorganic Biochemistry*, 2006, **100**, 891-904.
50. F. Kratz and L. Messori, *Journal of Inorganic Biochemistry*, 1993, **49**, 79-82.
51. A. Bergamo and G. Sava, *Dalton Transactions*, 2011, **40**, 7817-7823.
52. J. R. Durig, J. Danneman, W. D. Behnke and E. E. Mercer, *Chemico-Biological Interactions*, 1976, **13**, 287-294.
53. M. J. Clarke, S. Bitler, D. Rennert, M. Buchbinder and A. D. Kelman, *Journal of Inorganic Biochemistry*, 1980, **12**, 79-87.
54. M. J. Clarke, F. C. Zhu and D. R. Frasca, *Chemical Reviews*, 1999, **99**, 2511-2533.
55. E. S. Antonarakis and A. Emadi, *Cancer Chemother Pharmacol*, 2010, **66**, 1-9.
56. P. J. Dyson and G. Sava, *Dalton Transactions*, 2006, 1929-1933.

57. G. Sava, F. Frausin, M. Cocchietto, F. Vita, E. Podda, P. Spessotto, A. Furlani, V. Scarcia and G. Zabucchi, *European Journal of Cancer*, 2004, **40**, 1383-1396.
58. A. Vacca, M. Bruno, A. Boccarelli, M. Coluccia, D. Ribatti, A. Bergamo, S. Garbisa, L. Sartor and G. Sava, *British Journal of Cancer*, 2002, **86**, 993-998.
59. G. Sava, A. Bergamo, S. Zorzet, B. Gava, C. Casarsa, M. Cocchietto, A. Furlani, V. Scarcia, B. Serli, E. Iengo, E. Alessio and G. Mestroni, *European Journal of Cancer*, 2002, **38**, 427-435.
60. B. Sanna, M. Debidda, G. Pintus, B. Tadolini, A. M. Posadino, F. Bennardini, G. Sava and C. Ventura, *Archives of Biochemistry and Biophysics*, 2002, **403**, 209-218.
61. G. Pintus, B. Tadolini, A. M. Posadino, B. Sanna, M. Debidda, F. Bennardini, G. Sava and C. Ventura, *European Journal of Biochemistry*, 2002, **269**, 5861-5870.
62. B. Cebrian-Losantos, A. A. Krokhin, I. N. Stepanenko, R. Eichinger, M. A. Jakupec, V. B. Arion and B. K. Keppler, *Inorganic Chemistry*, 2007, **46**, 5023-5033.
63. J. M. Rademaker-Lakhai, D. van den Bongard, D. Pluim, J. H. Beijnen and J. H. M. Schellens, *Clinical Cancer Research*, 2004, **10**, 3717-3727.
64. M. R. Berger, F. T. Garzon, B. K. Keppler and D. Schmahl, *Anticancer Research*, 1989, **9**, 761-765.
65. F. T. Garzon, M. R. Berger, B. K. Keppler and D. Schmahl, *Cancer Chemotherapy and Pharmacology*, 1987, **19**, 347-349.
66. S. Kapitza, M. Pongratz, M. A. Jakupec, P. Heffeter, W. Berger, L. Lackinger, B. K. Keppler and B. Marian, *Journal of Cancer Research and Clinical Oncology*, 2005, **131**, 101-110.
67. C. G. Hartinger, M. A. Jakupec, S. Zorbas-Seifried, M. Groessl, A. Egger, W. Berger, H. Zorbas, P. J. Dyson and B. K. Keppler, *Chemistry & Biodiversity*, 2008, **5**, 2140-2155.
68. M. Pongratz, P. Schluga, M. A. Jakupec, V. B. Arion, C. G. Hartinger, G. Allmaier and B. K. Keppler, *Journal of Analytical Atomic Spectrometry*, 2004, **19**, 46-51.

69. A. Kung, T. Pieper and B. K. Keppler, *Journal of Chromatography B-Analytical Technologies in the Biomedical and Life Sciences*, 2001, **759**, 81-89.
70. A. Egger, V. B. Arion, E. Reisner, B. Cebrian-Losantos, S. Shova, G. Trettenhahn and B. K. Keppler, *Inorganic Chemistry*, 2005, **44**, 122-132.
71. J. Malina, O. Novakova, B. K. Keppler, E. Alessio and V. Brabec, *Journal of Biological Inorganic Chemistry*, 2001, **6**, 435-445.
72. S. Kapitza, M. A. Jakupec, M. Uhl, B. K. Keppler and B. Marian, *Cancer Letters*, 2005, **226**, 115-121.
73. F. Lentz, A. Drescher, A. Lindauer, M. Henke, R. A. Hilger, C. G. Hartinger, M. E. Scheulen, C. Dittrich, B. K. Keppler, U. Jaehde and R. Cent European Soc Anticanc Drug, *Anti-Cancer Drugs*, 2009, **20**, 97-103.
74. G. E. Buechel, I. N. Stepanenko, M. Hejl, M. A. Jakupec, B. K. Keppler and V. B. Arion, *Inorganic Chemistry*, 2011, **50**, 7690-7697.
75. M. J. Clarke, *Coordination Chemistry Reviews*, 2003, **236**, 209-233.
76. G. Süß-Fink, *Dalton Transactions*, 2010, **39**, 1673-1688.
77. A. Levina, A. Mitra and P. A. Lay, *Metallomics*, 2009, **1**, 458-470.
78. R. E. Morris, R. E. Aird, P. D. Murdoch, H. M. Chen, J. Cummings, N. D. Hughes, S. Parsons, A. Parkin, G. Boyd, D. I. Jodrell and P. J. Sadler, *Journal of Medicinal Chemistry*, 2001, **44**, 3616-3621.
79. C. S. Allardyce, P. J. Dyson, D. J. Ellis and S. L. Heath, *Chemical Communications*, 2001, 1396-1397.
80. R. E. Aird, J. Cummings, A. A. Ritchie, M. Muir, R. E. Morris, H. Chen, P. J. Sadler and D. I. Jodrell, *British Journal of Cancer*, 2002, **86**, 1652-1657.
81. S. M. Guichard, R. Else, E. Reid, B. Zeitlin, R. Aird, M. Muir, M. Dodds, H. Fiebig, P. J. Sadler and D. I. Jodrell, *Biochemical Pharmacology*, 2006, **71**, 408-415.
82. A. Habtemariam, M. Melchart, R. Fernandez, S. Parsons, I. D. H. Oswald, A. Parkin, F. P. A. Fabbiani, J. E. Davidson, A. Dawson, R. E. Aird, D. I. Jodrell and P. J. Sadler, *Journal of Medicinal Chemistry*, 2006, **49**, 6858-6868.
83. F. Y. Wang, A. Habtemariam, E. P. L. van der Geer, R. Fernandez, M. Melchart, R. J. Deeth, R. Aird, S. Guichard, F. P. A. Fabbiani, P. Lozano-Casal, I. D. H. Oswald, D. I. Jodrell, S. Parsons and P. J. Sadler, *Proceedings*

- of the National Academy of Sciences of the United States of America*, 2005, **102**, 18269-18274.
84. K. D. Camm, A. El-Sokkary, A. L. Gott, P. G. Stockley, T. Belyaeva and P. C. McGowan, *Dalton Transactions*, 2009, 10914-10925.
85. A. F. A. Peacock, A. Habtemariam, S. A. Moggach, A. Prescimone, S. Parsons and P. J. Sadler, *Inorganic Chemistry*, 2007, **46**, 4049-4059.
86. A. F. A. Peacock, S. Parsons and P. J. Sadler, *Journal of the American Chemical Society*, 2007, **129**, 3348-3357.
87. B. C. Behrens, T. C. Hamilton, H. Masuda, K. R. Grotzinger, J. Whangpeng, K. G. Louie, T. Knutsen, W. M. McKoy, R. C. Young and R. F. Ozols, *Cancer Research*, 1987, **47**, 414-418.
88. H. Masuda, R. F. Ozols, G. M. Lai, A. Fojo, M. Rothenberg and T. C. Hamilton, *Cancer Research*, 1988, **48**, 5713-5716.
89. T. Bugarcic, O. Novakova, A. Halamikova, L. Zerzankova, O. Vrana, J. Kasparkova, A. Habtemariam, S. Parsons, P. J. Sadler and V. Brabec, *Journal of Medicinal Chemistry*, 2008, **51**, 5310-5319.
90. H. M. Chen, J. A. Parkinson, S. Parsons, R. A. Coxall, R. O. Gould and P. J. Sadler, *Journal of the American Chemical Society*, 2002, **124**, 3064-3082.
91. S. Betanzos-Lara, L. Salassa, A. Habtemariam and P. J. Sadler, *Chemical Communications*, 2009, 6622-6624.
92. S. Betanzos-Lara, L. Salassa, A. Habtemariam, O. Novakova, A. M. Pizarro, G. J. Clarkson, B. Liskova, V. Brabec and P. J. Sadler, *Organometallics*, 2012, **31**, 3466-3479.
93. T. Bugarcic, A. Habtemariam, R. J. Deeth, F. P. A. Fabbiani, S. Parsons and P. J. Sadler, *Inorganic Chemistry*, 2009, **48**, 9444-9453.
94. A. F. A. Peacock, A. Habtemariam, R. Fernandez, V. Walland, F. P. A. Fabbiani, S. Parsons, R. E. Aird, D. I. Jodrell and P. J. Sadler, *Journal of the American Chemical Society*, 2006, **128**, 1739-1748.
95. F. Caruso, M. Rossi, A. Benson, C. Opazo, D. Freedman, E. Monti, M. B. Gariboldi, J. Shaulky, F. Marchetti, R. Pettinari and C. Pettinari, *Journal of Medicinal Chemistry*, 2012, **55**, 1072-1081.
96. H. M. Chen, J. A. Parkinson, R. E. Morris and P. J. Sadler, *Journal of the American Chemical Society*, 2003, **125**, 173-186.

97. F. Wang, H. M. Chen, S. Parsons, L. D. H. Oswald, J. E. Davidson and P. J. Sadler, *Chemistry-a European Journal*, 2003, **9**, 5810-5820.
98. H. K. Liu, F. Y. Wang, J. A. Parkinson, J. Bella and P. J. Sadler, *Chemistry-a European Journal*, 2006, **12**, 6151-6165.
99. H. K. Liu, S. J. Berners-Price, F. Y. Wang, J. A. Parkinson, J. J. Xu, J. Bella and P. J. Sadler, *Angewandte Chemie-International Edition*, 2006, **45**, 8153-8156.
100. H.-K. Liu, J. A. Parkinson, J. Bella, F. Wang and P. J. Sadler, *Chemical Science*, 2010, **1**, 258-270.
101. H. M. Chen, J. A. Parkinson, O. Novakova, J. Bella, F. Y. Wang, A. Dawson, R. Gould, S. Parsons, V. Brabec and P. J. Sadler, *Proceedings of the National Academy of Sciences of the United States of America*, 2003, **100**, 14623-14628.
102. O. Novakova, H. M. Chen, O. Vrana, A. Rodger, P. J. Sadler and V. Brabec, *Biochemistry*, 2003, **42**, 11544-11554.
103. C. Gossens, I. Tavernelli and U. Rothlisberger, *Journal of the American Chemical Society*, 2008, **130**, 10921-10928.
104. C. Gossens, I. Tavernelli and U. Rothlisberger, *Journal of Physical Chemistry A*, 2009, **113**, 11888-11897.
105. Z. Futera, J. Klenko, J. E. Sponer, J. Sponer and J. V. Burda, *Journal of Computational Chemistry*, 2009, **30**, 1758-1770.
106. R. L. Hayward, Q. C. Schornagel, R. Tente, J. C. Macpherson, R. E. Aird, S. Guichard, A. Habtemariam, P. Sadler and D. I. Jodrell, *Cancer Chemotherapy and Pharmacology*, 2005, **55**, 577-583.
107. F. Y. Wang, J. Bella, J. A. Parkinson and P. J. Sadler, *Journal of Biological Inorganic Chemistry*, 2005, **10**, 147-155.
108. F. Y. Wang, J. J. Xu, A. Habtemariam, J. Bella and P. J. Sadler, *Journal of the American Chemical Society*, 2005, **127**, 17734-17743.
109. J. Reedijk, *Chemical Reviews*, 1999, **99**, 2499-2510.
110. Y. Han, Q. Luo, X. Hao, X. Li, F. Wang, W. Hu, K. Wu, S. Lu and P. J. Sadler, *Dalton Transactions*, 2011, **40**, 11519-11529.
111. A. F. A. Peacock, M. Melchart, R. J. Deeth, A. Habtemariam, S. Parsons and P. J. Sadler, *Chemistry-a European Journal*, 2007, **13**, 2601-2613.

112. S. H. van Rijt, A. F. A. Peacock, R. D. L. Johnstone, S. Parsons and P. J. Sadler, *Inorganic Chemistry*, 2009, **48**, 1753-1762.
113. S. H. van Rijt, A. Mukherjee, A. M. Pizarro and P. J. Sadler, *Journal of Medicinal Chemistry*, 2010, **53**, 840-849.
114. H. Kostrohunova, J. Florian, O. Novakova, A. F. A. Peacock, P. J. Sadler and V. Brabec, *Journal of Medicinal Chemistry*, 2008, **51**, 3635-3643.
115. G. R. Martin and R. K. Jain, *Cancer Research*, 1994, **54**, 5670-5674.
116. C. Scolaro, A. Bergamo, L. Brescacin, R. Delfino, M. Cocchietto, G. Laurency, T. J. Geldbach, G. Sava and P. J. Dyson, *Journal of Medicinal Chemistry*, 2005, **48**, 4161-4171.
117. P. Nowak-Sliwinska, J. R. van Beijnum, A. Casini, A. A. Nazarov, G. Wagnieres, H. van den Bergh, P. J. Dyson and A. W. Griffioen, *Journal of Medicinal Chemistry*, 2011, **54**, 3895-3902.
118. C. Scolaro, C. G. Hartinger, C. S. Allardyce, B. K. Keppler and P. J. Dyson, *Journal of Inorganic Biochemistry*, 2008, **102**, 1743-1748.
119. A. K. Renfrew, A. D. Phillips, E. Tapavicza, R. Scopelliti, U. Rothlisberger and P. J. Dyson, *Organometallics*, 2009, **28**, 5061-5071.
120. A. Dorcier, C. G. Hartinger, R. Scopelliti, R. H. Fish, B. K. Keppler and P. J. Dyson, *Journal of Inorganic Biochemistry*, 2008, **102**, 1066-1076.
121. B. Wu, M. S. Ong, M. Groessl, Z. Adhireksan, C. G. Hartinger, P. J. Dyson and C. A. Davey, *Chemistry-a European Journal*, 2011, **17**, 3562-3566.
122. A. Bergamo, A. Masi, P. J. Dyson and G. Sava, *International Journal of Oncology*, 2008, **33**, 1281-1289.
123. A. Casini, C. Gabbiani, F. Sorrentino, M. P. Rigobello, A. Bindoli, T. J. Geldbach, A. Marrone, N. Re, C. G. Hartinger, P. J. Dyson and L. Messori, *Journal of Medicinal Chemistry*, 2008, **51**, 6773-6781.
124. A. A. Nazarov, J. Risse, W. H. Ang, F. Schmitt, O. Zava, A. Ruggi, M. Groessl, R. Scopelitti, L. Juillerat-Jeanneret, C. G. Hartinger and P. J. Dyson, *Inorganic Chemistry*, 2012, **51**, 3633-3639.
125. Y. Q. Tan, P. J. Dyson and W. H. Ang, *Organometallics*, 2011, **30**, 5965-5971.
126. C. G. Hartinger, A. Casini, C. Duhot, Y. O. Tsybin, L. Messori and P. J. Dyson, *Journal of Inorganic Biochemistry*, 2008, **102**, 2136-2141.

127. A. Casini, A. Karotki, C. Gabbiani, F. Rugi, M. Vasak, L. Messori and P. J. Dyson, *Metallomics*, 2009, **1**, 434-441.
128. S. Chatterjee, S. Kundu, A. Bhattacharyya, C. G. Hartinger and P. J. Dyson, *Journal of Biological Inorganic Chemistry*, 2008, **13**, 1149-1155.
129. A. Dorcier, W. H. Ang, S. Bolano, L. Gonsalvi, L. Juillerat-Jeannerat, G. Laurenczy, M. Peruzzini, A. D. Phillips, F. Zanobini and P. J. Dyson, *Organometallics*, 2006, **25**, 4090-4096.
130. C. Scolaro, T. J. Geldbach, S. Rochat, A. Dorcier, C. Gossens, A. Bergamo, M. Cocchietto, I. Tavernelli, G. Sava, U. Rothlisberger and P. J. Dyson, *Organometallics*, 2006, **25**, 756-765.
131. C. Scolaro, A. B. Chaplin, C. G. Hartinger, A. Bergamo, M. Cocchietto, B. K. Keppler, G. Sava and P. J. Dyson, *Dalton Transactions*, 2007, 5065-5072.
132. A. K. Renfrew, R. Scopelliti and P. J. Dyson, *Inorganic Chemistry*, 2010, **49**, 2239-2246.
133. A. K. Renfrew, A. D. Phillips, A. E. Egger, C. G. Hartinger, S. S. Bosquain, A. A. Nazarov, B. K. Keppler, L. Gonsalvi, M. Peruzzini and P. J. Dyson, *Organometallics*, 2009, **28**, 1165-1172.
134. I. Berger, M. Hanif, A. A. Nazarov, C. G. Hartinger, R. O. John, M. L. Kuznetsov, M. Groessl, F. Schmitt, O. Zava, F. Biba, V. B. Arion, M. Galanski, M. A. Jakupc, L. Juillerat-Jeanneret, P. J. Dyson and B. K. Keppler, *Chemistry-a European Journal*, 2008, **14**, 9046-9057.
135. W. H. Ang, E. Daldini, C. Scolaro, R. Scopelliti, L. Juillerat-Jeannerat and P. J. Dyson, *Inorganic Chemistry*, 2006, **45**, 9006-9013.
136. A. Casini, G. Mastrobuoni, W. H. Ang, C. Gabbiani, G. Pieraccini, G. Moneti, P. J. Dyson and L. Messori, *Chemmedchem*, 2007, **2**, 631-635.
137. C. A. Vock, A. K. Renfrew, R. Scopelliti, L. Juillerat-Jeanneret and P. J. Dyson, *European Journal of Inorganic Chemistry*, 2008, 1661-1671.
138. J. J. Wilson and S. J. Lippard, *Journal of Medicinal Chemistry*, 2012, **55**, 5326-5336.
139. W. H. Ang, L. J. Parker, A. De Luca, L. Juillerat-Jeanneret, C. J. Morton, M. Lo Bello, M. W. Parker and P. J. Dyson, *Angewandte Chemie-International Edition*, 2009, **48**, 3854-3857.
140. S. Chatterjee, I. Biondi, P. J. Dyson and A. Bhattacharyya, *Journal of Biological Inorganic Chemistry*, 2011, **16**, 715-724.

141. W. H. Ang, I. Khalaila, C. S. Allardyce, L. Juillerat-Jeanneret and P. J. Dyson, *Journal of the American Chemical Society*, 2005, **127**, 1382-1383.
142. S. J. Dougan, A. Habtemariam, S. E. McHale, S. Parsons and P. J. Sadler, *Proceedings of the National Academy of Sciences of the United States of America*, 2008, **105**, 11628-11633.
143. S. J. Dougan, M. Melchart, A. Habtemariam, S. Parsons and P. J. Sadler, *Inorganic Chemistry*, 2006, **45**, 10882-10894.
144. Y. Fu, A. Habtemariam, A. M. Pizarro, S. H. van Rijt, D. J. Healey, P. A. Cooper, S. D. Shnyder, G. J. Clarkson and P. J. Sadler, *Journal of Medicinal Chemistry*, 2010, **53**, 8192-8196.
145. Y. Fu, A. Habtemariam, A. M. B. H. Basri, D. Braddick, G. J. Clarkson and P. J. Sadler, *Dalton Transactions*, 2011, **40**, 10553-10562.
146. L. Zhang, P. Carroll and E. Meggers, *Organic Letters*, 2004, **6**, 521-523.
147. E. Meggers, *Chemical Communications*, 2009, 1001-1010.
148. H. Bregman, D. S. Williams, G. E. Atilla, P. J. Carroll and E. Meggers, *Journal of the American Chemical Society*, 2004, **126**, 13594-13595.
149. J. E. Debreczeni, A. N. Bullock, G. E. Atilla, D. S. Williams, H. Bregman, S. Knapp and E. Meggers, *Angewandte Chemie-International Edition*, 2006, **45**, 1580-1585.
150. K. S. M. Smalley, R. Contractor, N. K. Haass, A. N. Kulp, G. E. Atilla-Gokcumen, D. S. Williams, H. Bregman, K. T. Flaherty, M. S. Soengas, E. Meggers and M. Herlyn, *Cancer Research*, 2007, **67**, 209-217.
151. J. Maksimoska, D. S. Williams, G. E. Atilla-Gokcumen, K. S. M. Smalley, P. J. Carroll, R. D. Webster, P. Filippakopoulos, S. Knapp, M. Herlyn and E. Meggers, *Chemistry-a European Journal*, 2008, **14**, 4816-4822.
152. W. F. Schmid, R. O. John, V. B. Arion, M. A. Jakupec and B. K. Keppler, *Organometallics*, 2007, **26**, 6643-6652.
153. W. F. Schmid, R. O. John, G. Muehlgassner, P. Heffeter, M. A. Jakupec, M. Galanski, W. Berger, V. B. Arion and B. K. Keppler, *Journal of Medicinal Chemistry*, 2007, **50**, 6343-6355.
154. W. Ginzinger, G. Muehlgassner, V. B. Arion, M. A. Jakupec, A. Roller, M. Galanski, M. Reithofer, W. Berger and B. K. Keppler, *Journal of Medicinal Chemistry*, 2012, **55**, 3398-3413.

155. K. Wu, Q. Luo, W. Hu, X. Li, F. Wang, S. Xiong and P. J. Sadler, *Metallomics*, 2012, **4**, 139-148.
156. F. Pelletier, V. Comte, A. Massard, M. Wenzel, S. Toulot, P. Richard, M. Picquet, P. Le Gendre, O. Zava, F. Edafe, A. Casini and P. J. Dyson, *Journal of Medicinal Chemistry*, 2010, **53**, 6923-6933.
157. A. L. Noffke, A. Habtemariam, A. M. Pizarro and P. J. Sadler, *Chemical Communications*, 2012, **48**, 5219-5246.
158. F. H. Igney and P. H. Krammer, *Nature Reviews Cancer*, 2002, **2**, 277-288.
159. S. W. Lowe, H. E. Ruley, T. Jacks and D. E. Housman, *Cell*, 1993, **74**, 957-967.
160. M. Galanski, M. A. Jakupec and B. K. Keppler, *Current Medicinal Chemistry*, 2005, **12**, 2075-2094.
161. B. Serli, E. Zangrando, T. Gianferrara, C. Scolaro, P. J. Dyson, A. Bergamo and E. Alessio, *European Journal of Inorganic Chemistry*, 2005, 3423-3434.
162. I. Bratsos, S. Jedner, A. Bergamo, G. Sava, T. Gianferrara, E. Zangrando and E. Alessio, *Journal of Inorganic Biochemistry*, 2008, **102**, 1120-1133.
163. T. Bugarcic, A. Habtemariam, J. Stepankova, P. Heringova, J. Kasparikova, R. J. Deeth, R. D. L. Johnstone, A. Prescimone, A. Parkin, S. Parsons, V. Brabec and P. J. Sadler, *Inorganic Chemistry*, 2008, **47**, 11470-11486.
164. T. Gianferrara, A. Bergamo, I. Bratsos, B. Milani, C. Spagnul, G. Sava and E. Alessio, *Journal of Medicinal Chemistry*, 2010, **53**, 4678-4690.
165. I. Bratsos, D. Urankar, E. Zangrando, P. Genova-Kalou, J. Kosmrlj, E. Alessio and I. Turel, *Dalton Transactions*, 2011, **40**, 5188-5199.
166. I. Bratsos, E. Mitri, F. Ravalico, E. Zangrando, T. Gianferrara, A. Bergamo and E. Alessio, *Dalton Transactions*, 2012, **41**, 7358-7371.
167. T. Bowen, R. P. Planalp and M. W. Brechbiel, *Bioorganic & Medicinal Chemistry Letters*, 1996, **6**, 807-810.
168. L. Cronin, S. P. Foxon, P. J. Lusby and P. H. Walton, *Journal of Biological Inorganic Chemistry*, 2001, **6**, 367-377.
169. F. L. Urbach, J. E. Sarneski, L. J. Turner and D. H. Busch, *Inorganic Chemistry*, 1968, **7**, 2169-2171.
170. R. A. Wentworth and J. J. Felten, *Journal of the American Chemical Society*, 1968, **90**, 621-626.

171. F. Lions and K. V. Martin, *Journal of the American Chemical Society*, 1957, **79**, 1572-1575.
172. H. Y. Luo, N. Eberly, R. D. Rogers and M. W. Brechbiel, *Inorganic Chemistry*, 2001, **40**, 493-498.
173. B. Greener, L. Cronin, G. D. Wilson and P. H. Walton, *Journal of the Chemical Society-Dalton Transactions*, 1996, 401-403.
174. B. Greener, M. H. Moore and P. H. Walton, *Chemical Communications*, 1996, 27-28.
175. L. Cronin and P. H. Walton, *Chemical Communications*, 2003, 1572-1573.
176. S. V. Torti, F. M. Torti, S. P. Whitman, M. W. Brechbiel, G. Park and R. P. Planalp, *Blood*, 1998, **92**, 1384-1389.
177. G. Park, F. H. Lu, N. Ye, M. W. Brechbiel, S. V. Torti, F. M. Torti and R. P. Planalp, *Journal of Biological Inorganic Chemistry*, 1998, **3**, 449-457.
178. A. M. Samuni, M. C. Krishna, W. DeGraff, A. Russo, R. P. Planalp, M. W. Brechbiel and J. B. Mitchell, *Biochimica Et Biophysica Acta-General Subjects*, 2002, **1571**, 211-218.
179. R. D. Abeysinghe, B. T. Greene, R. Haynes, M. C. Willingham, J. L. Turner, R. P. Planalp, M. W. Brechbiel, F. M. Torti and S. V. Torti, *Carcinogenesis*, 2001, **22**, 1607-1614.
180. B. T. Greene, J. Thorburn, M. C. Willingham, A. Thorburn, R. P. Planalp, M. W. Brechbiel, J. Jennings-Gee, J. Wilkinson, F. M. Torti and S. V. Torti, *Journal of Biological Chemistry*, 2002, **277**, 25568-25575.
181. R. Zhao, R. P. Planalp, R. Ma, B. T. Greene, B. T. Jones, M. W. Brechbiel, F. M. Torti and S. V. Torti, *Biochemical Pharmacology*, 2004, **67**, 1677-1688.
182. M. L. Childers, F. Su, A. M. Przyborowska, B. Bishwokarma, G. Park, M. W. Brechbiel, S. V. Torti, F. M. Torti, G. Broker, J. S. Alexander, R. D. Rogers, K. Ruhlandt-Senge and R. P. Planalp, *European Journal of Inorganic Chemistry*, 2005, 3971-3982.
183. C. A. S. Regino, S. V. Torti, R. Ma, G. P. A. Yap, K. A. Kreisel, F. M. Torti, R. P. Planalp and M. W. Brechbiel, *Journal of Medicinal Chemistry*, 2005, **48**, 7993-7999.
184. H. S. Chong, F. M. Torti, S. V. Torti and M. W. Brechbiel, *Journal of Organic Chemistry*, 2002, **67**, 8072-8078.

185. H. S. Chong, S. V. Torti, R. Ma, F. M. Torti and M. W. Brechbiel, *Journal of Medicinal Chemistry*, 2004, **47**, 5230-5234.
186. K. Camphausen, M. Sproull, S. Tantama, S. Sankineni, T. Scott, C. Menard, C. N. Coleman and M. W. Brechbiel, *Bioorganic & Medicinal Chemistry*, 2003, **11**, 4287-4293.
187. N. Ye, G. Park, A. M. Przyborowska, P. E. Sloan, T. Clifford, C. B. Bauer, G. A. Broker, R. D. Rogers, R. Ma, S. V. Torti, M. W. Brechbiel and R. P. Planalp, *Dalton Transactions*, 2004, 1304-1311.
188. J. E. Sarneski, A. T. McPhail, K. D. Onan, L. E. Erickson and C. N. Reilley, *Journal of the American Chemical Society*, 1977, **99**, 7376-7378.
189. L. E. Erickson, D. J. Cook, G. D. Evans, J. E. Sarneski, P. J. Okarma and A. D. Sabatelli, *Inorganic Chemistry*, 1990, **29**, 1958-1967.
190. M. Yamaguchi, T. Iida and T. Yamagishi, *Inorganic Chemistry Communications*, 1998, **1**, 299-301.
191. M. A. Bennett, T. N. Huang, T. W. Matheson and A. K. Smith, *Inorganic Syntheses*, 1982, **21**, 74-78.
192. D. C. Wilson and J. H. Nelson, *Journal of Organometallic Chemistry*, 2003, **682**, 272-289.
193. S. J. Laplaca and J. A. Ibers, *Inorganic Chemistry*, 1965, **4**, 778-783.
194. A. R. Cowley, J. R. Dilworth and C. A. M. von Beckh, *Acta Crystallographica Section E-Structure Reports Online*, 2005, **61**, M1237-M1239.
195. P. S. Hallman, T. A. Stephenson and G. Wilkinson, in *Inorganic Syntheses*, ed. W. P. Robert, 2007, pp. 237-240.
196. R. D. Ernst, R. Basta and A. M. Arif, *Zeitschrift Fur Kristallographie-New Crystal Structures*, 2003, **218**, 49-51.
197. Blackmore, T., M. I. Bruce and F. G. A. Stone, *Journal of the Chemical Society a -Inorganic Physical Theoretical*, 1971, 2376-2382.
198. N. W. Alcock, I. D. Burns, K. S. Claire and A. F. Hill, *Inorganic Chemistry*, 1992, **31**, 2906-2908.
199. A. F. Hill, N. W. Alcock, J. C. Cannadine and G. R. Clark, *Journal of Organometallic Chemistry*, 1992, **426**, C40-C43.
200. M. Scholl, S. Ding, C. W. Lee and R. H. Grubbs, *Organic Letters*, 1999, **1**, 953-956.

201. P. Schwab, M. B. France, J. W. Ziller and R. H. Grubbs, *Angewandte Chemie-International Edition in English*, 1995, **34**, 2039-2041.
202. P. Schwab, R. H. Grubbs and J. W. Ziller, *Journal of the American Chemical Society*, 1996, **118**, 100-110.
203. B. Seiller, C. Bruneau and P. H. Dixneuf, *Journal of the Chemical Society-Chemical Communications*, 1994, 493-494.
204. M. Tokunaga and Y. Wakatsuki, *Angewandte Chemie-International Edition*, 1998, **37**, 2867-2869.
205. A. L. Gott, P. C. McGowan, T. J. Podesta and M. Thornton-Pett, *Journal of the Chemical Society-Dalton Transactions*, 2002, 3619-3623.
206. J. F. Malone, C. M. Murray, M. H. Charlton, R. Docherty and A. J. Lavery, *Journal of the Chemical Society-Faraday Transactions*, 1997, **93**, 3429-3436.
207. P. Vandersluis and A. L. Spek, *Acta Crystallographica Section A*, 1990, **46**, 194-201.
208. A. L. Spek, *Journal of Applied Crystallography*, 2003, **36**, 7-13.
209. G. Aullon, D. Bellamy, L. Brammer, E. A. Bruton and A. G. Orpen, *Chemical Communications*, 1998, 653-654.
210. A. G. Orpen and N. G. Connelly, *Journal of the Chemical Society-Chemical Communications*, 1985, 1310-1311.
211. B. J. Coe and S. J. Glenwright, *Coordination Chemistry Reviews*, 2000, **203**, 5-80.
212. E. R. T. Tiekink, *Zeitschrift Fur Kristallographie*, 1992, **198**, 158-161.
213. L. D. Field, B. A. Messerle, L. Soler, I. E. Buys and T. W. Hambley, *Journal of the Chemical Society-Dalton Transactions*, 2001, 1959-1965.
214. R. Lalrempuia, P. J. Carroll and M. R. Kollipara, *Journal of Coordination Chemistry*, 2003, **56**, 1499-1504.
215. J. R. Polam and L. C. Porter, *Inorganica Chimica Acta*, 1993, **205**, 119-121.
216. R. P. Schutte, S. J. Rettig and B. R. James, *Canadian Journal of Chemistry-Revue Canadienne De Chimie*, 1996, **74**, 2064-2072.
217. M. R. J. Elsegood, M. B. Smith and N. M. Sanchez-Ballester, *Acta Crystallographica Section E-Structure Reports Online*, 2006, **62**, M2838-M2840.
218. H. D. Hansen and J. H. Nelson, *Organometallics*, 2000, **19**, 4740-4755.

219. M. R. J. Elsegood and D. A. Tocher, *Polyhedron*, 1995, **14**, 3147-3156.
220. R. Taylor and O. Kennard, *Acta Crystallographica Section B-Structural Science*, 1983, **39**, 517-525.
221. M. Jimenez-Tenorio, M. D. Palacios, M. C. Puerta and P. Valerga, *Organometallics*, 2004, **23**, 504-510.
222. J. B. Zhang, K. A. Barakat, T. R. Cundari, T. B. Gunnoe, P. D. Boyle, J. L. Petersen and C. S. Day, *Inorganic Chemistry*, 2005, **44**, 8379-8390.
223. F. H. Allen, *Acta Crystallographica Section B-Structural Science*, 2002, **58**, 380-388.
224. Toxicological profile for methylene chloride, <http://www.atsdr.cdc.gov/ToxProfiles/tp14.pdf>, Accessed 27 July, 2012.
225. J. A. Davies, *Advances in Inorganic Chemistry*, 1981, **24**, 115-187.
226. A. B. Chaplin, C. Fellay, G. Laurency and P. J. Dyson, *Organometallics*, 2007, **26**, 586-593.
227. C. Landgrafe and W. S. Sheldrick, *Journal of the Chemical Society-Dalton Transactions*, 1994, 1885-1893.
228. J. Carmichael, J. B. Mitchell, W. G. Degraff, J. Gamson, A. F. Gazdar, B. E. Johnson, E. Glatstein and J. D. Minna, *British Journal of Cancer*, 1988, **57**, 540-547.
229. E. Iengo, E. Zangrando, E. Baiutti, F. Munini and E. Alessio, *European Journal of Inorganic Chemistry*, 2005, 1019-1031.
230. C. A. Vock, C. Scolaro, A. D. Phillips, R. Scopelliti, G. Sava and P. J. Dyson, *Journal of Medicinal Chemistry*, 2006, **49**, 5552-5561.
231. I. Bratsos, C. Simonin, E. Zangrando, T. Gianferrara, A. Bergamo and E. Alessio, *Dalton Transactions*, 2011, **40**, 9533-9543.
232. G. Sava, S. Zorzet, T. Giraldi, G. Mestroni and G. Zassinovich, *European Journal of Cancer & Clinical Oncology*, 1984, **20**, 841-847.
233. S. Cauci, E. Alessio, G. Mestroni and F. Quadrioglio, *Inorganica Chimica Acta-Bioinorganic Chemistry*, 1987, **137**, 19-24.
234. E. Alessio, G. Mestroni, G. Nardin, W. M. Attia, M. Calligaris, G. Sava and S. Zorzet, *Inorganic Chemistry*, 1988, **27**, 4099-4106.
235. G. Sava, S. Pacor, G. Mestroni and E. Alessio, *Clinical & Experimental Metastasis*, 1992, **10**, 273-280.

236. I. P. Evans, A. Spencer and G. Wilkinson, *Journal of the Chemical Society-Dalton Transactions*, 1973, 204-209.
237. W. A. Clucas, R. S. Armstrong, I. E. Buys, T. W. Hambley and K. W. Nugent, *Inorganic Chemistry*, 1996, **35**, 6789-6794.
238. L. V. Kononov and V. G. Pogareva, *Journal of Structural Chemistry*, 1981, **22**, 438-440.
239. M. Calligaris and O. Carugo, *Coordination Chemistry Reviews*, 1996, **153**, 83-154.
240. M. H. Wang, U. Englert and U. Kolle, *Journal of Organometallic Chemistry*, 1993, **453**, 127-131.
241. M. Calligaris, *Coordination Chemistry Reviews*, 2004, **248**, 351-375.
242. M. Stener and M. Calligaris, *Journal of Molecular Structure-Theochem*, 2000, **497**, 91-104.
243. E. Ruba, C. Gemel, C. Slugovc, K. Mereiter, R. Schmid and K. Kirchner, *Organometallics*, 1999, **18**, 2275-2280.
244. M. Chandra, D. S. Pandey, M. C. Puerta and P. Valerga, *Acta Crystallographica Section E-Structure Reports Online*, 2002, **58**, M28-M29.
245. T. J. Beasley, R. D. Brost, C. K. Chu, S. L. Grundy and S. R. Stobart, *Organometallics*, 1993, **12**, 4599-4606.
246. T. Mosmann, *Journal of Immunological Methods*, 1983, **65**, 55-63.
247. M. Jennerwein and P. A. Andrews, *Drug Metabolism and Disposition*, 1995, **23**, 178-184.
248. L. Helm, G. M. Nicolle and A. E. Merbach, *Advances in Inorganic Chemistry - Including Bioinorganic Studies, Vol 57*, 2005, **57**, 327-379.
249. P. Kuzmic, *Analytical Biochemistry*, 1996, **237**, 260-273.
250. V. Moreno, M. Font-Bardia, T. Calvet, J. Lorenzo, F. X. Aviles, M. H. Garcia, T. S. Morais, A. Valente and M. P. Robalo, *Journal of Inorganic Biochemistry*, 2011, **105**, 241-249.
251. L. Salassa, *European Journal of Inorganic Chemistry*, 2011, 4931-4947.
252. O. Novakova, J. Kasparkova, O. Vrana, P. M. Vanvliet, J. Reedijk and V. Brabec, *Biochemistry*, 1995, **34**, 12369-12378.
253. A. E. Friedman, J. C. Chambron, J. P. Sauvage, N. J. Turro and J. K. Barton, *Journal of the American Chemical Society*, 1990, **112**, 4960-4962.

254. Y. Jenkins, A. E. Friedman, N. J. Turro and J. K. Barton, *Biochemistry*, 1992, **31**, 10809-10816.
255. M. R. Gill, H. Derrat, C. G. W. Smythe, G. Battaglia and J. A. Thomas, *Chembiochem*, 2011, **12**, 877-880.
256. D. Sun, R. Zhang, F. Yuan, D. Liu, Y. Zhou and J. Liu, *Dalton Transactions*, 2012, **41**, 1734-1741.
257. G. R. Desiraju and T. Steiner, in *The weak hydrogen bond in structural chemistry and biology*, Oxford University Press, 1999, pp. 29-121.
258. M. T. Forel and Tranquil.M, *Spectrochimica Acta Part a-Molecular Spectroscopy*, 1970, **A 26**, 1023-1035.
259. G. R. Fulmer, A. J. M. Miller, N. H. Sherden, H. E. Gottlieb, A. Nudelman, B. M. Stoltz, J. E. Bercaw and K. I. Goldberg, *Organometallics*, 2010, **29**, 2176-2179.
260. M. Calligaris, *Croatia Chemica Acta*, 1999, **72**, 147-169.
261. R. Thomas, Shoemake.Cb and K. Eriks, *Acta Crystallographica*, 1966, **21**, 12-20.
262. C. V. Senoff, Maslowsk.E and R. G. Goel, *Canadian Journal of Chemistry*, 1971, **49**, 3585-3589.
263. F. C. March and G. Ferguson, *Canadian Journal of Chemistry*, 1971, **49**, 3590-3595.
264. M. O. Albers, D. J. Robinson, A. Shaver and E. Singleton, *Organometallics*, 1986, **5**, 2199-2205.
265. C. Slugovc, R. Schmid and K. Kirchner, *Coordination Chemistry Reviews*, 1999, **185-6**, 109-126.
266. S. J. Bernersprice, C. K. Mirabelli, R. K. Johnson, M. R. Mattern, F. L. McCabe, L. F. Faucette, C. M. Sung, S. M. Mong, P. J. Sadler and S. T. Crooke, *Cancer Research*, 1986, **46**, 5486-5493.
267. S. Das, S. Sinha, R. Britto, K. Somasundaram and A. G. Samuelson, *Journal of Inorganic Biochemistry*, 2010, **104**, 93-104.
268. J. M. Walker, A. McEwan, R. Pycko, M. L. Tassotto, C. Gottardo, J. Th'ng, R. Y. Wang and G. J. Spivak, *European Journal of Inorganic Chemistry*, 2009, 4629-4633.

269. W. H. Pearson, J. E. Shade, J. E. Brown and T. E. Bitterwolf, *Acta Crystallographica Section C-Crystal Structure Communications*, 1996, **52**, 1106-1110.
270. R. C. van der Drift, M. Gagliardo, H. Kooijman, A. L. Spek, E. Bouwman and E. Drent, *Journal of Organometallic Chemistry*, 2005, **690**, 1044-1055.
271. C. Dagueneat, R. Scopelliti and P. J. Dyson, *Organometallics*, 2004, **23**, 4849-4857.
272. I. S. Thorburn, S. J. Rettig and B. R. James, *Journal of Organometallic Chemistry*, 1985, **296**, 103-114.
273. Y. Takahashi, M. Akita, S. Hikichi and Y. Moro-oka, *Inorganic Chemistry*, 1998, **37**, 3186-3194.
274. J. Canivet, L. Karmazin-Brelot and G. Suss-Fink, *Journal of Organometallic Chemistry*, 2005, **690**, 3202-3211.
275. R. Fernandez, M. Melchart, A. Habtemariam, S. Parsons and P. J. Sadler, *Chemistry-a European Journal*, 2004, **10**, 5173-5179.
276. M. Gras, B. Therrien, G. Suss-Fink, O. Zava and P. J. Dyson, *Dalton Transactions*, 2010, **39**, 10305-10313.
277. J. Reedijk, *Pure and Applied Chemistry*, 1987, **59**, 181-192.
278. Z. J. Guo and P. J. Sadler, *Advances in Inorganic Chemistry*, Vol 49, 2000, **49**, 183-306.
279. A. Krezel and W. Bal, *Journal of Inorganic Biochemistry*, 2004, **98**, 161-166.
280. K. Popov, H. Ronkkomaki and L. H. J. Lajunen, *Pure and Applied Chemistry*, 2006, **78**, 663-675.
281. *Handbook of Chemistry and Physics*, CRC Press, 2007.
282. C. Gossens, A. Dorcier, P. J. Dyson and U. Rothlisberger, *Organometallics*, 2007, **26**, 3969-3975.
283. M. C. Lim and R. B. Martin, *Journal of Inorganic & Nuclear Chemistry*, 1976, **38**, 1911-1914.
284. M. Melchart, A. Habtemariam, O. Novakova, S. A. Moggach, F. P. A. Fabbiani, S. Parsons, V. Brabec and P. J. Sadler, *Inorganic Chemistry*, 2007, **46**, 8950-8962.
285. C. Pecklak-Scott, P. K. Smitherman, A. J. Townsend and C. S. Morrow, *Molecular Cancer Therapeutics*, 2008, **7**, 3247-3255.

286. B. R. James, E. Ochiai and G. I. Rempel, *Inorganic & Nuclear Chemistry Letters*, 1971, **7**, 781-784.
287. M. O. Albers, T. V. Ashworth, H. E. Oosthuizen, E. Singleton, J. S. Merola and R. T. Kacmarcik, *Inorganic Syntheses*, 1989, **26**, 68-77.
288. W. Luginbuhl, P. Zbinden, P. A. Pittet, T. Armbruster, H. B. Burgi, A. E. Merbach and A. Ludi, *Inorganic Chemistry*, 1991, **30**, 2350-2355.
289. A. M. McNair, D. C. Boyd and K. R. Mann, *Organometallics*, 1986, **5**, 303-310.
290. G. L. Hardgrove and D. H. Templeton, *Acta Crystallographica*, 1959, **12**, 28-32.
291. F. Grepioni, G. Cojazzi, D. Braga, E. Marseglia, L. Scaccianoce and B. F. G. Johnson, *Journal of the Chemical Society-Dalton Transactions*, 1999, 553-558.
292. "SMART" - control software Bruker SMART Apex X-ray Diffractometer. v5.625, Bruker-AXS GMBH, Karlsruhe, Germany.
293. "SAINT+" - integration software for Bruker SMART detectors. v6.45, Bruker-AXS GMBH, Karlsruhe, Germany.
294. G. M. Sheldrick, *Acta Crystallogr., Sect. B*, 2008, **64**, 112.
295. CrysAlisPro, Oxford Diffraction Ltd. Version 1.171.34.40
295. Empirical absorption correction using spherical harmonics, implemented in SCALE3 ABSPACK scaling algorithm within CrysAlisPro software, Oxford Diffraction Ltd. Version 1.171.34.40
297. "smtbx-flip" plug-in module to "Olex2" crystallography software, *J. Appl. Cryst.*, 2009 **42**, 339-341.
298. "SHELXL-97" - program for the Refinement of Crystal Structures. G. M. Sheldrick, University of Göttingen, Göttingen, Germany, 1997.
- 299 (a) P. Csaszar, P. Pulay, *Journal of Molecular Structure*, 1984, **114**, 31-34; (b) R. Ahlrichs, M. Bar, M. Haser, H. Horn, C. Kolmel, *Chemical Physics Letters*, 1989, **162**, 165-169; (c) K. Eichkorn, O. Treutler, H. Ohm, M. Haser; R. Ahlrichs, *Chemical Physics Letters*, 1995, **240**, 283-289; (d) O. Treutler, R. Ahlrichs, *Journal of Chemical Physics*, 1995, **102**, 346-354; (e) K. Eichkorn, F. Weigend, O. Treutler, R. Ahlrichs, *Theoretical Chemistry Accounts*, 1997, **97**, 119-124; (f) M. V. Arnim, R. Ahlrichs, *The Journal of Chemical Physics*, 1999, **111**, 9183-9190; (g) P. Deglmann, F. Furche,

Journal of Chemical Physics, 2002, **117**, 9535-9538; (h) P. Deglmann, F. Furche, R. Ahlrichs, *Chemical Physics Letters*, 2002, **362**, 511-518; (i) P. Deglmann, K. May, F. Furche, R. Ahlrichs, *Chemical Physics Letters*, 2004, **384**, 103-107.